Alma Mater Studiorum - Università di Bologna

DOTTORATO DI RICERCA IN

MECCANICA E SCIENZE AVANZATE DELL'INGEGNERIA

Ciclo 34

Settore Concorsuale: 09/C2 - FISICA TECNICA E INGEGNERIA NUCLEARE

Settore Scientifico Disciplinare: ING-IND/19 - IMPIANTI NUCLEARI

DEVELOPMENT OF A NUMERICAL PLATFORM FOR THE MODELING AND OPTIMAL CONTROL OF LIQUID METAL FLOWS

Presentata da: Valentina Giovacchini

Coordinatore Dottorato

Marco Carricato

Supervisore

Sandro Manservisi

Esame finale anno 2022

Contents

Abstract

The main purpose of this work is to develop a numerical platform for the turbulence modeling and optimal control of liquid metal flows. Thanks to their interesting thermal properties, liquid metals are widely studied as coolants for heat transfer applications in the nuclear context. However, due to their low Prandtl numbers, the standard turbulence models commonly used for coolants as air or water are inadequate. Advanced turbulence models able to capture the anisotropy in the flow and heat transfer are then necessary. In this thesis, a new anisotropic four-parameter turbulence model is presented and validated. The proposed model is based on explicit algebraic models and solves four additional transport equations for dynamical and thermal turbulent variables. For the validation of the model, several flow configurations are considered for different Reynolds and Prandtl numbers, namely fully developed flows in a plane channel and cylindrical pipe, and forced and mixed convection in a backward-facing step geometry. Since buoyancy effects cannot be neglected in liquid metals-cooled fast reactors, the second aim of this work is to provide mathematical and numerical tools for the simulation and optimization of liquid metals in mixed and natural convection. Optimal control problems for turbulent buoyant flows are studied and analyzed with the Lagrange multipliers method. Numerical algorithms for optimal control problems are integrated into the numerical platform and several simulations are performed to show the robustness, consistency, and feasibility of the method.

Introduction

Liquid metals, with their low Prandtl numbers, have gained increasing attention in recent years. Compared with other coolant fluids, such as air or water, liquid metals can withstand large heat fluxes, with moderate temperature gradients, thanks to their large thermal conductivity values. Furthermore, due to their high values of boiling temperature, some liquid metals, like sodium, can flow in the liquid phase at high temperatures without needing pressurized systems [1]. Thanks to these properties, liquid metals are currently considered in a broad range of industrial applications, including the production of steel and semiconductors, in thermal solar plants [2, 3] and in Generation IV liquid metal-cooled reactors [4, 5, 6]. Liquid metal-cooled reactors are expected to play an important role in the future of nuclear energy production due to their possibility to use natural resources efficiently and to reduce the volume and lifetime of nuclear waste [7]. The coolants considered for such reactors are sodium, lead, and lead alloys with Pr numbers ranging from 0.001 to 0.02.

In the nuclear context, thermal-hydraulics is regarded as one of the key issues in the project, design, and construction of liquid metal-cooled reactors. To solve thermal-hydraulic issues, nuclear engineers and researchers rely on analytical and empirical correlations, System Thermal-Hydraulics (STH) and Computational Fluid Dynamics (CFD) codes. Detailed measurements of local flow parameters in liquid metal-cooled reactors are challenging due to the opacity of the fluid, the anisotropy of the flows, and the strong buoyancy influence [8]. Detailed experimental measuring capa-

bilities are limited and numerical simulations of basic and complex flow configurations are more important for low Prandtl number fluids than in usual cases. In this respect, CFD is regarded as a valuable tool to analyze the thermal-hydraulics behavior of nuclear systems when very sophisticated models are required to accurately simulate turbulent liquid metals flow and heat transfer.

To provide an understanding of flow mechanisms, the common tool employed is the Direct Numerical Simulation (DNS). The DNS method is based on the complete three-dimensional and time-dependent conservation equations for mass, momentum, and energy. All the turbulence scales are resolved but this approach is affordable only for low and medium Reynolds numbers. Another approach for obtaining useful data and flow parameters is the Large Eddy Simulation (LES). With this technique, only the large and slow scales of turbulence are resolved by the grid and in time. The small scales have to be modeled by sub-grid scale models. This approach is a compromise between the accuracy of DNS and the low-computational cost of the Reynolds-Averaged Navier-Stokes (RANS) technique. RANS approach is based on the time-averaging operation applied to conservation equations. The operation introduces new turbulent unknowns, Reynolds stresses and turbulent heat fluxes, leading to a closure problem for the system of equations. This approach is the most commonly used in CFD codes for the simulation of complex systems. The introduced models to close RANS equations have to be carefully calibrated to predict accurately the flow and heat transfer behavior.

In the RANS framework, several models have been developed in past decades for the computation of the Reynolds stress tensor. First-order models are based on the isotropic eddy viscosity, while second-order models use transport equations for Reynolds stress tensor components. First and second-order models are integrated and available in most of the commercial codes. The first-order models are simple to implement but fail to predict flow features in several cases, while the second-order ones allow predicting the anisotropy in the flows but require a considerably increased numerical effort [9]. For the turbulent heat flux, only a few models have been developed and validated. Most of the commercial codes apply the Simple Gradient Diffusion Hypothesis (SGDH) based on the turbulent thermal diffusivity and a constant turbulent Prandtl number. However, this concept is inadequate in heat transfer problems involving low Prandtl number fluids

like liquid metals [10]. More sophisticated heat transfer models are necessary to correctly predict flow features and heat transfer phenomena in liquid metal flows. One of the most promising heat transfer models for liquid metals is the isotropic four-parameter turbulence model which is based on the SGDH hypothesis and solves two additional transport equations for thermal turbulent quantities [11, 12, 13, 14].

The abovementioned isotropic four-equation turbulence model is implemented in FEMuS, a finite element code integrated into the multiscale and multiphysics numerical platform FemusPlatform [15]. The numerical platform is based on the SALOME project and has been developed over the last years at the Laboratory of Montecuccolino of the University of Bologna. It is an environment where several numerical codes can be run together, allowing the simulation of complex physical phenomena on different physical scales [16, 17]. In particular, the numerical platform includes the multigrid finite element in-house code FEMuS for heat transfer, fluid flow, turbulence, fluid-structure modeling and adjoint optimal control; the open-source finite volume CFD software OpenFOAM; the multiscale neutronic code DONJON-DRAGON; and a STH code for thermal-hydraulic simulations.

In this framework, this Ph.D. thesis aims to propose and validate a new turbulence model for flow and heat transfer simulations of liquid metals based on the isotropic four-parameter turbulence model implemented in FEMuS. The new model for the closure of Reynolds stresses and turbulent heat fluxes adopts explicit algebraic models, which belong to a class of models between first and second-order models. Explicit algebraic models are characterized by the easy implementation of first-order models but they can capture the anisotropy in the flow and heat transfer as second-order models. The explicit algebraic stress and heat transfer model requires the solution of transport equations for four parameters, thus it is referred to as the anisotropic four-parameter turbulence model [18, 19, 20]. The new model is implemented into FEMuS and its validation is performed by referring to DNS data and empirical correlations. The upgrade of the four-parameter turbulence model aims to improve the multiphysics and multiscale simulations involving liquid metals performed by using the numerical platform.

In the project, design, and optimization of liquid metal-cooled reactors, the optimal control theory can be exploited. The optimal design of natural and mixed convection systems is crucial in the thermal-hydraulics of lead-

cooled fast reactors, where cooling is guaranteed by natural convection. Optimization techniques can be used to find the optimal wall temperature or heat flux to achieve specified objectives inside heat exchangers, nuclear cores, primary and secondary circuit pipes. There are many objectives of interest in this kind of application, i.e. flow matching, drag minimization, enhancing or reducing turbulence, and hot spot reduction.

In liquid metal-cooled reactors, the buoyancy forces have a strong influence on the flow. In particular, the thermodynamic properties of lead allow a high level of natural circulation cooling in the primary system of lead-cooled reactors. In the design and optimization of core cooling in lead-cooled reactors, the strong natural circulation characteristics during both operation and shutdown conditions cannot be neglected [21]. However, optimal control problems for natural or mixed convection in turbulent conditions have not been considered so far. Optimal control problems for the Boussinesq system in laminar condition have been studied focusing on the stationary boundary and distributed control problems [22, 23, 24, 25, 26] to find the optimal wall temperature, heat source or force in the case of electrically conductive fluids as liquid metals. Since the role of turbulence has not been considered yet in the optimal control for liquid metal flows in mixed and natural convection, this Ph.D. thesis aims to treat mathematically and numerically the optimal control of turbulent buoyant flows [27, 28]. The new adjoint solvers for the optimal control of Boussinesq equations in laminar and turbulent conditions are implemented into the numerical platform, in particular into the finite element code FEMuS.

This thesis is divided into two main parts, dealing with the turbulence modeling and the optimal control of liquid metal flows. The first part is devoted to flow and heat transfer modeling for low Prandtl number fluids. In Chapter 1 the main features of turbulent flows are presented and particular attention is given to wall turbulence and its characteristics. The Reynolds averaging operation is presented and applied to conservation equations. The problem of their closure is treated in Chapter 2. The standard closure models are presented based on linear eddy viscosity and eddy thermal diffusivity models, focusing on the treatment of wall flows. Then, the explicit algebraic models for Reynolds stresses and turbulent heat fluxes are derived and the anisotropic four-parameter turbulence model is presented. In Chapter 3, a validation of the model is proposed through numerical simulations performed by using FEMuS and considering several flow con-

figurations in different conditions of Reynolds and Prandtl numbers. In the second part, the study of optimal boundary control problems for buoyant turbulent flows is presented. In Chapter 4 the main features of an optimal control problem are described for the case of mixed or natural convection in laminar flows. Numerical results are presented to show and compare the effectiveness of the main control mechanisms, i.e. Dirichlet, Neumann and distributed controls. In Chapter 5 the role of turbulence is taken into account. The optimal control problem is analyzed from a mathematical point of view for the Dirichlet optimal control. Numerical results obtained by using FEMuS are presented and discussed.

PART I

Liquid metals turbulence modeling

CHAPTER 1

Turbulent flows

In this chapter, we consider the conservation equations of mass, momentum, and energy that describe the state of an incompressible Newtonian fluid. Buoyancy effects are considered in the framework of the Oberbeck-Boussinesq approximation. When turbulence occurs, statistical tools for the description of random variables characterizing turbulent flows may be required, such as probability density function, mean, fluctuation, and standard deviation. When the random fields can be decomposed into mean and fluctuating parts, the conservation equations can be time-averaged following the Reynolds averaging procedure. With the averaging operation, a set of equations for the mean fields can be obtained. However, in the attempt to close the averaged system of equations, new unknown correlations appear during the averaging process. The well-known problem of the new system closure is treated in Chapter 2.

Turbulence can be generated by frictional forces acting over solid walls, or by the flow of layers of fluids with different velocities. The turbulence generated and continuously affected by fixed walls is designated as wall turbulence, while turbulence generated by two adjacent layers of fluid in absence of walls is called free turbulence. In this Ph.D. thesis, we are particularly interested in wall turbulence and wall flows. The main features of wall turbulence, like the one occurring in channel and pipe flows, are

presented and described in the last section of this chapter.

1.1. Conservation equations for incompressible flows

In this section, the conservation equation of mass, momentum and energy for an incompressible Newtonian fluid are derived and discussed. The Oberbeck-Boussinesq approximation is also considered and the corresponding equations are reported. In the following, the Einstein summation notation is employed.

1.1.1. Conservation of mass

The conservation of mass equation, or continuity equation, states that the time rate of change of mass in a fixed volume is equal to the net rate of mass flow across the surface

$$\frac{\partial \rho}{\partial t} + \frac{\partial}{\partial x_i}(\rho u_i) = 0\,, \tag{1.1}$$

where ρ is the density of the medium and u_i is the i-component of the velocity vector $\mathbf{u}$. By introducing the Eulerian derivative $D/Dt = \partial/\partial t + \mathbf{u} \cdot \nabla$, the continuity equation can be expressed in the advective form as

$$\frac{D\rho}{Dt} + \rho \frac{\partial u_i}{\partial x_i} = 0\,. \tag{1.2}$$

When the fluid density changes are negligible, the medium is incompressible and the Eulerian derivative of the density field vanishes. The continuity equation becomes

$$\frac{\partial u_i}{\partial x_i} = 0\,, \tag{1.3}$$

which is often referred to as the incompressibility condition.

1.1.2. Conservation of momentum

The conservation equation of momentum, or Navier-Stokes equation, can be written as

$$\frac{\partial (\rho u_i)}{\partial t} + \frac{\partial}{\partial x_j}(\rho u_i u_j) = \frac{\partial \sigma_{ij}}{\partial x_j} + \rho f_i\,, \tag{1.4}$$

where σ_{ij} is the Cauchy stress tensor and f_i is the i-component of the total body force vector $\mathbf{f}$. For incompressible flows, the momentum conservation

equation is reduced to the advective form

$$\rho \frac{Du_i}{Dt} = \frac{\partial \sigma_{ij}}{\partial x_j} + \rho f_i \,. \tag{1.5}$$

The principle of conservation of angular momentum states that in absence of distributed couples the stress tensor is symmetric $\sigma_{ij} = \sigma_{ji}$. Thus, it can be decomposed into isotropic and deviatoric parts

$$\sigma_{ij} = -p\delta_{ij} + \tau_{ij} \,, \tag{1.6}$$

where p is the hydrostatic pressure and τ_{ij} is the viscous stress tensor. For Newtonian fluids, the viscous stress tensor is related to the strain rate tensor S_{ij} by

$$\tau_{ij} = C_{ijkl} S_{kl} \,, \tag{1.7}$$

where C_{ijkl} is the fourth-order tensor of viscosities of the fluid and S_{ij} is the strain rate tensor or rate of deformation tensor

$$S_{ij} = \frac{1}{2}\Big(\frac{\partial u_i}{\partial x_j} + \frac{\partial u_j}{\partial x_i}\Big) \,. \tag{1.8}$$

For an isotropic viscous fluid, the fourth-order tensor C_{ijkl} can be expressed in terms of the Lamè constants η and μ

$$\tau_{ij} = \eta(\operatorname{tr} \mathbf{S})\delta_{ij} + 2\mu S_{ij} \,, \tag{1.9}$$

where $(\operatorname{tr} \mathbf{S}) = S_{ii}$ denotes the trace of the strain rate tensor $\mathbf{S}$. The second Lamè coefficient μ is referred to as dynamic viscosity of the fluid. For an incompressible fluid $(\operatorname{tr} \mathbf{S}) = 0$, then Equation (1.9) and (1.6) become

$$\tau_{ij} = 2\mu S_{ij} \,, \quad \sigma_{ij} = -p\delta_{ij} + 2\mu S_{ij} \,. \tag{1.10}$$

The Navier Stokes equation (1.5) can be then written as

$$\rho \frac{Du_i}{Dt} = -\frac{\partial p}{\partial x_i} + \frac{\partial}{\partial x_j}\Big[\mu\Big(\frac{\partial u_i}{\partial x_j} + \frac{\partial u_j}{\partial x_i}\Big)\Big] + \rho f_i \,. \tag{1.11}$$

or

$$\frac{Du_i}{Dt} = -\frac{1}{\rho}\frac{\partial p}{\partial x_i} + \frac{\partial}{\partial x_j}\Big[\nu\Big(\frac{\partial u_i}{\partial x_j} + \frac{\partial u_j}{\partial x_i}\Big)\Big] + f_i \,. \tag{1.12}$$

where $\nu = \mu/\rho$ is the kinematic viscosity.

1.1.3. Conservation of energy

The law of conservation of energy states that the time rate of change of the local energy is equal to the sum of the rate of work done by applied forces and the change of heat content per unit of time. The conservation of energy can be expressed as

$$\frac{\partial(\rho e)}{\partial t} + \frac{\partial \rho e u_i}{\partial x_i} = -\frac{\partial q_i}{\partial x_i} + \frac{\partial \sigma_{ij} u_j}{\partial x_i} + Q + \rho f_i u_i \,, \tag{1.13}$$

where $e = \upsilon + \frac{1}{2} u_i u_i$ is the total energy, υ is the internal energy, q_i is the i-component of the heat flux vector and Q is the internal heat generation. For incompressible flows, an equation for the internal energy υ can be derived

$$\frac{\partial(\rho \upsilon)}{\partial t} + \frac{\partial \rho \upsilon u_i}{\partial x_i} = -\frac{\partial q_i}{\partial x_i} + Q + \Phi \,, \tag{1.14}$$

where $\Phi = \sigma_{ij} \partial u_i / \partial x_j$ is a dissipation function that can be expressed for a Newtonian and isotropic fluid as

$$\Phi = (-p\delta_{ij} + \tau_{ik}) \frac{\partial u_i}{\partial x_j} \,. \tag{1.15}$$

The internal energy equation can be simplified by expanding the derivatives on the left-hand side of the equation. Using the continuity equation we obtain the advective form of the energy equation

$$\rho \frac{D\upsilon}{Dt} = -\frac{\partial q_i}{\partial x_i} + Q + \Phi \,. \tag{1.16}$$

We now introduce constitutive relations for the internal energy υ and the heat flux q_i to formulate the conservation equations in terms of the temperature T. The internal energy can be related to two intensive thermodynamic variables, such as temperature T and specific volume $v = 1/\rho$, thus $\upsilon = \upsilon(T, v)$. The change of internal energy is

$$d\upsilon = \left.\frac{\partial \upsilon}{\partial T}\right|_v dT + \left.\frac{\partial \upsilon}{\partial v}\right|_T dv = c_v dT + \left(T \left.\frac{\partial p}{\partial T}\right|_v - p\right) dv \,, \tag{1.17}$$

where c_v is the specific heat at constant volume. When converted to a material derivative and multiplying for the density ρ one can write

$$\rho \frac{D\upsilon}{Dt} = \rho c_v \frac{DT}{Dt} + \left(T \left.\frac{\partial p}{\partial T}\right|_v - p\right) \rho \frac{Dv}{Dt} \,. \tag{1.18}$$

Since $v = 1/\rho$, the term $\rho Dv/Dt$ can be rewritten as $\partial u_i/\partial x_i$, and for an incompressible flow the second term on the right-hand side of (1.18) is zero. Moreover, $c_v \approx c_p \approx c$, where c is the specific heat and c_p is the specific heat at constant pressure, then $\rho Dv/Dt = \rho c DT/Dt$ for incompressible flows.

The constitutive relation for the heat flux is the Fourier law for heat conduction, which states that

$$q_i = -\lambda_{ij}\frac{\partial T}{\partial x_j}\,, \tag{1.19}$$

where λ_{ij} denotes the conductivity tensor of order two. For an isotropic medium $\lambda_{ij} = \lambda\delta_{ij}$, where λ denotes the isotropic thermal conductivity. The conservation equation of energy can be then written as

$$\rho c\frac{DT}{Dt} = \frac{\partial}{\partial x_i}\Big(\lambda\frac{\partial T}{\partial x_i}\Big) + Q + \Phi\,, \tag{1.20}$$

or

$$\frac{DT}{Dt} = \frac{\partial}{\partial x_i}\Big(\alpha\frac{\partial T}{\partial x_i}\Big) + \frac{Q}{\rho c} + \frac{\Phi}{\rho c}\,, \tag{1.21}$$

where $\alpha = \lambda/(\rho c)$ is the thermal diffusivity. The dissipation function is important in some special cases involving very high shear rates, such as bearings and hydraulic systems. In most other cases the dissipation function can be neglected, and the energy equation further simplifies

$$\frac{DT}{Dt} = \frac{\partial}{\partial x_i}\Big(\alpha\frac{\partial T}{\partial x_i}\Big) + \frac{Q}{\rho c}\,. \tag{1.22}$$

1.1.4. Approximation of Oberbeck-Boussinesq

The Oberbeck-Boussinesq approximation is a widely used procedure to solve non-isothermal flows without having to solve for the full compressible formulation of the conservation equations (1.1), (1.4) and (1.13). This approximation assumes that variations in density ρ do not affect the flow field, except that they give rise to buoyancy forces. Thus, we can consider $\rho = \rho_0$ except for the gravity term. Under this approximation, the continuity equation reduces to the incompressibility condition (1.3). When one considers $\rho\mathbf{f} = \rho\mathbf{g}$, where $\mathbf{g}$ is the gravitational acceleration, the Navier-Stokes equation can be written in the following form

$$\rho_0\frac{Du_i}{Dt} = -\frac{\partial p}{\partial x_i} + \frac{\partial}{\partial x_j}\Big[\mu\Big(\frac{\partial u_i}{\partial x_j} + \frac{\partial u_j}{\partial x_i}\Big)\Big] + \rho g_i\,. \tag{1.23}$$

The fluid density ρ is replaced by a constant density ρ_0 except in the body force term representing the buoyancy force. The buoyancy term can be rewritten as

$$\rho g_i = (\rho_0 + \Delta\rho) g_i \,, \tag{1.24}$$

where $\Delta\rho = \rho - \rho_0$. The buoyancy term $\Delta\rho g_i$ can be further rewritten as $\Delta\rho g_i = (\rho - \rho_0) g_i = -\rho_0 (T - T_0)\beta g_i$ where β is the coefficient of thermal expansion. This yields

$$\rho_0 \frac{Du_i}{Dt} = -\frac{\partial p}{\partial x_i} + \frac{\partial}{\partial x_j}\Big[\mu\Big(\frac{\partial u_i}{\partial x_j} + \frac{\partial u_j}{\partial x_i}\Big)\Big] + \rho_0 g_i - \rho_0 (T - T_0)\beta g_i \,, \tag{1.25}$$

which is often written as

$$\rho_0 \frac{Du_i}{Dt} = -\frac{\partial p'}{\partial x_i} + \frac{\partial}{\partial x_j}\Big[\mu\Big(\frac{\partial u_i}{\partial x_j} + \frac{\partial u_j}{\partial x_i}\Big)\Big] - \rho_0 (T - T_0)\beta g_i \,, \tag{1.26}$$

where $p' = p - \rho g h$ with h representing the elevation.

In the energy conservation equation, the density ρ and the heat capacity c are assumed constant and the dissipation function is neglected. Under the Oberbeck-Boussinesq assumption, the conservation equations are the following

$$\frac{\partial u_i}{\partial x_i} = 0 \,, \tag{1.27}$$

$$\frac{Du_i}{Dt} = -\frac{1}{\rho}\frac{\partial p}{\partial x_i} + \frac{\partial}{\partial x_j}\Big[\nu\Big(\frac{\partial u_i}{\partial x_j} + \frac{\partial u_j}{\partial x_i}\Big)\Big] - g_i \beta T \,, \tag{1.28}$$

$$\frac{DT}{Dt} = \frac{\partial}{\partial x_i}\Big(\alpha \frac{\partial T}{\partial x_i}\Big) + \frac{Q}{\rho c} \,, \tag{1.29}$$

where ρ and c are constant.

1.2. Statistical description of turbulent flows

In a turbulent flow, the velocity field $\mathbf{u}(\mathbf{x}, t)$, the pressure field $p(\mathbf{x}, t)$ and the temperature field $T(\mathbf{x}, t)$ are random variables. Consider a fluid flow experiment that can be repeated many times under a specific set of conditions and consider an event A. If the event A inevitably occurs, then A is certain; if the event cannot occur, then it is impossible. If A may occur, or it may but need not occur, the event is random. The fact that $\mathbf{u}(\mathbf{x}, t)$, $p(\mathbf{x}, t)$ and $T(\mathbf{x}, t)$ are random variables means that they do not

have a unique value every time the experiment is repeated under the same set of conditions [29].

The random nature of turbulence arises a consistency issue with the deterministic nature of the Navier-Stokes and energy equations. Even though the conservation equations of mass, momentum and energy are deterministic, the solutions are random because in any turbulent flow there are perturbations in initial conditions, boundary conditions and material properties and at the high Reynolds numbers of turbulent flows, the evolution of the flow field is extremely sensitive to small changes in initial conditions, boundary conditions, and material properties [29].

In this section, following the discussion proposed by Pope [29], we introduce various statistical quantities to describe turbulent flows, such as means, probability density functions, and two-point correlations. For all these quantities, it is possible to derive evolution equations starting from the Navier-Stokes and energy equations. In particular, we derive the equations that govern the mean velocity $\langle \mathbf{u}(\mathbf{x}, t) \rangle$, pressure $\langle p(\mathbf{x}, t) \rangle$ and temperature $\langle T(\mathbf{x}, t) \rangle$ fields.

Random variables. Let u be a particular component of the velocity at a specified position $\mathbf{x}$ and time t. The component u is a random variable. We introduce an independent variable v defined as the sample-space variable corresponding to u. Different events such as $B = \{u < v_b\}$ or $C = \{v_a < u < v_b\}$ correspond to different regions of the sample space.

The probability of the event B is written as $p = P(B) = P\{u < v_b\}$. For an impossible event $p = 0$, while for a certain event $p = 1$. The probability of any event can be determined from the cumulative distribution function defined by $\mathcal{F}(v) = P\{u < v\}$. According to this definition, we can write $P(B) = P\{u < v_b\} = \mathcal{F}(v_b)$ and $P(C) = P\{v_a < u < v_b\} = P\{u < v_b\} - P\{u < v_a\} = \mathcal{F}(v_b) - \mathcal{F}(v_a)$. The main properties of the cumulative distribution function can be consulted in [29].

We can introduce the probability density function $f(v)$, defined as the derivative of the cumulative distribution function

$$f(v) = \frac{d\mathcal{F}(v)}{dv}\,. \tag{1.30}$$

From the properties of the cumulative distribution function, it follows that $f(v) \geq 0$, since $\mathcal{F}(v)$ is a non-decreasing function. For other properties, the reader can consult [29].

The probability density function $f(v)$ or the cumulative distribution function $\mathcal{F}(v)$ fully characterize the random variable u. Two or more random variables that have the same probability density function are said to be identically distributed or statistically identical. Examples of the probability distribution are the uniform distribution, the exponential distribution, the normal or Gaussian distribution, and so on.

The mean of the random variable u is defined as

$$\langle u \rangle = \int_{-\infty}^{\infty} v f(v) dv \,. \tag{1.31}$$

More in general, if $\phi(u)$ is a function of u, the mean of $\phi(u)$ is

$$\langle \phi(u) \rangle = \int_{-\infty}^{\infty} \phi(v) f(v) dv \,. \tag{1.32}$$

The means $\langle u \rangle$ and $\langle \phi(u) \rangle$ are not random variables and $\langle \langle u \rangle \rangle = \langle u \rangle$. The operator $\langle \cdot, \cdot \rangle$ is a linear operator, then if $\phi(u)$ and $\xi(u)$ are functions of u, a and b are constants, we have

$$\langle a\phi(u) + b\xi(u) \rangle = a\langle \phi(u) \rangle + b\langle \xi(u) \rangle \,. \tag{1.33}$$

We now define the fluctuation in u as

$$u' = u - \langle u \rangle \,. \tag{1.34}$$

The variance of u is defined as the mean-square fluctuation

$$\langle u'^2 \rangle = \int_{-\infty}^{\infty} (v - \langle u \rangle)^2 f(v) dv \,, \tag{1.35}$$

while the standard deviation or root-mean-square of u is the square-root of the variance, i.e. $u_{rms} = \langle u'^2 \rangle^{1/2}$.

Random joint variables. Since the velocity field $\mathbf{u}(\mathbf{x}, t)$ is a vector, we need to extend the definitions presented to two or more random variables. We consider the components of velocity (u_1, u_2, u_3) at a specified position $\mathbf{x}$ and time t in a turbulent flow. The sample-space variables corresponding to the random variables $\mathbf{u} = \{u_1, u_2, u_3\}$ are denoted by $\mathbf{v} = \{v_1, v_2, v_3\}$. Considering the two components u_1 and u_2, we can define the cumulative distribution function of the joint random variables (u_1, u_2) as

$$\mathcal{F}_{12}(v_1, v_2) = P\{u_1 < v_1, u_2 < v_2\} \,, \tag{1.36}$$

while the joint probability density function is defined as

$$f_{12}(v_1, v_2) = \frac{\partial^2 \mathcal{F}_{12}(v_1, v_2)}{\partial v_1 \partial v_2} \,. \tag{1.37}$$

If $\phi(u_1, u_2)$ is a function of the random variables, its mean is defined by

$$\langle \phi(u_1, u_2) \rangle = \iint_{-\infty}^{\infty} \phi(v_1, v_2) f_{12}(v_1, v_2) dv_1 dv_2 \,. \tag{1.38}$$

Let $u_1' = u_1 - \langle u_1 \rangle$, $u_2' = u_2 - \langle u_2 \rangle$ be the fluctuations, then the covariance of u_1 and u_2 is

$$\langle u_1' u_2' \rangle = \iint_{-\infty}^{\infty} (v_1 - \langle u_1 \rangle)(v_2 - \langle u_2 \rangle) f_{12}(v_1, v_2) dv_1 dv_2 \,, \tag{1.39}$$

and the correlation coefficient is

$$\rho_{12} = \frac{\langle u_1' u_2' \rangle}{(\langle u_1'^2 \rangle \langle u_2'^2 \rangle)^{1/2}} \,, \tag{1.40}$$

and $-1 \leq \rho_{12} \leq 1$. We have a positive correlation coefficient when positive excursions from the mean for one random variable are preferentially associated with positive excursions for the other random variable. It is negative when positive excursions for one random variable are preferentially associated with negative excursions for the other. If ρ_{12} is zero then the random variables u_1 and u_2 are uncorrelated. If $\rho_{12} = 1$, u_1 and u_2 are perfectly correlated; if $\rho_{12} = -1$, u_1 and u_2 are perfectly negatively correlated.

Random processes. Let $u(t)$ be a time-dependent velocity component at a specified position $\mathbf{x}$. Such a random variable is called random process.

At each time, the random variable $u(t)$ is characterized by its one-time cumulative density function, $\mathcal{F}(v, t) = P\{u(t) < v\}$, or by its one-time probability density function $f(v, t) = \partial \mathcal{F}(v, t)/\partial v$. However, these quantities do not contain information about $u(t)$ at two or more times, then we introduce the N-time joint cumulative density function of the random process $u(t)$ defines as

$$\mathcal{F}_N(v_1, t_1; \ldots; v_N, t_N) = P\{u(t_1) < v_1, \ldots, u(t_N) < v_N\} \,, \tag{1.41}$$

where $\{t_1, \ldots, t_N\}$ are specified time points. To completely characterize the random process, it is necessary to know the joint cumulative density function for all instants of time, which is in general impossible. If the process

is statistically stationary, we have considerable simplifications. A process is statistically stationary if, for all positive intervals Δt and all choices of $\{t_1, \ldots, t_N\}$, we have

$$f(v_1, t_1 + \Delta t; \ldots; v_N, t_N + \Delta t) = f(v_1, t_1 \ldots; v_N, t_N)\,. \tag{1.42}$$

A turbulent flow, after an initial transient period, can reach a statistically stationary state in which the statistics, for example the mean of the variance, are independent of time, even though the flow variables vary with time. For a statistically stationary process, the simplest multi-time statistic that we introduce is the autocovariance

$$R(s) = \langle u'(t)u'(t+s)\rangle\,, \tag{1.43}$$

or the autocorrelation function

$$\rho(s) = \frac{\langle u'(t)u'(t+s)\rangle}{\langle u'(t)^2\rangle}\,, \tag{1.44}$$

which is the correlation coefficient between the process at times t and $t+s$, then we have $-1 \leq \rho(s) \leq 1$ and $\rho(0) = 1$.

Random fields. Now we are ready to treat the velocity field $\mathbf{u}(\mathbf{x}, t)$ which is a time-dependent random vector field. We need to extend the tools presented so far. We can have one-point or N-point statistics. The one-point one-time joint cumulative distributed function is

$$\mathcal{F}(\mathbf{v}, \mathbf{x}, t) = P\{u_i(\mathbf{x}, t) < v_i, i = 1, 2, 3\}\,, \tag{1.45}$$

and then the one-point one-time joint probability density function

$$f(\mathbf{v}; \mathbf{x}, t) = \frac{\partial^3 \mathcal{F}(\mathbf{v}, \mathbf{x}, t)}{\partial v_1 \partial v_2 \partial v_3}\,. \tag{1.46}$$

At each point $\mathbf{x}$ and time t this function fully characterizes the random velocity vector but it does not contain any information at two or more times or positions. The mean velocity field is

$$\langle \mathbf{u}(\mathbf{x}, t)\rangle = \iiint_{-\infty}^{\infty} \mathbf{v} f(\mathbf{v}; \mathbf{x}, t) d\mathbf{v}\,, \tag{1.47}$$

and the one-point one-time covariance of the velocity is $\langle u_i'(\mathbf{x}, t)u_j'(\mathbf{x}, t)\rangle$. These covariances, as we will see in the next section, are called Reynolds stresses and are written $\langle u_i' u_j'\rangle$.

The N-point N-time joint probability density function can be defined as an extension of (1.41). Considering a specific set of positions and times $\{\mathbf{x}^{(n)}, t^{(n)}\}$ with $n = 1, \ldots, N$, we can define the joint probability density function at these N space-time points as

$$f_N(\mathbf{v}^{(1)}, \mathbf{x}^{(1)}, t^{(1)}; \ldots; \mathbf{v}^{(N)}, \mathbf{x}^{(N)}, t^{(N)}) \,. \tag{1.48}$$

The determination of this N-point probability density function for all space-time points is impossible, thus a random velocity field cannot be fully characterized. However, there are some simplifications if the field is statistically stationary, homogeneous, or isotropic.

The random field $\mathbf{u}(\mathbf{x}, t)$ is statistically stationary if all statistics are invariant under a shift in time, which means that f_N in (1.48) is unchanged if $(\mathbf{x}^{(n)}, t^{(n)})$ is replaced by $(\mathbf{x}^{(n)}, t^{(n)} + \Delta t)$ for all N point, where Δt is the time shift. Similarly, the field $\mathbf{u}(\mathbf{x}, t)$ is statistically homogeneous if all statistics are invariant under a shift in position, then f_N in (1.48) is unchanged if $(\mathbf{x}^{(n)}, t^{(n)})$ is replaced by $(\mathbf{x}^{(n)} + \mathbf{X}^{(n)}, t^{(n)})$ for all N point, where $\mathbf{X}^{(n)}$ is the shift in position. We have homogeneous turbulence when the fluctuating velocity $\mathbf{u}'(\mathbf{x}, t)$ is statistically homogeneous. Moreover, turbulent flows can be statistically two-dimensional or one dimensional when the statistics are independent of one or two coordinates respectively, such as in a channel flow. The random field $\mathbf{u}(\mathbf{x}, t)$ is statistically isotropic if it is statistically homogeneous and statistically invariant under rotations and reflections of coordinate system, which means that f_N in (1.48) is unchanged if $\mathbf{u}(\mathbf{x}^{(n)}, t^{(n)})$ is replaced by $\overline{\mathbf{u}}(\overline{\mathbf{x}}^{(n)}, t^{(n)})$ for all N point, where $\overline{\mathbf{x}}$ and $\overline{\mathbf{u}}$ denote the position and random velocity field in any coordinate system obtained by rotation and reflections of the coordinate axes.

The simplest statistic containing some information on the spatial structure of the random field is the two-point one-time autocovariance

$$R_{ij}(\mathbf{r}, \mathbf{x}, t) = \langle \mathbf{u}'_i(\mathbf{x}, t) \mathbf{u}'_j(\mathbf{x} + \mathbf{r}, t) \rangle \,, \tag{1.49}$$

which is often referred to as two-point correlation.

Reynolds averaging. We have given a definition for the mean of a random field $\mathbf{u}(\mathbf{x}, t)$ in (1.47) using the probability density function $f(\mathbf{v}; \mathbf{x}, t)$. The probability density function cannot be determined, then we present averaging operations used to estimate $\langle \mathbf{u}(\mathbf{x}, t) \rangle$, introduced by Reynolds. The three forms of Reynolds averaging most used in turbulent flow experiments

and simulations are the time average, spatial average and the ensemble average. For statistically stationary flows the time average over a time interval Δt is the most suitable and it is defined as

$$\langle \mathbf{u}(\mathbf{x},t)\rangle = \lim_{T\to\infty} \frac{1}{T}\int_t^{t+T} \mathbf{u}(\mathbf{x},t)dt\,. \tag{1.50}$$

For homogeneous turbulence the spacial average is the most appropriate. We average over all spatial coordinates by doing the following volume integral

$$\langle \mathbf{u}(\mathbf{x},t)\rangle = \lim_{V\to\infty} \frac{1}{V}\iiint \mathbf{u}(\mathbf{x},t)dV\,. \tag{1.51}$$

For flows that can be repeated or replicated N times, the ensemble average is defined by

$$\langle \mathbf{u}(\mathbf{x},t)\rangle = \lim_{N\to\infty} \frac{1}{N}\sum_{n=1}^{N} \mathbf{u}^{(n)}(\mathbf{x},t)\,. \tag{1.52}$$

For turbulence that is both stationary and homogeneous, we may assume that these three averages are all equal.

1.3. The RANS equations

In the previous section, various statistical quantities have been introduced to describe turbulent flows, i.e. mean, covariance, probability density functions, two-point correlations, etc. It is possible to derive equations for the evolution of all these quantities starting from the Navier-Stokes and energy equations. The Reynolds decomposition involves the decomposition of the dynamic and thermal fields into their mean and their fluctuation, i.e.

$$\mathbf{u}(\mathbf{x},t) = \langle \mathbf{u}(\mathbf{x},t)\rangle + \mathbf{u}'(\mathbf{x},t)\,, \tag{1.53}$$

$$p(\mathbf{x},t) = \langle p(\mathbf{x},t)\rangle + p'(\mathbf{x},t)\,, \tag{1.54}$$

$$T(\mathbf{x},t) = \langle T(\mathbf{x},t)\rangle + T'(\mathbf{x},t)\,, \tag{1.55}$$

where the mean operator $\langle\cdot,\cdot\rangle$ is the time average defined in (1.50).

1.3.1. The Reynolds-Averaged Navier-Stokes equation

Applying the Reynolds decomposition and taking the mean of the continuity and Navier-Stokes equations (1.27)-(1.28), we obtain

$$\frac{\partial\langle u_i\rangle}{\partial x_i} = 0\,, \tag{1.56}$$

$$\frac{D\langle u_i\rangle}{Dt} = -\frac{1}{\rho}\frac{\partial\langle p\rangle}{\partial x_i} + \frac{\partial}{\partial x_j}\Big[\nu\Big(\frac{\partial\langle u_i\rangle}{\partial x_j} + \frac{\partial\langle u_j\rangle}{\partial x_i}\Big) - \langle u_i' u_j'\rangle\Big] + \\ -g_i\beta\langle T\rangle\,. \tag{1.57}$$

The Reynolds-averaged conservation of mass (1.56) is identical to instantaneous continuity equation (1.27) with the mean velocity $\langle\mathbf{u}\rangle$ replacing the instantaneous velocity $\mathbf{u}$. We can show that also the fluctuation $\mathbf{u}'$ has zero divergence, subtracting (1.56) from (1.27). Aside from replacement of instantaneous variables by mean values, the only difference between the Reynolds-Averaged Navier-Stokes (1.57) and instantaneous momentum equation (1.28) is the appearance of the velocity covariance $\langle u_i' u_j'\rangle$, which is called Reynolds stress tensor.

To understand why we refer to this term as stress, we rewrite the Reynolds-Averaged Navier-Stokes equation (1.57) as

$$\rho\frac{D\langle u_i\rangle}{Dt} = \frac{\partial}{\partial x_j}\Big[\mu\Big(\frac{\partial\langle u_i\rangle}{\partial x_j} + \frac{\partial\langle u_j\rangle}{\partial x_i}\Big) - \langle p\rangle\delta_{ij} - \rho\langle u_i' u_j'\rangle\Big] - \rho g_i\beta\langle T\rangle\,, \tag{1.58}$$

and the term in square brackets represents the sum of three stresses: the viscous stress, the isotropic stress $\langle p\rangle\delta_{ij}$ from the mean pressure field and the apparent stress arising from the fluctuating velocity field, $\rho\langle u_i' u_j'\rangle$. It is as if the turbulent fluctuations have given rise to additional stresses. We can express the rate of gain of momentum within a fixed control volume V due to flow through the surface S as

$$\dot{M}_i = \oint_S \rho u_i(-u_j n_j)dS\,, \tag{1.59}$$

where the i-component of momentum per unit volume is ρu_i and the volume flow rate per unit area into V through S is $-u_j n_j$. The mean of the i-component of this equation is

$$\langle\dot{M}_i\rangle = \oint_S -\rho(\langle u_i\rangle\langle u_j\rangle + \langle u_i' u_j'\rangle)n_j dS\,, \tag{1.60}$$

and applying the divergence theorem

$$\langle\dot{M}_i\rangle = \int_V -\rho\frac{\partial}{\partial x_j}(\langle u_i\rangle\langle u_j\rangle + \langle u_i' u_j'\rangle)dV\,. \tag{1.61}$$

Thus, for the control volume V, the Reynolds stress that appears in the Reynolds-Averaged Navier-Stokes equation (1.57) and acts like stresses, actually represents the mean momentum flux due to the fluctuating velocity

on the boundary S, $\rho\langle u_i' u_j'\rangle n_j$. Then $\langle u_i' u_j'\rangle$ is not a real stress in the conventional sense of the word but it represents the mean momentum fluxes induced by the turbulence. However, as far as we consider the mean flow, we can capture the effects of these fluxes by pretending that $\langle u_i' u_j'\rangle$ is a stress.

The Reynolds stress tensor is symmetric, $\langle u_i' u_j'\rangle = \langle u_j' u_i'\rangle$, and thus has six independent components. The diagonal components, $\langle u'^2\rangle$, $\langle v'^2\rangle$ and $\langle w'^2\rangle$, are called normal stresses, while the off-diagonal components, $\langle u'v'\rangle$, $\langle u'w'\rangle$ and $\langle v'w'\rangle$, are named shear stresses. The turbulent kinetic energy $k(\mathbf{x}, t)$ is defined to be half the trace of the Reynolds stress tensor

$$k = \frac{1}{2}\langle u_i' u_i'\rangle \,. \tag{1.62}$$

We can distinguish isotropic and anisotropic stresses, in particular

$$\langle u_i' u_j'\rangle = \frac{2}{3}k\delta_{ij} + a_{ij} \,, \tag{1.63}$$

where $2/3k\delta_{ij}$ is the isotropic stress and the deviatoric anisotropic part is a_{ij}. Equation (1.63) is often reformulated using the normalized anisotropic tensor b_{ij}, defined as $b_{ij} = (\langle u_i' u_j'\rangle - 2/3k\delta_{ij})/(2k)$, into the following expression

$$\langle u_i' u_j'\rangle = \frac{2}{3}k\delta_{ij} + 2kb_{ij} \,. \tag{1.64}$$

It is only the anisotropic tensor a_{ij} that is effective in transporting momentum since we have

$$\begin{aligned}\frac{D\langle u_i\rangle}{Dt} = &-\frac{1}{\rho}\frac{\partial}{\partial x_i}\Big(\langle p\rangle + \frac{2}{3}\rho k\Big) + \frac{\partial}{\partial x_j}\Big[\nu\Big(\frac{\partial\langle u_i\rangle}{\partial x_j} + \frac{\partial\langle u_j\rangle}{\partial x_i}\Big) - a_{ij}\Big] + \\ &- g_i\beta\langle T\rangle \,,\end{aligned} \tag{1.65}$$

and then the isotropic component $2/3k$ can be absorbed in a modified mean pressure.

1.3.2. Reynolds-Averaged energy equation

The conservation equation for $\langle T\rangle$ is obtained by applying the same procedure used to obtain the Reynolds-Averaged Navier-Stokes equation. Using the Reynolds decomposition reported in Equation (1.55), the time-averaged energy equation (1.29) is

$$\frac{D\langle T\rangle}{Dt} = \frac{\partial}{\partial x_i}\Big(\alpha\frac{\partial\langle T\rangle}{\partial x_i} - \langle u_i' T'\rangle\Big) + \frac{Q}{\rho c} \,. \tag{1.66}$$

where the velocity-temperature covariance $\langle u_i' T' \rangle$ is a vector, which is called turbulent heat flux or scalar flux. It represents the flux of the temperature due to the fluctuating velocity field. In this equation, the turbulent heat flux plays an analogous role to that of the Reynolds stresses in the mean momentum equation.

1.3.3. The closure problem

Hereinafter we refer to (1.56), (1.57) and (1.66) as Reynolds-Averaged Navier-Stokes and energy system, or more concisely RANS system. This system is not closed, since the averaging operation has introduced as unknowns the six independent components of the Reynolds stresses and the three components of the turbulent heat flux. If we take a non-statistical approach, we have governing equations which are deterministic, but the solutions are random fields. On the other hand, if we take a statistical approach, then the quantities we are interested in are non-random and perfectly reproducible in any experiment, but we cannot find a closed set of equations that describes them. In the attempt to close (1.57) and (1.66), we derive the exact transport equations for velocity covariance $\langle u_i' u_j' \rangle$ and velocity-temperature covariance $\langle u_i' T' \rangle$, by following [30].

The Reynolds-Stress transport equation

To predict the behavior of the mean flow through the Reynolds-Averaged Navier-Stokes equation (1.57), we need to know the velocity covariance or Reynolds stresses. Following [31], we derive the equation for $\langle u_i' u_j' \rangle$ using the Reynolds-Averaged Navier-Stokes equation (1.57) and the momentum equation (1.28) for the instantaneous velocity $\mathbf{u}$. Subtracting (1.57) from (1.28), we obtain a transport equation for the fluctuating velocity field

$$\begin{aligned} \frac{\partial u_i'}{\partial t} + \langle u_j \rangle \frac{\partial u_i'}{\partial x_j} + u_j' \frac{\partial \langle u_i \rangle}{\partial x_j} + u_j' \frac{\partial u_i'}{\partial x_j} = -\frac{1}{\rho} \frac{\partial p'}{\partial x_i} + \\ + \frac{\partial}{\partial x_j} \left[\nu \left(\frac{\partial u_i'}{\partial x_j} + \frac{\partial u_j'}{\partial x_i} \right) + \langle u_i' u_j' \rangle \right] - g_i \beta T' \,. \end{aligned} \tag{1.67}$$

The transport equation for $\langle u_i' u_j' \rangle$ can be obtained by multiplying the i-th equation (1.67) by u_j' and the j-th equation by u_i' and time-averaging the

sum of the two resulting equations

$$\begin{aligned}\frac{\partial\langle u_i'u_j'\rangle}{\partial t}+\langle u_k\rangle\frac{\partial\langle u_i'u_j'\rangle}{\partial x_k}+\langle u_i'u_k'\rangle\frac{\partial\langle u_j\rangle}{\partial x_k}+\langle u_j'u_k'\rangle\frac{\partial\langle u_i\rangle}{\partial x_k}+\\ +\frac{\partial}{\partial x_k}\langle u_i'u_j'u_k'\rangle=-\frac{1}{\rho}\Big(\langle u_i'\frac{\partial p'}{\partial x_j}\rangle+\langle u_j'\frac{\partial p'}{\partial x_i}\rangle\Big)+\\ +\nu\Big(\langle u_j'\frac{\partial^2 u_i'}{\partial x_k^2}\rangle+\langle u_i'\frac{\partial^2 u_j'}{\partial x_k^2}\rangle\Big)+\langle u_j'\frac{\partial u_k'u_i'}{\partial x_k}\rangle+\langle u_i'\frac{\partial u_k'u_j'}{\partial x_k}\rangle\\ -\beta(g_j\langle u_i'T'\rangle+g_i\langle u_j'T'\rangle)\,.\end{aligned}\tag{1.68}$$

The first term on the right-hand-side represents the pressure gradient interaction with the turbulent fluctuation. This term can be rewritten

$$\begin{aligned}-\frac{1}{\rho}\Big(\langle u_i'\frac{\partial p'}{\partial x_j}\rangle+\langle u_j'\frac{\partial p'}{\partial x_i}\rangle\Big)=-\frac{1}{\rho}\Big(\frac{\partial\langle u_j'p'\rangle}{\partial x_i}-\langle p'\frac{\partial u_j'}{\partial x_i}\rangle\Big)+\\ -\frac{1}{\rho}\Big(\frac{\partial\langle u_i'p'\rangle}{\partial x_j}-\langle p'\frac{\partial u_i'}{\partial x_j}\rangle\Big)=\frac{1}{\rho}\Big(\langle p'\frac{\partial u_j'}{\partial x_i}\rangle+\langle p'\frac{\partial u_i'}{\partial x_j}\rangle\Big)+\\ -\frac{1}{\rho}\frac{\partial}{\partial x_k}\Big(\langle p'\delta_{ki}u_j'\rangle+\langle p'\delta_{kj}u_i'\rangle\Big)\,.\end{aligned}\tag{1.69}$$

Similarly, the second term on the right-hand-side represents the viscous dissipation of the turbulent fluctuations and can be rewritten as follows

$$\nu\Big(\langle u_j'\frac{\partial^2 u_i'}{\partial x_k^2}\rangle+\langle u_i'\frac{\partial^2 u_j'}{\partial x_k^2}\rangle\Big)=\nu\Big(\frac{\partial^2\langle u_i'u_j'\rangle}{\partial x_k^2}-2\langle\frac{\partial u_i'}{\partial x_k}\frac{\partial u_j'}{\partial x_k}\rangle\Big)\,.\tag{1.70}$$

With these modifications, the Reynolds-stress equation can be written

$$\begin{aligned}\frac{D\langle u_i'u_j'\rangle}{Dt}=-\langle u_i'u_k'\rangle\frac{\partial\langle u_j\rangle}{\partial x_k}-\langle u_j'u_k'\rangle\frac{\partial\langle u_i\rangle}{\partial x_k}-2\nu\langle\frac{\partial u_i'}{\partial x_k}\frac{\partial u_j'}{\partial x_k}\rangle+\\ +\frac{1}{\rho}\Big(\langle p'\frac{\partial u_j'}{\partial x_i}\rangle+\langle p'\frac{\partial u_i'}{\partial x_j}\rangle\Big)+\frac{\partial}{\partial x_k}\Big(\nu\frac{\partial\langle u_i'u_j'\rangle}{\partial x_k}-\langle u_i'u_j'u_k'\rangle+\\ -\langle\frac{p'}{\rho}(\delta_{ki}u_j'+\delta_{kj}u_i')\rangle\Big)-\beta(g_j\langle u_i'T'\rangle+g_i\langle u_j'T'\rangle)\,,\end{aligned}\tag{1.71}$$

or, more concisely, we can formulate the Reynolds-stress equation in its most recognizable form

$$\frac{D\langle u_i'u_j'\rangle}{Dt}=\mathcal{P}_{ij}-\varepsilon_{ij}+\Pi_{ij}+\mathcal{D}_{ij}+\mathcal{G}_{ij}\,,\tag{1.72}$$

where $\mathcal{P}_{ij}$ is the production tensor, ε_{ij} is the dissipation tensor, Π_{ij} is the pressure-strain correlation, $\mathcal{D}_{ij}$ is the diffusion term and $\mathcal{G}_{ij}$ is the buoyant source term

$$\mathcal{P}_{ij} = -\langle u_i' u_k' \rangle \frac{\partial \langle u_j \rangle}{\partial x_k} - \langle u_j' u_k' \rangle \frac{\partial \langle u_i \rangle}{\partial x_k}\,, \tag{1.73}$$

$$\varepsilon_{ij} = 2\nu \langle \frac{\partial u_i'}{\partial x_k} \frac{\partial u_j'}{\partial x_k} \rangle\,, \tag{1.74}$$

$$\Pi_{ij} = \frac{1}{\rho}\Big(\langle p' \frac{\partial u_j'}{\partial x_i} \rangle + \langle p' \frac{\partial u_i'}{\partial x_j} \rangle \Big)\,, \tag{1.75}$$

$$\mathcal{D}_{ij} = \frac{\partial}{\partial x_k}\Big(\nu \frac{\partial \langle u_i' u_j' \rangle}{\partial x_k} - \langle u_i' u_j' u_k' \rangle - \langle \frac{p'}{\rho}(\delta_{ki} u_j' + \delta_{kj} u_i') \rangle \Big)\,, \tag{1.76}$$

$$\mathcal{G}_{ij} = -\beta (g_j \langle u_i' T' \rangle + g_i \langle u_j' T' \rangle)\,. \tag{1.77}$$

The production tensor $\mathcal{P}_{ij}$ represents the production of turbulent stresses by the gradient of the mean velocity. This is the mechanism by which energy is transferred from the mean flow to the fluctuating velocity components. The pressure-strain correlation Π_{ij} represents the correlation of pressure and velocity gradient. For an incompressible flow, the pressure fluctuations are directly connected to the velocity fluctuations. Indeed, the fluctuation of the pressure field must respond to changes in the flow instantaneously and globally to enforce incompressibility. The diffusion term $\mathcal{D}_{ij}$ represents the diffusive transport of turbulent stresses away from sources of production, such as channel walls. This diffusion is affected by spatial gradients in turbulence intensity, viscous forces, and pressure fluctuations. Lastly, the buoyant term $\mathcal{G}_{ij}$ is a source depending on the interaction between the gravity vector and turbulent heat flux components. While the production term $\mathcal{P}_{ij}$ is closed and does not require modeling, the other terms, like pressure-strain correlation Π_{ij} and dissipation tensor ε_{ij}, are unclosed and require closure models.

The turbulent kinetic energy equation

We can derive a transport equation for the turbulent kinetic energy (1.62) by taking the half-trace of the Reynolds stress equation (1.71) [31]

$$\begin{aligned} \frac{Dk}{Dt} = &-\langle u_i' u_k' \rangle \frac{\partial \langle u_i \rangle}{\partial x_k} - \nu \langle \frac{\partial u_i'}{\partial x_k} \frac{\partial u_i'}{\partial x_k} \rangle + \frac{\partial}{\partial x_k}\Big(\nu \frac{\partial k}{\partial x_k} - \frac{1}{2}\langle u_i' u_i' u_k' \rangle + \\ &- \frac{\langle p' u_k' \rangle}{\rho} \Big) - \beta g_i \langle u_i' T' \rangle\,, \end{aligned} \tag{1.78}$$

Notice that the pressure-strain correlation term has vanished upon contraction since the flow is assumed to be incompressible. We can write the equation in a more compact form

$$\frac{Dk}{Dt} = \mathcal{P} - \varepsilon + \mathcal{D} + \mathcal{G}\,, \tag{1.79}$$

where

$$\mathcal{P} = -\langle u_i' u_k' \rangle \frac{\partial \langle u_i \rangle}{\partial x_k}\,, \tag{1.80}$$

$$\varepsilon = \nu \langle \frac{\partial u_i'}{\partial x_k} \frac{\partial u_i'}{\partial x_k} \rangle\,, \tag{1.81}$$

$$\mathcal{D} = \frac{\partial}{\partial x_k}\Big(\nu \frac{\partial k}{\partial x_k} - \frac{1}{2}\langle u_i' u_i' u_k' \rangle - \frac{\langle p' u_k' \rangle}{\rho}\Big)\,, \tag{1.82}$$

$$\mathcal{G} = -\beta g_i \langle u_i' T' \rangle\,. \tag{1.83}$$

The first term on the right-hand side of (1.79) is known as production $\mathcal{P}$ and represents the rate at which kinetic energy is transferred from the mean flow to the turbulence. The second term is called dissipation ε and it is the rate at which turbulent kinetic energy is converted into thermal internal energy. We have then the diffusive contribution $\mathcal{D}$ that consists of three terms. The term involving $\nu \partial k / \partial x_k$ is the molecular diffusion and represents the diffusion of turbulent energy caused by the molecular transport process. We refer to the triple velocity correlation term $\langle u_i' u_i' u_k' \rangle$ as turbulent transport and regard it as the rate at which turbulent energy is transported through the fluid by turbulent fluctuations. We have then the pressure diffusion, another form of turbulent transport resulting from the correlation of pressure and velocity fluctuations $\langle p' u_k' \rangle$. Lastly, $\mathcal{G}$ is the source term due to the buoyancy. Thus, the turbulent kinetic energy evolves as a result of shear production, diffusion and viscous dissipation. The unsteady term, convection and molecular diffusion are in closed form while production, dissipation, turbulent transport and pressure diffusion involve unknown correlations. Thus, the turbulent kinetic energy transport equation is not closed.

The dissipation rate equation

To close the turbulent kinetic energy transport equation, we can try to derive transport equations for the unknown correlations appearing in its

expression. An attempt can be done to construct the transport equation for the scalar dissipation rate ε. This is accomplished by differentiating the transport equation for velocity fluctuation (1.67) with respect to x_k, multiplying by $2\nu\partial u_i'/\partial x_k$ and time-averaging. The equation obtained in [32] is the following

$$\begin{aligned}\frac{D\varepsilon}{Dt} = &-2\nu\Big(\langle\frac{\partial u_i'}{\partial x_k}\frac{\partial u_j'}{\partial x_k}\rangle + \langle\frac{\partial u_k'}{\partial x_j}\frac{\partial u_k'}{\partial x_i}\rangle\Big)\frac{\partial\langle u_i\rangle}{\partial x_j} - 2\nu g_i\beta\langle\frac{\partial T'}{\partial x_k}\frac{\partial u_i'}{\partial x_k}\rangle + \\ &- 2\nu\Big(\langle\frac{\partial u_i'}{\partial x_k}\frac{\partial u_j'}{\partial x_k}\frac{\partial u_i'}{\partial x_j}\rangle + \langle u_j'\frac{\partial u_i'}{\partial x_k}\rangle\frac{\partial^2 u_i}{\partial x_j\partial x_k} + \nu\langle\frac{\partial^2 u_i'}{\partial x_j\partial x_k}^2\rangle\Big) + \\ &+ \frac{\partial}{\partial x_j}\Big[\nu\frac{\partial\varepsilon}{\partial x_j} - \nu\langle u_j'\frac{\partial u_i'}{\partial x_k}\frac{\partial u_i'}{\partial x_k}\rangle - \frac{2\nu}{\rho}\langle\frac{\partial u_j'}{\partial x_k}\frac{\partial p'}{\partial x_k}\rangle\Big].\end{aligned} \tag{1.84}$$

This equation is more complicated than the turbulent kinetic energy equation and involves several new double and triple correlations of fluctuating velocity, velocity gradient and pressure. We can rewrite (1.84) in the compact form

$$\frac{D\varepsilon}{Dt} = \mathcal{P}_\varepsilon + \mathcal{G}_\varepsilon - \varepsilon_\varepsilon + \mathcal{D}_\varepsilon\,, \tag{1.85}$$

where

$$\mathcal{P}_\varepsilon = -2\nu\Big(\langle\frac{\partial u_i'}{\partial x_k}\frac{\partial u_j'}{\partial x_k}\rangle + \langle\frac{\partial u_k'}{\partial x_j}\frac{\partial u_k'}{\partial x_i}\rangle\Big)\frac{\partial\langle u_i\rangle}{\partial x_j}\,, \tag{1.86}$$

$$\mathcal{G}_\varepsilon = -2\nu g_i\beta\langle\frac{\partial T'}{\partial x_k}\frac{\partial u_i'}{\partial x_k}\rangle\,, \tag{1.87}$$

$$\varepsilon_\varepsilon = 2\nu\Big(\langle\frac{\partial u_i'}{\partial x_k}\frac{\partial u_j'}{\partial x_k}\frac{\partial u_i'}{\partial x_j}\rangle + \langle u_j'\frac{\partial u_i'}{\partial x_k}\rangle\frac{\partial^2 u_i}{\partial x_j\partial x_k} + \nu\langle\frac{\partial^2 u_i'}{\partial x_j\partial x_k}^2\rangle\Big), \tag{1.88}$$

$$\mathcal{D}_\varepsilon = \frac{\partial}{\partial x_j}\Big[\nu\frac{\partial\varepsilon}{\partial x_j} - \nu\langle u_j'\frac{\partial u_i'}{\partial x_k}\frac{\partial u_i'}{\partial x_k}\rangle - \frac{2\nu}{\rho}\langle\frac{\partial u_j'}{\partial x_k}\frac{\partial p'}{\partial x_k}\rangle\Big]. \tag{1.89}$$

The terms on the first line of the right-hand side of equation (1.84) are the production of dissipation by shear $\mathcal{P}_\varepsilon$ and buoyancy $\mathcal{G}_\varepsilon$, respectively. The terms on the second line represent the dissipation of dissipation rate, ε_ε, and the terms on the third line are the diffusion term $\mathcal{D}_\varepsilon$, given by the sum of the molecular diffusion of dissipation and the turbulent transport of dissipation. Almost all correlations appearing on the right-hand side are additional unknowns, then also this equation is not closed.

The turbulent heat flux transport equation

To close the Reynolds-Averaged energy equation, we try to derive a transport equation for the velocity-temperature correlation appearing on the right-hand side of (1.66). To obtain the transport equation for the turbulent heat flux, we follow the procedure indicated in [33]. We multiply the i-th fluctuating velocity component by the equation for the instantaneous temperature (1.29) and add it to the i-th instantaneous Navier-Stokes equation (1.28) multiplied by the fluctuating temperature T' and then by time-averaging the result is

$$\begin{aligned}\frac{D\langle u_i'T'\rangle}{Dt} = &-\Big(\langle u_k'T'\rangle\frac{\partial\langle u_i\rangle}{\partial x_k} + \langle u_k'u_i'\rangle\frac{\partial\langle T\rangle}{\partial x_k}\Big) - \beta g_i\langle T'^2\rangle + \\ &- (\alpha+\nu)\langle\frac{\partial T'}{\partial x_k}\frac{\partial u_i'}{\partial x_k}\rangle - \frac{\partial}{\partial x_k}\Big(\langle u_k'u_i'T'\rangle + \frac{\langle p'T'\rangle}{\rho}\delta_{ik} + \\ &- \alpha\langle u_i'\frac{\partial T'}{\partial x_k}\rangle - \nu\langle T'\frac{\partial u_i'}{\partial x_k}\rangle\Big) + \langle\frac{p'}{\rho}\frac{\partial T'}{\partial x_i}\rangle\,,\end{aligned} \tag{1.90}$$

we can formulate this equation in the more compact form

$$\frac{D\langle u_i'T'\rangle}{Dt} = \mathcal{P}_{i\theta} + \mathcal{G}_{i\theta} - \varepsilon_{i\theta} + \mathcal{D}_{i\theta} + \Pi_{i\theta}\,, \tag{1.91}$$

where $\mathcal{P}_{i\theta}$ is the rate of production of $\langle u_i'T'\rangle$, $\mathcal{G}_{i\theta}$ is a production term due to buoyancy, $\varepsilon_{i\theta}$ represents the rate of dissipation by molecular processes, $\mathcal{D}_{ij}$ represents the turbulent and molecular transport term and finally $\Pi_{i\theta}$ is the fluctuating pressure-temperature gradient correlation

$$\mathcal{P}_{i\theta} = -\langle u_k'T'\rangle\frac{\partial\langle u_i\rangle}{\partial x_k} - \langle u_k'u_i'\rangle\frac{\partial\langle T\rangle}{\partial x_k}\,, \tag{1.92}$$

$$\mathcal{G}_{i\theta} = -\beta g_i\langle T'^2\rangle\,, \tag{1.93}$$

$$\varepsilon_{i\theta} = -(\alpha+\nu)\langle\frac{\partial T'}{\partial x_k}\frac{\partial u_i'}{\partial x_k}\rangle\,, \tag{1.94}$$

$$\mathcal{D}_{i\theta} = -\frac{\partial}{\partial x_k}\Big(\langle u_k'u_i'T'\rangle + \frac{\langle p'T'\rangle}{\rho} - \alpha\langle u_i'\frac{\partial T'}{\partial x_k}\rangle - \nu\langle T'\frac{\partial u_i'}{\partial x_k}\rangle\Big)\,, \tag{1.95}$$

$$\Pi_{i\theta} = -\langle\frac{p'}{\rho}\frac{\partial T'}{\partial x_i}\rangle\,. \tag{1.96}$$

The production term $\mathcal{P}_{i\theta}$ expresses the rate of creation of $\langle u_i'T'\rangle$ due to the combined actions of mean velocity and mean temperature gradients. The former tends to increase the velocity fluctuations, the latter the magnitude of the temperature fluctuations. The dissipative correlation $\varepsilon_{i\theta}$ is zero

in isotropic turbulence and will be negligible also in non-isotropic turbulence, provided that the turbulence Reynolds number is high. The pressure-temperature gradient correlation $\Pi_{i\theta}$ is the counterpart of the pressure-strain correlation in the stress equations. With the direct dissipation negligible, this provides the mechanism which limits the growth of the fluxes [34]. The equation (1.90) cannot be solved in the presented form, then modeling is required.

The temperature variance transport equation

The transport equation for the temperature variance $\langle T'^2 \rangle$ is obtained by multiplying the equation for the instantaneous temperature (1.29) by T' and averaging [34]. The result may be written as

$$\begin{aligned} \frac{D\frac{1}{2}\langle T'^2\rangle}{Dt} = &-\langle u_j' T'\rangle \frac{\partial \langle T\rangle}{\partial x_j} - \alpha \langle \frac{\partial T'}{\partial x_j}\frac{\partial T'}{\partial x_j}\rangle + \\ &+ \frac{\partial}{\partial x_j}\Big(\alpha \frac{\partial \frac{1}{2}\langle T'^2\rangle}{\partial x_j} - \frac{\langle u_j' T'^2\rangle}{2}\Big)\,. \end{aligned} \tag{1.97}$$

We introduce k_θ defined as the half-temperature variance $\frac{1}{2}\langle T'^2\rangle$ and we formulate (1.97) as

$$\frac{Dk_\theta}{Dt} = \mathcal{P}_\theta - \varepsilon_\theta + \mathcal{D}_\theta\,, \tag{1.98}$$

where $\mathcal{P}_\theta$ is the production rate of temperature fluctuations by the temperature gradient, ε_θ is the dissipation of fluctuations due to molecular diffusion, and $\mathcal{D}_\theta$ represents the diffusive transport produced by molecular and turbulent velocity fluctuations

$$\mathcal{P}_\theta = -\langle u_j' T'\rangle \frac{\partial \langle T\rangle}{\partial x_j}\,, \tag{1.99}$$

$$\varepsilon_\theta = \alpha \langle \frac{\partial T'}{\partial x_j}\frac{\partial T'}{\partial x_j}\rangle\,, \tag{1.100}$$

$$\mathcal{D}_\theta = \frac{\partial}{\partial x_j}\Big(\alpha \frac{\partial \langle k_\theta\rangle}{\partial x_j} - \frac{\langle u_j' T'^2\rangle}{2}\Big)\,. \tag{1.101}$$

As expected, equation (1.97) contains correlations ($\langle u_j' T'^2\rangle$) and dissipation (ε_θ) terms which introduce new unknowns and make the equation undetermined.

The dissipation rate of temperature variance equation

The transport equation for the dissipation rate of fluctuations ε_θ is obtained by taking the derivative of the equation of the instantaneous temperature $\langle T\rangle + T'$ with respect to x_j, multiplying by $2\alpha\partial T'/\partial x_j$ and averaging [34]

$$\begin{aligned}\frac{D\varepsilon_\theta}{Dt} = &-2\alpha\langle\frac{\partial T'}{\partial x_k}\frac{\partial u_j'}{\partial x_k}\rangle\frac{\partial\langle T\rangle}{\partial x_j} - 2\alpha\langle u_j'\frac{\partial T'}{\partial x_k}\rangle\frac{\partial^2\langle T\rangle}{\partial x_j\partial x_k} + \\ &- 2\alpha\langle\frac{\partial T'}{\partial x_k}\frac{\partial T'}{\partial x_j}\rangle\frac{\partial\langle u_j\rangle}{\partial x_k} - 2\alpha\langle\frac{\partial T'}{\partial x_k}\frac{\partial u_j'}{\partial x_k}\frac{\partial T'}{\partial x_j}\rangle + \\ &- 2\alpha^2\langle\Big(\frac{\partial^2 T'}{\partial x_j\partial x_k}\Big)^2\rangle - \frac{\partial}{\partial x_j}\Big(\langle\varepsilon_\theta' u_j'\rangle - \alpha\frac{\partial\varepsilon_\theta}{\partial x_j}\Big)\,.\end{aligned} \tag{1.102}$$

where $\varepsilon_\theta' = \alpha(\partial T'/\partial x_k)(\partial T'/\partial x_k)$ and $\varepsilon_\theta = \langle\varepsilon_\theta'\rangle$. We can rewrite the equation in a more compact form

$$\frac{D\varepsilon_\theta}{Dt} = \mathcal{P}_{1\varepsilon_\theta} + \mathcal{P}_{2\varepsilon_\theta} + \mathcal{P}_{3\varepsilon_\theta} + \mathcal{P}_{\varepsilon_\theta} - \varepsilon_{\varepsilon_\theta} + \mathcal{D}_{\varepsilon_\theta}\,, \tag{1.103}$$

where

$$\mathcal{P}_{1\varepsilon_\theta} = -2\alpha\langle\frac{\partial T'}{\partial x_k}\frac{\partial u_j'}{\partial x_k}\rangle\frac{\partial\langle T\rangle}{\partial x_j}\,, \tag{1.104}$$

$$\mathcal{P}_{2\varepsilon_\theta} = -2\alpha\langle u_j'\frac{\partial T'}{\partial x_k}\rangle\frac{\partial^2\langle T\rangle}{\partial x_j\partial x_k}\,, \tag{1.105}$$

$$\mathcal{P}_{3\varepsilon_\theta} = -2\alpha\langle\frac{\partial T'}{\partial x_k}\frac{\partial T'}{\partial x_j}\rangle\frac{\partial\langle u_j\rangle}{\partial x_k}\,, \tag{1.106}$$

$$\mathcal{P}_{\varepsilon_\theta} = -2\alpha\langle\frac{\partial T'}{\partial x_k}\frac{\partial u_j'}{\partial x_k}\frac{\partial T'}{\partial x_j}\rangle\,, \tag{1.107}$$

$$\varepsilon_{\varepsilon_\theta} = -2\alpha^2\langle\Big(\frac{\partial^2 T'}{\partial x_j\partial x_k}\Big)^2\rangle\,, \tag{1.108}$$

$$\mathcal{D}_{\varepsilon_\theta} = -\frac{\partial}{\partial x_j}\Big(\langle\varepsilon_\theta' u_j'\rangle - \alpha\frac{\partial\varepsilon_\theta}{\partial x_j}\Big)\,. \tag{1.109}$$

The first four terms $\mathcal{P}_{1\varepsilon_\theta}$, $\mathcal{P}_{2\varepsilon_\theta}$, $\mathcal{P}_{3\varepsilon_\theta}$ and $\mathcal{P}_{\varepsilon_\theta}$ in the right-hand side are production terms for ε_θ. The direct mean-field generation terms ($\mathcal{P}_{1\varepsilon_\theta}$, $\mathcal{P}_{2\varepsilon_\theta}$ and $\mathcal{P}_{3\varepsilon_\theta}$) are negligible at high Reynolds number, but they become important in the immediate neighborhood of a wall. Anyway, the production term $\mathcal{P}_{\varepsilon_\theta}$ due to fine scale turbulence interactions is dominant. The term $\varepsilon_{\varepsilon_\theta}$ represents the dissipation contribution due to fine-scale turbulence interactions. The remaining term $\mathcal{D}_{\varepsilon_\theta}$ represents the turbulent and molecular diffusion contributions. All the correlations appearing in equation (1.102) are unknown quantities.

1.4. Wall turbulence

Most turbulent flows are bounded by one or more solid surfaces. The presence of a boundary has a deep influence on turbulent flows. Wall-bounded flows are usually divided into internal flows (pipe, channel, ducts) and external flows (boundary layers). In this dissemination we will treat only internal flows, in particular in this section we analyze the channel and pipe flows, that are of practical importance and played a prominent role in the historical development of the study of turbulent flows. The classical problems of flow in a channel and a pipe are the idealized cases of an infinitely long channel or pipe. This approximation is appropriate if we are not too close to the inlet of the channel/pipe so that the flow has become fully developed. In fully-developed flows, the mean velocity vector is parallel to the wall and the near-wall behavior in each of these cases is similar and responds to the so-called law of the wall. We follow the discussion reported in [29].

1.4.1. Channel flow

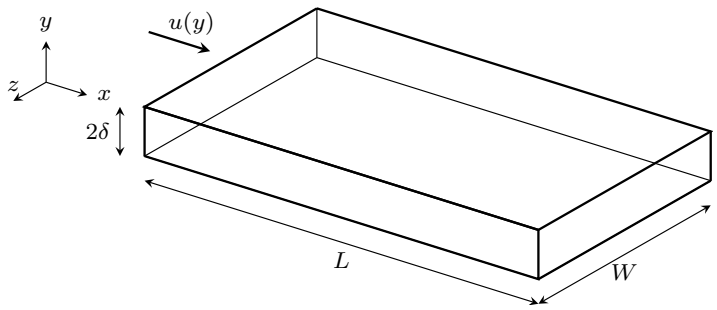

Figure 1.1: Schematic of a channel flow.

As sketched in Figure 1.1, we consider the flow through the rectangular duct of height 2δ. The duct is long $L/\delta \gg 1$ and has a large aspect ratio $W/\delta \gg 1$. The mean flow is mainly in the axial direction x with the mean velocity varying principally in the wall-normal direction y. The bottom and top walls are respectively at $y = 0$ and $y = 2\delta$. The extent of the channel in the spanwise direction is large compared with δ so that the flow is statistically independent of z. The center-line is defined by $y = \delta$ and $z = 0$.

The velocity $\mathbf{u}$ in the three coordinate directions is (u, v, w) with mean $(\langle u\rangle, \langle v\rangle, \langle w\rangle)$ and fluctuations (u', v', w'). At the walls, mean and fluctuat-

ing velocity are equal to zero, i.e. $\langle u\rangle = \langle v\rangle = \langle w\rangle = 0$ and $u_i' = v_i' = w_i' = 0$. At the entry of the channel, there is a flow-development region. We confine our attention to the fully developed region where velocity statistics no longer vary with the streamwise direction. Then, the fully developed channel flow is statistically stationary and statistically one-dimensional, with velocity statistics depending only on y. The Reynolds number used to characterize the flow is $Re = 2\delta U_b/\nu$, where U_b is the bulk velocity evaluated with the integral $U_b = (\int_0^\delta \langle u\rangle dy)/\delta$.

Since $\langle w\rangle = 0$ and $\langle u\rangle$ are independent of x, the mean continuity equation (1.56) reduces to

$$\frac{d\langle v\rangle}{dy} = 0\,. \tag{1.110}$$

With the boundary condition $\langle v\rangle = 0$ on the walls, (1.110) indicates that $\langle v\rangle$ vanishes for all y. The x and y components of (1.57) reduce to

$$\frac{\partial}{\partial y}\Big(\nu\frac{\partial\langle u\rangle}{\partial y} - \langle u'v'\rangle\Big) = \frac{1}{\rho}\frac{\partial\langle p\rangle}{\partial x}\,, \tag{1.111}$$

$$\frac{\partial}{\partial y}\Big(-\langle v'v'\rangle\Big) = \frac{1}{\rho}\frac{\partial\langle p\rangle}{\partial y}\,. \tag{1.112}$$

Firstly, we rewrite (1.112) in the following form

$$\frac{\partial}{\partial y}\Big(\langle v'v'\rangle + \frac{\langle p\rangle}{\rho}\Big) = 0\,, \tag{1.113}$$

and we introduce the modified pressure $p_w = \langle p\rangle + \rho\langle v'v'\rangle$, which is named wall pressure since $p_w = \langle p\rangle_{y=0}$. From (1.113) we deduce that p_w is a function of x alone and since $\langle v'v'\rangle$ is independent of x we can rewrite (1.111) as

$$\frac{\partial}{\partial y}\Big(\nu\frac{\partial\langle u\rangle}{\partial y} - \langle u'v'\rangle\Big) = \frac{1}{\rho}\frac{\partial p_w}{\partial x}\,. \tag{1.114}$$

We introduce the total shear stress defined as the sum of the viscous $\tau = \rho\nu d\langle u\rangle/dy$ and turbulent shear stress $\tau_R = -\rho\langle u'v'\rangle$

$$\tau_{eff}(y) = \rho\nu\frac{d\langle u\rangle}{dy} - \rho\langle u'v'\rangle\,, \tag{1.115}$$

and we rewrite (1.114) using the ordinary derivatives

$$\frac{d\tau_{eff}}{dy} = \frac{dp_w}{dx}\,. \tag{1.116}$$

The left-hand side and the right-hand side of (1.116) are independent of x and y respectively then we can deduce that both $d\tau_{eff}/dy$ and dp_w/dx are constant. We can express the mean pressure gradient in terms of the wall shear stress

$$\tau_w = \tau_{eff}|_{y=0} = \tau|_{y=0} = \rho\nu \frac{d\langle u\rangle}{dy}\bigg|_{y=0}, \tag{1.117}$$

which is due entirely to the viscous contribution since $\rho\langle u'v'\rangle = 0$ at the walls. Integrating (1.116) along y from the wall $y = 0$, where $\tau_{eff} = \tau_w$, to the mid-plane $y = \delta$ where $\tau_{eff} = 0$, we obtain

$$-\frac{dp_w}{dx} = \frac{\tau_w}{\delta}\,. \tag{1.118}$$

The solution of Equation (1.116) can be then written as

$$\tau_{eff}(y) = \tau_w\left(1 - \frac{y}{\delta}\right), \tag{1.119}$$

so the total shear stress is equal to its viscous contribution along the walls and vanishes at the center-line of the channel. The flow in the fully developed region of a plane channel is then driven by the constant pressure gradient, which is balanced by the shear stress gradient. For a given pressure gradient dp_w/dx and channel half-width δ, the shear stress profile is given by (1.118) and (1.119) and it is independent of the fluid properties. We now define appropriate viscous scales for the near-wall region. The friction velocity is

$$u_\tau = \sqrt{\frac{\tau_w}{\rho}} \tag{1.120}$$

and using this velocity scale we can define the friction Reynolds number as $Re_\tau = u_\tau\delta/\nu$, which characterizes the turbulent behavior of the flow. The pressure gradient driving the flow can be expressed using the friction quantities

$$-\frac{dp_w}{dx} = \frac{\rho u_\tau^2}{\delta} = \frac{\rho Re_\tau^2\nu^2}{\delta^3}\,. \tag{1.121}$$

Let δ_ν be the viscous length-scale defined as $\delta_\nu = \nu/u_\tau$, then the distance from the wall measured in viscous length is denoted by

$$y^+ = \frac{y}{\delta_\nu} = \frac{u_\tau y}{\nu}\,. \tag{1.122}$$

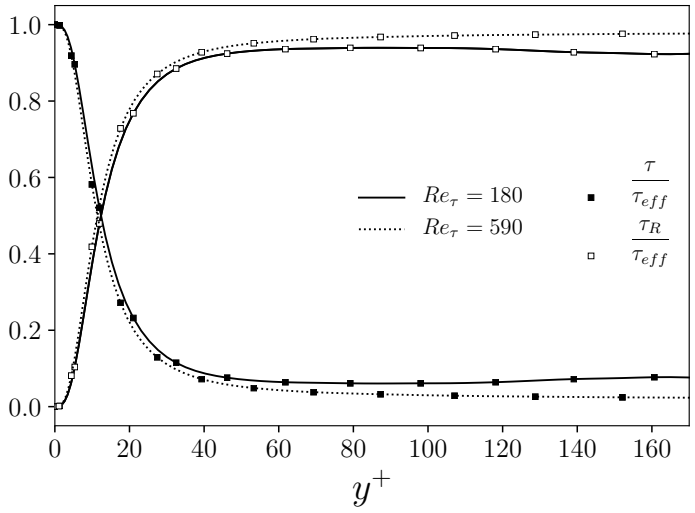

Figure 1.2: Profiles of the fractional contributions of the viscous stress τ and Reynolds stress τ_R to the total stress τ_{eff} with y^+. DNS data from [35] for $Re_\tau = 180$ and 590.

Different regions in the near-wall flow can be defined on the basis of y^+ defined in (1.122). Figure 1.2 shows the contributions of the viscous stress τ and Reynolds stress τ_R to the total stress τ_{eff}, defined in (1.115), plotted against y^+ for $Re_\tau = 180$ and 590. Close to the wall, for $y^+ < 50$, we can observe an important contribution of the molecular viscosity on the shear stress. In this region, which is usually named viscous wall region, rapid variations in both τ and τ_R occur. Although the sum of the two stresses is constant, we move rapidly from a situation in which τ_{eff} is purely viscous at $y = 0$, i.e. $\tau_{eff} \approx \tau$, to a situation in which $\tau_{eff} \approx \tau_R$ at a short distance from the wall. The sub-region where the Reynolds stress tensor is small compared to the viscous stress is called viscous sub-layer, with $y^+ < 5$. For $y^+ > 50$, the direct effect of viscosity is negligible, then $\tau_{eff} \approx \tau_R$, and this region is called outer region.

Now we consider the condition of thermally fully developed flow [31]. A uniform heat flux q_w is imposed at the walls of the plane channel. Due to the convective heat transfer between the fluid and the walls, the mean temperature $\langle T \rangle$ changes with x, then the condition of thermally fully developed flow is certainly different from the hydrodynamic case for which $\partial \langle u \rangle / \partial x = 0$. If there is heat transfer, $\partial \langle T \rangle / \partial x$ is not zero and the mean temperature is a function of x and y. Let T_b be the bulk mean temperature

defined as $T_b(x) = (\int_0^\delta \langle T\rangle\langle u\rangle dy)/(\int_0^\delta \langle u\rangle dy)$ then the Newton's law of cooling states

$$q_w = h(T_w - T_b)\,, \tag{1.123}$$

where T_w is the wall temperature and h is the heat transfer coefficient.

We introduce the non-dimensional temperature $(T_w - T)/(T_w - T_b)$ which is independent of x in the thermally fully developed condition [36]. It means that although the temperature profile changes with x, the relative shape of the profile does not change

$$\frac{\partial}{\partial x}\left[\frac{T_w(x) - \langle T\rangle(x,y)}{T_w(x) - T_b(x)}\right] = 0\,. \tag{1.124}$$

From (1.124) we find

$$\frac{\partial\langle T\rangle}{\partial x} = \frac{dT_w}{dx}\frac{\langle T\rangle - T_w}{T_w - T_b} + \frac{dT_b}{dx}\frac{T_b - \langle T\rangle}{T_w - T_b}\,. \tag{1.125}$$

Since q_w is constant, we have from (1.123) that $dT_w/dx = dT_b/dx$. Then (1.125) gives

$$\frac{\partial\langle T\rangle}{\partial x} = \frac{dT_b}{dx}\,. \tag{1.126}$$

We can apply an energy balance to the plane channel to determine the variation of the bulk temperature with x

$$dq = \dot{q}_w P dx = \dot{m} c_p dT_b\,, \tag{1.127}$$

where P is the surface perimeter and $\dot{m} = \rho U_b A$ is the mass flow rate entering into the channel section with area A. We can deduce from (1.127)

$$\frac{dT_b}{dx} = \frac{\dot{q}_w P}{\rho U_b A c_p} = \frac{4\dot{q}_w}{\rho U_b D_h c_p}\,. \tag{1.128}$$

where $D_h = 4A/P$ is the hydraulic diameter. With these specifications, we can write the energy equation (1.66) for thermally fully developed flows in the following form

$$\frac{\partial}{\partial y}\left[\alpha\frac{\partial\langle T\rangle}{\partial y} - \langle v'T'\rangle\right] = \langle u\rangle\frac{4\dot{q}_w}{\rho U_b D_h c_p}\,, \tag{1.129}$$

where $D_h = 4\delta$.

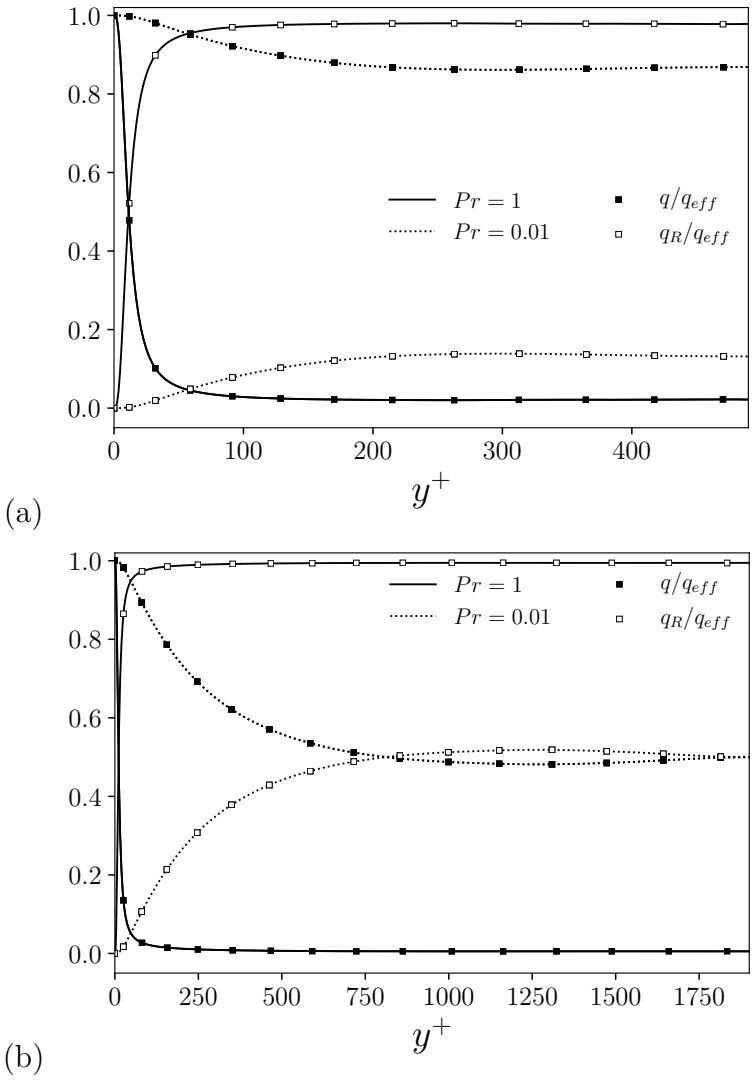

Figure 1.3: Profiles of the fractional contributions of the molecular q and turbulent heat flux q_R to the total heat flux q_{eff} with y^+. DNS data with Prandtl number $Pr = 0.01$ and 1 and friction Reynolds number $Re_\tau = 500$ (a) and $Re_\tau = 2000$ (b).

Let q_{eff} be the total heat flux given by the sum of the molecular $q = \alpha\partial\langle T\rangle/\partial y$ and turbulent $q_R = -\langle v'T'\rangle$ terms. Figure 1.3 shows the contributions of the molecular and turbulent heat flux to the total heat flux q_{eff} for medium and low Prandtl numbers, $Pr = 1$ and 0.01, considering medium and high Reynolds friction numbers, $Re_\tau = 500$ and 2000. The DNS data are taken from Alcántara-Ávila et al. [37]. For medium Pr numbers, i.e.

$Pr = 1$, and for both Reynolds numbers, we can observe a near-wall region where the thermal conductivity is dominant and the turbulent heat flux is negligible. This region is the viscous thermal layer. Increasing the distance from the wall, we observe rapid variations on both contributions, and, for high y^+, the molecular conductivity becomes negligible. This behavior is analogous to the one we have described for the total shear stress τ_{eff} in Figure 1.2. For this reason, the dynamic and thermal boundary layers are often considered similar for medium Prandtl numbers.

For $Pr = 0.01$ we can observe a totally different behavior. In Figure 1.3a, the thermal conductivity is dominant everywhere and the turbulent heat flux is almost negligible. In Figure 1.3b, with a high Reynolds number, the turbulent heat flux increases and, at the center of the channel, the viscous and turbulent contributions have the same importance. However, there is no region where the viscous contribution vanishes. For low Prandtl number fluids, the viscous thermal layer is thicker than for medium-high Prandtl number fluids and no similarity exists between thermal and dynamic boundary layers.

1.4.2. Pipe flow

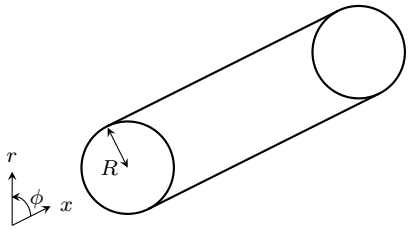

Figure 1.4: Schematic of a pipe flow.

We consider the fully developed turbulent flow in a long pipe of circular cross-section, with internal diameter $D = 2R$. A representative schematic of the pipe is reported in Figure 1.4. The velocity components $\langle u \rangle, \langle v \rangle, \langle w \rangle$ denote the flow in the x, r and ϕ directions. The analysis of fully-developed flows along a pipe is quite similar to the one presented for the plane channel, indeed the fully-developed pipe-flow is statistically stationary and statistically one-dimensional, with velocity statistics independent of x and ϕ. The Reynolds number used to characterize the flow is $Re = 2RU_b/\nu$, where U_b is the bulk velocity evaluated with the integral $U_b = (\int_0^R 2\pi r \langle u \rangle dr)/\pi R^2$. We denote the distance from the center of the pipe by r.

Since $\langle w\rangle = 0$ and $\langle u\rangle$ is independent of x, the continuity equation (1.56) states

$$\frac{1}{r}\frac{\partial r\langle v\rangle}{\partial r} = 0\,, \tag{1.130}$$

then the radial velocity component $\langle v\rangle$ does not vary across the pipe. Since $\langle v\rangle$ must vanish at the pipe walls, we conclude that $\langle v\rangle = 0$ everywhere over the fully-developed region. The x and r components of (1.57) reduce to

$$\frac{1}{r}\frac{\partial}{\partial r} r\Big(\nu\frac{\partial\langle u\rangle}{\partial r} - \langle u'v'\rangle\Big) = \frac{1}{\rho}\frac{\partial\langle p\rangle}{\partial x}\,, \tag{1.131}$$

$$-\frac{1}{r}\frac{\partial}{\partial r} r\langle v'v'\rangle - \frac{\langle w'w'\rangle}{r} = \frac{1}{\rho}\frac{\partial\langle p\rangle}{\partial r}\,. \tag{1.132}$$

We can rewrite (1.132) as

$$\frac{\partial}{\partial r}\Big(\frac{\langle p\rangle}{\rho} + \langle v'v'\rangle\Big) = -\frac{\langle v'v'\rangle + \langle w'w'\rangle}{r}\,. \tag{1.133}$$

Integrating Equation (1.133) from a generic position r to the wall $r = R$, we obtain

$$\Big[\frac{\langle p\rangle}{\rho} + \langle v'v'\rangle\Big]_r^R = \frac{p_w}{\rho} - \frac{\langle p\rangle}{\rho} - \langle v'v'\rangle = -\int_r^R \frac{\langle v'v'\rangle + \langle w'w'\rangle}{\bar{r}} d\bar{r} \tag{1.134}$$

where $p_w = \langle p\rangle_{r=R}$ is the wall pressure. From (1.134) we obtain that the pressure in the radial direction changes across the duct due to the presence of the turbulent stresses

$$\langle p\rangle = p_w - \rho\langle v'v'\rangle + \rho\int_r^R \frac{\langle v'v'\rangle + \langle w'w'\rangle}{\bar{r}} d\bar{r}\,. \tag{1.135}$$

Since the turbulent stresses depend only on the radial coordinates, differentiating Equation (1.135) with respect to x we obtain

$$\frac{\partial\langle p\rangle}{\partial x} = \frac{dp_w}{dx}\,. \tag{1.136}$$

We consider now (1.131) for the x-component of mean momentum equation. Let τ_{eff} be the total shear stress defined as the sum of viscous and Reynolds stresses. Since the pressure gradient is independent of r, integrating along the radial direction from the center-line $r = 0$ to the wall $r = R$ we obtain

the relation between the pressure-gradient and the shear stress at the wall $\tau_w = \nu du/dr|_{r=R}$

$$\frac{dp_w}{dx} = \frac{2\tau_w}{R}\,, \tag{1.137}$$

or using the friction velocity and the friction Reynolds number

$$\frac{dp_w}{dx} = \frac{2\rho u_\tau^2}{R} = \frac{2\rho R e_\tau^2 \nu^2}{R^3}\,. \tag{1.138}$$

Now, integrating along the radial direction from the center-line $r = 0$ to the generic r

$$\tau_{eff}(r) = \frac{r}{2}\frac{dp_w}{dx} = \frac{r}{R}\tau_w\,. \tag{1.139}$$

If we define y as the distance from the wall $R - r$, we obtain

$$\tau_{eff}(y) = \tau_w\Big(1 - \frac{y}{R}\Big)\,, \tag{1.140}$$

which is the same solution expressed in (1.119) for the fully-developed channel flow, then all the conclusions about mean flow obtained for channel flows apply equally to pipe flows.

Now we consider the condition of thermally fully developed flow also for the pipe. Let $\dot{q}_w$ be a uniform heat flow set on the wall. The mean temperature $\langle T(x,r)\rangle$ depends on both radial and axial coordinates. We introduce the bulk temperature $T_b(x)$ defined as

$$T_b(x) = \frac{\int_0^R \langle T(x,r)\rangle\langle u(r)\rangle r dr}{\int_0^R \langle u(r)\rangle r dr}\,. \tag{1.141}$$

As for the plane channel, we define the condition of thermally fully developed flow as the condition in which the dimensionless temperature $(T_w - T)/(T_w - T_b)$ is independent of x. Following the same steps presented in the previous section, we can write the mean temperature equation as

$$\frac{1}{r}\frac{\partial}{\partial r}\Big[r\Big(\alpha\frac{\partial\langle T\rangle}{\partial r} - \langle v'T'\rangle\Big)\Big] = \langle u\rangle\frac{4\dot{q}_w}{\rho U_b D_h c_p}\,, \tag{1.142}$$

where $D_h = 2R$.

1.4.3. Law of the wall for velocity

In this section, we aim to characterize the mean velocity profiles. Fully developed channel or pipe flows are completely specified by ν, δ (or R for the pipe) and u_τ (or the pressure gradient dp_w/dx). Following [29, 38], we can form two independent non-dimensional groups from ν, δ, u_τ and y and the mean velocity profile can be written as

$$\langle u \rangle = u_\tau F\Big(\frac{y}{\delta}, Re_\tau\Big)\,, \tag{1.143}$$

where F is a universal non-dimensional function to be determined. We express the mean velocity gradient in terms of non-dimensional parameters

$$\frac{d\langle u \rangle}{dy} = \frac{u_\tau}{y}\phi\Big(\frac{y}{\delta_\nu}, \frac{y}{\delta}\Big)\,, \tag{1.144}$$

where ϕ is a universal non-dimensional function.

In the inner region, close to the wall where $y/\delta \ll 1$, the mean velocity profile is determined by the viscous scales and it is independent of the channel half-width δ. This implies that the function $\phi(y/\delta_\nu, y/\delta)$ tends asymptotically to a function $\widetilde{\phi}(y/\delta_\nu)$ as $y/\delta \to 0$. Under this assumption, Equation (1.144) becomes

$$\frac{d\langle u \rangle}{dy} = \frac{u_\tau}{y}\widetilde{\phi}\Big(\frac{y}{\delta_\nu}\Big)\,, \quad \text{for } \frac{y}{\delta} \ll 1\,, \tag{1.145}$$

or in non-dimensional form

$$\frac{du^+}{dy^+} = \frac{1}{y^+}\widetilde{\phi}(y^+)\,, \tag{1.146}$$

where $u^+ = \langle u \rangle / u_\tau$ is the non-dimensional mean velocity. The integral of (1.146) is known as law of the wall

$$u^+ = f(y^+)\,, \tag{1.147}$$

which states that u^+ depends only on y^+ for $y/\delta \ll 1$. The function f is universal for channel flows, pipes and boundary layers. The Taylor-series expansion for $f(y^+)$ around $y^+ = 0$ is

$$f(y^+) = y^+ + \mathcal{O}(y^{+2})\,, \tag{1.148}$$

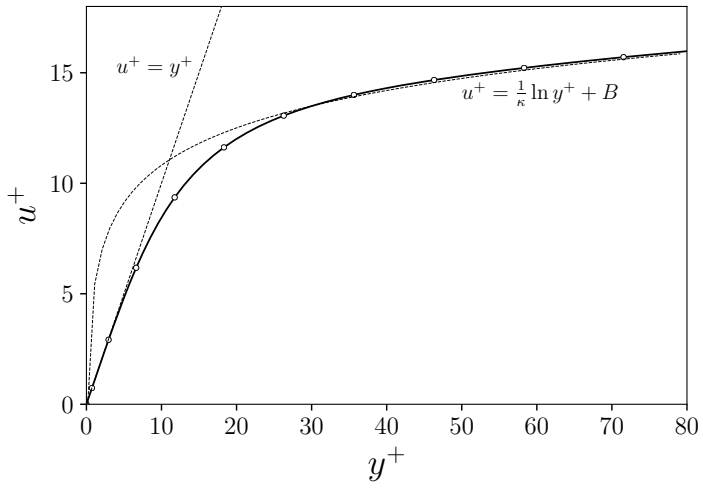

Figure 1.5: Profiles of the non-dimensional mean velocity u^+ versus y^+ showing the law of the wall. DNS data for a plane channel with $Re_\tau = 395$ [39].

then for small values of y^+ a linear relation holds

$$u^+ = y^+ \quad \text{for } \frac{y}{\delta} \ll 1 \text{ and } y^+ \ll 1\,. \tag{1.149}$$

Figure 1.5 shows the profile of u^+ in the near wall-region obtained from direct numerical simulations [39] for a turbulent flow in a plane channel with $Re_\tau = 395$. The linear relation holds in the viscous sub-layer $y^+ < 5$, also known as linear region, whereas for greater values of y^+ the discrepancies from this trend are significant.

As we have mentioned before, for large values of y^+ it can be supposed that viscosity effects are negligible and then the dependence of $\widetilde{\phi}(y/\delta_\nu)$ on ν, expressed in Equation (1.145), vanishes and $\widetilde{\phi}$ takes a constant value

$$\widetilde{\phi}\Big(\frac{y}{\delta_\nu}\Big) = \frac{1}{\kappa}\,, \quad \text{for } \frac{y}{\delta} \ll 1 \text{ and } y^+ \gg 1\,. \tag{1.150}$$

Substituting in (1.146) the expression of $\widetilde{\phi}$ and integrating, we find

$$u^+ = \frac{1}{\kappa}\ln(y^+) + B\,, \quad \text{for } \frac{y}{\delta} \ll 1 \text{ and } y^+ \gg 1\,, \tag{1.151}$$

that is the logarithmic law of the wall. By experiments, this is valid with $\kappa = 0.41$ and $B = 5.2$ for $y^+ > 30$ and $y/\delta < 0.1$-0.2 approximately, provided that the bulk Reynolds number is not too small. In Figure 1.5 we can observe the comparison between the logarithmic law of the wall and the

DNS data. There is a perfect agreement between the two lines for $y^+ > 30$ and this region is called log-law region. The region between the viscous sub-layer ($y^+ < 5$) and the log-law region ($y^+ > 30$) is named buffer layer.

We now analyze the outer region ($y^+ > 50$), where the viscous stresses are negligible and then we can assume that $\phi(y/\delta_\nu, y/\delta)$ is independent of ν and y/δ_ν. This implies that for large y/δ_ν, the function $\phi(y/\delta_\nu, y/\delta)$ tends asymptotically to $\hat{\phi}(y/\delta)$. Integrating (1.144) between the center-line $y = \delta$ and a generic y we obtain the velocity defect law

$$\frac{u_0 - \langle u \rangle}{u_\tau} = \hat{f}\left(\frac{y}{\delta}\right), \quad \text{for } y^+ > 50 \tag{1.152}$$

where $\hat{f}$ is a non-dimensional function and, unlike f in (1.147), is not universal. Then, Equation (1.152) states that the departure of $\langle u \rangle$ from the center-line velocity u_0 normalized by u_τ depends only on y/δ.

1.4.4. Law of the wall for temperature

The law of the wall for temperature can be derived by analogous dimensional analysis that we have reported for the law of the wall for velocity.

For $y \ll \delta$ and $y \ll \delta_T$, where δ_T is the thickness of the thermal boundary layer, the temperature measured with respect to the wall, $T_w - \langle T \rangle$, depends only on the wall shear stress τ_w, on the wall heat flux q_w, on the distance from the wall y and on the fluid properties ν, ρ, c_p and α. Following [38], the dimensional analysis gives

$$T_w - \langle T \rangle = T_\tau F_T(y^+, Pr, B_q), \quad \text{for } y \ll \delta \text{ and } y \ll \delta_T \tag{1.153}$$

where F_T is a universal non-dimensional function to be determined and $T_\tau = q_w/(\rho c_p u_\tau)$ is the friction temperature. The non-dimensional parameter $y^+ = u_\tau y/\nu$ is the distance from the wall in wall units, $Pr = \nu/\alpha$ is the Prandtl number and the last parameter $B_q = q_w/(u_\tau \tau_w)$ represents the ratio of wall heat flux to the internal source due to viscous dissipation. In low-speed flows, this parameter can be ignored. By considering the mean temperature gradient in terms of non-dimensional parameters, we can write

$$\frac{\partial \langle T \rangle}{\partial y} = -\frac{T_\tau}{y}\phi_T(y^+, Pr). \tag{1.154}$$

which is similar to (1.145). In the immediate vicinity of the wall, for $y^+ \ll 1$, the molecular heat transfer dominates and a molecular transport sublayer

adjacent to the wall exists [40]. The distribution of the dimensionless temperature $T^+ = (T_w - \langle T \rangle)/T_\tau$ in the molecular heat conduction layer is given by

$$T^+ = Pry^+ , \quad \text{for } \frac{y}{\delta} \ll 1 \text{ and } y^+Pr \ll 1 . \tag{1.155}$$

The dimensionless thickness of the molecular transport sublayer depends

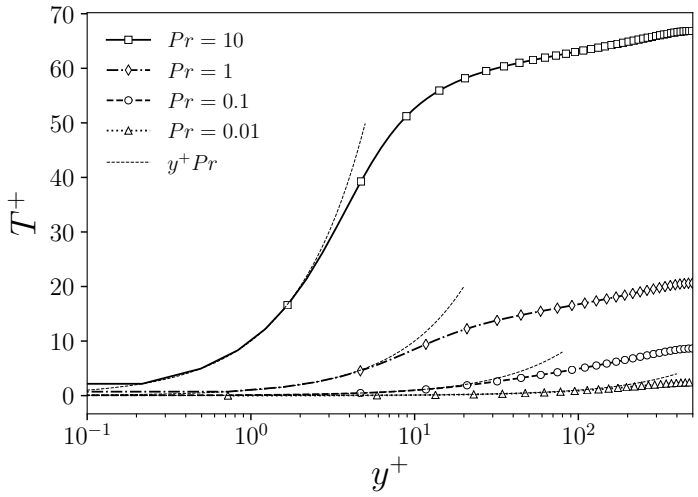

Figure 1.6: Profiles of the non-dimensional mean temperature T^+ versus y^+ showing the law of the wall $T^+ = Pry^+$ in the molecular transport sublayer. DNS data from [37] for $Pr = 1, 0.1$ and 0.01, $Re_\tau = 500$.

on the Pr number, as we can see in Figure 1.6. If $Pr \gg 1$, the molecular transport sublayer is immersed in the dynamic viscous sublayer, then $y_\alpha^+ < y_\nu^+$ and $y_\alpha^+ \approx 12/Pr^{1/3}$. For fluids with $Pr \approx 1$ the velocity and temperature fields are approximately similar, then the viscous and the molecular sublayer have about the same depth and $y_\alpha^+ \approx y_\nu^+ \approx 30$. When $Pr \ll 1$ the sublayer of molecular heat conduction is thicker than the viscous sublayer, $y_\alpha^+ > y_\nu^+$ and it spreads from the wall to the velocity logarithmic region and $y_\alpha^+ \approx 2/Pr$ [41].

If y^+ and y^+Pr are large, the effects of viscosity and thermal diffusivity on heat transfer are small, then the function ϕ_T should tend to a constant, $1/\kappa_T$, and we can write Equation (1.154) as

$$\frac{\partial T^+}{\partial y^+} = \frac{1}{\kappa_T y^+} , \quad \text{for } \frac{y}{\delta} \ll 1 \text{ and } y^+Pr \gg 1 , \tag{1.156}$$

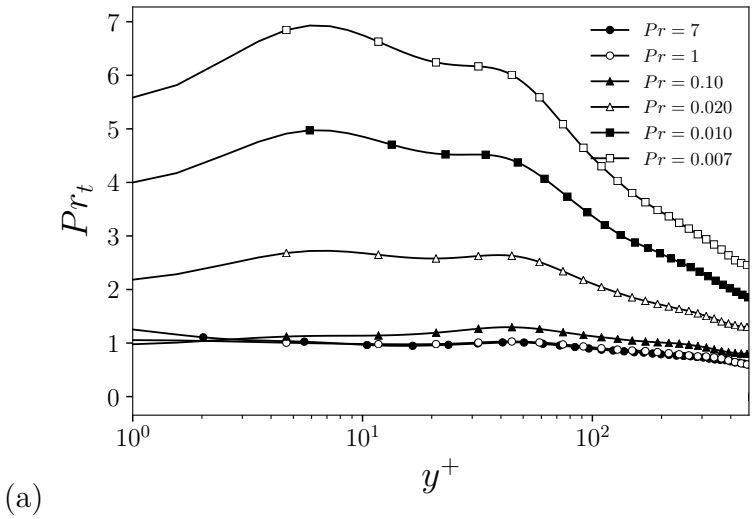

(a)

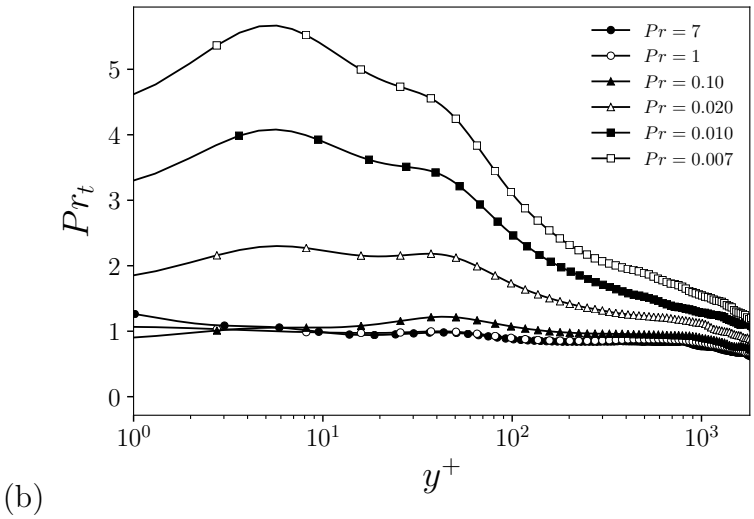

(b)

Figure 1.7: Profiles of turbulent Prandtl number Pr_t with y^+. DNS data from Alcántara-Ávila et al. [37] with friction Reynolds number $Re_\tau = 500$ (a) and $Re_\tau = 2000$ (b) for several Pr numbers.

which integrates to give

$$T^+ = \frac{1}{\kappa_T}\ln(y^+) + B_T\,, \qquad \text{for } \frac{y}{\delta} \ll 1 \text{ and } y^+ Pr \gg 1 \tag{1.157}$$

where B_T is a function of Pr and the coefficient κ_T is usually considered as a constant with value $\kappa_T \approx 0.48$ [38, 40]. Kader [40] proposed the following correlation for Pr number from 0.006 to 40000

$$B(T) = (3.85Pr^{1/3} - 1.3)^2 + 2.12\ln(Pr). \tag{1.158}$$

The turbulent Prandtl number Pr_t is the ratio of the apparent viscosity to the apparent thermal diffusivity, i.e.

$$Pr_t = \frac{\langle u'v' \rangle / (\partial \langle u \rangle / \partial y)}{\langle v'T' \rangle / (\partial \langle T \rangle / \partial y)} \,. \tag{1.159}$$

In the region of validity of both velocity (1.151) and temperature (1.156) logarithmic laws, in which $\langle u'v' \rangle$ and $\langle v'T' \rangle$ are almost constant, we have $Pr_t = \kappa/\kappa_T$, then $Pr = 0.85$.

The turbulent Prandtl number is shown as a function of y^+ in Figure 1.7 for $Re_\tau = 500$ and 2000. We can observe that Pr_t is approximately constant and equal to 1 for medium and high molecular Prandtl number ($Pr = 0.1, 1, 7$). The turbulent Prandtl number becomes almost independent of y^+ and Pr as the wall is approached, except for low Prandtl numbers. The turbulent Prandtl number has higher values for low Prandtl fluids along the whole channel, not only in the wall proximity. Moreover, the turbulent Prandtl number depends significantly on the Reynolds number [42, 37]. Increasing the Reynolds number Re_τ, the turbulent Prandtl number moves toward the value for the larger Pr. Then the high value of Pr_t for a low Prandtl number fluid is caused by the effect of the low Reynolds number. With the increase of the Reynolds number, the turbulent heat transport contributes more dominantly compared to the conduction effect [42].

CHAPTER 2

Turbulence modeling

In Chapter 1 we have introduced the statistical tools commonly employed for the study of turbulent flows. In contrast to laminar flows, deterministic equations such as continuity, momentum, and energy equations have random solutions when the flow is turbulent. Applying the Reynolds averaging operation, it is possible to derive the so-called Reynolds-Averaged Navier-Stokes and energy equations for the mean velocity $\langle \mathbf{u} \rangle$, pressure $\langle p \rangle$ and temperature $\langle T \rangle$ fields. However, the obtained system of equations is not closed because the averaging operation has introduced additional statistic unknowns, the velocity covariance or Reynolds stresses $\langle u_i' u_j' \rangle$, and the velocity-temperature covariance or turbulent heat flux $\langle u_i' T' \rangle$.

Several models have been developed in past decades for the computation of the Reynolds stress tensor $\langle u_i' u_j' \rangle$. The first-order models are based on the Boussinesq assumption, which hypothesizes a linear relationship between Reynolds stresses $\langle u_i' u_j' \rangle$ and the mean strain-rate tensor S_{ij} through an isotropic eddy viscosity ν_t, which is usually determined using two-equation turbulence models. The Reynolds-stress models are second-order models and use transport equations for each component of the Reynolds stress tensor. From an academic point of view, the second-order models would be the best modeling for anisotropic momentum transfer, but the usage of these techniques requires a considerably increased numerical effort [9].

For the turbulent heat flux $\langle u_i' T' \rangle$, only a restricted number of models have been developed and validated. Most of them are first-order models based on the Simple Gradient Diffusion Hypothesis (SGDH), which assumes the similarity between the turbulent heat flux and the molecular heat conduction introducing the turbulent thermal diffusivity α_t and the turbulent Prandtl number Pr_t, which is often set equal to a constant value in the range 0.8–1. This concept can reproduce reasonable results in the forced convection regime and for fluids with $Pr \approx 1$, whereas it is inadequate for applications involving non-unity Prandtl number fluids like liquid metals and/or non-negligible buoyancy effects [10]. For these applications, the most promising models require the introduction of additional transport equations. In [43, 44], an implicit Algebraic Heat Flux Model has been proposed and implemented in STAR-CCM+. Its closure requires one additional transport equation for the evaluation of the temperature variance $\langle T'^2 \rangle$. In [43], the thermal model has been coupled with a low-Reynolds linear k-ε model, while in [44], the coupling with a second-order Reynolds-stress model has shown better results. In [11, 12, 13, 14], an isotropic four-parameter model (I4P) has been proposed and implemented in FEMuS. The model introduces two additional thermal transport equations for the evaluation of the squared temperature fluctuations k_θ and its dissipation ε_θ. In the original formulation of this model, the turbulent heat flux is evaluated with an SGDH approach.

In this Ph.D. thesis, an anisotropic version of the above-mentioned four-parameter model is proposed. For the closure of the momentum equation, we suggest an Explicit Algebraic Stress Model, instead of the Boussinesq assumption used in the isotropic model I4P, and for the modeling of the turbulent heat flux, we propose an Explicit Algebraic Heat Flux Model, instead of the SGDH hypothesis applied in I4P model. For the closure of $\langle u_i' u_j' \rangle$ and $\langle u_i' T' \rangle$, we can solve the four transport model equations of the isotropic model (k-ε-k_θ-ε_θ, k-ω-k_θ-ω_θ or K-Ω-K_θ-Ω_θ).

The chapter is structured as follows: firstly, we introduce the Boussinesq assumption and the linear eddy viscosity models, giving particular attention to k-ε and k-ω models. We also report the near-wall treatment employed in the isotropic four-parameter model. We then introduce the eddy thermal diffusivity models based on the SGDH hypothesis, in particular, we describe the k_θ-ε_θ and k_θ-ω_θ models. The description of the near-wall treatment for thermal variables used in the isotropic four-parameter model is reported.

To propose the anisotropic version of the isotropic four-parameter model, we describe the procedure of derivation of the explicit algebraic stress and heat flux models. Finally, we present the anisotropic four-parameter model, developed, implemented, and validated during this Ph.D. project.

2.1. Eddy viscosity models

The simplest turbulence models used in the RANS framework employ the Boussinesq eddy viscosity approximation to compute the Reynolds stress components as the product of an eddy viscosity ν_t and the mean strain rate tensor S_{ij} defined in (1.8). The eddy viscosity hypothesis is mathematically analogous to the constitutive relation between stress and rate of strain for a Newtonian fluid. According to the eddy viscosity hypothesis, there exists the following relation

$$\langle u_i' u_j' \rangle = \frac{2}{3} k \delta_{ij} - 2\nu_t S_{ij} \,, \tag{2.1}$$

which means that the deviatoric part of Reynolds stress a_{ij}, introduced in (1.63), is proportional to the mean rate of strain

$$a_{ij} = \langle u_i' u_j' \rangle - \frac{2}{3} k \delta_{ij} = -2\nu_t S_{ij} \,. \tag{2.2}$$

The mean momentum equation (1.65) incorporating the eddy viscosity hypothesis is

$$\begin{aligned} \frac{D\langle u_i \rangle}{Dt} = &-\frac{1}{\rho} \frac{\partial}{\partial x_i} \Big(\langle p \rangle + \frac{2}{3} \rho k \Big) + \frac{\partial}{\partial x_j} \Big[\nu_{eff} \Big(\frac{\partial \langle u_i \rangle}{\partial x_j} + \frac{\partial \langle u_j \rangle}{\partial x_i} \Big) \Big] + \\ &- g_i \beta \langle T \rangle \,, \end{aligned} \tag{2.3}$$

where $\nu_{eff} = \nu + \nu_t$ is the effective viscosity. Equation (2.3) has the same form as Navier-Stokes equation (1.28) with $\langle \mathbf{u} \rangle$ and ν_{eff} in place of $\mathbf{u}$ and ν and with the modified mean pressure $\langle p \rangle + 2/3 \rho k$. Then, the convenience of the eddy viscosity hypothesis is the possibility to maintain the same form of differential equations for laminar and turbulent flows, allowing the use of the same numerical scheme [30]. Moreover, since in general $\nu_t > \nu$, this formulation of the problem can be rather robust numerically, especially if compared to alternative forms of maintaining the Reynolds stress gradient explicitly in (1.57) [45]. However, one of the most evident deficiencies of the model is the isotropy of the eddy viscosity, which is a consequence of the

Boussinesq approximation which assumes a direct proportionality between the turbulent stress and the mean strain rate. Due to this assumption, the model fails to predict the anisotropy in simple configurations such as fully developed plane channel flows. In fact, due to the symmetry of this configuration $\partial\langle u\rangle/\partial x = \partial\langle v\rangle/\partial y = \partial\langle v\rangle/\partial x = 0$. The linear eddy viscosity model yields

$$\langle u'u'\rangle = \langle v'v'\rangle = \langle w'w'\rangle = \frac{2}{3}k\,, \tag{2.4}$$

which is in contradiction with DNS data reported in Figure 2.1 for a turbulent fully developed flow over a plane channel with $Re_\tau = 590$. In Figure 2.1 the dimensionless normal stresses, $\langle u'u'\rangle^+$, $\langle v'v'\rangle^+$ and $\langle w'w'\rangle^+$, are reported, where the squared friction velocity u_τ^2 is used to normalize the quantities. The streamwise normal stress $\langle u'u'\rangle^+$ presents a maximum value in the near-wall region that is considerably higher than the peak values of wall-normal normal stress $\langle v'v'\rangle^+$ and spanwise normal stress $\langle w'w'\rangle^+$.

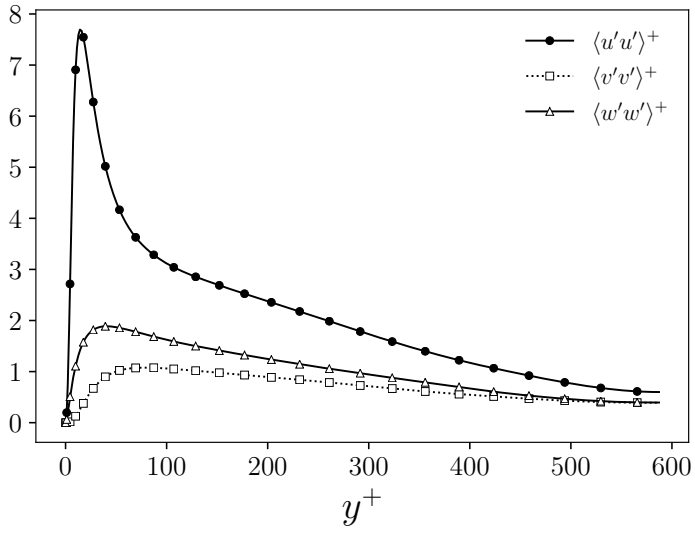

Figure 2.1: The $\langle u_i'u_i'\rangle^+$ distribution from data of direct numerical simulation of fully developed plane turbulent channel flow for $Re_\tau = 590$ [35].

Nonlinear eddy viscosity models extend in a general manner the representation reported in (2.1), since they express the Reynolds stress in the more general form

$$\langle u_i'u_j'\rangle = \frac{2}{3}k\delta_{ij} + \sum_{n=1}^{N}\alpha^{(n)}T_{ij}^{(n)}\,, \tag{2.5}$$

where $T_{ij}^{(n)}$ are the tensor bases and $\alpha^{(n)}$ are the expansion coefficients which need to be determined.

When using the eddy viscosity approximation, the problem of the closure is considerably simplified since the only additional unknown in Equation (2.3) is the eddy viscosity ν_t, instead of the six independent components of the Reynolds stress tensor. The eddy viscosity can be written as the product of a velocity scale υ and a length scale ℓ, then $\nu_t = \upsilon\ell$ [29]. There are different levels of closure, depending on the number of differential equations solved to determine the two scales. In algebraic or zero-equation models the velocity and length scales are specified algebraically, while in one-equation models the velocity scale is obtained by the transport equation for the turbulent kinetic energy, and the length scale is specified algebraically. In two-equation models, differential transport equations are used for both scales. The turbulent velocity scale is based on the turbulent kinetic energy equation, while the length scale ℓ is estimated through the dissipation rate ε or the dissipation rate per unit of turbulent kinetic energy ω. In the next paragraphs, the modeled transport equations for k-ε and k-ω model are presented and discussed.

2.1.1. The k-ε model

The k-ε model belongs to the class of two-equation models, in which two additional transport equations are solved for the turbulent kinetic energy k and the dissipation rate ε. These two quantities can be used to form a length scale $\ell \propto k^{3/2}/\varepsilon$ and a velocity scale $\upsilon \propto k^{1/2}$. From these scales, the turbulent viscosity is specified as

$$\nu_t = c_\mu \frac{k^2}{\varepsilon} \,. \tag{2.6}$$

The exact transport equation for turbulent kinetic energy has been derived in Chapter 1 and the differential equation is reported in (1.78). In this equation, the terms Dk/Dt, $\mathcal{P}$, ε and $\mathcal{G}$ are in a closed form given the eddy viscosity hypothesis and an appropriate closure model for the turbulent heat flux appearing in the expression of $\mathcal{G}$. With the eddy viscosity hypothesis, the production term $\mathcal{P}$ is expressed as $\mathcal{P} = -\langle u_i' u_j' \rangle \partial u_i/\partial x_j = 2\nu_t S^2$, where we have decomposed the velocity gradient tensor into the symmetric strain rate tensor S_{ij} and the antisymmetric rotation rate tensor $\Omega_{ij} = (\partial u_i/\partial x_j - \partial u_j/\partial x_i)/2$. Moreover, we have used $S_{ij}S_{ij} = S^2$ and $S_{ij}\Omega_{ij} = 0$.

The remaining unknown is the diffusion term $\mathcal{D}$, given by the sum of

viscous, turbulent and pressure diffusion terms. The viscous diffusion term is in a closed form, while the correlations need to be modeled. Referring to the standard k-ε model due to Jones and Launder [46], we apply the gradient-diffusion hypothesis for the turbulent diffusion terms

$$-\frac{1}{2}\langle u_i' u_i' u_k' \rangle - \frac{\langle p' u_k' \rangle}{\rho} \approx \frac{\nu_t}{\sigma_k}\frac{\partial k}{\partial x_k}\,, \tag{2.7}$$

where σ_k is a closure coefficient called effective Prandtl-Schmidt number for diffusion that is taken as a constant in incompressible flows. The modeled transport equation for turbulent kinetic energy can be then written in the following form

$$\frac{Dk}{Dt} = \frac{\partial}{\partial x_k}\left[\left(\nu + \frac{\nu_t}{\sigma_k}\right)\frac{\partial k}{\partial x_k}\right] + 2\nu_t S^2 - \varepsilon + \mathcal{G}\,. \tag{2.8}$$

The exact transport equation of the rate of dissipation of turbulent kinetic energy ε is reported in (1.84). The only terms in a closed-form are $D\varepsilon/Dt$ and the molecular diffusion. For the other terms, we introduce the standard closure assumptions [32, 47]. The production term $\mathcal{P}_\varepsilon$ is modeled by

$$\mathcal{P}_\varepsilon = c_{\varepsilon 1}\frac{\varepsilon}{k}\langle u_i' u_k' \rangle \frac{\partial \langle u_i \rangle}{\partial x_k} = c_{\varepsilon 1}\frac{\varepsilon}{k} 2\nu_t S^2\,, \tag{2.9}$$

where $c_{\varepsilon 1}$ is constant. The buoyancy source term is given by $\mathcal{G}_\varepsilon = c_b \varepsilon/k \mathcal{G}$, and the dissipation term is modeled by $\varepsilon_\varepsilon = c_{\varepsilon_2}\varepsilon^2/k$, while the diffusion term is modeled by a gradient-diffusion hypothesis

$$\mathcal{D}_\varepsilon = \frac{\partial}{\partial x_j}\left[\left(\nu + \frac{\nu_t}{\sigma_\varepsilon}\right)\frac{\partial \varepsilon}{\partial x_j}\right], \tag{2.10}$$

having neglected the diffusion transport of ε by pressure fluctuations. With these closure assumptions, the final form of the transport equation for the dissipation rate can be written as

$$\frac{D\varepsilon}{Dt} = \frac{\partial}{\partial x_j}\left(\nu + \frac{\nu_t}{\sigma_\varepsilon}\right)\frac{\partial \varepsilon}{\partial x_j} + c_{\varepsilon 1}\frac{\varepsilon}{k}\mathcal{P} - c_{\varepsilon_2}\frac{\varepsilon^2}{k} + c_b\frac{\varepsilon}{k}\mathcal{G}\,. \tag{2.11}$$

The standard values of all the model coefficients are [30]

$$c_\mu = 0.09\,, c_{\varepsilon 1} = 1.45\,, c_{\varepsilon 2} = 1.9\,, c_b = 1.2\,, \sigma_k = 1.0\,, \sigma_\varepsilon = 1.3\,. \tag{2.12}$$

The coefficients reported in (2.12) are assumed constants, but it is only an

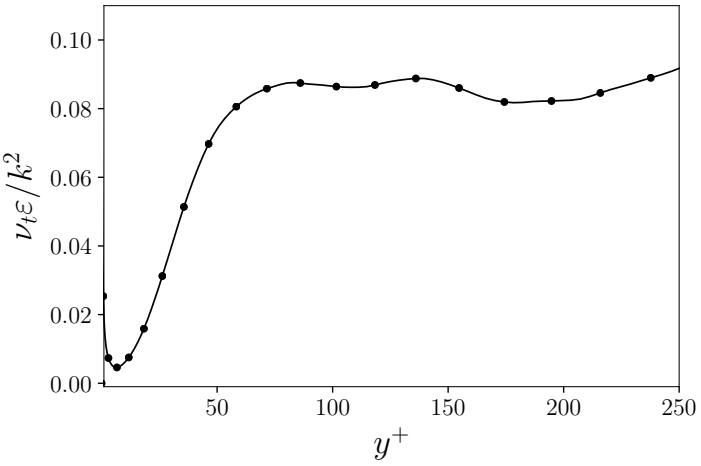

Figure 2.2: The profile of $\nu_t\varepsilon/k^2$ from DNS of channel flow at $Re_\tau = 395$ [35].

approximation that can be acceptable for simple flows, but it can be quite inaccurate for complex flows. Figure 2.2 shows the quantity $\nu_t\varepsilon/k^2$, corresponding to the coefficient c_μ from Equation (2.6), calculated from DNS data of fully developed turbulent channel flow. This quantity is approximately constant with a value of around 0.09, except for the near-wall region ($y^+ < 50$). Changes in the standard k-ε model are required to apply to the near-wall region, since the assumption of c_μ constant in this region is inadequate [29, 48].

2.1.2. The k-ω model

The k-ω model is a two-equation turbulence model. Its first formulation was proposed by Kolmogorov in 1942 and the model has evolved over the decades. Let ω be the specific dissipation rate of turbulent kinetic energy, a turbulent quantity whose dimensions are inversely proportional to time, defined as

$$\omega = \frac{\varepsilon}{c_\mu k}\,. \tag{2.13}$$

In a k-ω model, the eddy viscosity is computed as the ratio of turbulent kinetic energy and its specific dissipation rate $\nu_t = k/\omega$. The transport equation for turbulent kinetic energy proposed by Wilcox [49], can be obtained from (2.8) replacing the dissipation term with the relation $\varepsilon = \beta^* k\omega$

derived from the definition (2.13), where $\beta^* = c_\mu$,

$$\frac{Dk}{Dt} = \frac{\partial}{\partial x_k}\left[\left(\nu + \frac{\nu_t}{\sigma_k}\right)\frac{\partial k}{\partial x_k}\right] + \mathcal{P} - \beta^* k\omega \,. \tag{2.14}$$

The transport equation for the specific dissipation rate proposed by Wilcox [49] can be formulated

$$\frac{D\omega}{Dt} = \frac{\partial}{\partial x_k}\left[\left(\nu + \frac{\nu_t}{\sigma_\omega}\right)\frac{\partial \omega}{\partial x_k}\right] + \gamma\frac{\omega}{k}\mathcal{P} - \beta\omega^2 + \gamma\frac{\omega}{k}\mathcal{G} \,, \tag{2.15}$$

where

$$\beta = \frac{3}{40} \,, \beta^* = 0.09 \,, \gamma = \frac{5}{9} \,, \sigma_k = \sigma_\omega = 2 \,. \tag{2.16}$$

The k-ω model here presented differs from the standard k-ε model previously reported [29]. To better understand the differences between the two models, we can derive the ω equation implied by the k-ε model. From Equation (2.11) taking $\sigma_k = \sigma_\varepsilon = \sigma_\omega$ for simplicity, the result is

$$\begin{aligned}\frac{D\omega}{Dt} = \frac{\partial}{\partial x_k}\left[\left(\nu + \frac{\nu_t}{\sigma_\omega}\right)\frac{\partial \omega}{\partial x_k}\right] + \frac{2}{k}\left(\nu + \frac{\nu_t}{\sigma_\omega}\right)\frac{\partial k}{\partial x_j}\frac{\partial \omega}{\partial x_j} + \\ + (c_{\varepsilon 1} - 1)\frac{\omega}{k}\mathcal{P} - (c_{\varepsilon 2} - 1)c_\mu\omega^2 + (c_b - 1)\frac{\omega}{k}\mathcal{G} \,.\end{aligned} \tag{2.17}$$

For homogeneous turbulence, the choice of $\gamma = c_{\varepsilon 1} - 1$ and $\beta = c_{\varepsilon 2} - 1$ makes the models (2.15) and (2.17) identical. However, for inhomogeneous turbulence, the k-ε model written as a k-ω model presents an additional term, which is the term in Equation (2.17) given by the scalar product of turbulent kinetic energy gradient and its specific dissipation rate gradient. This term is often called cross-diffusion.

2.1.3. Near-wall treatment

In a turbulent flow, the presence of a wall causes different effects. Firstly, the turbulent Reynolds number Re_τ tends to zero as the wall is approached. Thus, we have a predominant effect of molecular viscosity on the flow structures in the proximity of the wall. Moreover, as the wall is approached, the turbulence tends to a two-component limit because the velocity fluctuations in the wall-normal direction damp [48]. The influence of low Reynolds numbers and the wall proximity have to be taken into account to predict the near-wall turbulence. The standard two-equation models necessitate modifications to capture these effects. While the forms of the basic k-ε

Table 2.1: Near-wall Taylor expansion for the components of the mean velocity $\langle u_i \rangle$ and fluctuating velocity u_i'.

Mean Components	Fluctuating components
$\langle u \rangle = A_1 y + A_2 y^2 + A_3 y^3 + \dots$	$u' = a_1 y + a_2 y^2 + a_3 y^3 + \dots$
$\langle v \rangle = B_2 y^2 + B_3 y^3 + \dots$	$v' = b_2 y^2 + b_3 y^3 + \dots$
$\langle w \rangle = C_1 y + C_2 y^2 + C_3 y^3 + \dots$	$w' = c_1 y + c_2 y^2 + c_3 y^3 + \dots$

models have not changed since the form proposed in the 1970s, the same is not true for the near-wall treatment of basic two-equation turbulence models. Jones and Launder were the first to extend the original k-ε model to the low-Reynolds number form that allows calculations in the proximity of walls [50]. As new detailed DNS data for the viscous near-wall region are available, turbulence models are continually developed and improved to become more and more accurate. For the various low-Reynolds k-ε models proposed, the relation for determining the eddy viscosity ν_t can be written as

$$\nu_t = c_\mu f_\mu \frac{k^2}{\varepsilon}\,, \tag{2.18}$$

where the damping function f_μ has been introduced to reduce the eddy viscosity near the wall and takes into account low-Reynolds numbers and wall-proximity effects. Since the introduction of f_μ aims to capture the limiting behavior of the wall turbulence, we report in Table 2.1 the Taylor expansion of each component of velocity in terms of the distance from the wall y.

In the vicinity of the wall, the following relations hold

$$k = \frac{1}{2}\{\langle u'^2 \rangle + \langle v'^2 \rangle + \langle w'^2 \rangle\} \approx \frac{1}{2}(a_1^2 + c_1^2) y^2\,, \tag{2.19}$$

$$\varepsilon = \nu \langle \left(\frac{du'}{dy}\right)^2 + \left(\frac{dv'}{dy}\right)^2 + \left(\frac{dw'}{dy}\right)^2 \rangle \approx \nu(a_1^2 + c_1^2)\,, \tag{2.20}$$

$$\nu_t = \langle u'v' \rangle / \frac{d\langle u \rangle}{dy} \approx \frac{a_1 b_2}{A_1} y^3\,. \tag{2.21}$$

From Equation (2.18) and (2.21), the model function f_μ has to satisfy $f_\mu \propto y^{-1}$ since $k^2/\varepsilon \propto y^4$. The function f_μ has to be modeled to account for the near-wall behavior and low-Reynolds effects, then it might be formulated as a function of the dimensionless wall distance y^+ and turbulent Reynolds

number $R_t = k^2/\nu\varepsilon$, defined using $k^{1/2}$ as velocity scale and $k^{3/2}/\varepsilon$ as length scale. Among the existing low-Reynolds number k-ε models, the model developed by Abe et al. [51] is regarded as one of the most reliable. The model can reproduce the near-wall limiting behavior and provides accurate predictions in both attached and detached wall flows. Most of the low-Reynolds k-ε models fail to predict separating and reattaching flows, since the dimensionless wall distance $y^+ = u_\tau y/\nu$ vanishes around separating and reattaching points where the friction velocity u_τ is zero. From the near-wall expansion, we find that the the friction velocity u_τ, defined in Equation (1.120), is expressed as

$$u_\tau = \sqrt{\frac{\tau_w}{\rho}} = \sqrt{\nu \frac{d\langle u \rangle}{dy}\Big|_{y=0}} = \sqrt{\nu A_1}\,, \tag{2.22}$$

then the velocity scale is determined by the mean velocity component A_1, which vanishes in separating and reattaching points. In [51], Abe et al. proposed to use the Kolmogorov velocity scale $u_\varepsilon = (\nu\varepsilon)^{1/4} \approx \nu^{1/2}(a_1^2 + c_1^2)^{1/4}$ for the definition of the dimensionless wall distance $R_d = y u_\varepsilon/\nu$. Since the Kolmogorov velocity scale u_ε has a finite value near wall, we have $R_d \propto y$ for $y \to 0$. According to [52], the damping function f_μ is modeled as

$$f_\mu = \Big\{1 + \frac{35}{R_t^{3/4}} \exp\Big[-\Big(\frac{R_t}{30}\Big)^{3/4}\Big]\Big\}\Big\{1 - \exp\Big[-\Big(\frac{R_d}{26}\Big)^2\Big]\Big\}\,. \tag{2.23}$$

Away from the wall, where R_t and R_d become large, $f_\mu \approx 1$ then $\nu_t = c_\mu k^2/\varepsilon$, while as the wall is approached, $f_\mu \approx y^{-1}$ and ν_t is reduced. It is necessary to observe that with the Boussinesq assumption of the isotropic model we are not able to capture the near-wall behavior of the stresses $\langle v'v' \rangle \propto y^4$, $\langle u'u' \rangle \propto y^2$ and $\langle w'^2 \rangle \propto y^2$. Indeed, applying (2.1), all the stresses are $\propto y^2$ at the wall, while the turbulent shear stress near-wall behavior is correctly represented $\langle u'v' \rangle \propto y^3$.

In low-Reynolds k-ε models, also the coefficient $c_{\varepsilon 2}$ which appears in the dissipation term of ε Equation (2.11) has to be modeled, since its value is influenced by the near-wall region. In addition, the destruction of dissipation rate $c_{\varepsilon 2}\varepsilon^2/k$ is singular at the wall since ε is finite and k vanishes. Let f_ε be the damping function appearing in the low-Reynolds ε modeled transport equation

$$\frac{D\varepsilon}{Dt} = \frac{\partial}{\partial x_j}\Big[\Big(\nu + \frac{\nu_t}{\sigma_\varepsilon}\Big)\frac{\partial \varepsilon}{\partial x_j}\Big] + c_{\varepsilon 1}\frac{\varepsilon}{k}\mathcal{P} - c_{\varepsilon_2} f_\varepsilon \frac{\varepsilon^2}{k} + c_b \frac{\varepsilon}{k}\mathcal{G}\,. \tag{2.24}$$

From Equation (2.24), the following equation holds at $y = 0$

$$\nu \frac{\partial^2 \varepsilon}{\partial y^2} = c_{\varepsilon 2} f_\varepsilon \frac{\varepsilon^2}{k} \,. \tag{2.25}$$

Since ε and its derivatives are not infinite at the wall, the left-hand side is of order y^0 then $f_\varepsilon \propto y^2$ is required to satisfy equation (2.25). In free turbulence, the limiting behavior requires

$$f_\varepsilon = 1 - 0.3 \exp\Big[- \Big(\frac{R_t}{A_u} \Big)^2 \Big] \,, \tag{2.26}$$

that is of order y^0 near the wall due to the factor 0.3 in front of the exponential term. Thus, the following expression is proposed to respect both near-wall and free turbulence limiting behavior

$$f_\varepsilon = \Big\{ 1 - 0.3 \exp\Big[- \Big(\frac{R_t}{6.5} \Big)^2 \Big] \Big\} \Big\{ 1 - \exp\Big[- \Big(\frac{R_d}{3.7} \Big)^2 \Big] \Big\} \,, \tag{2.27}$$

where the second factor is of order y^2 near the wall then $f_\varepsilon \propto y^2$ as required. The low-Reynolds k-ε model uses the following set of model constants

$$c_\mu = 0.09 \,, \sigma_k = 1.4 \,, \sigma_\varepsilon = 1.4 \,, c_{\varepsilon 1} = 1.5 \,, c_{\varepsilon 2} = 1.9 \,. \tag{2.28}$$

Let us now consider the k-ω derived from the low-Reynolds k-ε model just described. Using the definition reported in Equation (2.13) and substituting in Equation (2.24) we obtain

$$\begin{aligned} \frac{D\omega}{Dt} = \frac{\partial}{\partial x_k} \Big[\Big(\nu + \frac{\nu_t}{\sigma_\omega} \Big) \frac{\partial \omega}{\partial x_k} \Big] + \frac{2}{k} \Big(\nu + \frac{\nu_t}{\sigma_\omega} \Big) \frac{\partial k}{\partial x_j} \frac{\partial \omega}{\partial x_j} + \\ + (c_{\varepsilon 1} - 1) \frac{\omega}{k} \mathcal{P} - (c_{\varepsilon 2} f_\varepsilon - 1) c_\mu \omega^2 + (c_b - 1) \frac{\omega}{k} \mathcal{G} \,, \end{aligned} \tag{2.29}$$

where $c_{\varepsilon 1}$, $c_{\varepsilon 2}$ and f_ε are defined in (2.27) and (2.28).

The isotropic four-parameter turbulence model adopts the expression of ν_t, f_μ and f_ε reported in (2.18), (2.23) and (2.27), respectively. The model can be formulated in terms of k-ε, k-ω or using the logarithmic version of the variables, as presented in [12].

2.2. Eddy thermal diffusivity models

The Reynolds-Averaged energy equation (1.66) contains as additional unknowns the three components of the turbulent heat flux. This term can

be closed at different levels. The most common turbulent heat flux modeling method is based on the generalized gradient diffusion hypothesis (GGDH), which assumes for the unknown turbulent heat flux terms the following relation

$$\langle u_i' T' \rangle = -\alpha_t^{ij} \frac{\partial \langle T \rangle}{\partial x_j} \,, \tag{2.30}$$

where the introduced unknown α_t^{ij} is the tensor of the eddy thermal diffusivities. In most models, the anisotropic eddy thermal diffusivity tensor α_t^{ij} is replaced by an isotropic scalar eddy thermal diffusivity α_t. This means that each heat flux component $\langle u_i' T' \rangle$ is governed by the same eddy thermal conductivity. Moreover, each heat flux component is aligned with the corresponding mean temperature gradient component

$$\langle u_i' T' \rangle = -\alpha_t \frac{\partial \langle T \rangle}{\partial x_i} \,. \tag{2.31}$$

This simplification is usually referred to as the simple gradient diffusion hypothesis (SGDH).

To the best of our knowledge, none of the large commercial codes has up to now a well-validated model for the scalar eddy thermal diffusivity [53]. Almost all the commercial codes apply the Reynolds analogy, which assumes similarity in the turbulent transport features of momentum and heat. According to the Reynolds analogy, the isotropic eddy thermal diffusivity α_t is assumed to be proportional to the eddy viscosity ν_t. The proportionality factor is the inverse of the turbulent Prandtl number Pr_t

$$\langle u_i' T' \rangle = -\frac{\nu_t}{Pr_t} \frac{\partial \langle T \rangle}{\partial x_i} \,, \tag{2.32}$$

so the closure problem is shifted to the unknown proportionality factor Pr_t and the averaged energy equation can be expressed as

$$\frac{D\langle T \rangle}{Dt} = \frac{\partial}{\partial x_i} \left[\left(\alpha + \frac{\nu_t}{Pr_t} \right) \frac{\partial \langle T \rangle}{\partial x_i} \right] . \tag{2.33}$$

The turbulent Prandtl number has been already defined in Equation (1.159) as the ratio of the apparent viscosity to the apparent thermal diffusivity

$$Pr_t = \frac{\nu_t}{\alpha_t} = \frac{\langle u'v' \rangle}{\langle v'T' \rangle} \frac{\partial \langle u \rangle / \partial y}{\partial \langle T \rangle / \partial y} \,. \tag{2.34}$$

Usually, a spatially constant value of $Pr_t = 0.9$ is applied for all types of flows, for all Prandtl numbers, and all Reynolds stress tensor models [53]. From Figure 1.7a,b, we observe that Pr_t is approximately constant for medium and high molecular Prandtl numbers, but for low Prandtl numbers, it depends on many parameters, such as the Reynolds number and the distance from the wall, then more sophisticated closure models are required to overcome the Reynolds analogy deficiencies.

For low Prandtl number fluids, models which solve one, two, or more additional transport equations are preferred. There exist then three-parameter or three-equation turbulence models, where k and ε are used for closing the dynamic turbulence and the temperature variance $k_\theta = \langle T'^2 \rangle / 2$ is solved for the thermal turbulence, and four-parameter or four-equation turbulence models, which solve also for the dissipation rate of the temperature fluctuations ε_θ [9]. Using three or four-equation models, it is possible to express the isotropic scalar eddy thermal diffusivity as

$$\alpha_t = C_\lambda k \tau_m \,, \tag{2.35}$$

where τ_m is the mixed time scale. In three-equation turbulence models τ_m is determined using only the temperature variance k_θ, while in four-equation turbulence models the mixed time scale is evaluated using also the dissipation rate of temperature fluctuations ε_θ [44]. In the following, we focus on four-parameter turbulence models which are employed in the isotropic four-parameter turbulence model.

2.2.1. The k_θ-ε_θ model

The exact transport equation for temperature variance k_θ is reported in Equation (1.97). The production $\mathcal{P}_\theta$, dissipation ε_θ and viscous diffusion terms are in closed forms, whereas the turbulent diffusion term needs to be modeled. In particular, in the framework of the isotropic four-parameter model, and more in general of SGDH models, $\mathcal{P}_\theta$ is expressed as

$$\mathcal{P}_\theta = -\langle u_j' T' \rangle \frac{\partial \langle T \rangle}{\partial x_j} = \alpha_t \frac{\partial \langle T \rangle}{\partial x_j} \frac{\partial \langle T \rangle}{\partial x_j} \,, \tag{2.36}$$

while, according to [11, 4, 12], the turbulent diffusion term is modeled applying a standard gradient diffusion model

$$\mathcal{D}_\theta = \frac{\partial}{\partial x_j} \Big(\alpha \frac{\partial k_\theta}{\partial x_j} - \frac{\langle u_j' T'^2 \rangle}{2} \Big) = \frac{\partial}{\partial x_j} \Big(\alpha \frac{\partial k_\theta}{\partial x_j} + \frac{\alpha_t}{\sigma_{k_\theta}} \frac{\partial k_\theta}{\partial x_j} \Big) \,, \tag{2.37}$$

where σ_{k_θ} is a model constant.

The exact transport equation for the dissipation of temperature variance ε_θ has been derived in Chapter 1 and it is reported in Equation (1.102). The direct mean-field generation terms in the ε_θ are negligible when the turbulence Reynolds number is large, but they become important in the immediate vicinity of the wall because of the sharp decrease of the turbulent Reynolds number $R_t = k^2/\nu\varepsilon$ values. In the isotropic four-parameter model [11, 4, 12], the unknown source and dissipation terms in Equation (1.102) are written as follows

$$\begin{aligned}\mathcal{P}_{1\varepsilon_\theta} + \mathcal{P}_{3\varepsilon_\theta} + \mathcal{P}_{\varepsilon_\theta} - \varepsilon_{\varepsilon_\theta} &= -2\alpha\langle\frac{\partial T'}{\partial x_k}\frac{\partial u_j'}{\partial x_k}\rangle\frac{\partial\langle T\rangle}{\partial x_j} + \\ &- 2\alpha\langle\frac{\partial T'}{\partial x_k}\frac{\partial T'}{\partial x_j}\rangle\frac{\partial\langle u_j\rangle}{\partial x_k} - 2\alpha\langle\frac{\partial T'}{\partial x_k}\frac{\partial u_j'}{\partial x_k}\frac{\partial T'}{\partial x_j}\rangle - 2\alpha^2\langle\Big(\frac{\partial^2 T'}{\partial x_j\partial x_k}\Big)^2\rangle + \\ &= c_{p1}\frac{\varepsilon_\theta}{k_\theta}\mathcal{P}_\theta + c_{p2}\frac{\varepsilon_\theta}{k}\mathcal{P} - c_{d1}\frac{\varepsilon_\theta^2}{k_\theta} - c_{d2}\frac{\varepsilon\varepsilon_\theta}{k}\,,\end{aligned} \tag{2.38}$$

where $\mathcal{P}_\theta = -\langle u_j'T'\rangle\partial\langle T\rangle/\partial x_j$ and $\mathcal{P} = -\langle u_i'u_j'\rangle\partial\langle u_i\rangle/\partial x_j$. The production term $P_{2\varepsilon_\theta}$ is usually neglected. The coefficient c_{d2} is the following model function

$$c_{d2} = \Big\{1.9\Big[1 - 0.3\exp\Big(-\frac{R_t^2}{42.25}\Big)\Big] - 1\Big\}\Big[1 - \exp\Big(-\frac{R_d^2}{25}\Big)\Big]\,, \tag{2.39}$$

while $c_{p1} = 0.925$, $c_{p2} = 0.9$, $c_{d1} = 0.9$ [11, 4, 12]. The turbulent diffusion term is modeled applying the gradient diffusion model, then we have

$$\mathcal{D}_{\varepsilon_\theta} = \frac{\partial}{\partial x_j}\Big(\alpha\frac{\partial\varepsilon_\theta}{\partial x_j} - \langle\varepsilon_\theta' u_j'\rangle\Big) = \frac{\partial}{\partial x_j}\Big(\alpha\frac{\partial\varepsilon_\theta}{\partial x_j} + \frac{\alpha_t}{\sigma_{\varepsilon_\theta}}\frac{\partial\varepsilon_\theta}{\partial x_j}\Big)\,, \tag{2.40}$$

where $\sigma_{\varepsilon_\theta}$ is a model constant. In the isotropic four-parameter turbulence model, σ_{k_θ} and $\sigma_{\varepsilon_\theta}$ are set equal to 1.4 [11, 4, 12]. The modeled equations assume then the following form

$$\frac{\partial k_\theta}{\partial t} + \langle u_j\rangle\frac{\partial k_\theta}{\partial x_j} = \frac{\partial}{\partial x_j}\Big[\Big(\alpha + \frac{\alpha_t}{\sigma_{k_\theta}}\Big)\frac{\partial k_\theta}{\partial x_j}\Big] + \mathcal{P}_\theta - \varepsilon_\theta\,, \tag{2.41}$$

and

$$\begin{aligned}\frac{\partial\varepsilon_\theta}{\partial t} + \langle u_j\rangle\frac{\partial\varepsilon_\theta}{\partial x_j} = \frac{\partial}{\partial x_j}\Big[\Big(\alpha + \frac{\alpha_t}{\sigma_{\varepsilon_\theta}}\Big)\frac{\partial\varepsilon_\theta}{\partial x_j}\Big] + c_{p1}\frac{\varepsilon_\theta}{k_\theta}\mathcal{P}_\theta + c_{p2}\frac{\varepsilon_\theta}{k}\mathcal{P} + \\ - c_{d1}\frac{\varepsilon_\theta^2}{k_\theta} - c_{d2}\frac{\varepsilon\varepsilon_\theta}{k}\,.\end{aligned} \tag{2.42}$$

2.2.2. The k_θ-ω_θ model

In the literature, many applications of k-ω models can be found for the study of dynamical turbulence, but only few applications are present for a k_θ-ω_θ model for thermal turbulence. The k-ω-k_θ-ω_θ turbulence model has been proposed as a possible formulation of the isotropic four-parameter model to overcome the poor numerical convergence that the k-ε-k_θ-ε_θ may show [12]. Let ω_θ be the specific dissipation rate of temperature variance, defined

$$\omega_\theta = \frac{\varepsilon_\theta}{c_\mu k_\theta}\,. \tag{2.43}$$

The k_θ-ω_θ turbulence model has been derived in [12] starting from the k_θ-ε_θ model, specifically substituting the definition of (2.43) into (2.41) and (2.42). The new system of equations is

$$\frac{\partial k_\theta}{\partial t} + \langle u_j\rangle \frac{\partial k_\theta}{\partial x_j} = \frac{\partial}{\partial x_j}\left[\left(\alpha + \frac{\alpha_t}{\sigma_{k_\theta}}\right)\frac{\partial k_\theta}{\partial x_j}\right] + \mathcal{P}_\theta - c_\mu k_\theta \omega_\theta\,, \tag{2.44}$$

$$\begin{aligned}\frac{\partial \omega_\theta}{\partial t} + \langle u_j\rangle \frac{\partial \omega_\theta}{\partial x_j} = \frac{\partial}{\partial x_j}\left[\left(\alpha + \frac{\alpha_t}{\sigma_{\omega_\theta}}\right)\frac{\partial \omega_\theta}{\partial x_j}\right] + \frac{2}{k_\theta}\left(\alpha + \frac{\alpha_t}{\sigma_{\omega_\theta}}\right)\frac{\partial k_\theta}{\partial x_j}\frac{\partial \omega_\theta}{\partial x_j} + \\ + (c_{p1}-1)\frac{\omega_\theta}{k_\theta}\mathcal{P}_\theta + c_{p2}\frac{\omega_\theta}{k}\mathcal{P} - (c_{d1}-1)\omega_\theta^2 - c_{d2}c_\mu\omega_\theta\omega\,.\end{aligned} \tag{2.45}$$

In the k_θ-ω_θ formulation of the isotropic four-parameter model [12], special attention was paid to the model coefficients c_{p1} and c_{d1} since these coefficients must be greater than one to avoid negative model coefficients for the production and dissipation term of ω_θ. The values of these coefficients were then modified from the original k-ε-k_θ-ε_θ model, and they are set $c_{p1} = 1.025$ and $c_{d1} = 1.1$ according to [12]. The model coefficients c_{p2}, c_{d2}, σ_{k_θ} and $\sigma_{\omega_\theta} = \sigma_{\varepsilon_\theta}$ are the ones proposed for the k-ε-k_θ-ε_θ model.

2.2.3. Near-wall treatment

To predict the heat transfer in wall flows, the characteristic time scale τ_m of Equation (2.35) plays a key role. We present the modeling of τ_m as reported in [11, 4, 54, 12, 14, 13]. The mixed time scale τ_m is a function of the time-scale ratio of the thermal to mechanical turbulent time scales

$$R = \tau_\theta/\tau_u = \frac{k_\theta \varepsilon}{k \varepsilon_\theta}\,, \tag{2.46}$$

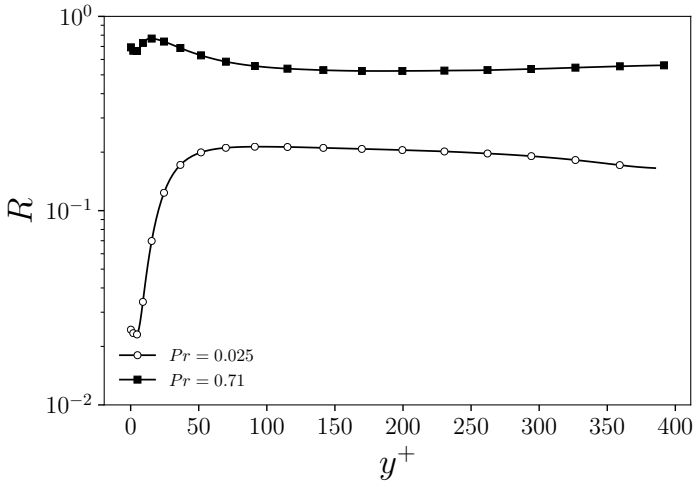

Figure 2.3: time-scale ratio of the thermal to mechanical turbulent time scales R for $Re_\tau = 395$ and $Pr = 0.025, 0.71$ [35].

where $\tau_u = k/\varepsilon$ and $\tau_\theta = k_\theta/\varepsilon_\theta$ are the dynamic and thermal time scales, respectively. In three-equation turbulence models, the time-scale ratio R is assumed as constant, whereas in four-equation turbulence models can be computed by its definition (2.46).

The near-wall Taylor expansion for the mean temperature $\langle T \rangle$ and fluctuating temperature T' is the following

$$\langle T \rangle = A_\theta + B_\theta y + C_\theta y^2 + \dots \qquad T' = a_\theta + b_\theta y + c_\theta y^2 + \dots . \tag{2.47}$$

In the case of a constant wall temperature boundary condition, namely $T = T_w$, the condition must be fulfilled by both temperature and fluctuating values, so that $T' = 0$ and $a_\theta = 0$ along the wall. When a uniform heat flux is imposed at the wall, we have that $A_\theta = 0$ and a_θ can be null or not. If we consider the fluctuations null, we have the following near-wall Taylor expansion

$$\langle T \rangle = B_\theta y + C_\theta y^2 + \dots \qquad T' = b_\theta y + c_\theta y^2 + \dots . \tag{2.48}$$

Thus

$$k_\theta = \frac{1}{2}\langle T'^2 \rangle \approx b_\theta^2 y^2 , \qquad \varepsilon_\theta = \alpha \langle \frac{\partial T'}{\partial x_j} \frac{\partial T'}{\partial x_j} \rangle \approx \alpha b_\theta^2 . \tag{2.49}$$

Thus, recalling (2.19) and (2.20), we can see that R tends exactly to Pr when the wall is approached.

The time-scale ratio R is shown in Figure 2.3 for $Pr = 0.71$ and $Pr = 0.025$. From Figure 2.3 we can see that the wall limiting value of R is equal to the Prandtl number, as already shown from the near-wall Taylor expansion. In the central region, for $Pr = 0.71$ the time-scale ratio R is about 0.5 which is the value usually assumed in three-equation turbulence models [44].

The characteristic time scale τ_m is usually defined as the harmonic average of the dynamical time scale $\tau_u = k/\varepsilon$ and the thermal time scale $\tau_t = k_\theta/\varepsilon_\theta$

$$\tau_m \propto \frac{1}{1/\tau_u + C_m/\tau_t} = \tau_u \frac{R}{C_m + R}\,. \tag{2.50}$$

The shortest time scale among τ_u and τ_t is the most important for turbulent heat flux [55]. In the bulk region, τ_m is independent of the time ratio R, and the turbulent diffusion is assumed to be dominated only by velocity fluctuations. In the bulk region, therefore, we assume $\tau_m \propto \tau_u/Pr_{t,\infty}$, where $Pr_{t,\infty}$ can be assumed constant and uniform or can be modeled, for example by means of Kays model $Pr_t = 0.85 + 0.7/Pr\nu_t$ [56]. A model function in the τ_m expression has been introduced in [11, 4, 12, 13] to account for the wall-proximity effects. For the near-wall region, the characteristic time scale is $\tau_m \propto \sqrt{2R}/PrR_t^{\frac{3}{4}}$. The characteristic thermal time scale is then modeled as

$$\tau_m = \tau_u f_{1t}\Big(\frac{1}{Pr_t} + \frac{2R}{R + C_\gamma} f_{2t} + 1.3\frac{\sqrt{2R}}{PrR_t^{3/4}} f_{3t}\Big)\,, \tag{2.51}$$

where $C_\gamma = 0.25/Pr^{\frac{1}{4}}$. The model function f_{1t} accounts for wall proximity effects

$$f_{1t} = \Big[1 - \exp\Big(-\frac{R_d}{14}\Big)\Big]\Big[1 - \exp\Big(-\frac{\sqrt{Pr}R_d}{14}\Big)\Big]\,. \tag{2.52}$$

The blending functions f_{2t} and f_{3t} have been defined in [11] as

$$f_{2t} = \exp\Big[-\Big(\frac{R_t}{500}\Big)^2\Big]\,,\; f_{3t} = \exp\Big[-\Big(\frac{R_t}{200}\Big)^2\Big]\,. \tag{2.53}$$

The near-wall behavior of the characteristic time scale is $\tau_m \propto y$, thus the isotropic eddy thermal diffusivity α_t is proportional to y^3 from (2.35). When

a uniform heat flux is applied, from Table 2.1 and Equation (2.48), the near-wall behavior of the wall-normal and streamwise turbulent heat fluxes are given by

$$\langle v'T' \rangle = b_2 b_\theta y^3 + \dots , \tag{2.54}$$

$$\langle u'T' \rangle = a_1 b_\theta y^2 + \dots . \tag{2.55}$$

From Equation (2.31), the modeled wall-normal turbulent heat flux is proportional to y^3 in agreement with Equation (2.54). In contrast, the streamwise turbulent heat flux $\langle u'T' \rangle$ near-wall behavior cannot be represented by Equation (2.31) which gives $\langle u'T' \rangle = 0$ along the wall.

2.3. Explicit algebraic stress models

Explicit Algebraic Stress Models (EASM) are special nonlinear eddy viscosity models, where the expansion coefficients in (2.5) are derived starting from Reynolds-stress models. In this section, we report the derivation of algebraic stress models following Pope [29, 57], Gatski et al. [58], Rodi [59] and Abe et al. [52].

By introducing an approximation for the transport terms, a Reynolds-stress model can be reduced to a set of algebraic equations for each component. These equations form an algebraic stress model which implicitly determines the Reynolds stresses as a function of k, ε, and the mean velocity gradient. Because of the approximation involved, the algebraic stress models are less general and accurate than Reynolds-stress models, however, they are widely used because of their simplicity. A standard Reynolds-stress model transport equation is

$$\frac{D\langle u_i' u_j' \rangle}{Dt} - \mathcal{D}_{ij} = \mathcal{P}_{ij} - \varepsilon_{ij} + \Pi_{ij} , \tag{2.56}$$

where the buoyancy source term $\mathcal{G}_{ij}$ is neglected to simplify the derivation. The terms on the right-hand side are local, algebraic functions of $\langle u \rangle$, $\langle p \rangle$, $\langle u_i' u_j' \rangle$ and ε and they do not involve derivatives of the Reynolds stress tensor. In algebraic stress models, the transport terms on the left-hand side, $D\langle u_i' u_j' \rangle / Dt - \mathcal{D}_{ij}$, are approximated by an algebraic expression, so that the whole equation becomes algebraic. The simplest way to model the terms is to neglect them, imposing the equilibrium hypothesis. However, the complete neglect of the transport terms is inconsistent unless $\mathcal{P} = \varepsilon$,

since the half trace of Equation (2.56) is

$$\frac{Dk}{Dt} - \mathcal{D} = \mathcal{P} - \varepsilon\,, \tag{2.57}$$

where $k = \frac{1}{2}\langle u_i' u_i' \rangle$, $\mathcal{D} = \frac{1}{2}\mathcal{D}_{ii}$, $\mathcal{P} = \frac{1}{2}\mathcal{P}_{ii}$ and $\varepsilon = \frac{1}{2}\varepsilon_{ij}$. Rodi introduced the more general weak-equilibrium assumption [59]. The Reynolds stresses can be decomposed as

$$\langle u_i' u_j' \rangle = k\frac{\langle u_i' u_j' \rangle}{k} = k\Big(2b_{ij} + \frac{2}{3}\delta_{ij}\Big)\,, \tag{2.58}$$

where b_{ij} is the normalized anisotropy tensor. Then, the spatial and temporal variations in $\langle u_i' u_j' \rangle$ can be considered to be due to variations in k and b_{ij}. In the weak-equilibrium assumption, the variations in $\langle u_i' u_j' \rangle / k$, or in b_{ij}, are neglected but the variations in $\langle u_i' u_j' \rangle$ due to those in k are considered. This leads to the approximation

$$\frac{D\langle u_i' u_j' \rangle}{Dt} = \frac{\langle u_i' u_j' \rangle}{k}\frac{Dk}{Dt} + k\frac{D}{Dt}\frac{\langle u_i' u_j' \rangle}{k} \approx \frac{\langle u_i' u_j' \rangle}{k}\frac{Dk}{Dt}\,. \tag{2.59}$$

The same approximation applied to the entire transport term brings to

$$\frac{D\langle u_i' u_j' \rangle}{Dt} - \mathcal{D}_{ij} \approx \frac{\langle u_i' u_j' \rangle}{k}\Big(\frac{Dk}{Dt} - \mathcal{D}\Big) = \frac{\langle u_i' u_j' \rangle}{k}(\mathcal{P} - \varepsilon)\,, \tag{2.60}$$

where we have used (2.57). The weak equilibrium assumption (2.60) leads to the general form of the algebraic stress model

$$\frac{\langle u_i' u_j' \rangle}{k}(\mathcal{P} - \varepsilon) = \mathcal{P}_{ij} + \Pi_{ij} - \varepsilon_{ij}\,. \tag{2.61}$$

In physical terms, this is an equilibrium for which convective and transport effects can be neglected. Even though it constitutes an idealization, this equilibrium hypothesis is achievable in physical cases such as the homogeneous shear flow and the logarithmic region of an equilibrium turbulent boundary layer [58]. The mean velocity gradient is usually decomposed into symmetric and antisymmetric parts, $\partial\langle u_i \rangle / \partial x_j = S_{ij} + \Omega_{ij}$, where S_{ij} is the strain-rate tensor and Ω_{ij} is the vorticity tensor

$$S_{ij} = \frac{1}{2}\Big(\frac{\partial\langle u_i \rangle}{\partial x_j} + \frac{\partial\langle u_j \rangle}{\partial x_i}\Big)\,, \quad \Omega_{ij} = \frac{1}{2}\Big(\frac{\partial\langle u_i \rangle}{\partial x_j} - \frac{\partial\langle u_j \rangle}{\partial x_i}\Big)\,. \tag{2.62}$$

The production P_{ij} term of (2.61) can be formulated as

$$\begin{aligned}\mathcal{P}_{ij} &= -\langle u_i' u_k' \rangle \frac{\partial \langle u_j \rangle}{\partial x_k} - \langle u_j' u_k' \rangle \frac{\partial \langle u_i \rangle}{\partial x_k} = \\ &= -2k b_{ik} S_{jk} - 2k b_{jk} S_{ik} - 2k b_{ik} \Omega_{jk} - 2k b_{jk} \Omega_{ik} - \frac{4}{3} k S_{ij} \,.\end{aligned} \tag{2.63}$$

The left-hand side of equation (2.61) can be written as

$$\frac{\langle u_i' u_j' \rangle}{k} (\mathcal{P} - \varepsilon) = 2 b_{ij} (\mathcal{P} - \varepsilon) + \frac{2}{3} \delta_{ij} \mathcal{P} - \frac{2}{3} \delta_{ij} \varepsilon \,, \tag{2.64}$$

where the term $\frac{2}{3}\delta_{ij}\mathcal{P}$ can be formulated taking the half trace of $\mathcal{P}_{ij}$ expressed in Equation (2.63)

$$\frac{2}{3} \delta_{ij} \mathcal{P} = \frac{2}{3} \delta_{ij} P_{ll} = -\frac{4}{3} k \delta_{ij} b_{lm} S_{lm} \,. \tag{2.65}$$

The dissipation rate tensor ε_{ij} can be split into isotropic and deviatoric parts $\varepsilon_{ij} = \frac{2}{3}\delta_{ij}\varepsilon + \varepsilon_{D,ij}$. Then, we obtain

$$\begin{aligned}(\mathcal{P} - \varepsilon) b_{ij} = &-\frac{2}{3} k S_{ij} - k \Big(b_{ik} S_{jk} + b_{jk} S_{ik} - \frac{2}{3} b_{lm} S_{lm} \delta_{ij} \Big) + \\ &- k (b_{ik} \Omega_{jk} + b_{jk} \Omega_{ik}) + \frac{1}{2} \Pi_{ij} - \frac{1}{2} \varepsilon_{D,ij} \,.\end{aligned} \tag{2.66}$$

Let Φ_{ij} be the difference of pressure-strain correlation and the deviatoric part of the dissipation rate tensor $\Phi_{ij} = \Pi_{ij} - \varepsilon_{D,ij}$. In all the commonly used second-order closure models, Φ_{ij} is modeled in the general form [60]

$$\Phi_{ij} = \varepsilon \mathcal{A}_{ij}(\mathbf{b}) + k \mathcal{M}_{ijkl}(\mathbf{b}) \frac{\partial \langle u_k \rangle}{\partial x_l} \,. \tag{2.67}$$

The substitution of (2.67) into (2.66) yields a closed system of algebraic equations for the determination of the Reynolds stress anisotropy tensor and this constitutes the general form of algebraic stress models. These models are implicit, since the Reynolds stress tensor appears on both sides of the equation. If models for Φ_{ij} are linear in the anisotropy tensor $\mathbf{b}$, then it is possible to obtain an explicit expression for b_{ij} in terms of the mean velocity gradients. The procedure is based on techniques from linear algebra. Pope [57] obtained an explicit relation for b_{ij} starting from (2.66) for two-dimensional flows, and Gatski [58] extended the procedure for three-dimensional flows. Explicit models bring considerable savings in

computational cost, avoiding the need for matrix inversions, which is the main drawback of implicit algebraic stress models. Gatski et. al [58] proposed as most general linear in the anisotropy tensor b_{ij} form of (2.67) the following expression

$$\begin{aligned}\Phi_{ij} = &-C_1\varepsilon b_{ij} + C_2 k S_{ij} + C_3 k\Big(b_{ik}S_{jk} + b_{jk}S_{ik} - \frac{2}{3}b_{mn}S_{mn}\delta_{ij}\Big) + \\ &+ C_4 k(b_{ik}\Omega_{jk} + b_{jk}\Omega_{ik})\,,\end{aligned} \tag{2.68}$$

where the closure coefficients can be functions of the invariants of b_{ij}. The direct substitution of (2.68) into (2.66) leads to

$$\begin{aligned}b_{ij} = \frac{1}{2}\tau\Big[&\Big(C_2 - \frac{4}{3}\Big)S_{ij} + (C_4 - 2)(b_{ik}\Omega_{jk} + b_{jk}\Omega_{ik}) + \\ &+ (C_3 - 2)\Big(b_{ik}S_{jk} + b_{jk}S_{ik} - \frac{2}{3}b_{lm}S_{lm}\delta_{ij}\Big)\Big]\,,\end{aligned} \tag{2.69}$$

where the turbulence time scale τ is defined as

$$\tau = \frac{k}{\varepsilon}\Big(\frac{1}{2}C_1 + \frac{\mathcal{P}}{\varepsilon} - 1\Big)^{-1}\,. \tag{2.70}$$

By introducing the dimensionless variables

$$b^*_{ij} = \frac{C_3 - 2}{C_2 - \frac{4}{3}}b_{ij}\,, \quad S^*_{ij} = \frac{1}{2}\tau(2 - C_3)S_{ij}\,, \quad \Omega^*_{ij} = \frac{1}{2}\tau(2 - C_4)\Omega_{ij}\,, \tag{2.71}$$

equation (2.69) reduces to the simpler form

$$b^*_{ij} = -S^*_{ij} - \Big(b^*_{ik}S^*_{jk} + b^*_{jk}S^*_{ik} - \frac{2}{3}b^*_{lm}S^*_{lm}\delta_{ij}\Big) + b^*_{ik}\Omega^*_{kj} + b^*_{jk}\Omega^*_{ki}\,, \tag{2.72}$$

which can be written in matrix form as

$$\mathbf{b}^* = -\mathbf{S}^* - \Big(\mathbf{b}^*\mathbf{S}^* + \mathbf{S}^*\mathbf{b}^* + \frac{2}{3}\{\mathbf{b}^*\mathbf{S}^*\}\mathbf{I}\Big) + \mathbf{b}^*\mathbf{\Omega}^* + \mathbf{\Omega}^*\mathbf{b}^*\,, \tag{2.73}$$

where $\{\cdot\}$ denotes the trace operator, i.e. $\{\mathbf{b}^*\mathbf{S}^*\} = \mathrm{tr}(\mathbf{b}^*\mathbf{S}^*)$, and $\mathbf{I}$ is the unit tensor. According to Gatski et al. [58], the solution of (2.73) can be written as

$$\mathbf{b}^* = \sum_{\lambda} G^{(\lambda)}\mathbf{T}^{(\lambda)}\,, \tag{2.74}$$

where $\mathbf{T}^{(\lambda)}$ is the integrity basis for functions of a symmetric and antisymmetric tensors and $G^{(\lambda)}$ are scalar functions of the irreducible invariants of

$\mathbf{S}^*$ and $\mathbf{\Omega}^*$ [58]. Equation (2.74) means that Reynolds stresses are known functions of a finite number of known tensors $\mathbf{T}^{(\lambda)}$ and the same number of unknown scalars $G^{(\lambda)}$, which are functions of a finite number of known invariants. Since $\mathbf{b}^*$ is symmetric and has zero-trace, the tensors $\mathbf{T}^{(\lambda)}$ are linearly independent symmetric tensors with zero-trace. For two-dimensional flows, there are only three linearly independent tensors that are symmetric and have zero trace [57]

$$\mathbf{T}^{(1)} = \mathbf{S}^*\,, \quad \mathbf{T}^{(2)} = \mathbf{S}^*\mathbf{\Omega}^* - \mathbf{\Omega}^*\mathbf{S}^*\,, \quad \mathbf{T}^{(3)} = \mathbf{S}^{*2} - \frac{1}{3}\{\mathbf{S}^{*2}\}\mathbf{I}\,, \tag{2.75}$$

and there are only two non-zero independent invariants, i.e. $\{\mathbf{S}^{*2}\}$ and $\{\mathbf{\Omega}^{*2}\}$. Then, we have

$$G^{(\lambda)} = G^{(\lambda)}(\{\mathbf{S}^{*2}\}, \{\mathbf{\Omega}^{*2}\})\,, \tag{2.76}$$

with $\lambda = 1, 2, 3$. For the general three-dimensional case there are ten linearly independent tensors

$$\begin{aligned}
&\mathbf{T}^{(1)} = \mathbf{S}^*\,, && \mathbf{T}^{(6)} = \mathbf{\Omega}^{*2}\mathbf{S}^* - \mathbf{S}^*\mathbf{\Omega}^{*2} - \frac{2}{3}\mathbf{I}\{\mathbf{S}^*\mathbf{\Omega}^{*2}\}\,,\\
&\mathbf{T}^{(2)} = \mathbf{S}^*\mathbf{\Omega}^* - \mathbf{\Omega}^*\mathbf{S}^*\,, && \mathbf{T}^{(7)} = \mathbf{\Omega}^*\mathbf{S}^*\mathbf{\Omega}^{*2} - \mathbf{\Omega}^{*2}\mathbf{S}^*\mathbf{\Omega}^*\,,\\
&\mathbf{T}^{(3)} = \mathbf{S}^{*2} - \frac{1}{3}\{\mathbf{S}^{*2}\}\mathbf{I}\,, && \mathbf{T}^{(8)} = \mathbf{S}^*\mathbf{\Omega}^*\mathbf{S}^{*2} - \mathbf{S}^{*2}\mathbf{\Omega}^*\mathbf{S}^*\,,\\
&\mathbf{T}^{(4)} = \mathbf{\Omega}^{*2} - \frac{1}{3}\{\mathbf{\Omega}^{*2}\}\mathbf{I}\,, && \mathbf{T}^{(9)} = \mathbf{\Omega}^{*2}\mathbf{S}^{*2} + \mathbf{S}^{*2}\mathbf{\Omega}^{*2} - \frac{2}{3}\mathbf{I}\{\mathbf{S}^{*2}\mathbf{\Omega}^{*2}\}\,,\\
&\mathbf{T}^{(5)} = \mathbf{\Omega}^*\mathbf{S}^{*2} - \mathbf{S}^{*2}\mathbf{\Omega}^*\,, && \mathbf{T}^{(10)} = \mathbf{\Omega}^*\mathbf{S}^{*2}\mathbf{\Omega}^{*2} - \mathbf{\Omega}^{*2}\mathbf{S}^{*2}\mathbf{\Omega}^*\,,
\end{aligned} \tag{2.77}$$

and five invariants [61]

$$\{\mathbf{S}^{*2}\}\,, \quad \{\mathbf{\Omega}^{*2}\}\,, \quad \{\mathbf{S}^{*3}\}\,, \quad \{\mathbf{\Omega}^{*2}\mathbf{S}^*\}\,, \quad \{\mathbf{\Omega}^{*2}\mathbf{S}^{*2}\}\,, \tag{2.78}$$

then the scalar functions are

$$G^{(\lambda)} = G^{(\lambda)}(\{\mathbf{S}^{*2}\}, \{\mathbf{\Omega}^{*2}\}, \{\mathbf{S}^{*3}\}, \{\mathbf{\Omega}^{*2}\mathbf{S}^*\}, \{\mathbf{\Omega}^{*2}\mathbf{S}^{*2}\})\,, \tag{2.79}$$

with $\lambda = 1, 2, \ldots, 10$. The direct substitution of (2.74) into Equation (2.73) yields

$$\begin{aligned}
\sum_\lambda G^{(\lambda)}\mathbf{T}^{(\lambda)} = &-\sum_\lambda \delta_{1\lambda}\mathbf{T}^{(\lambda)} - \sum_\lambda G^{(\lambda)}\Big(\mathbf{T}^{(\lambda)}\mathbf{S}^* + \mathbf{S}^*\mathbf{T}^{(\lambda)} + \\
&+ \frac{2}{3}\{\mathbf{T}^{(\lambda)}\mathbf{S}^*\}\mathbf{I} - \mathbf{T}^{(\lambda)}\mathbf{\Omega}^* - \mathbf{\Omega}^*\mathbf{T}^{(\lambda)}\Big)\,,
\end{aligned} \tag{2.80}$$

where we have used $\mathbf{S}^* = \mathbf{T}^1$. Since $\mathbf{T}$ is an integrity basis, we can expand any polynomial in $\mathbf{S}^*$ and $\mathbf{\Omega}^*$ in the integrity basis, also the terms on the right-hand side of Equation (2.80). According to Gatski et al. [58], it is possible to define scalar functions H and J as follows

$$\mathbf{T}^{(\lambda)}\mathbf{S}^* + \mathbf{S}^*\mathbf{T}^{(\lambda)} - \frac{2}{3}\{\mathbf{T}^{(\lambda)}\mathbf{S}^*\} = \sum_\gamma H_{\lambda\gamma}\mathbf{T}^{(\gamma)}\,, \tag{2.81}$$

$$\mathbf{T}^{(\lambda)}\mathbf{\Omega}^* + \mathbf{\Omega}^*\mathbf{T}^{(\lambda)} = \sum_\gamma J_{\lambda\gamma}\mathbf{T}^{(\gamma)}\,, \tag{2.82}$$

and substituting into (2.80) gives

$$\sum_\lambda G^{(\lambda)}\mathbf{T}^{(\lambda)} = -\sum_\lambda \delta_{1\lambda}\mathbf{T}^{(\lambda)} - \sum_\lambda G^{(\lambda)}\Big(\sum_\gamma (H_{\lambda\gamma}\mathbf{T}^{(\gamma)} + J_{\lambda\gamma}\mathbf{T}^{(\gamma)})\Big)\,. \tag{2.83}$$

Since the tensors $\mathbf{T}$ are independent, their coefficients on either side of (2.83) may be equated

$$G^{(\lambda)} = -\delta_{1\lambda} - \sum_\gamma G^{(\lambda)}H_{\lambda\gamma} + \sum_\gamma G^{(\lambda)}J_{\lambda\gamma}\,. \tag{2.84}$$

The 10×10 matrices $H_{\lambda\gamma}$ and $J_{\lambda\gamma}$ are reported in the Appendix of [58]. The system (2.84) is a 10×10 linear system of equations for the determination of $G^{(\lambda)}$ which can be written in the matrix form

$$\mathbf{AG} = \mathbf{B}\,, \tag{2.85}$$

where the component of $\mathbf{A}$, $\mathbf{G}$ and $\mathbf{B}$ are given by $A_{\lambda\gamma} = -\delta_{\lambda\gamma} - H_{\lambda\gamma} + J_{\lambda\gamma}$, $G_\lambda = G^{(\lambda)}$, $B_\lambda = \delta_{1\lambda}$. The solution to (2.85) is given by $G^{(\lambda)} = A^{-1}_{\lambda\gamma}B_\lambda$, then in order to obtain the expression of $G^{(\lambda)}$ it is necessary to analytically invert the matrix $\mathbf{A}$. From the inversion of $\mathbf{A}$, Gatski et al. [58] obtained

$$\begin{aligned}
G^{(1)} &= -\frac{1}{2}(6 - 3\{\mathbf{S}^{*2}\} - 21\{\mathbf{\Omega}^{*2}\} - 2\{\mathbf{S}^{*3}\} + 30\{\mathbf{S}^*\mathbf{\Omega}^{*2}\})/D\,,\\
G^{(2)} &= -(3 + 3\{\mathbf{S}^{*2}\} - 6\{\mathbf{\Omega}^{*2}\} + 2\{\mathbf{S}^{*3}\} + 6\{\mathbf{S}^*\mathbf{\Omega}^{*2}\})/D\,,\\
G^{(3)} &= (6 - 3\{\mathbf{S}^{*2}\} - 12\{\mathbf{\Omega}^{*2}\} - 2\{\mathbf{S}^{*3}\} - 6\{\mathbf{S}^*\mathbf{\Omega}^{*2}\})/D\,,\\
G^{(4)} &= -3(3\{\mathbf{S}^{*2}\} + 2\{\mathbf{S}^{*3}\} + 6\{\mathbf{S}^*\mathbf{\Omega}^{*2}\})/D\,,\\
G^{(5)} &= G^{(6)} = -G^{(7)} = -G^{(8)} = -9/D\,,\\
G^{(9)} &= 19/D\,,\ G^{(10)} = 0\,,
\end{aligned} \tag{2.86}$$

where the denominator D is given by

$$\begin{aligned}
D = 3 &- \frac{7}{2}\{\mathbf{S}^{*2}\} + \{\mathbf{S}^{*2}\}^2 - \frac{15}{2}\{\mathbf{\Omega}^{*2}\} - 8\{\mathbf{S}^{*2}\}\{\mathbf{\Omega}^{*2}\} + 3\{\mathbf{\Omega}^{*2}\}^2\\
&- \{\mathbf{S}^{*3}\} + \frac{2}{3}\{\mathbf{\Omega}^{*2}\}\{\mathbf{S}^{*3}\} + 21\{\mathbf{S}^*\mathbf{\Omega}^{*2}\} + 24\{\mathbf{S}^{*2}\mathbf{\Omega}^{*2}\}\\
&+ 2\{\mathbf{S}^{*2}\}\{\mathbf{S}^*\mathbf{\Omega}^{*2}\} - 6\{\mathbf{\Omega}^{*2}\}\{\mathbf{S}^*\mathbf{\Omega}^{*2}\}\,.
\end{aligned} \tag{2.87}$$

To obtain the three-dimensional form of $\mathbf{b}^*$ it is necessary to expand the expression reported in Equation (2.74) using the integrity basis of (2.77) and the coefficients of (2.86). We do not report the three-dimensional form of $\mathbf{b}^*$ because of the complexity of its expression. The three-dimensional form reduces to Pope's form in the two-dimensional limit, where the invariants $\{\mathbf{S}^{*3}\}$ and $\{\mathbf{S}^*\mathbf{\Omega}^{*2}\}$ are zero and $\{\mathbf{S}^{*2}\mathbf{\Omega}^{*2}\}$ becomes equal to $\frac{1}{2}\{\mathbf{S}^{*2}\}\{\mathbf{\Omega}^{*2}\}$ [57]. Using this reduction and the integrity basis (2.75), the resulting expression for $G^{(\lambda)}$ in the two-dimensional limit becomes

$$\begin{aligned} G^{(1)} &= -\frac{3}{3-2\{\mathbf{S}^{*2}\}-6\{\mathbf{\Omega}^{*2}\}}\,, \quad G^{(2)} = -\frac{3}{3-2\{\mathbf{S}^{*2}\}-6\{\mathbf{\Omega}^{*2}\}}\,, \\ G^{(3)} &= \frac{6}{3-2\{\mathbf{S}^{*2}\}-6\{\mathbf{\Omega}^{*2}\}}\,. \end{aligned} \tag{2.88}$$

Expanding Equation (2.74) in the two-dimensional case, the following formal expression for the anisotropy tensor $\mathbf{b}^*$ can be obtained [57]

$$\mathbf{b}^* = \frac{3(-\mathbf{S}^* - \mathbf{S}^*\mathbf{\Omega}^* + \mathbf{\Omega}^*\mathbf{S}^* + 2\mathbf{S}^{*2} - 2\{\mathbf{S}^{*2}\}\mathbf{I}/3)}{3-2\{\mathbf{S}^{*2}\}-6\{\mathbf{\Omega}^{*2}\}}\,. \tag{2.89}$$

The Reynolds-stress expression given by Equation (2.89) is expected to apply to many types of turbulent flows not deviating from the equilibrium state. However, this model cannot express the correct turbulent phenomena in the near-wall region where both molecular and turbulent diffusion becomes large and the flow greatly deviates from the local equilibrium state. In other words, the characteristic time scale given by Equation (2.70) is not appropriate to represent the near-wall behavior of turbulence. Moreover, mathematical inaccuracies may occur with the increase of $\{\mathbf{S}^{*2}\}$ because the denominator of the coefficients $G^{(\lambda)}$ can be zero or negative. This may happen in complex non-equilibrium turbulent flows with large strain rates. Also, this is an issue for the calculation of turbulent flows that achieve equilibrium but it is necessary to compute through a transient state which is far from the equilibrium. Thus, there is the need to regularize the explicit algebraic stress model. We rewrite the coefficient on the right-hand side of Equation (2.89)

$$\frac{3}{3-2\{\mathbf{S}^{*2}\}-6\{\mathbf{\Omega}^{*2}\}} = \frac{3}{3-2S^{*2}+6\Omega^{*2}}\,, \tag{2.90}$$

where

$$S^{*2} = S^*_{ij}S^*_{ij} = \{\mathbf{S}^{*2}\}\,, \quad \Omega^{*2} = \Omega^*_{ij}\Omega^*_{ij} = -\{\mathbf{\Omega}^{*2}\}\,. \tag{2.91}$$

It is clear from (2.90) that for sufficiently large strain rates singularities can occur and, on the other hand, the rotational strains do not cause any problem. We rewrite the right-hand side of equation (2.90) as

$$\frac{3}{3-2S^{*2}+6\Omega^{*2}} = \frac{1}{1+\frac{22}{3}(\frac{\Omega^{*2}}{4})+\frac{2}{3}(\frac{\Omega^{*2}}{4}-S^{*2})}\,. \tag{2.92}$$

The parameter $(\Omega^{*2}/4 - S^{*2})$ is one of the most important measures in turbulence because it indicates how the flow field deviates from the condition of pure shear flow. In a pure shear flow, only S_{12}, $S_{21} = S_{12}$, $\Omega_{12} = S_{12}$ and $\Omega_{21} = -S_{12}$ exist so that $(\Omega^{*2}/4 - S^{*2}) = 0$. When the flow greatly deviates from pure shear flow, the normal strain rate may be much larger than the shear strain rate, resulting in $S^{*2} \gg \Omega^{*2}/4$ and this can lead to improper or singular behavior. On that basis, Abe et al. [52] modified (2.92) introducing the model function f_B to guarantee non-negative turbulent intensities under the condition $S^{*2} \gg \Omega^{*2}/4$

$$\frac{1}{1+\frac{22}{3}(\frac{\Omega^{*2}}{4})+\frac{2}{3}(\frac{\Omega^{*2}}{4}-S^{*2})f_B}\,. \tag{2.93}$$

The effect of f_B disappears in pure shear flows, such as fully developed channel flow and homogeneous shear flow, then Abe et. al [52] adopted the following formulation which satisfies this requirement

$$f_B = 1 + C_\eta\Big(\frac{\Omega^{*2}}{4} - S^{*2}\Big)\,, \tag{2.94}$$

where C_η is a model constant.

With the modification proposed in (2.93), the mathematical inaccuracies occurring when $S^{*2} \gg 0$ are prevented. However, the model is still unable to represent the near-wall turbulence. Abe et al, [52] proposed modifications on the turbulence time scale τ and on coefficients of (2.71) to account for the near-wall and low-Reynolds number effects leading to an appropriate expression in both homogeneous and wall turbulent shear flows. The final expression of the normalized anisotropy tensor is

$$b^*_{ij} = \frac{-S^*_{ij} - (S^*_{ik}\Omega^*_{kj} - \Omega^*_{ik}S^*_{kj}) + 2(S^*_{ik}S^*_{kj} - S^*_{mn}S^*_{mn}\delta_{ij}/3)}{1+\frac{22}{3}(\frac{\Omega^{*2}}{4})+\frac{2}{3}(\frac{\Omega^{*2}}{4}-S^{*2})f_B}\,, \tag{2.95}$$

where the dimensionless forms are

$$b^*_{ij} = C_D b_{ij}\,, \quad S^*_{ij} = C_D\tau S_{ij}\,, \quad \Omega^*_{ij} = 2C_D\tau\Omega_{ij}\,, \tag{2.96}$$

with C_D a model constant. The near-wall and low-Reynolds number effects can be modeled through the definition of the characteristic time scale of turbulence τ according to [52, 62, 63].

2.4. Explicit algebraic heat flux model

Beyond the turbulent heat flux models based on the Generalized and Simple Gradient Diffusion Hypothesis, there is a class of models that helps to get rid of the gradient assumption. This class is named Algebraic Heat Flux Models (AHFM), and through this approach it is possible to model the turbulent heat flux in convection flows in which temperature gradients become approximately zero. The exact transport equation for turbulent heat flux is given by Equation (1.90), and neglecting the buoyancy source term it can be expressed in the more compact form

$$\frac{D\langle u_i' T'\rangle}{Dt} - \mathcal{D}_{i\theta} = \mathcal{P}_{i\theta} - \varepsilon_{i\theta} + \Pi_{i\theta}\,. \tag{2.97}$$

Following the procedure presented by Abe et al. [62], we define the normalized heat flux a_j^* as $a_j^* = \langle u_j' T'\rangle / \sqrt{k k_\theta}$. Then, the spatial and temporal variations in $\langle u_j' T'\rangle$ can be considered to be due to variations in k, k_θ and a_j^*. According to the weak-equilibrium assumption already used for the derivation of the Algebraic Stress Model, the variations in a_j^* are neglected but the variations in $\langle u_j' T'\rangle$ due to those in k and k_θ are considered [34]. This leads to the approximation

$$\begin{aligned}\frac{D\langle u_j' T'\rangle}{Dt} = \frac{D(a_j^*\sqrt{k k_\theta})}{Dt} = a_j^*\sqrt{k_\theta}\frac{D\sqrt{k}}{Dt} + a_j^*\sqrt{k}\frac{D\sqrt{k_\theta}}{Dt} + \\ + \sqrt{k k_\theta}\frac{Da_j^*}{Dt} \approx a_j^*\frac{\sqrt{k_\theta}}{2\sqrt{k}}\frac{Dk}{Dt} + a_j^*\frac{\sqrt{k}}{2\sqrt{k_\theta}}\frac{Dk_\theta}{Dt}\,.\end{aligned} \tag{2.98}$$

The same approximation applied to the entire transport term brings to

$$\begin{aligned}\frac{D\langle u_i' T'\rangle}{Dt} - \mathcal{D}_{i\theta} \approx a_j^*\frac{\sqrt{k_\theta}}{2\sqrt{k}}(\mathcal{P} - \varepsilon) + a_j^*\frac{\sqrt{k}}{2\sqrt{k_\theta}}(\mathcal{P}_\theta - \varepsilon_\theta) = \\ \frac{a_j^*\sqrt{k k_\theta}}{2}\Big[\frac{1}{\tau_u}\Big(\frac{\mathcal{P}}{\varepsilon} - 1\Big) + \frac{1}{\tau_\theta}\Big(\frac{\mathcal{P}_\theta}{\varepsilon_\theta} - 1\Big)\Big]\,.\end{aligned} \tag{2.99}$$

The use of the weak equilibrium assumption (2.99) leads to the general form of the algebraic turbulent heat flux model

$$\frac{a_j^*\sqrt{k k_\theta}}{2}\Big[\frac{1}{\tau_u}\Big(\frac{\mathcal{P}}{\varepsilon} - 1\Big) + \frac{1}{\tau_\theta}\Big(\frac{\mathcal{P}_\theta}{\varepsilon_\theta} - 1\Big)\Big] = \mathcal{P}_{j\theta} + \Pi_{j\theta} - \varepsilon_{j\theta}\,, \tag{2.100}$$

where $\mathcal{P}_{j\theta} = -\langle u'_k T' \rangle \partial \langle u_j \rangle / \partial x_k - \langle u'_k u'_j \rangle \partial \langle T \rangle / \partial x_k$ is the production term of the turbulent heat flux and it is in a closed form, while for the pressure temperature gradient correlation $\Pi_{j\theta}$ and the dissipation rate $\varepsilon_{j\theta}$ closure models are required. The most general linear expression for the term $\Pi_{j\theta} - \varepsilon_{j\theta}$ was proposed by Launder [34]

$$\Pi_{j\theta} - \varepsilon_{j\theta} = -c_{t1} \frac{\langle u'_j T' \rangle}{\tau_u} + c_{t2} \langle u'_k T' \rangle \frac{\partial \langle u_j \rangle}{\partial x_k} + c_{t3} \langle u'_k T' \rangle \frac{\partial \langle u_k \rangle}{\partial x_j}\,, \tag{2.101}$$

where c_{t1}, c_{t2} and c_{t3} are model constants. Recalling the decomposition of Reynolds stresses into isotropic and anisotropic parts reported in Equation (2.58), $\langle u'_i u'_j \rangle = 2/3 k \delta_{ij} + 2 k b_{ij}$, the right-hand side of (2.100) can be reformulated as

$$\begin{aligned} \mathcal{P}_{j\theta} + \Pi_{j\theta} - \varepsilon_{j\theta} = & -a^*_k \sqrt{k k_\theta} (S_{jk} + \Omega_{jk}) + \\ & - \Big(\frac{2}{3} k \delta_{jk} + 2 k b_{jk} \Big) \frac{\partial \langle T \rangle}{\partial x_k} - c_{t1} a^*_j \frac{\sqrt{k k_\theta}}{\tau_u} + \\ & + c_{t2} a^*_k \sqrt{k k_\theta} (S_{jk} + \Omega_{jk}) + c_{t3} a^*_k \sqrt{k k_\theta} (S_{kj} + \Omega_{jk})\,. \end{aligned} \tag{2.102}$$

The term in a^*_j can be moved into the left-hand side of Equation (2.100), then after some manipulations Abe et al. [62] obtained

$$\begin{aligned} \frac{c_{t1}}{\tau_u} \Big[1 + \frac{1}{2 c_{t1}} \Big(\frac{\mathcal{P}}{\varepsilon} - 1 \Big) + \frac{1}{2 c_{t1} R} \Big(\frac{\mathcal{P}_\theta}{\varepsilon_\theta} - 1 \Big) \Big] a^*_j = & \\ = -\frac{2}{3} (3 b_{jk} + \delta_{jk}) \frac{\sqrt{k}}{\sqrt{k_\theta}} \frac{\partial \langle T \rangle}{\partial x_k} + [(c_{t2} - 1)(S_{jk} + \Omega_{jk}) + & \\ + c_{t3} (S_{jk} - \Omega_{jk})] a^*_k\,. & \end{aligned} \tag{2.103}$$

Introducing $c_{T1} = 1/c_{t1}$, $c_{T2} = (1 - c_t 2)/c_{t1}$, $c_{T3} = c_{t3}/c_{t1}$ and

$$\tau_m = \tau_u \Big\{ 1 + \frac{1}{2 c_{t1}} \Big(\frac{\mathcal{P}}{\varepsilon} - 1 \Big) + \frac{1}{2 c_{t1} R} \Big(\frac{\mathcal{P}_\theta}{\varepsilon_\theta} - 1 \Big) \Big\}^{-1}\,, \tag{2.104}$$

equation (2.103) can be rewritten as

$$\begin{aligned} a^*_j = -\frac{2}{3} c_{T1} (3 b_{jk} + \delta_{jk}) \tau_m \frac{\sqrt{k}}{\sqrt{k_\theta}} \frac{\partial \langle T \rangle}{\partial x_k} - [(c_{T2} - c_{T3}) \tau_m S_{jk} + & \\ + (c_{T2} + c_{T3}) \tau_m \Omega_{jk}] a^*_k\,. & \end{aligned} \tag{2.105}$$

The expression obtained in Equation (2.105) represents the implicit form of the Algebraic Stress Models since the normalized turbulent heat flux

appears on both sides of the equation. The following normalized variables are introduced

$$b^*_{jk} = 3b_{jk}\,, \quad S^*_{jk} = (c_{T2} - c_{T3})\tau_m S_{jk}\,, \quad \Omega^*_{jk} = (c_{T2} + c_{T3})\tau_m \Omega_{jk}\,, \\ \frac{\partial \langle T \rangle}{\partial x_k}^* = \frac{2}{3} c_{T1} \tau_m \frac{\sqrt{k}}{\sqrt{k_\theta}} \frac{\partial \langle T \rangle}{\partial x_k}\,, \tag{2.106}$$

thus (2.105) reduces to the simplified form

$$a^*_j = -(b^*_{jk} + \delta^*_{jk}) \frac{\partial \langle T \rangle}{\partial x_k}^* - (S^*_{jk} + \Omega^*_{jk}) a^*_k\,. \tag{2.107}$$

In the two-dimensional space, the explicit expression for the normalized turbulent heat flux can be obtained [62]

$$a^*_j = \frac{2[-(\delta_{jk} + b^*_{jk}) + (\delta_{lk} + b^*_{lk})(S^*_{jl} + \Omega^*_{jl})]}{2 + \Omega^{*2} - S^{*2}} \frac{\partial \langle T \rangle}{\partial x_k}^*\,, \tag{2.108}$$

where Ω^{*2} and S^{*2} are defined in Equation (2.91). Explicit Algebraic Heat Flux Models (EAHFM) are based on Equation (2.108).

The expression that we have obtained following [62] is expected to apply to various types of turbulent heat transfer fields not deviating from the equilibrium state. This model, however, may not express the correct turbulent heat transfer phenomena in the near-wall region where the viscous and turbulent diffusion becomes dominant and the heat transfer greatly deviates from the local equilibrium state. Thus, the characteristic time scale given by Equation (2.104) is not appropriate to represent the near-wall turbulent heat transfer.

2.5. The anisotropic four-parameter model

In this section, we finally present the anisotropic four-parameter turbulence model (A4P) developed and implemented in the multigrid finite element code FEMuS of the numerical platform FemusPlatform [15] for the flow and heat transfer modeling in low Prandtl number fluids. Throughout this chapter, we have presented linear eddy viscosity and SGDH models that are the most used and implemented in commercial codes. In particular, we have described the several forms of the isotropic four-parameter model [12, 13] already implemented in FEMuS. The abovementioned models present drawbacks and deficiencies for the modeling of complex and anisotropic flows, such as wall-bounded flows [9].

To capture the anisotropy in the fluids, we need to leave the assumption of isotropic eddy viscosity. Reynolds-stress models would be the best choice, but they would involve a not negligible computational effort [9]. Algebraic stress models are a calibrated compromise between the accuracy of Reynolds-stress models and the simplicity of eddy viscosity models. Thus, in the anisotropic version of the four-parameter model, we adopt an algebraic model for the Reynolds stress closure.

For heat transfer modeling, few models have been developed so far. Most commercial codes are based on Reynolds Analogy and the assumption of a constant turbulent Prandtl number [9]. This assumption is acceptable for fluids with Pr number around the unity, but it is inconsistent for fluids with a Prandtl number that deviates considerably from unity [53]. Moreover, the usual assumption of alignment between the mean temperature gradient and the turbulent heat flux components leads to total underpredictions in convection cases in which gradients are approximately zero [9]. Starting from the isotropic four-parameter model, we adopt an explicit algebraic model for the turbulent heat flux closure.

One of the aims of this Ph.D. thesis is deriving, presenting, and validating the new anisotropic turbulence model which employs explicit algebraic models for Reynolds stresses and turbulent heat fluxes and uses four parameters for determining the characteristic dynamic and thermal time scales. In the previous section, the basis of the anisotropic four-parameter model has been introduced, and in the next paragraphs, a complete description of the model is proposed. Moreover, in Chapter 3, a validation of the new turbulence model is presented.

2.5.1. Dynamic turbulence modeling

The governing equations for the velocity field are written as

$$\frac{\partial u_i}{\partial x_i} = 0\,, \tag{2.109}$$

$$\frac{Du_i}{Dt} = -\frac{1}{\rho}\frac{\partial p}{\partial x_i} + \frac{\partial}{\partial x_j}\Big[\nu\Big(\frac{\partial u_i}{\partial x_j} + \frac{\partial u_j}{\partial x_i}\Big) - \langle u_i' u_j' \rangle\Big]\,. \tag{2.110}$$

For the closure of the Reynolds-Averaged Navier-Stokes equation, we use the Explicit Algebraic Stress Model derived in the previous sections under the hypothesis of local equilibrium. Following Hattori et al. [63], we can

write the dimensional form of the explicit algebraic stress model as follows

$$\begin{aligned}\langle u_i' u_j' \rangle = &\frac{2}{3} k \delta_{ij} - \frac{2\nu_t}{f_R} S_{ij} + \\ &- \frac{4 C_D k f_\tau}{f_R} \Big(S_{ik}\Omega_{kj} - \Omega_{ik} S_{kj} - S_{ik} S_{kj} + \frac{1}{3} S^2 \delta_{ij} \Big) ,\end{aligned} \tag{2.111}$$

where $C_D = 0.8$, f_R is given by

$$f_R = 1 + \frac{22}{3} (C_D \tau_{R_0})^2 \Omega^2 + \frac{2}{3} (C_D \tau_{R_0})^2 (\Omega^2 - S^2) f_B \,, \tag{2.112}$$

and the quantity τ_{R_0} is the characteristic time scale of turbulence defined as $\tau_{R_0} = \nu_t / k$, where ν_t has been defined in (2.18), as $c_\mu f_\mu k^2 / \varepsilon$. The values assigned to the constant c_μ is the standard value 0.09 and the damping function f_μ is the one reported in Equation (2.23), according to [52].

The function f_τ has been introduced by Hattori et al. [63] and reproduces the wall-limiting behavior and anisotropy of the Reynolds normal stress components near the wall. It is defined as

$$f_\tau = \tau_{R_0}^2 + \tau_{R_W}^2 \,, \tag{2.113}$$

where τ_{R_W} is the wall reflection time scale, defined in [63] as

$$\tau_{R_W} = \sqrt{\frac{f_R}{6 C_D f_{S\Omega}}} \Big(1 - \frac{3 C_{v1} f_{v2}}{8} \Big) f_{v1}^2 \,, \tag{2.114}$$

where $f_{v2} = 1 - \exp(-\sqrt{R_t}/100)$ [63], $f_{v1} = \exp(-R_{tm}^2/2025)$ [64], and $C_{v1} = 0.4$ [65, 63, 64]. In the model function f_{v1}, the modified Reynolds number R_{tm} appears and it has been defined in [63] as follows

$$R_{tm} = \frac{130 R_d R_t^{\frac{1}{4}}}{130 R_t^{\frac{1}{4}} + R_d} \,. \tag{2.115}$$

The modeling of the function $f_{S\Omega}$ is a crucial aspect. In [63] the following expression is suggested for $f_{S\Omega}$

$$f_{S\Omega} = \frac{\Omega^2}{2} + \frac{S^2}{3} - \Big[\Big(\sqrt{\frac{S^2}{2}} - \sqrt{\frac{\Omega^2}{2}} \Big) f_w(1) \Big]^2 , \tag{2.116}$$

with $f_w(1) = \exp(-R_{tm}^2)$.

Once the model for $\langle u_i' u_j' \rangle$ and ν_t is chosen, it is necessary to compute the variables appearing in the model functions, in particular the turbulent

kinetic energy k and the characteristic time scale τ_u. We use the logarithmic turbulence model K-Ω proposed in [13, 16], which improves the stability of a standard k-ω model since the state variables are maintained always positive during the solution process [66]. This is important because the eddy viscosity may assume negative values compromising the stability of the numerical solution algorithm. The specific dissipation rate of turbulent kinetic energy ω and the logarithmic form of k and ω are defined as

$$\omega = \frac{\varepsilon}{c_\mu k}, \quad \Omega = \ln(\omega)\,, \quad K = \ln(k)\,. \tag{2.117}$$

The system of equations for the K-Ω model is the following

$$\begin{aligned} \frac{DK}{Dt} = \frac{\partial}{\partial x_i}\Big[\Big(\nu + \frac{\nu_t}{\sigma_k}\Big)\frac{\partial K}{\partial x_i}\Big] + \Big(\nu + \frac{\nu_t}{\sigma_k}\Big)\frac{\partial K}{\partial x_i}\frac{\partial K}{\partial x_i} + \\ + \frac{\mathcal{P}}{e^K} + \frac{\mathcal{G}}{e^K} - c_\mu e^{\Omega}\,, \end{aligned} \tag{2.118}$$

$$\begin{aligned} \frac{D\Omega}{Dt} = \frac{\partial}{\partial x_i}\Big[\Big(\nu + \frac{\nu_t}{\sigma_\omega}\Big)\frac{\partial \Omega}{\partial x_i}\Big] + \Big(\nu + \frac{\nu_t}{\sigma_\omega}\Big)\frac{\partial \Omega}{\partial x_i}\frac{\partial \Omega}{\partial x_i} + \\ + \frac{\mathcal{P}}{e^K}(c_{\varepsilon 1} - 1) + 2\Big(\nu + \frac{\nu_t}{\sigma_\omega}\Big)\frac{\partial K}{\partial x_i}\frac{\partial \Omega}{\partial x_i} + \\ + (c_b - 1)\frac{\mathcal{G}}{e^K} - c_\mu(c_{\varepsilon 2} f_\varepsilon - 1)e^{\Omega}\,. \end{aligned} \tag{2.119}$$

where $\mathcal{P} = -\langle u_i' u_j'\rangle \partial u_i/\partial x_j$is the production rate of turbulent kinetic energy and $\mathcal{G} = -\beta g_i \langle u_i' T'\rangle$ is the source term for buoyant flows. We recall from [12, 13, 14, 16] the model constant values $\sigma_k = \sigma_\omega = 1.4$, $c_{\varepsilon 1} = 1.9$, $c_{\varepsilon 2} = 1.5$, $c_b = 1.2$, $c_\mu = 0.9$, while the model function f_ε is given in (2.27).

2.5.2. Thermal turbulence modeling

The governing equation for the mean temperature field can be written as

$$\frac{DT}{Dt} = \frac{\partial}{\partial x_i}\Big(\alpha \frac{\partial T}{\partial x_i} - \langle u_i' T'\rangle\Big) + \frac{Q}{\rho c}\,. \tag{2.120}$$

For the closure of the Reynolds-Averaged energy equation, we use the Explicit Algebraic Heat Flux model derived in the previous sections. Recalling the definitions in (2.106), the Equation (2.108) can be written in the dimensional form

$$\begin{aligned} \langle u_j' T'\rangle = \frac{c_{T1}\tau_m}{f_{RT}}\Big\{ - \delta_{jl} + \\ \tau_m[(c_{T2} + c_{T3})\Omega_{jl} + (c_{T2} - c_{T3})S_{jl}]\Big\}\langle u_l' u_k'\rangle \frac{\partial \langle T\rangle}{\partial x_k}\,, \end{aligned} \tag{2.121}$$

where $c_{T1} = 0.18$, $c_{T2} = 0.18$, and $c_{T3} = 0.02$ [62] are model constants and the coefficient f_{RT} is given by the following expression proposed in [62]

$$f_{RT} = 1 + \frac{1}{2}\tau_m^2[(c_{T2} + c_{T3})^2\Omega^2 - (c_{T2} - c_{T3})^2 S^2]\,. \tag{2.122}$$

In contrast to conventional models, the turbulent heat fluxes and the mean temperature gradient components in (2.121) are not necessary aligned because of the effects of the mean shear rate and anisotropy in the flow field. This expression is closely related to the existing models. When considering only the first term of (2.121), the Generalized Gradient Diffusion Hypothesis (GGDH) model is obtained

$$\langle u_j' T' \rangle = -\frac{c_{T1}\tau_m}{f_{RT}} \langle u_j' u_k' \rangle \frac{\partial \langle T \rangle}{\partial x_k}\,. \tag{2.123}$$

Comparing (2.123) with (2.30), the eddy thermal diffusivities are given by

$$\alpha_t^{ij} = \frac{c_{T1}\tau_m}{f_{RT}} \langle u_j' u_k' \rangle\,. \tag{2.124}$$

To predict the heat transfer in both free and wall turbulent flows, we use the characteristic time scale of the isotropic four-parameter model reported in (2.51) which appropriately represents heat transfer phenomena for low Prandtl number fluids. In order to evaluate k_θ and ε_θ appearing in the model functions, we use the logarithmic K_θ-Ω_θ turbulence model proposed in [16, 13], where K_θ and Ω_θ represent the logarithmic values of mean temperature fluctuations k_θ and its dissipation rate ω_θ, defined as $\omega_\theta = \varepsilon_\theta / c_\mu k_\theta$. According to [13], the transport equations for the logarithmic quantities can be written as

$$\begin{aligned} \frac{DK_\theta}{Dt} = \frac{\partial}{\partial x_i}\left[\left(\alpha + \frac{\alpha_t}{\sigma_{k\theta}}\right)\frac{\partial K_\theta}{\partial x_i}\right] + \left(\alpha + \frac{\alpha_t}{\sigma_{k\theta}}\right)\frac{\partial K_\theta}{\partial x_i}\frac{\partial K_\theta}{\partial x_i} + \\ + \frac{\mathcal{P}_\theta}{e^{K_\theta}} - c_\mu e^{\Omega_\theta}\,, \end{aligned} \tag{2.125}$$

$$\begin{aligned} \frac{D\Omega_\theta}{Dt} = \frac{\partial}{\partial x_i}\left[\left(\alpha + \frac{\alpha_t}{\sigma_{\omega_\theta}}\right)\frac{\partial \Omega_\theta}{\partial x_i}\right] + \left(\alpha + \frac{\alpha_t}{\sigma_{\omega_\theta}}\right)\frac{\partial \Omega_\theta}{\partial x_i}\frac{\partial \Omega_\theta}{\partial x_i} + \\ 2\left(\alpha + \frac{\alpha_t}{\sigma_{\omega_\theta}}\right)\frac{\partial K_\theta}{\partial x_i}\frac{\partial \Omega_\theta}{\partial x_i} + \frac{\mathcal{P}_\theta}{e^{K_\theta}}(c_{p1} - 1) + \\ -(c_{d1} - 1)c_\mu e^{\Omega_\theta} - c_{d2}c_\mu e^{\Omega} + c_{p2}\frac{\mathcal{P}}{e^K}\,, \end{aligned} \tag{2.126}$$

where $\mathcal{P}_\theta = -\langle u_j' T' \rangle \partial T/\partial x_j$, $\mathcal{P} = -\langle u_i' u_j' \rangle \partial u_i/\partial x_j$ and c_{d2} is the following model function

$$c_{d2} = \Big\{1.9\Big[1 - 0.3\exp\Big(-\frac{R_t^2}{42.25}\Big)\Big] - 1\Big\}\Big[1 - \exp\Big(-\frac{R_d^2}{25}\Big)\Big]\,, \quad (2.127)$$

while $c_{p1} = 1.025$, $c_{p2} = 0.9$, $c_{d1} = 1.1$, and $\sigma_{k_\theta} = \sigma_{\omega_\theta} = 1.4$ [12, 16, 14, 13]. The eddy thermal diffusivity appearing in the diffusive terms of (2.125) and (2.126) is simplified as the scalar quantity $\alpha_t = c_\lambda k \tau_m$ of Equation (2.35), with $c_\lambda = 0.1$.

2.5.3. Boundary conditions

In this subsection, we describe the boundary conditions that can be imposed on the state variables of the turbulence model. When a near-wall approach with no wall functions is used, the boundary conditions can be computed by a near-wall Taylor series expansion for the turbulence variables. For the description of the boundary conditions we refer to the case of the plane channel of Figure 1.1, where y is the wall distance, x is the streamwise coordinate, and z is the spanwise one. Moreover, v, u, and w are respectively the wall-normal, streamwise, and spanwise velocity components. In Table 2.1 we have reported the expansion for the mean and fluctuating velocity. Following the definitions, we obtain the following dynamical turbulence variable expansions

$$k_w \approx \frac{1}{2}(a_1^2 + c_1^2)y^2 = \frac{1}{2}\xi y^2\,, \quad K_w \approx \ln\Big(\frac{1}{2}\xi y^2\Big)\,, \quad (2.128)$$

$$\varepsilon_w \approx \nu(a_1^2 + c_1^2) = \nu\xi\,, \quad (2.129)$$

$$\omega_w \approx \frac{2\nu}{c_\mu y^2}\,, \quad \Omega_w \approx \ln\Big(\frac{2\nu}{c_\mu y^2}\Big)\,, \quad (2.130)$$

where the lower-script w means the near-wall behavior. Since the value of ξ depends on the components of fluctuating velocity and it is not known a priori, we transform the Dirichlet conditions (2.128) into Neumann conditions. By taking the derivative of k in the wall-normal direction y, we obtain $\partial k/\partial y|_w = \xi y = 2k_w/y$, and considering the same derivative for the logarithmic variable $\partial K/\partial y|_w = 2/y$, then for both variables it is possible to impose Neumann boundary conditions. The dissipation of turbulent kinetic energy ε has a constant near-wall value which can be determined from k_w, in particular $\varepsilon = 2k_w/y^2$, thus an exact Dirichlet boundary condition cannot be imposed on ε, but the value of ξ is iteratively calculated from the value

of k on the wall and this can lead to convergence issues [12]. This aspect does not affect ω and Ω since their values on the walls depend only on the kinematic viscosity of the fluid ν, on the wall distance y and on the model constant c_μ. For these variables, we can then impose the exact Dirichlet conditions (2.130).

The issue of boundary conditions on fluctuating thermal variables is still an open question [11, 55, 67, 42]. For the energy equation, we can impose a constant wall temperature or a uniform wall heat flux. In the case of a constant wall temperature boundary condition, the fluctuations T' vanish along the wall. If a constant heat flux is applied, then temperature fluctuations can be considered null or not. If we assume that the temperature fluctuations are null (MX boundary conditions) we have the near-wall expansion reported in Equation (2.48), then from definitions we obtain the following expressions

$$k_\theta \approx \frac{1}{2} b_\theta^2 y^2 \,, \quad K_\theta \approx \ln\left(\frac{1}{2} b_\theta^2 y^2\right), \tag{2.131}$$

$$\varepsilon_\theta \approx \alpha b_\theta^2 \,, \tag{2.132}$$

$$\omega_\theta \approx \frac{2\alpha}{c_\mu y^2} \,, \quad \Omega_\theta \approx \ln\left(\frac{2\alpha}{c_\mu y^2}\right). \tag{2.133}$$

As in the dynamical turbulence case, the expressions of k_θ, ε_θ and K_θ depend on b_θ which is not known a priori. We can then reformulate (2.131) considering the derivative of k_θ and K_θ in the wall normal direction y as

$$\left.\frac{\partial k_\theta}{\partial y}\right|_w = b_\theta^2 y = \frac{2 k_{\theta w}}{y} \,, \quad \left.\frac{\partial K_\theta}{\partial y}\right|_w = \frac{2}{y} \,, \tag{2.134}$$

and impose Neumann boundary conditions. The quantity $\varepsilon_{\theta w}$ is affected by the same issue of ε_w since we cannot impose an exact Dirichlet condition on this variable but only apply a Dirichlet boundary condition with a value αb_θ^2 that changes iteration by iteration. For ω_θ and Ω_θ we can impose the exact Dirichlet conditions (2.133).

CHAPTER 3

Validation of the anisotropic four-parameter model

In this section, we aim to validate the anisotropic four-parameter turbulence model that is illustrated in Chapter 2. The anisotropic four-parameter model is validated by simulating different benchmark configurations. First, we consider heat transfer in fully developed turbulent flows. We perform several numerical simulations of low Prandtl number fluids over a plane channel configuration at different friction Reynolds numbers Re_τ. The results obtained with the anisotropic four-parameter model are compared with the available reference DNS data [42, 68, 37]. Secondly, the flow in a cylindrical pipe in fully developed conditions is considered. For this configuration, few DNS data are available for low Prandtl number fluids, then our simulation results are compared with the available DNS data and with empirical correlations for integral quantities, such as the Nusselt number. Lastly, a more complex configuration as a backward-facing step geometry is considered and the numerical results are compared with DNS data in forced and mixed convection regimes [69]. Also in this case the choice of Reynolds, Prandtl, and Richardson numbers for computations depends on the available DNS data in the literature. Preliminary results of the proposed validation are presented in [18, 20, 19].

The simulations have been performed using the in-house finite element multigrid code FEMuS developed at the Laboratory of Montecuccolino of the University of Bologna [15]. The code is based on a C++ main program that handles several external open-source libraries, such as MPI and PETSc libraries. In the turbulence framework, FEMuS contains solvers for Reynolds-Averaged Navier-Stokes and energy equations, and several formulations of the isotropic four-parameter turbulence model (k-ε-k_θ-ε_θ, k-ω-k_θ-ω_θ, K-Ω-K_θ-Ω_θ).

During this Ph.D. project, new solvers for Reynolds stresses and turbulent heat flux based on Explicit Algebraic Models have been developed and integrated into the finite element code FEMuS. The new solvers resolve the algebraic equations reported in (2.111) and (2.121) discretized with a finite element approach. The obtained fields act as explicit source terms in the Reynolds-Averaged Navier-Stokes and energy equations, as reported in (2.110) and (2.120), and they are used to compute explicitly the source and dissipation terms in the four-parameter equations. In FEMuS, both isotropic and anisotropic four-parameter turbulence models are now available.

3.1. Fully-developed turbulent flows

3.1.1. Plane channel flow

The plane channel flow configuration has been investigated by different authors in the framework of turbulence modeling [70, 71]. Several DNS databases have been created for this geometry, where the channel flow is characterized by flow parameters such as Re_τ, Pr and Gr. For the validation of the anisotropic four-parameter turbulence model, we refer to the dimensionless parameters of the available DNS data. We consider two different Pr numbers, 0.025 and 0.01, corresponding to liquid lead and sodium. In literature, for $Pr = 0.025$, the available DNS data refer to the friction Reynolds numbers $Re_\tau = 180$, 395, 640, 1020 [42], while for $Pr = 0.01$ we consider the friction Reynolds numbers $Re_t = 180$, 395, 590 [68] and 1000 [37].

The main features of plane channel flows are presented in Chapter 1 and a representative schematic of the geometry is reported in Figure 1.1. The conservation equations governing the flow state are (1.111), (1.112) and (1.129). The pressure gradient driving the fully developed flow can be

computed using (1.121), given the fluid properties, geometry, and target friction Reynolds number Re_τ.

Due to the symmetry of the problem, the computational domain can be simplified as reported in Figure 3.1, where a section of height L_y of the half-channel can be observed. In the figure, $L_x = 0.03025m$ corresponds to the half-channel width, previously indicated with δ. A uniform heat flux q equal to $3.6 \times 10^5\, W/m^2$ is imposed at the walls. In Figure 3.1 the inlet section is indicated as Γ_i, the outlet Γ_o, the heated wall Γ_w and the symmetry axis of the channel Γ_{sym}. Periodic boundary conditions are imposed in the inlet and outlet sections. We indicate with y the streamwise direction and x the wall-normal direction. In Table 3.1 the fluid properties are reported, with the first value of the thermal conductivity λ referring to the case of $Pr = 0.025$, and the second one for the case of $Pr = 0.01$. For the thermal simulations, we introduce the variable $\theta = T - T_{w0} - L_y \Delta T_b$, where ΔT_b is the bulk temperature increment over a streamwise length equal to Ly, T_{w0} is a constant value on Γ_w and L_y is the axial length of the computational domain. Due to the symmetry of the problem, the computation domain is half-channel geometry. A mesh refinement near the wall Γ_w is performed to have the first mesh point in the viscous layer, $x^+ < 1$, where the non-dimensional distance from the wall x^+ is defined as $(L_x - x)u_\tau/\nu$.

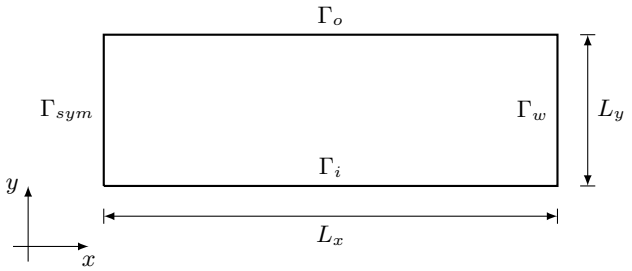

Figure 3.1: Plane channel: schematic of the computational domain.

The variables are normalized using wall units, i.e. the friction velocity u_τ, friction temperature T_τ and kinematic viscosity ν. The friction velocity is used to normalize the velocity $v^+ = v/u_\tau$ and the components of the Reynolds stress tensor $\langle u_i' u_j' \rangle^+ = \langle u_i' u_j' \rangle / u_\tau^2$. The friction temperature $T_\tau = q/u_\tau \rho C_p$ is used to normalize the temperature $\theta^+ = \theta/T_\tau$ and the components of the turbulent heat flux $\langle u_i' \theta' \rangle^+ = \langle u_i' \theta' \rangle / u_\tau T_\tau$.

The results obtained using the anisotropic four-parameter model (4AP) are shown in comparison with the available DNS data and the results ob-

Table 3.1: Plane channel flow: physical properties employed for the numerical simulations.

Property	Symbol	Value	Units
Viscosity	μ	0.001844	$Pa\,s$
Density	ρ	10340	kg/m^3
Thermal conductivity	λ	$10.72 - 26.88$	$W/(mK)$
Specific heat	c	145.75	$J/(kgK)$

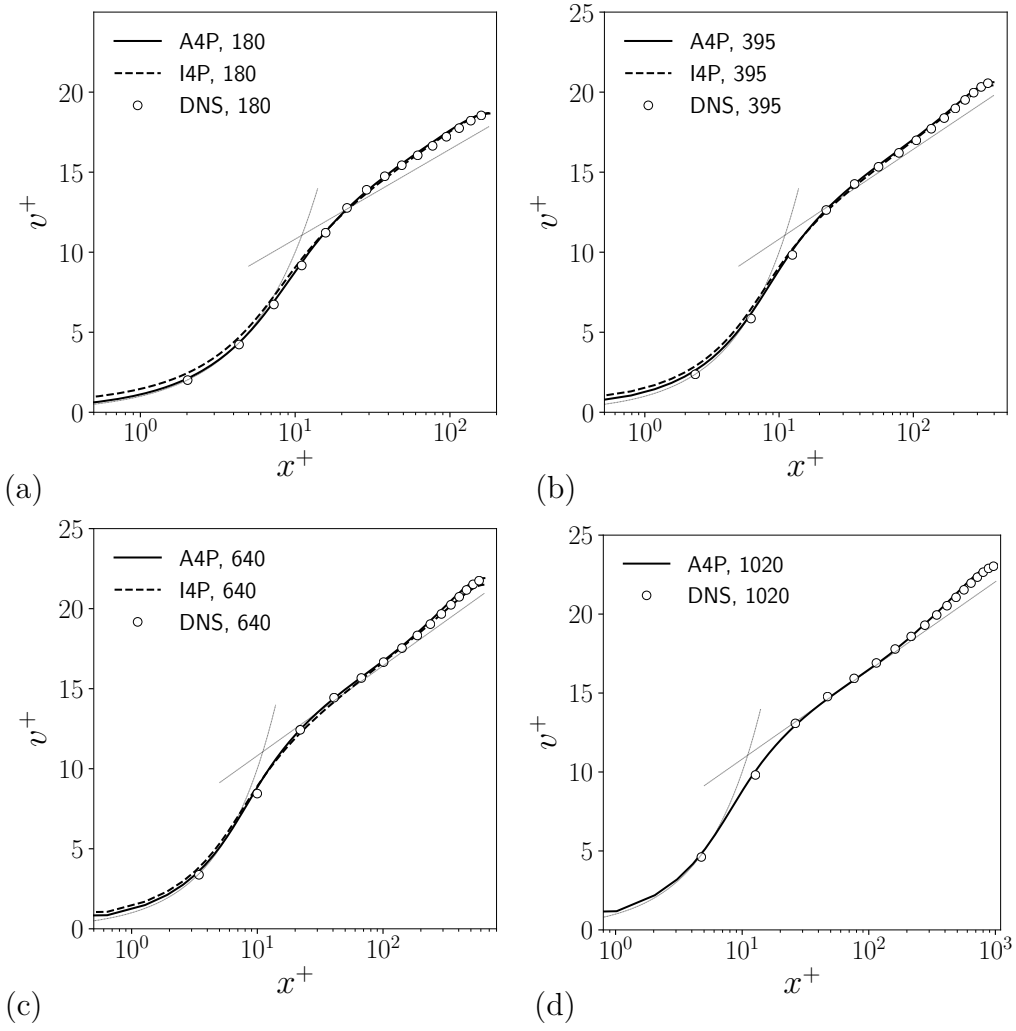

Figure 3.2: Plane channel flow: non-dimensional velocity v^+ profiles for $Re_\tau = 180$ (a), 395 (b), 640 (c) and 1020 (d).

Table 3.2: Plane channel flow: values of the pressure gradient expressed in Pa/m for DNS and for 4AP simulations. Relative errors of 4AP simulations with respect to reference DNS.

Re_τ	$(dP/dy)_{DNS}$	$(dP/dy)_{4AP}$	ϵ_r
180	0.00003723	0.00003710	0.353%
395	0.0001793	0.0001790	0.150%
640	0.0004706	0.0004698	0.167%
1020	0.001195	0.001193	0.225%

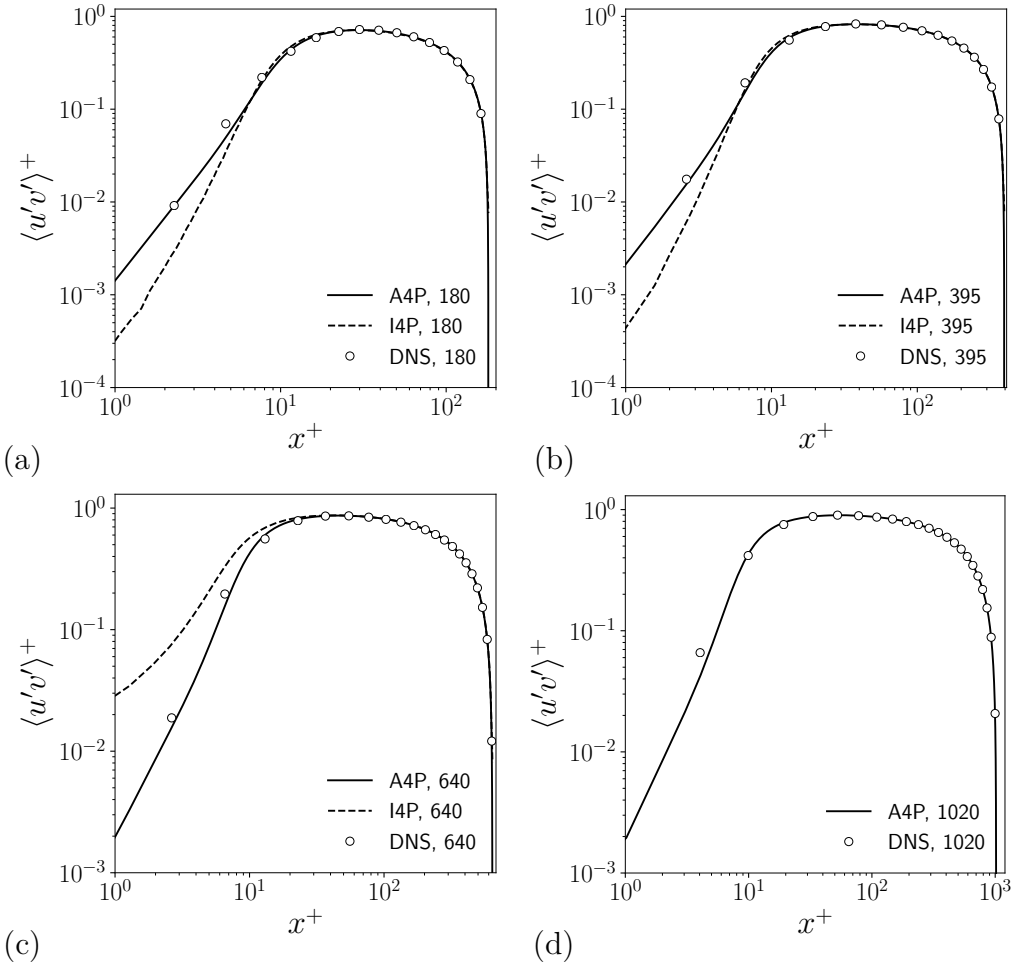

Figure 3.3: Plane channel flow: non-dimensional turbulent shear stress $\langle u'v' \rangle^+$ for $Re_\tau = 180$ (a), 395 (b) 640 (c) and 1020 (d).

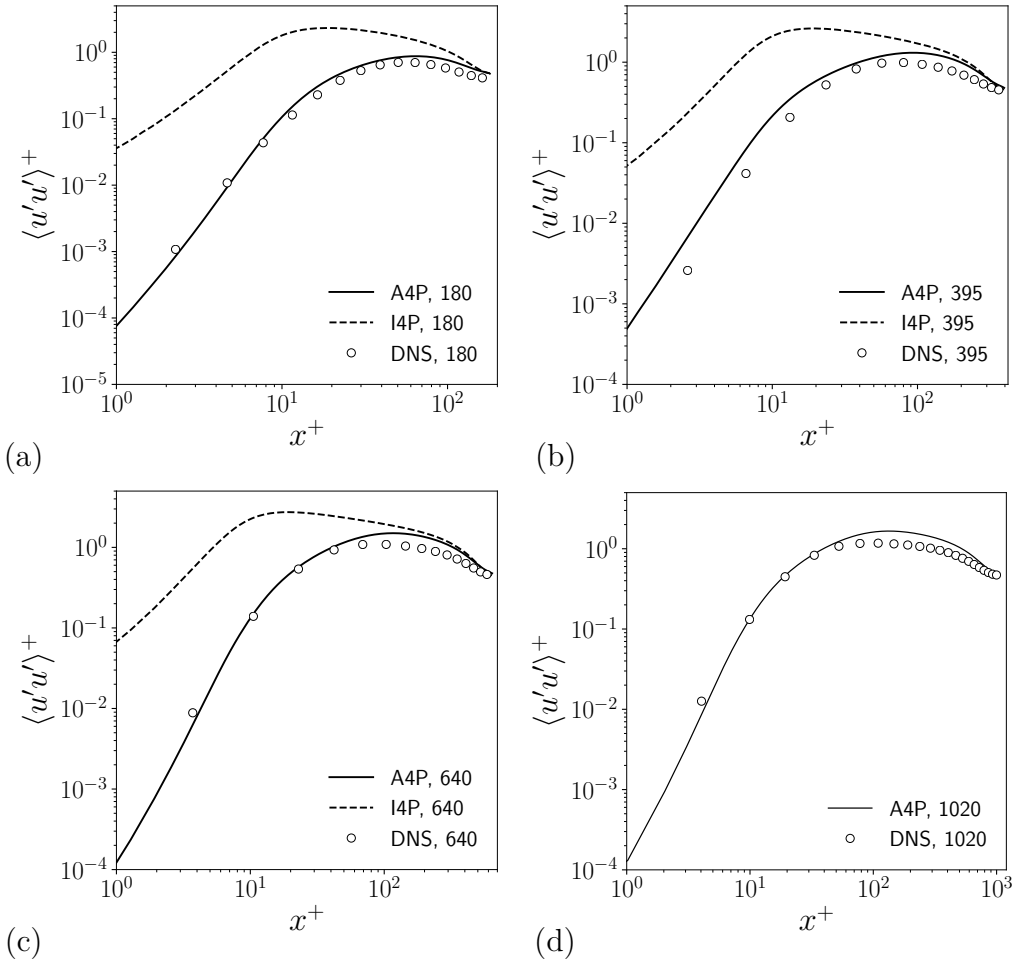

Figure 3.4: Plane channel flow: non-dimensional turbulent wall-normal normal stress $\langle u'u' \rangle^+$ for $Re_\tau = 180$ (a), 395 (b) 640 (c) and 1020 (d).

tained using the isotropic version of the model (I4P). In particular, we refer to the results published in [12] for $Pr = 0.025$ and in [13] for $Pr = 0.01$. In those works, the Reynolds friction numbers considered are 180, 395, 640, and 950, thus the comparison for the case $Re_\tau = 1020$ is not shown.

In Figure 3.2 the non-dimensional streamwise velocity v^+ is plotted against the non-dimensional distance from the wall x^+, for different Re_τ numbers, i.e. 180, 395, 640 and 1020, corresponding to the Reynolds numbers $Re \approx 5700$, 14100, 24400 and 41400 respectively. The linear and logarithmic profiles of the law of the wall have been reported with dotted lines. The comparison with DNS data shows a good matching in the linear and logarithmic regions for the different cases of Re_τ. Both the anisotropic (A4P)

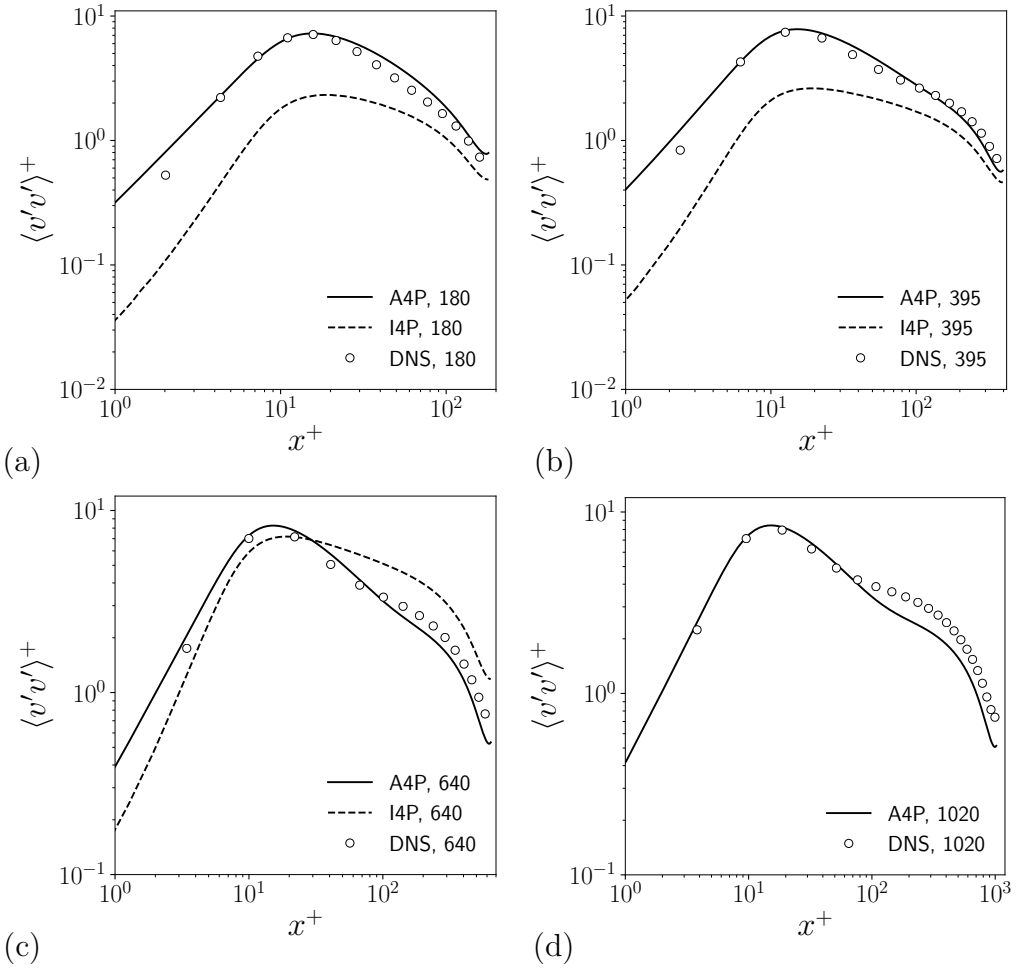

Figure 3.5: Plane channel flow: non-dimensional turbulent streamwise normal stress $\langle v'v' \rangle^+$ for $Re_\tau = 180$ (a), 395 (b) 640 (c) and 1020 (d).

and the isotropic (I4P) models show good agreement with the reference data and there are no appreciable discrepancies between the two models.

In Table 3.2, we report the pressure gradient values $(dP/dy)_{4AP}$ obtained with the 4AP model for all the considered Re_τ numbers. We also report the reference DNS values $(dP/dy)_{DNS}$ computed with (1.121). The relative error $\epsilon_r = [(dP/dy)_{4AP} - (dP/dy)_{DNS}]/(dP/dy)_{DNS}$ is shown. The relative error is below 0.4% for all cases, then the model is very accurate in predicting the correct pressure losses.

The dimensionless shear turbulent stress tensor $\langle u'v' \rangle^+$ is plotted against the non-dimensional distance from the wall x^+ in logarithmic scale for the different Re_τ numbers. The logarithmic scale allows focusing on the near-

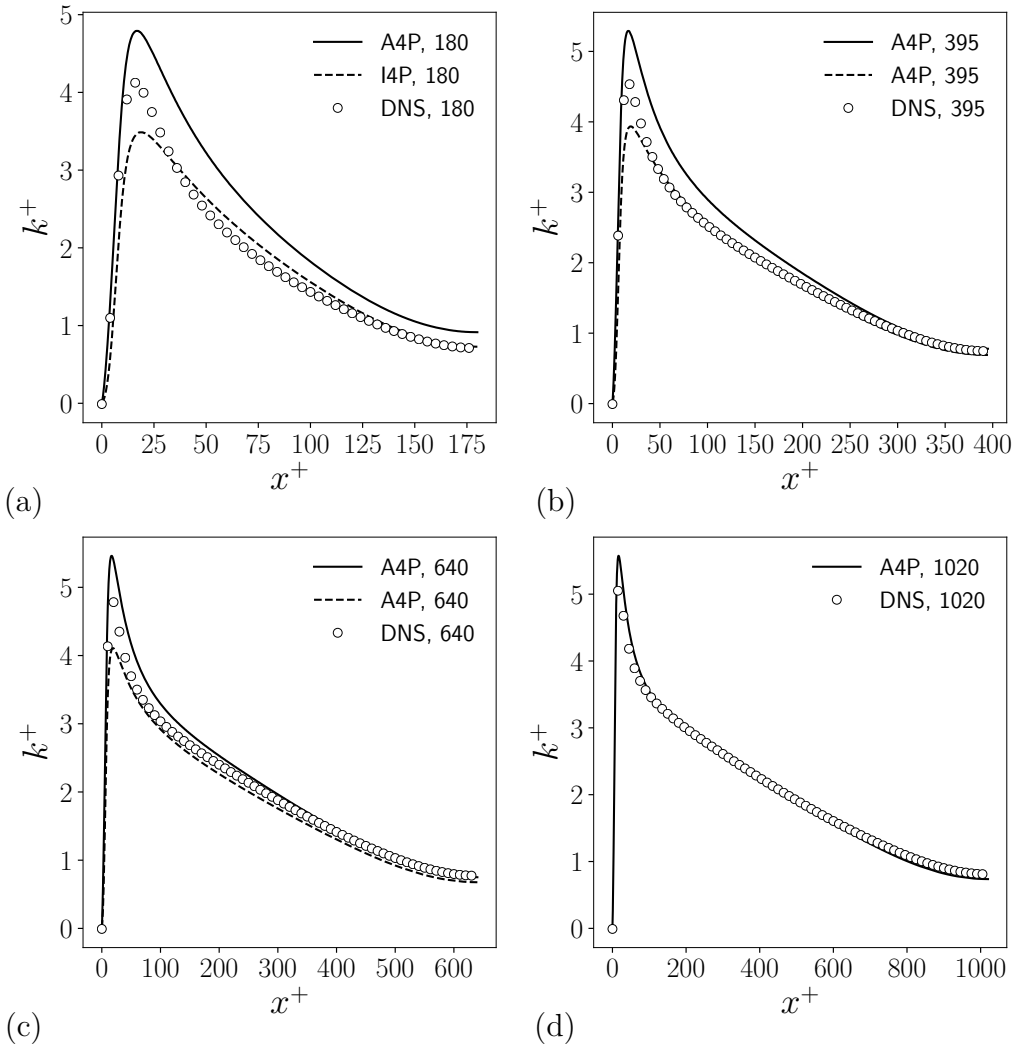

Figure 3.6: Plane channel flow: non-dimensional turbulent kinetic energy k^+ for $Re_\tau = 180$ (a), 395 (b) 640 (c) and 1020 (d).

wall behavior of the turbulent shear stress. We can observe that the simulation results with the anisotropic model (4AP) overlap perfectly with the reference data, both in the near-wall and bulk regions. Even though the results obtained with the isotropic model (I4P) show some discrepancies with DNS data in the linear region, both the anisotropic and isotropic models can accurately estimate the turbulent shear stress.

The other Reynolds stress components are characterized by more marked differences between simulation results and DNS data. The wall-normal normal stresses $\langle u'u' \rangle^+$ are shown in Figure 3.4 for the considered Re_τ numbers.

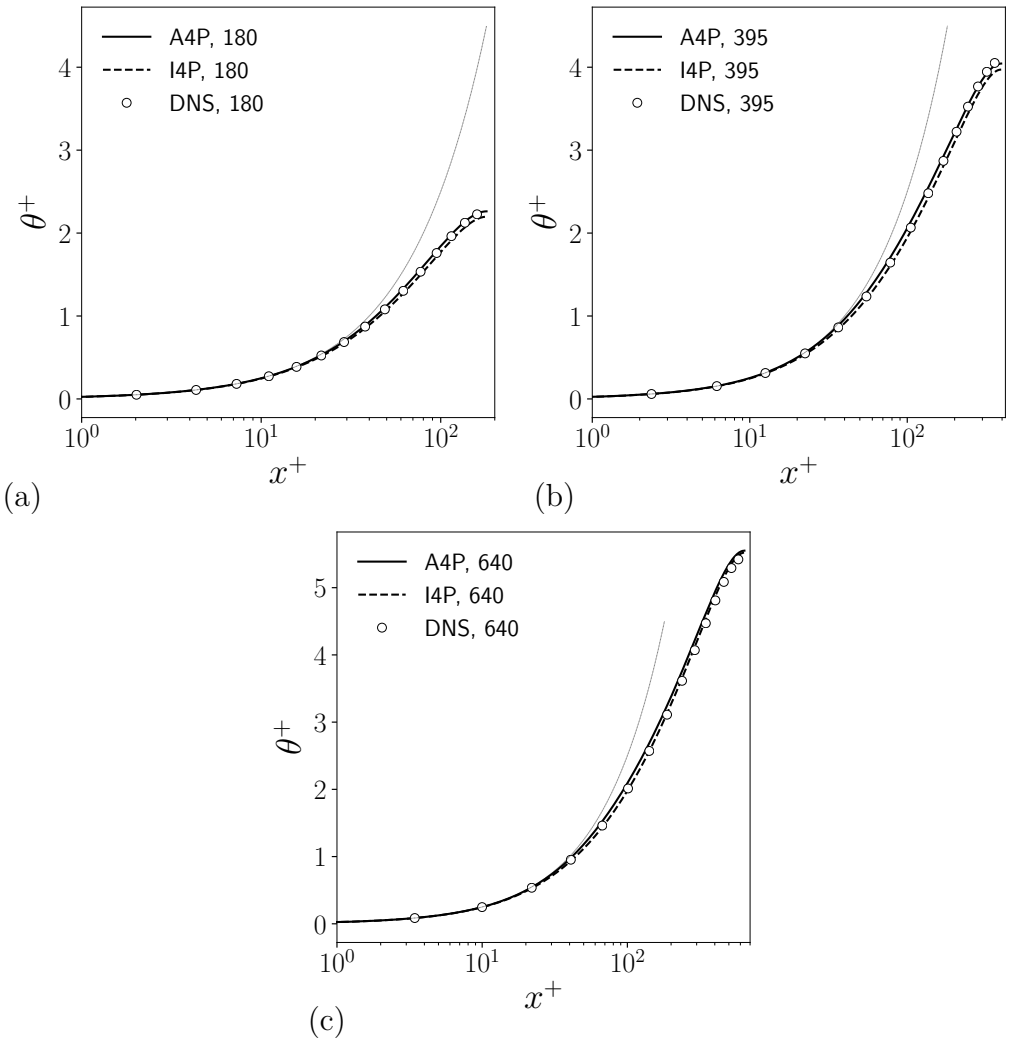

Figure 3.7: Plane channel flow: non-dimensional mean temperature profile θ^+ with $Pr = 0.025$ for different $Re_\tau = 180$ (a), 395 (b) and 640 (c).

The profiles are plotted against the dimensionless wall distance on logarithmic scale. For the isotropic four-parameter model (I4P), the wall-normal normal turbulent stress is computed considering the Boussinesq assumption, then $\langle u'u' \rangle = 2/3k$ since $\partial u/\partial x = 0$. The near-wall behavior of the wall-normal normal stress is well-estimated by the anisotropic four-parameter model (4AP). However, we can observe an overall overestimation of the peak of $\langle u'u' \rangle^+$ in the bulk region. Thanks to the explicit algebraic stress model, we can estimate $\langle u'u' \rangle^+$ with greater accuracy than we do with the isotropic model, above all in the near-wall region.

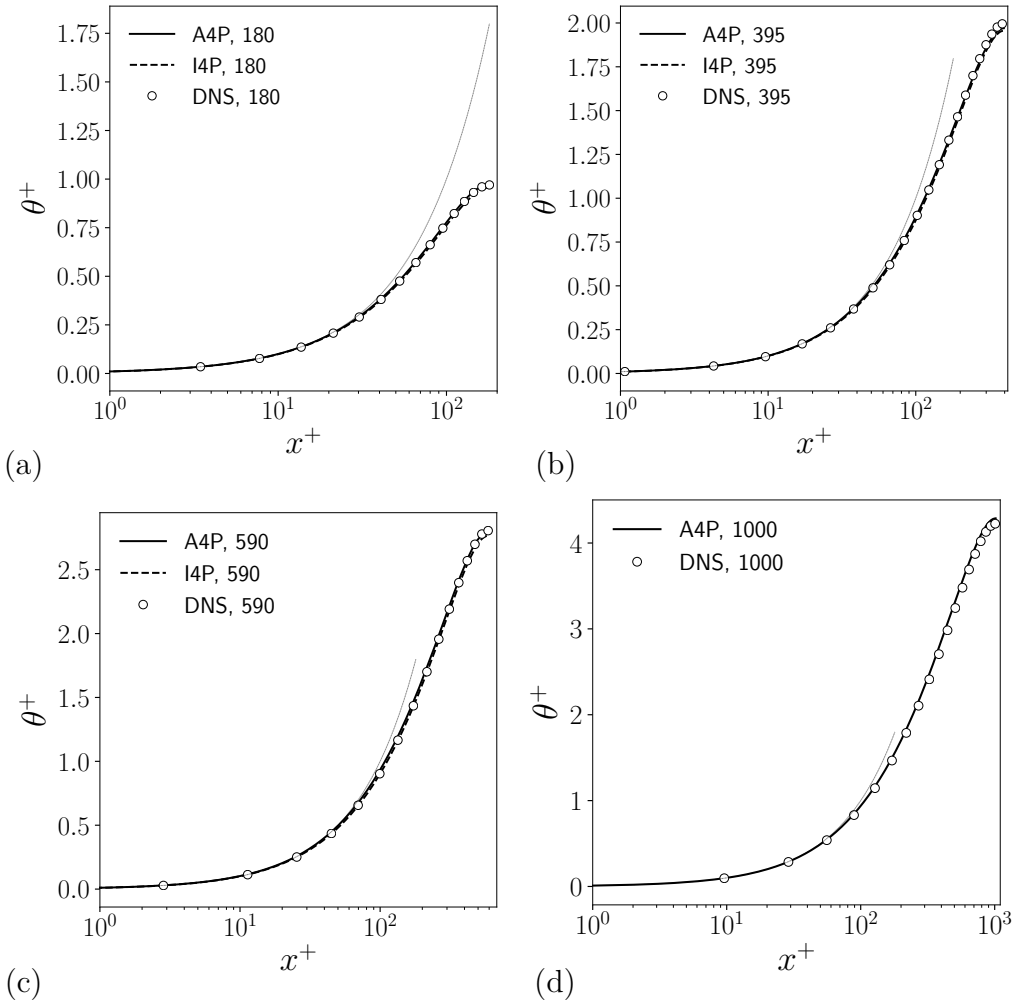

Figure 3.8: Plane channel flow: non-dimensional mean temperature profile θ^+ with $Pr = 0.01$ for different $Re_\tau = 180$ (a), 395 (b), 590 (c) and 1000 (d).

In Figure 3.5, the non-dimensional turbulent streamwise normal stress $\langle v'v' \rangle^+$ is shown plotted against the wall distance in logarithmic scale. For the isotropic four-parameter model (I4P), the streamwise normal turbulent stress is computed considering the Boussinesq assumption, then $\langle v'v' \rangle = 2/3k$ since $\partial v/\partial y = 0$. We can observe an overall satisfactory agreement between the anisotropic model and DNS for every Re_τ, even though the profiles obtained with numerical simulation overestimate the maximum of the stress and underestimate the bulk behavior. The near-wall behavior of the wall-normal normal stress is well-estimated by the anisotropic four-parameter model (4AP). Comparing the results with I4P profiles, we

can affirm that the adoption of the anisotropic model allows improving the estimation of the streamwise wall-normal component as well.

The turbulent normal stresses $\langle u'u' \rangle$ and $\langle v'v' \rangle$ do not affect the velocity field in this flow configuration. Due to the hypothesis of fully developed flow, only the turbulent shear stress appears in (1.111) and (1.112). For this reason, the prediction of the velocity field with the isotropic model is in good agreement with DNS data. However, for the anisotropic four-parameter model, the accurate estimation of the normal stresses is crucial since they affect the computation of the turbulent heat flux components.

Lastly, the dimensionless turbulent kinetic energy k^+ is reported in Figure 3.6 plotted against the non-dimensional wall distance x^+. The near-wall peaks are slightly overestimated for all Reynolds numbers, using the anisotropic model (4AP). For low Reynolds numbers, the turbulent kinetic energy is also overestimated in the central region of the channel. When increasing the Reynolds number, the turbulent kinetic energy perfectly matches the DNS reference data in the region far from the wall. With the isotropic model (I4P), the near-wall peaks are slightly underestimated for all Reynolds numbers, but the bulk behavior is well-predicted even for low Reynolds numbers.

The numerical results of thermal fields for $Pr = 0.025$ and $Pr = 0.01$ are now reported and discussed. The non-dimensional temperature profiles are shown in Figure 3.7 and 3.8 for $Pr = 0.025$ and $Pr = 0.01$ respectively. The linear profile of the law of the wall for the temperature, $\theta^+ = y^+ Pr$ is reported with dotted lines. The results obtained using the anisotropic four-parameter model (4AP) are compared with DNS data. Moreover, the results obtained with the isotropic model [12, 13] are also shown. The profiles are plotted against the dimensionless wall distance with a logarithmic scale. The temperature field is in good agreement with the reference DNS data for all the Pr and Re_τ numbers considered. There are no appreciable discrepancies between the results obtained with the anisotropic and isotropic models. For low Reynolds numbers and $Pr = 0.025$, we can observe a slight underestimation of the temperature profile in the bulk region obtained with the isotropic model.

In Figure 3.9 the dimensionless wall-normal turbulent heat flux $\langle u'\theta' \rangle^+$ profiles are reported for different Re_τ and Pr numbers. For shortness, only two cases of different Re_τ are shown for each Pr number. In Figures 3.9a and 3.9b the plots show the results for $Pr = 0.025$, while in Figures 3.9c and

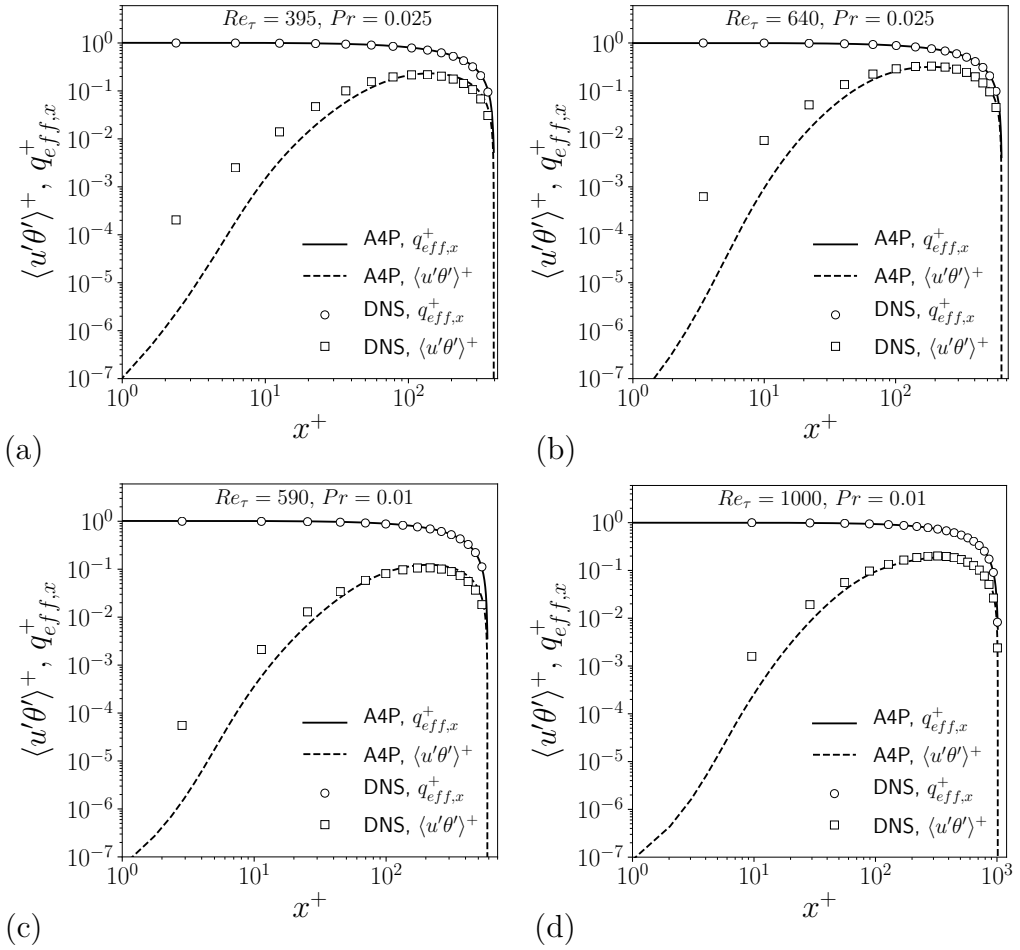

Figure 3.9: Plane channel flow: non-dimensional wall-normal total heat flux q^+_{eff} and non-dimensional wall-normal turbulent heat flux $\langle u'\theta' \rangle^+$ for $Re_\tau = 395\,, Pr = 0.025$ (a), $Re_\tau = 640\,, Pr = 0.025$ (b), $Re_\tau = 590\,, Pr = 0.01$ (c) and $Re_\tau = 1000\,, Pr = 0.01$ (d).

3.9d for $Pr = 0.01$. We also report the effective wall-normal heat flux $q^+_{eff,x}$ which is defined as the sum of the molecular heat flux and the turbulent heat flux in the wall-normal direction, i.e.

$$q^+_{eff,x} = \left(\alpha \frac{\partial \theta}{\partial x}\right)^+ - \langle u'\theta' \rangle^+ . \tag{3.1}$$

We can notice some discrepancies for the $\langle u'\theta' \rangle^+$ component from DNS data in the near-wall region. However, in this region the thermal conductivity contribution is dominant with negligible turbulent heat flux, then the total heat flux $q^+_{eff,x}$ is almost equal to the molecular heat flux. Thus,

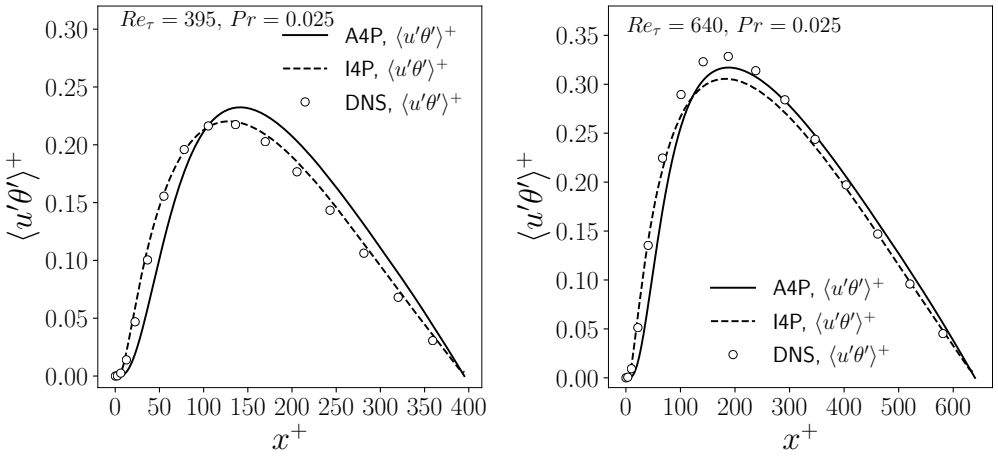

Figure 3.10: Plane channel flow: non-dimensional wall-normal total heat flux q^+_{eff} and non-dimensional wall-normal turbulent heat flux $\langle u'\theta' \rangle^+$ for $Pr = 0.025$ and $Re_\tau = 395$ (a) and $Re_\tau = 640$ (b).

the bad prediction of $\langle u'\theta' \rangle^+$ in this region does not affect the total heat flux and, consequently, the mean temperature field. In addition, we can observe that for the high Reynolds numbers, Figure 3.9b and d, the prediction of the wall-normal heat flux is in perfect agreement with DNS data in the far-wall region. The profiles of the wall-normal turbulent heat flux obtained with the isotropic model are shown in Figure 3.10 for the comparison with the anisotropic results, considering $Re_\tau = 395$ and 640 with $Pr = 0.025$. The isotropic model estimates accurately the near-wall behavior. Indeed, the mixed time scale τ_m is calibrated for the isotropic version of the model. To better estimate the near-wall behavior with the anisotropic model, it would be necessary to adapt the near-wall expression of τ_m. For high Reynolds numbers, the bulk behavior seems better estimated by the anisotropic model.

In Figure 3.11 the non-dimensional streamwise turbulent heat flux $\langle v'\theta' \rangle^+$ is shown for $Pr = 0.025$ and $Pr = 0.01$. The streamwise component of the turbulent heat flux is underestimated for all the cases with respect to the DNS reference data. We can then conclude that the anisotropic four-parameter turbulence model is not able to properly predict this component in the plane channel configuration. However, this bad prediction does not affect the mean temperature estimation. Indeed, due to the symmetry of the plane channel configuration, the mean temperature field is only affected by

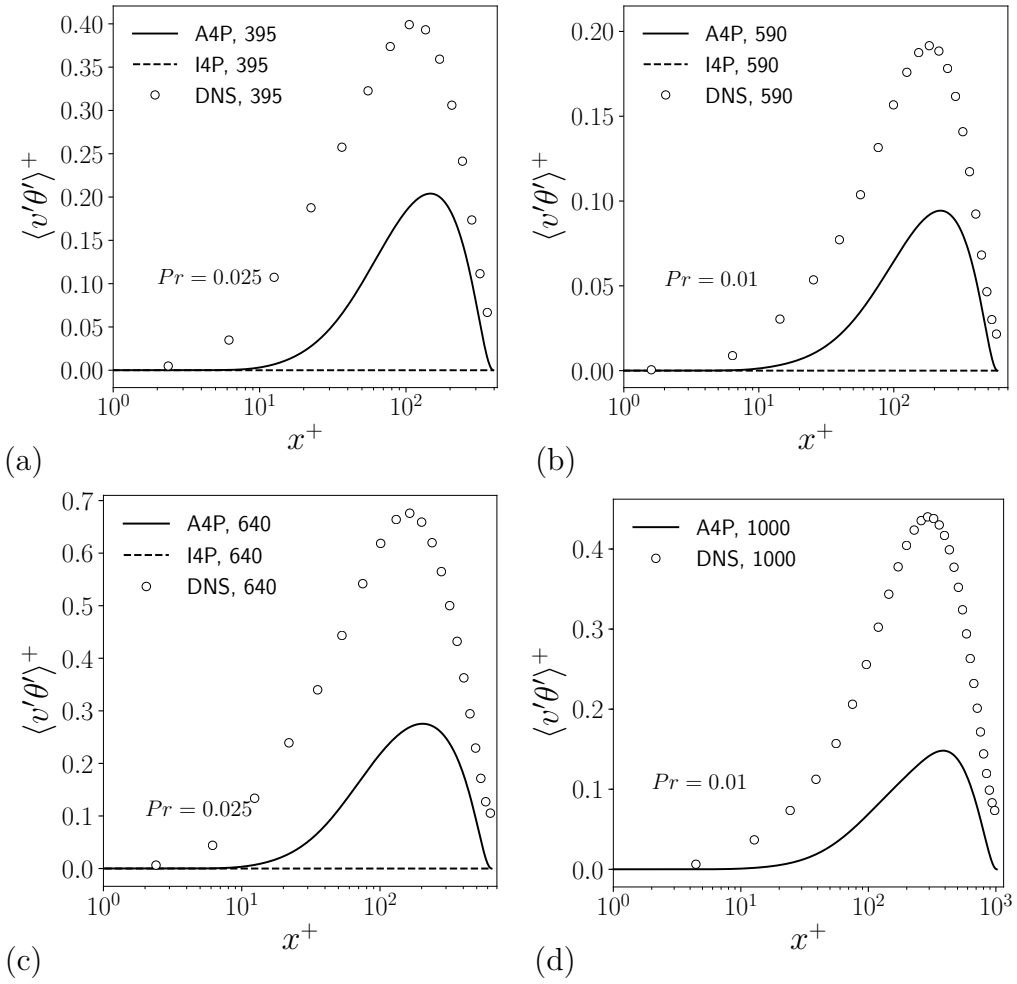

Figure 3.11: Plane channel flow: non-dimensional streamwise turbulent heat flux $\langle v'\theta' \rangle^+$ for $Pr = 0.025$ and $Re_\tau = 395$ (a), $Pr = 0.01$ and $Re_\tau = 590$ (b), $Pr = 0.025$ and $Re_\tau = 640$ (c) and $Pr = 0.01$ and $Re_\tau = 1000$ (d).

the wall-normal component of molecular and turbulent heat flux. Moreover, we underline that with the isotropic model (I4P), the streamwise turbulent heat flux component is identically zero in this configuration since it is computed as $\langle v'\theta' \rangle^+ = -\alpha_t \partial\theta/\partial y$ and $\partial\theta/\partial y = 0$.

3.1.2. Pipe flow

In this subsection, we report the results of numerical simulations performed considering a turbulent fully developed flow along a cylindrical pipe. The main features of pipe flows are presented in Chapter 1 and a representa-

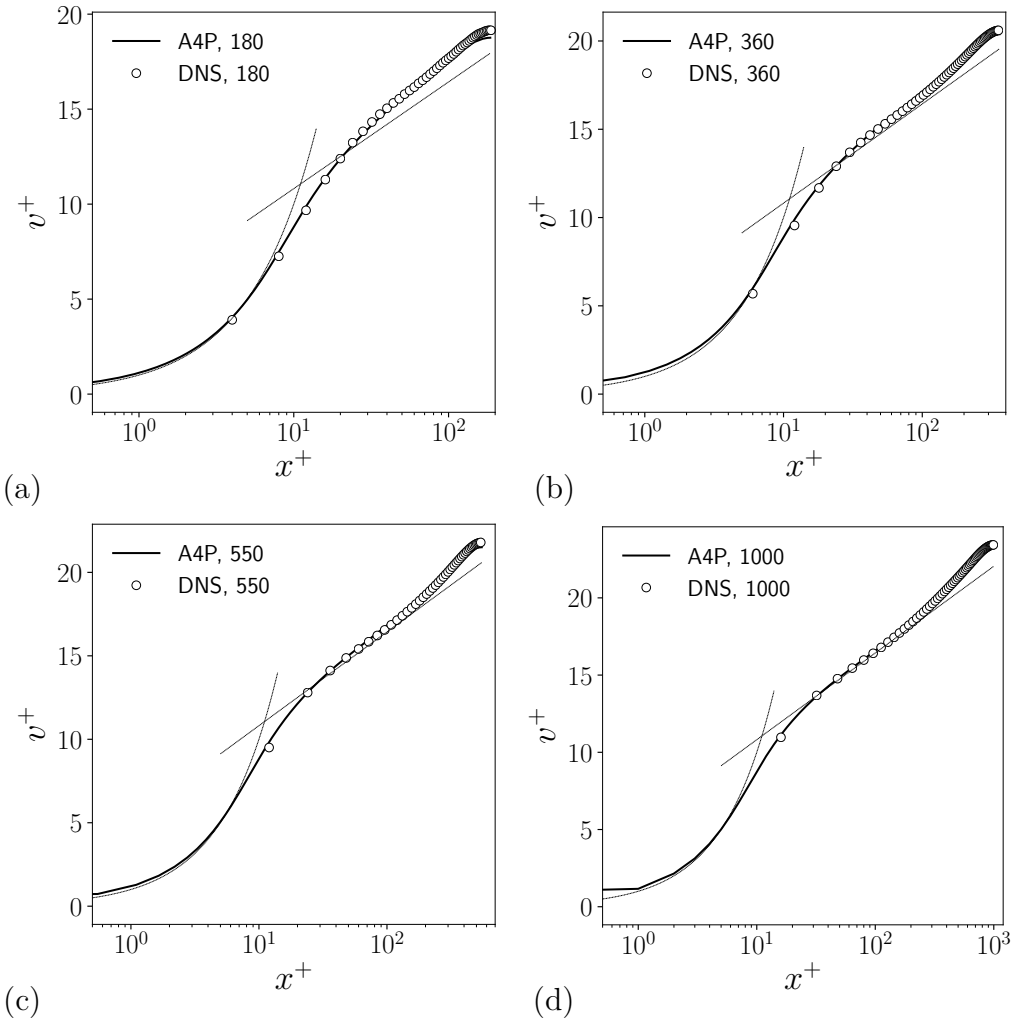

Figure 3.12: Pipe flow: non-dimensional velocity v^+ profiles for $Re_\tau = 180$ (a), 360 (b), 550 (c) and 1000 (d).

tive schematic of the geometry is reported in Figure 1.4. The conservation equations governing the flow state are (1.131), (1.132) and (1.142). The pressure gradient driving the fully developed pipe flow has been derived in Equation (1.138) and given as a function of $2\rho Re_\tau^2 \nu^2 / R^3$. Thus, with Reynolds friction numbers being equal, the pressure gradient in the pipe is double the pressure gradient in the channel. The computational domain is the same reported in Figure 3.1 for the plane channel configuration where x is the radial direction and y is the axial one. The half-channel width L_x corresponds to the pipe radius R, namely $D = 2L_x = 0.0605\ m$. A

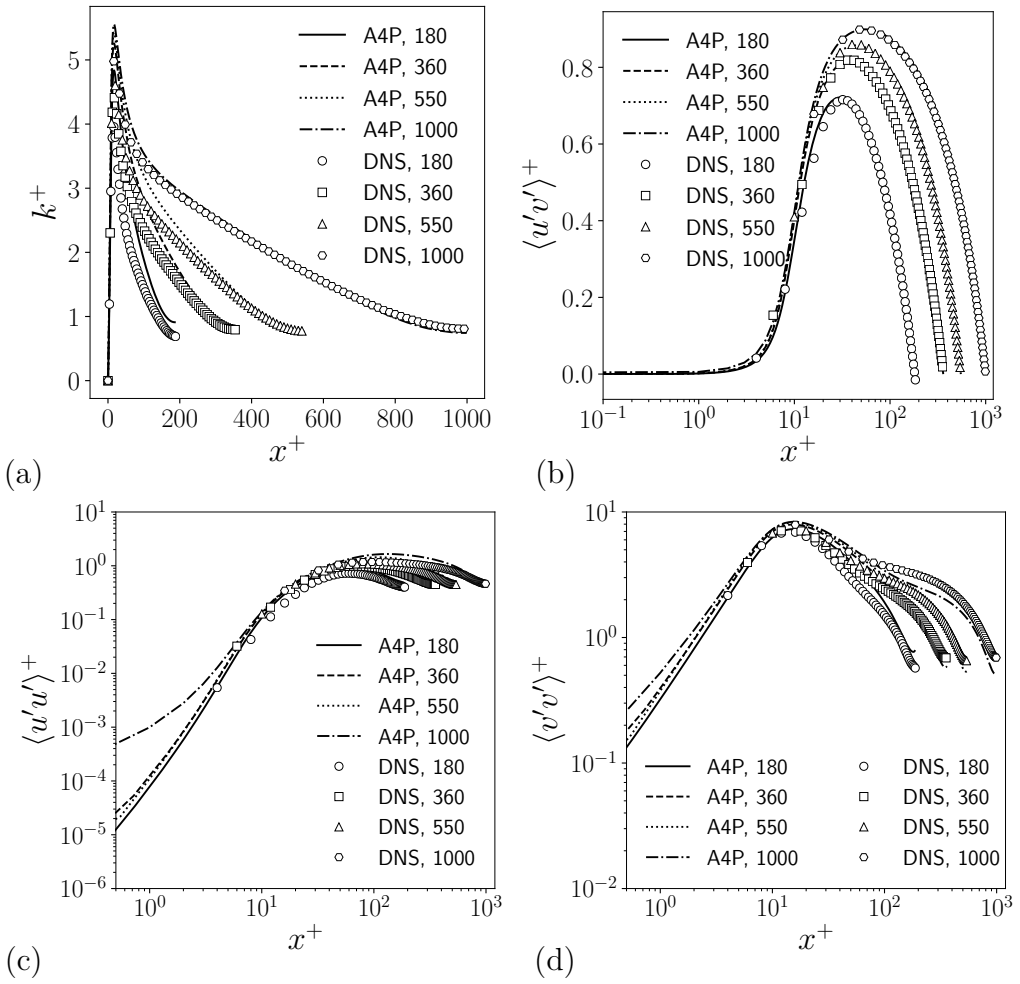

Figure 3.13: Pipe flow: non-dimensional turbulent kinetic energy k^+(a), turbulent shear stress $\langle u'v' \rangle^+$ (b), wall-normal normal stress $\langle u'u' \rangle^+$ (c) and streamwise normal stress $\langle v'v' \rangle^+$ (d) for different $Re_\tau = 180$, 360, 550, 1000.

uniform heat flux $q = 3.6 \times 10^5\, W/m^2$ acts on the pipe walls. Tests have been performed considering $Re_\tau = 180$, 360, 550 and 1000 since DNS reference data are available for dynamic fields [72]. However, there are very few DNS data of thermal fields of low Prandtl number fluids. The only available study is for $Pr = 0.026$ and $Re_\tau = 180$ [72]. For this reason, the validation of the anisotropic four-parameter model in the pipe configuration involves the comparison of dynamical fields between numerical results and DNS data. For the thermal validation, we can compare our results only with the DNS data for $Re_\tau = 180$. For the highest Reynolds numbers, we

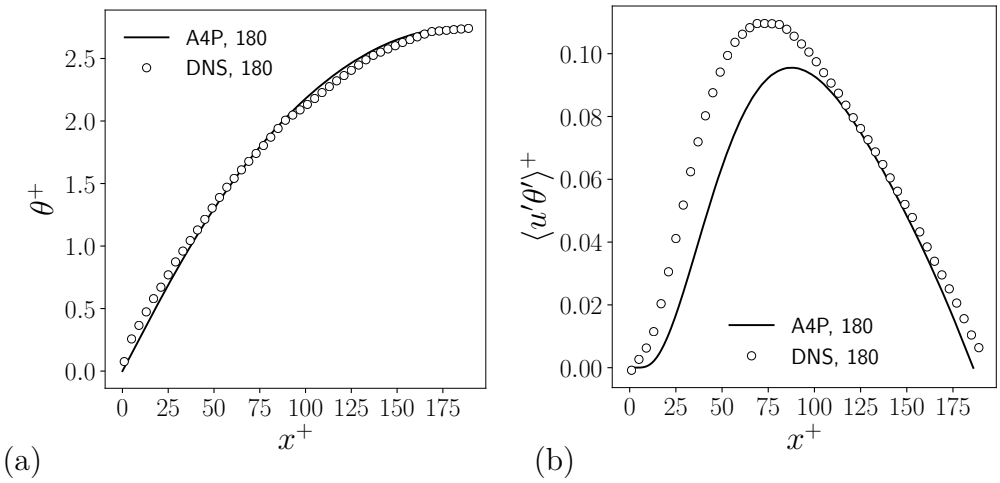

Figure 3.14: Pipe flow: non-dimensional mean temperature θ^+ (a) and wall-normal heat flux $\langle u'\theta' \rangle^+$ (b) for $Re_\tau = 180$.

propose a validation through empirical correlations.

The profiles of dimensionless velocity $v^+ = v/u_\tau$ are reported in Figure 3.12 for the different Reynolds friction numbers, $Re_\tau = 180$ (a), 360 (b), 550 (c) and 1000 (d). The corresponding bulk Reynolds numbers $Re = 2RU_b/\nu$ are 5410, 11800, 19100 and 38000, where U_b is the bulk velocity. For all the considered Reynolds numbers, the numerical results and reference data perfectly overlap.

In Figure 3.13a is reported the non-dimensional turbulent kinetic energy $k^+ = k/u_\tau^2$. By the comparison between numerical results and DNS data, an overall overestimation of the near-wall peak can be observed. For high Reynolds numbers, the bulk behavior of turbulent kinetic energy is in good agreement with reference data. The dimensionless turbulent shear stress $\langle u'v' \rangle^+ = \langle u'v' \rangle / u_\tau^2$ is reported in Figure 3.13b. This Reynolds stress component is in agreement with DNS data in analogy to the plane channel configuration. The dimensionless wall-normal normal stress $\langle u'u' \rangle^+ = \langle u'u' \rangle / u_\tau^2$ and streamwise normal stress $\langle v'v' \rangle^+ = \langle v'v' \rangle / u_\tau^2$ are respectively shown in Figure 3.13c and d. The same trends we have observed for the plane channel are recognizable. The peaks in the Reynolds normal stresses are overestimated. In the bulk region, our prediction of the streamwise normal stress is in good agreement with DNS data, while the wall-normal normal stress is overrated along the whole pipe cross-section.

The thermal fields are shown in Figure 3.14. The dimensionless temper-

Table 3.3: Pipe flow: flow and heat transfer parameters of the simulations.

Case	Re_τ	Re	Pe	Nu
a	180	5410	141	6.5
b	360	11800	296	7.7
c	550	19100	480	8.2
d	1000	38000	950	10.5

ature $\theta^+ = \theta/T_\tau$ is reported in Figure 3.14a for $Re_\tau = 180$ since DNS data are not available for higher values of the Reynolds friction number. From the comparison with DNS data for $Re_\tau = 180$, we can observe that the temperature is correctly predicted. In 3.14b the non-dimensional wall-normal turbulent heat flux $\langle u'\theta'\rangle^+ = \langle u'\theta'\rangle/(u_\tau T_\tau)$ is reported for $Re_\tau = 180$. By comparing the simulation result with the DNS profile, we can see that the maximum value is underestimated but the bulk flow behavior is in agreement with the reference.

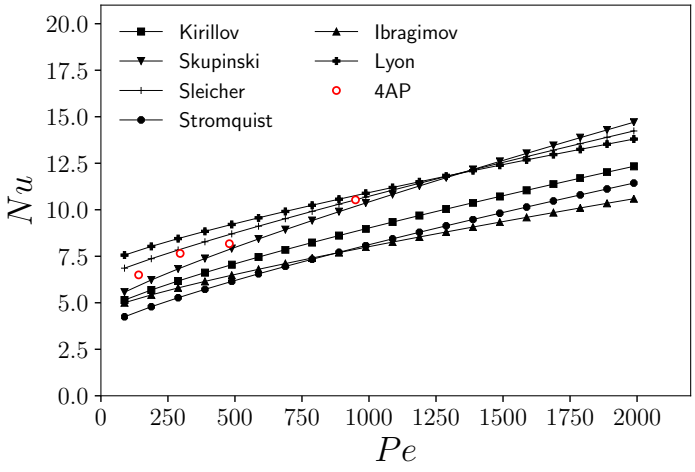

Figure 3.15: Pipe flow: profiles of Nusselt number as a function of Peclet number according to empirical correlations. Simulations results reported in red.

Since DNS data for low Prandtl numbers are insufficient to validate the thermal simulation, we use integral quantities. For low Prandtl number fluids, several empirical correlations exist based on experiments that predict the Nusselt number as a function of the Peclet number. The Nusselt number is the ratio of convective to conductive heat transfer $Nu = hD/\lambda$, while the

Peclet number is the ratio of advective transport rate and diffusive transport rate $Pe = RePr$, where h is the convective heat transfer coefficient of the flow introduced in Newton's law of cooling (1.123) then $h = q_w/(T_w - T_b)$. The bulk temperature T_b for a cylinder is given by Equation (1.141). One of the first empirical correlations was proposed by Lyon in [73]

$$Nu = 7 + 0.025\Big(\frac{Pe}{Pr_t}\Big)^{0.8}, \tag{3.2}$$

where $Pr_t = 1.8$. Other empirical correlations proposed are the following

$$Nu = 4.5 + 0.018Pe^{0.8}, \qquad 10^4 \leqslant Re \leqslant 5 \times 10^6, \tag{3.3}$$
$$Nu = 4.82 + 0.0185Pe^{0.827}, \qquad 10^4 \leqslant Re \leqslant 5 \times 10^6, \tag{3.4}$$
$$Nu = 6.3 + 0.0167Pe^{0.85}Pr^{0.08}, \qquad 10^4 \leqslant Re \leqslant 5 \times 10^6, \tag{3.5}$$
$$Nu = 3.6 + 0.018Pe^{0.8}, \qquad 88 \leqslant Pe \leqslant 4000, \tag{3.6}$$
$$Nu = 4.5 + 0.014Pe^{0.8}, \qquad 10^4 \leqslant Re \leqslant 5 \times 10^6, \tag{3.7}$$

which are introduced respectively by Kirillov and Ushakov [74], Skupinski [75], Sleicher [76], Stromquist [77] and Ibragimov [78]. In Figure 3.15 the above-mentioned correlations are plotted. The Nusselt and Peclet numbers corresponding to each simulation are evaluated and reported in Table 3.3. The results obtained for the four simulations are plotted in Figure 3.15 and marked by red circles. The points are in the range of Nusselt numbers identified by empirical correlations.

3.2. Backward-facing step flow

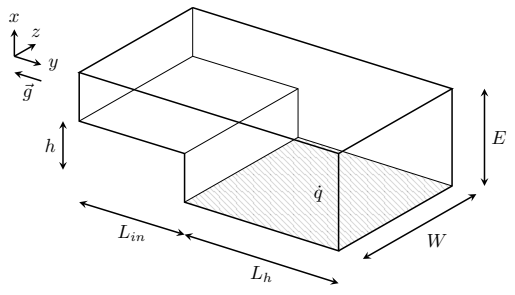

Figure 3.16: Backward-facing step geometry.

In this subsection, we report the results obtained for the simulation of a turbulent flow of liquid sodium over a vertical backward-facing step. This

Table 3.4: Backward-facing step: geometrical parameters of the simulated domain.

L_{in}/h	L_h/h	W	E_r	Re	Pr	Ri
2	20	0	1.5	4805	0.0088	0 - 0.338

Table 3.5: Backward-facing step: physical properties employed for the numerical simulations.

Property	Symbol	Value	Units
Viscosity	μ	0.00054335	$Pa\,s$
Density	ρ	914.6	kg/m^3
Thermal conductivity	λ	84.119	$W/(mK)$
Specific heat	c	1362.3	$J/(kgK)$
Coefficient of expansion	β	2.5684×10^{-4}	K^{-1}

type of flow has been extensively studied in the literature. In [79, 69, 80, 81] DNS simulations with different Reynolds numbers have been performed, in forced and/or mixed convection regimes. In [82] a comparison between the solutions of a RANS system of equations closed with various turbulence models is proposed for the forced convection case, showing that four-equation turbulence models, coupled with nonlinear expressions for the Reynolds stress tensor, allow improving the predictions of the turbulent heat flux. In [43] an anisotropic three-equation turbulence model has been proposed and applied to this configuration in forced and mixed convection regimes showing promising potential for the prediction of the turbulent heat flux. In [14] RANS simulations have been performed with an isotropic four-parameter turbulence model in forced and mixed convection regimes considering a linear expression for the Reynolds stress tensor and the turbulent heat flux. Results are promising in both regimes but the adoption of the anisotropic formulation that we are proposing could improve the prediction of the turbulent heat flux components.

The computational domain reproduces the reference DNS domain [69] and a representative schematic is reported in Figure 3.16. The inlet section length is L_{in}, the step height is h, the domain width is W and the downstream channel height is E. The expansion ratio is $E_r = E/(E-h)$. The geometrical parameters of the simulated domain are reported in Table 3.4.

Table 3.6: Number of bi-quadratic cells and nodes for the four grids of the mesh sensitivity study. Predicted reattachment y_r/h point location and relative deviation with respect to the finest mesh.

	Mesh 1	Mesh 2	Mesh 3	Mesh 4
Cells	11853	16298	24760	30689
Nodes	45289	62705	95885	119211
y_r/h	6.77	6.65	6.68	6.69
ϵ_{y_r}	1.19%	−0.60%	−0.15%	-

We have considered two different values of Richardson number $Ri = g\beta\Delta Th/U_b^2$, $Ri = 0$ corresponding to forced convection and $Ri = 0.338$ corresponding to mixed convection regime. In terms of boundary conditions, a fully developed inflow condition has been set for the velocity field and turbulent variables corresponding to $Re_\tau = hu_\tau/\nu \approx 300$ and $Re_b = 2hU_b/\nu = 9610$. The Reynolds number is calculated with respect to the inlet channel width $2h$ and the bulk inlet velocity U_b. For the temperature, a uniform value is set, i.e. $T_{ref} = 423.15K$. The same temperature is used as the reference value for the evaluation of liquid sodium properties reported in Table 3.5, using the correlations reported for liquid sodium in [83]. At this temperature, the Prandtl number is 0.0088. At the outlet section, an outflow boundary condition is imposed on the velocity field and for all the other variables homogeneous Neumann conditions are set. All the remaining boundaries have been treated as adiabatic no-slip walls, except for the wall behind the step where a uniform heat flux $\dot{q}$ is imposed. Numerical simulations have been performed for the forced and mixed convection calculations using the anisotropic four-parameter turbulence model and the results are compared with DNS data and with the isotropic model.

3.2.1. Mesh sensitivity study

A mesh sensitivity study has been performed for the forced convection case considering four different grids reported in Figure 3.17. Mesh cells are clustered near the corner step and reattachment zone. Mesh refinement is performed near wall boundaries to obtain a non-dimensional wall distance $x^+ < 1$ on the first mesh point near wall boundaries. The number of bi-quadratic cells and nodes are reported in Table 3.6 for all the considered grids.

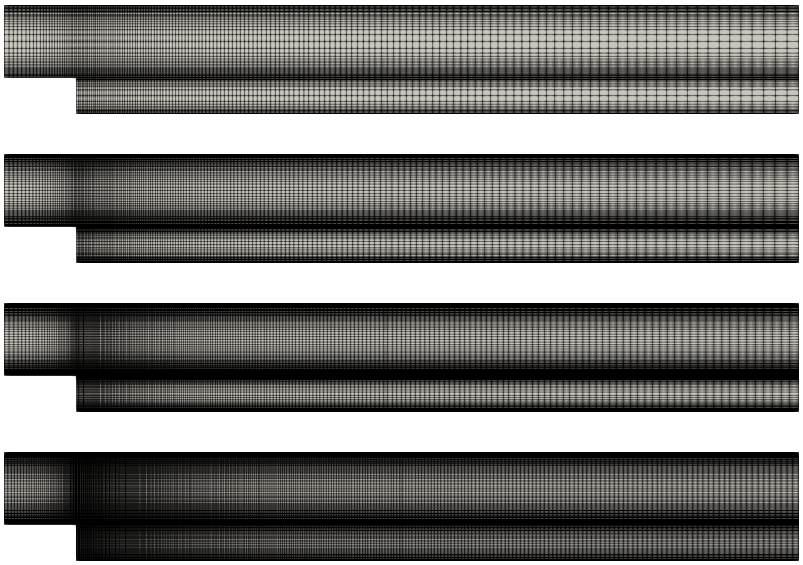

Figure 3.17: View of the four grids considered in the mesh sensitivity study.

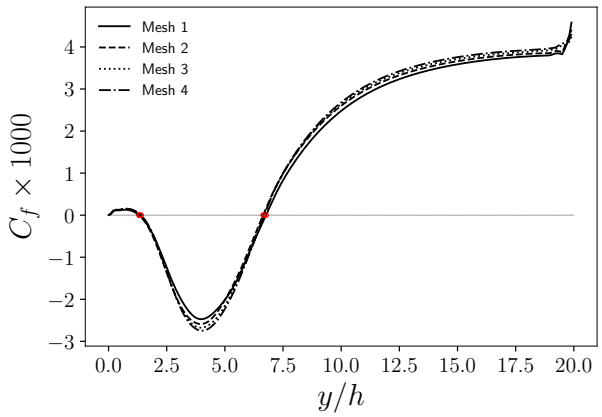

Figure 3.18: Skin friction coefficient C_f along the heated wall.

A typical feature of the backward-facing step flow in the forced convection regime is the presence of detachment and reattachment points behind the step. The streamwise location of the reattachment point y_r is usually used as a parameter to evaluate the sensitivity of the numerical results to the mesh resolution [43]. The detachment and reattachment points are the locations where the skin friction coefficient $C_f = 2\tau_w/\rho U_b^2$ changes its signs along the heated wall. The profiles of the skin friction coefficients and the detachment and reattachment points locations are shown in Figure 3.18.

The calculated y_r values are reported in Table 3.6 for the four different grids. We also report the relative deviation of the calculated y_r with respect to the most refined mesh, i.e. Mesh 4. From Table 3.6, it can be seen that the relative deviation of y_r for Mesh 3 is below to 0.5%. Therefore, Mesh 3 has been employed for all the calculations.

3.2.2. Forced convection

Dynamic fields

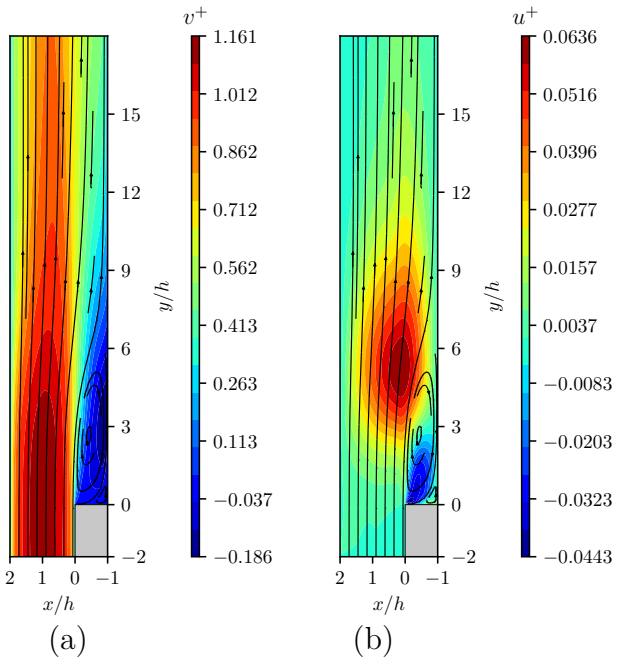

Figure 3.19: Contours of the non-dimensional streamwise velocity $v^+ = v/U_b$ (a) and wall-normal velocity $u^+ = u/U_b$ (b) with streamlines of the velocity field.

The dimensionless dynamic fields are reported and compared with DNS data for the case $Ri = 0$ corresponding to the forced convection regime. The contours of the non-dimensional streamwise $v^+ = v/U_b$ and wall-normal velocity component $u^+ = u/U_b$ are respectively reported in Figure 3.19a and b. The streamlines of the velocity field are also shown. The typical flow features for a backward-facing step configuration are observed, i.e. the flow separation taking place behind the step, the reattachment of the flow, the formation of two main vortexes behind the step: a bigger one rotating in the clockwise direction and a smaller one rotating in the opposite direction.

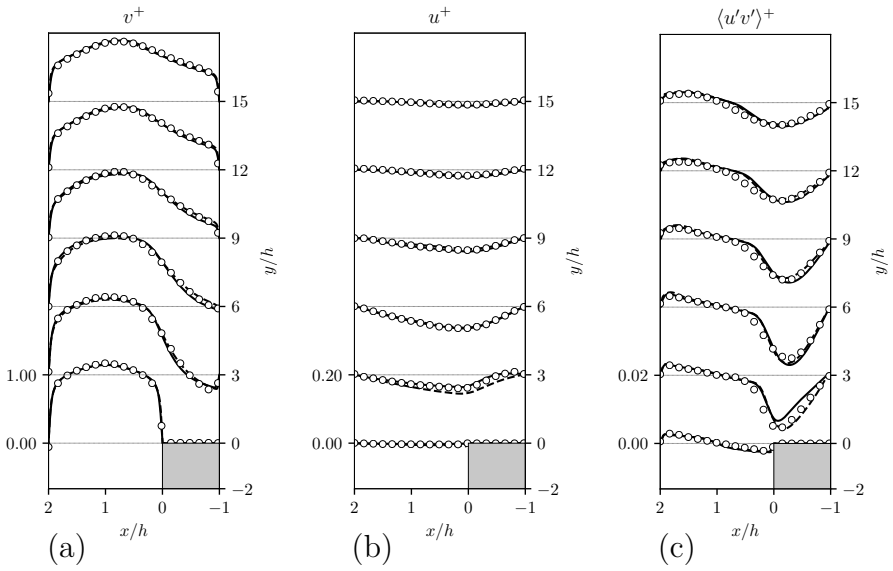

Figure 3.20: Profile of dynamical fields for $Ri = 0$: mean streamwise velocity v^+ (a), mean wall-normal velocity u^+ (b) and shear stress $\langle u'v' \rangle^+$ (c). —: 4AP; ---: I4P ∘ : DNS data.

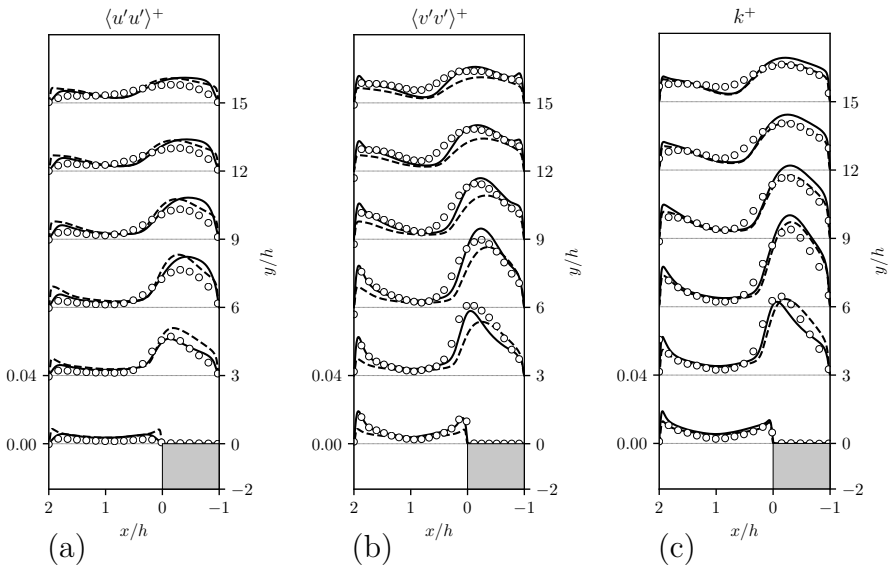

Figure 3.21: Profile of dynamical fields for $Ri = 0$: wall-normal normal stress $\langle u'u' \rangle^+$ (a), streamwise normal stress $\langle v'v' \rangle^+$ (b) and turbulent kinetic energy k^+ (c). —: 4AP; ---: I4P ∘ : DNS data.

Non-dimensional profiles of velocity are reported in solid lines for several streamwise coordinate y/h values for the anisotropic model (4AP). The

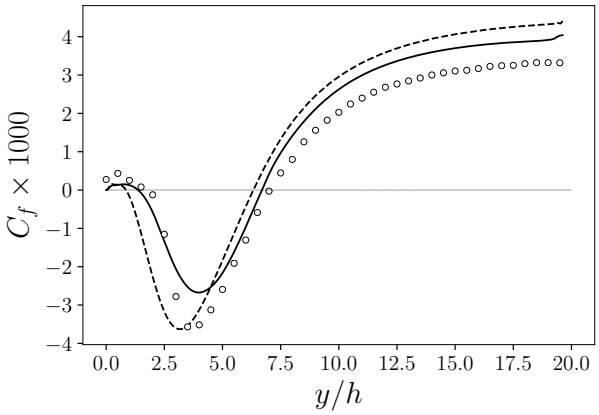

Figure 3.22: Skin friction coefficient C_f along the heated wall. —: 4AP; ---: I4P ◦ : DNS data.

streamwise positions included in these plots correspond to the locations where DNS data are available [69]. Numerical results obtained with the isotropic model (I4P) are also shown [14]. The streamwise v^+ and wall-normal velocity component u^+ are reported respectively in Figure 3.20a and Figure 3.20b. The velocity field prediction with the anisotropic four-parameter model is in good agreement with DNS results, while the isotropic model shows a slight deviation of the wall-normal velocity u^+ from DNS data at the non-dimensional height $y/h = 3$. The typical features of the flow over a backward-facing step, i.e. the separation and reattachment behind the step, can be observed from the plot taken at $y/h = 3$ where v^+ assumes negative values close to the heated wall.

In Figure 3.20c the non-dimensional turbulent shear stress $\langle u'v' \rangle^+ = \langle u'v' \rangle / U_b^2$ is reported in comparison with DNS data. The turbulent shear stress is mainly present in the layer behind the step at $x/h \approx 0$. For the isotropic four-parameter model results, we have computed the shear stress as $\langle u'v' \rangle = \nu_t(\partial u/\partial y + \partial v/\partial x)$. The evaluations obtained with both isotropic and anisotropic models are in good agreement with DNS data.

The wall-normal normal stress $\langle u'u' \rangle^+ = \langle u'u' \rangle / U_b^2$ and the streamwise normal stress $\langle v'v' \rangle^+ = \langle v'v' \rangle / U_b^2$ are reported respectively in Figure 3.21a and 3.21b. In Figure 3.21c the turbulent kinetic energy $k^+ = k/U_b^2$ is shown. These turbulent fields present a general good agreement with DNS data even though there are some discrepancies in the region behind the step. For the isotropic four-parameter model simulations, we have computed $\langle u'u' \rangle =$

$2/3k + 2\nu_t \partial u/\partial x$ and $\langle v'v' \rangle = 2/3k + 2\nu_t \partial v/\partial y$, according to Boussinesq approximation.

In Figure 3.22 the skin friction coefficient C_f along the heated wall is reported. The skin friction profile is subjected to a double change of sign, denoting the presence of two reattachment points. The skin friction coefficient assumes negative values in the recirculation zone, which is composed of a large clockwise rotating vortex. Directly behind the step, the principal recirculating vortex causes a secondary vortex rotating in the opposite direction. The position of the first reattachment point is approximately $y/h \approx 1.36$ for the anisotropic four-parameter model and $y/h \approx 1.91$ for DNS data. The second reattachment point is located approximately at $y/h \approx 6.68$. The DNS data give this point at $y/h \approx 7.01$, while Kasagi [84] gives this point at $y/h \approx 6.51$ through measurements.

Thermal fields

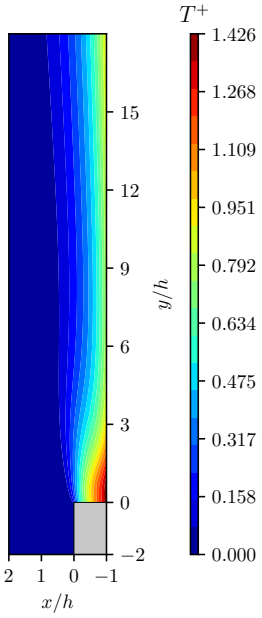

Figure 3.23: Contours of the non-dimensional temperature $T^+ = (T - T_{ref})/\Delta T$ for $Ri = 0$.

We now propose a comparison for thermal fields between the results obtained with the anisotropic four-parameter model and DNS data for the forced convection case. In Figure 3.23 contours of the non-dimensional

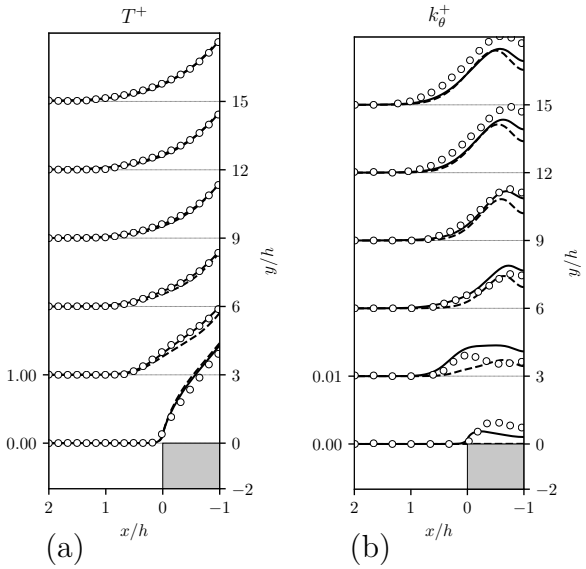

Figure 3.24: Profile of thermal fields for $Ri = 0$: mean temperature T^+ (a) and temperature fluctuations k_θ^+ (b). —: 4AP; ---: I4P ∘ : DNS data.

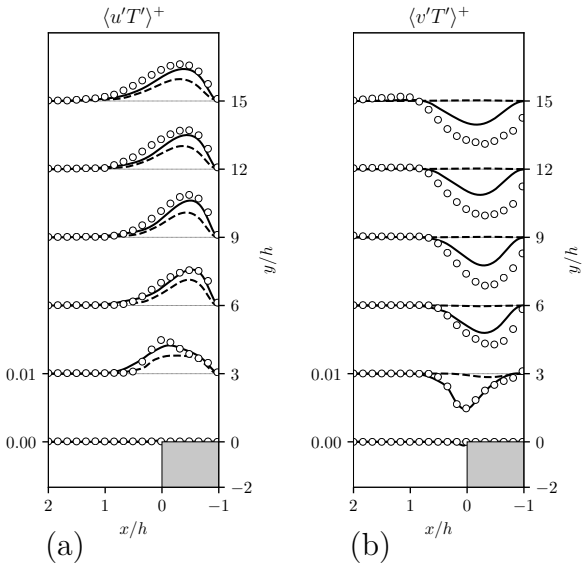

Figure 3.25: Profile of thermal fields for $Ri = 0$: mean wall-normal turbulent heat flux $\langle u'T'\rangle^+$ (a) and mean streamwise turbulent heat flux $\langle v'T'\rangle^+$(b). —: 4AP; ---: I4P ∘ : DNS data.

temperature $T^+ = (T - T_{ref})/\Delta T$ are reported for the simulation with the anisotropic four-parameter model. The hot fluid is located in the corner

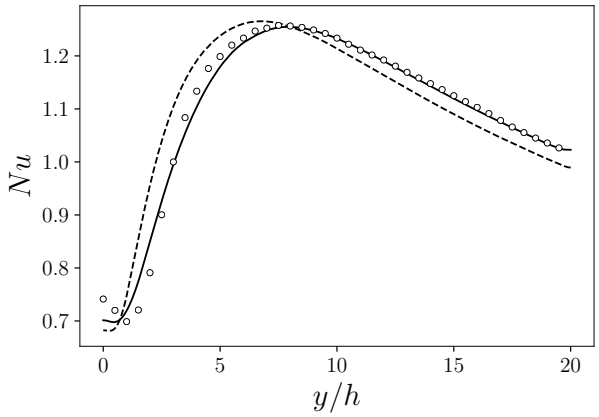

Figure 3.26: Nusselt number Nu along the heated wall for $Ri = 0$. —: 4AP; ---: I4P ◦ : DNS data.

between the step and the heated wall. A strong temperature increase is observed moving from the insulated wall towards the heated wall. The highest wall temperature is located in the recirculation zone and reaches a maximum closely behind the step due to the reduced heat transfer due to the backward flow.

Non-dimensional profiles of the mean temperature $T^+ = T/\Delta T$ are reported in Figure 3.24a for different values of streamwise coordinate y/h. The temperature difference ΔT is defined using the applied heat flux $\dot{q}$ setting $\Delta T = \dot{q}h/\lambda$, where λ is the liquid sodium thermal conductivity calculated for $T = T_{ref}$. The discrepancies with DNS results are limited to the plot taken at $y/h = 0$ where the temperature is slightly overestimated. With the isotropic model, the major discrepancies with DNS values are found on the plots taken at $y/h = 0$ and $y/h = 3$ where an over and underprediction of T^+ is respectively obtained. Non-dimensional mean squared temperature fluctuations $k_\theta^+ = 2k\theta/\Delta T^2$ are shown in Figure 3.24b for anisotropic and isotropic models. We observe good agreement with DNS results.

The turbulent heat flux along wall-normal $\langle u'T'\rangle^+ = \langle u'T'\rangle/(U_b\Delta T)$ and streamwise $\langle v'T'\rangle^+ = \langle v'T'\rangle/(U_b\Delta T)$ directions are reported respectively in Figure 3.25a and Figure 3.25b. The anisotropic model allows improving the prediction of the streamwise component which is completely underestimated with the isotropic model. The isotropic model assumes a unique scalar thermal diffusivity α_t for both turbulent heat flux components, i.e. $\langle u'T'\rangle = \alpha_t \partial T/\partial x$ and $\langle v'T'\rangle = \alpha_t \partial T/\partial y$. However, the mean temperature gradient

along the streamwise direction is small and for this reason the streamwise component is totally underestimated. With the proposed anisotropic model, the wall-normal component shows a better agreement with DNS data and the streamwise component results are only slightly underestimated.

The Nusselt number profile along the heated wall is shown in Figure 3.26. The Nusselt number is computed as $Nu = \dot{q}h/(T - T_{ref})\lambda$. When the Nusselt value is around 1 then the heat transfer is mostly diffusive due to the low Prandtl number of the liquid metal. Inside the recirculation zone, we have $Nu < 1$ then the heat transfer is prevented by the recirculating flow. As one can see in Figure 3.26, in the recirculation zone the Nusselt number is slightly overestimated with the isotropic model, while the anisotropic model is in good agreement with DNS data in all the regions.

3.2.3. Mixed convection

Dynamic fields

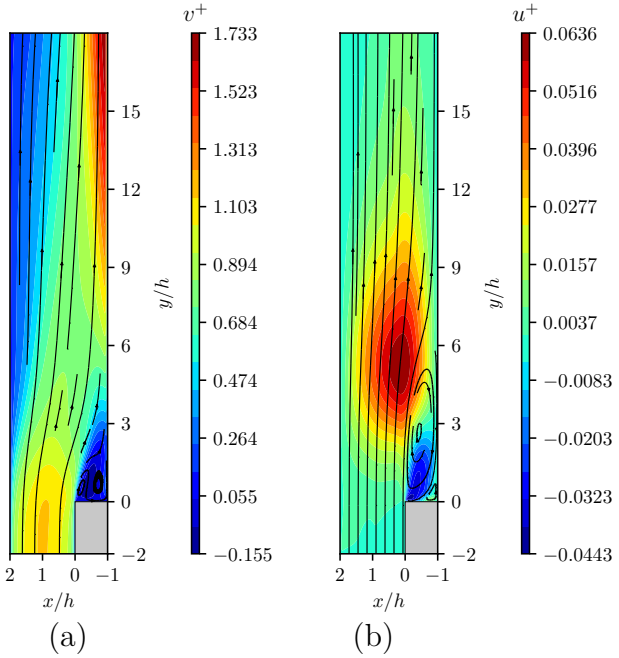

Figure 3.27: Contours of the non-dimensional streamwise velocity $v^+ = v/U_b$ (a) and wall-normal velocity $u^+ = u/U_b$ (b) with streamlines of the velocity field for $Ri = 0.338$.

In this section, the numerical results for flow fields are compared with DNS data and isotropic results for $Ri = 0.338$ corresponding to the mixed

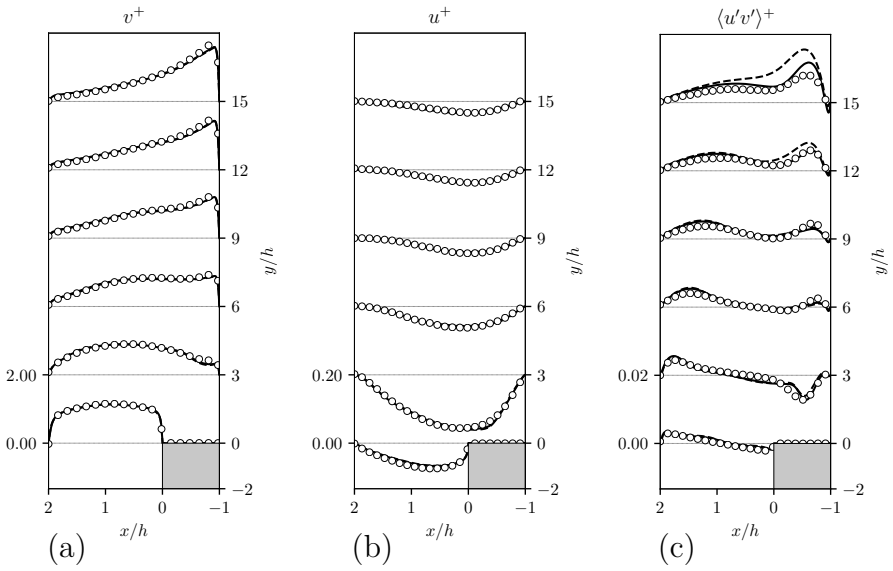

Figure 3.28: Profile of dynamical fields: mean streamwise velocity v^+ (a) mean wall-normal velocity u^+ (b) and shear stress $\langle u'v'^+ \rangle$ (c) for $Ri = 0.338$. —: 4AP; ---: I4P ∘ : DNS data.

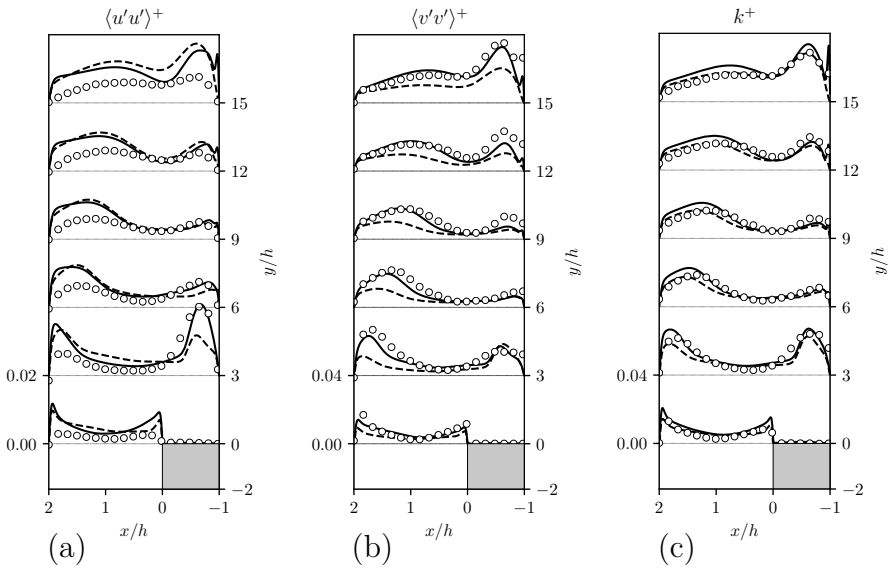

Figure 3.29: Profile of dynamical fields: wall-normal normal stress $\langle u'u' \rangle^+$ (a), streamwise normal stress $\langle v'v' \rangle^+$ (b) and turbulent kinetic energy k^+ (c) for $Ri = 0.338$.—: 4AP; ---: I4P ∘ : DNS data.

convection case. In Figure 3.27 the contours of the non-dimensional streamwise $v^+ = v/U_b$ and wall-normal $u^+ = u/U_b$ velocity components are shown.

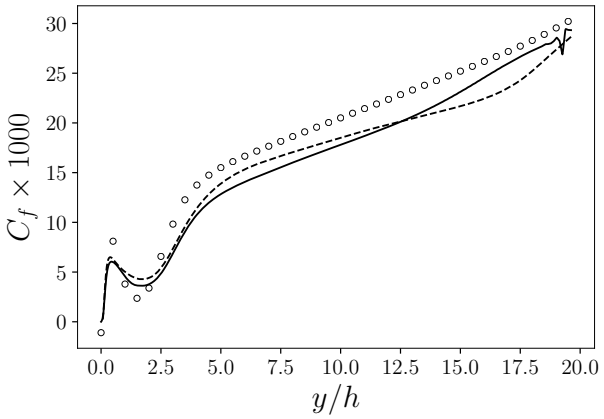

Figure 3.30: Skin friction coefficient C_f along the heated wall for $Ri = 0.338$. —: 4AP; ---: I4P ∘ : DNS data.

Also the streamlines of the velocity field are reported. In the proximity of the heated wall, $x/h = -1$, the fluid is warmer and is accelerated by buoyancy forces. Due to the continuity, the fluid from the rest of the domain is accelerated towards the heated wall and the streamwise velocity decreases strongly towards the insulated wall beyond $y/h = 6$. Buoyancy forces accelerate the hot fluid near the heated wall in streamwise direction and act against the rotation of the large clockwise rotating vortex found in the case of forced convection. Thus, the eddy rotating in the counterclockwise direction grows while the clockwise rotating vortex is reduced in size and completely detached from the wall.

Non-dimensional profiles of velocity are reported for several streamwise coordinate y/h values, for mixed convection regime. The streamwise $v^+ = v/U_b$ and wall-normal velocity component $u^+ = u/U_b$ are reported respectively in Figure 3.28a and Fig 3.28b. A jet flow develops near the heated wall due to the acceleration of the fluid caused by buoyancy. As a consequence, away from the heated wall, the streamwise velocity is significantly reduced. In Figure 3.28c the non-dimensional shear stress component $\langle u'v' \rangle^+ = \langle u'v' \rangle / U_b^2$ is reported in comparison with DNS data for mixed convection regime. The prediction of the shear stress is in good agreement with reference data but some discrepancies are observed near the heated wall in the locations $y/h > 9$.

The wall-normal normal stress $\langle u'u' \rangle^+ = \langle u'u' \rangle / U_b^2$ and the streamwise normal stress $\langle v'v' \rangle^+ = \langle v'v' \rangle / U_b^2$ are reported respectively in Figure 3.29a

and 3.21b for $Ri = 0.338$. In Figure 3.29c the turbulent kinetic energy $k^+ = k/U_b^2$ is shown. Buoyancy accelerates the warm fluid near the heated wall and generates strong wall shear stress. Shear stress, in turn, leads to the production of normal stresses. This effect can be seen by the peak of the streamwise normal stress $\langle v'v' \rangle^+$ and turbulent kinetic energy at $y/h > 12$ for $-1 < x/h < 0$. Some discrepancies in the prediction of the wall-normal normal stress can be observed in the near-wall region at the insulated wall.

In Figure 3.30 the skin friction coefficient C_f along the heated wall is reported for $Ri = 0.338$. The skin friction is positive along the heated channel since the clockwise rotating vortex is substantially reduced in size and completely detaches from the wall. The skin friction coefficient in the wall jet region increases almost linearly with the streamwise coordinate y/h. The skin coefficient with the anisotropic four-parameter model is slightly underestimated.

Thermal fields

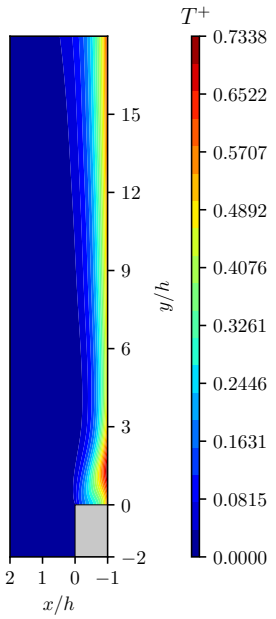

Figure 3.31: Contour of the non-dimensional temperature $T^+ = (T - T_{ref})/\Delta T$ for $Ri = 0.338$.

In Figure 3.31 contours of the non-dimensional temperature $T^+ = (T - T_{ref})/\Delta T$ are reported for the mixed convection case. Due to the influence

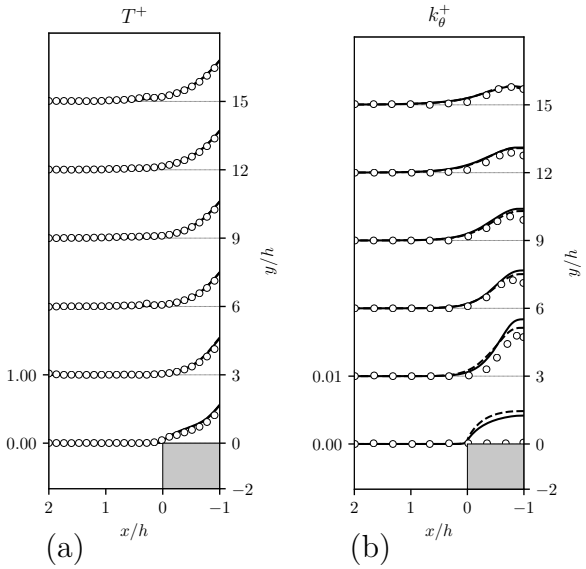

Figure 3.32: Profile of thermal fields for $Ri = 0.338$: mean temperature T^+ (a) and temperature fluctuations k_θ^+ (b). —: 4AP; ---: I4P ∘ : DNS data.

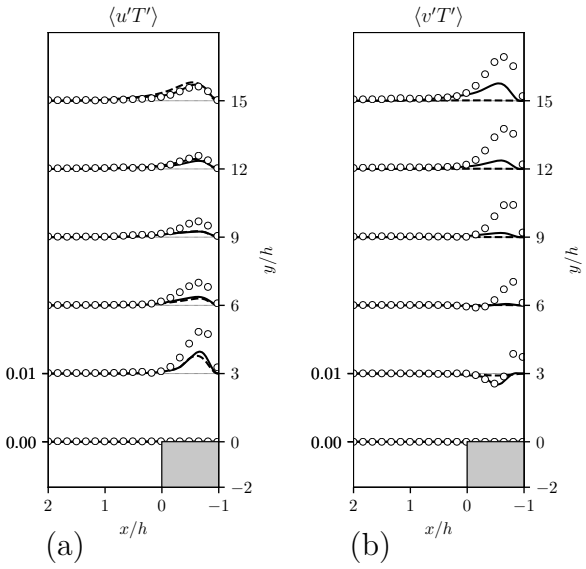

Figure 3.33: Profile of thermal fields for $Ri = 0.338$: mean wall-normal turbulent heat flux $\langle u'T' \rangle^+$ (a) and mean streamwise turbulent heat flux $\langle v'T' \rangle^+$(b). —: 4AP; ---: I4P ∘ : DNS data.

of buoyancy, heat transfer changes substantially. The wall temperature is substantially reduced in the mixed case compared to the forced case as a

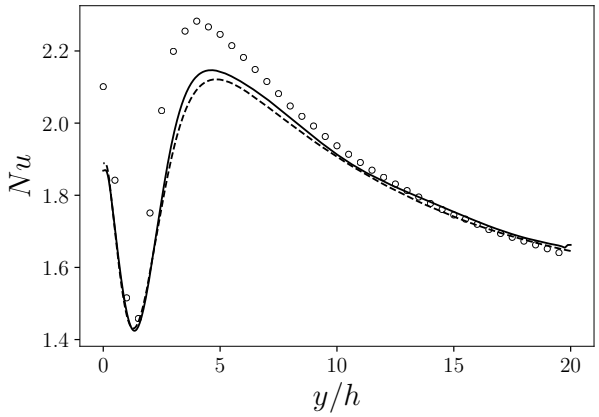

Figure 3.34: Nusselt number Nu along the heated wall for $Ri = 0.338$. —: 4AP; ---: I4P ◦ : DNS data.

result of enhanced heat transfer at the wall. Moreover, the mean temperature field is altered according to the modified flow field in the recirculation zone.

Non-dimensional profiles of temperature are reported in Figure 3.32a for different values of streamwise coordinate y/h. An overall good agreement with DNS data is obtained. A slight deviation from DNS results is observed on the plot at $y/h = 3$. There are no evident discrepancies between isotropic and anisotropic results. The non-dimensional temperature variance is reported in Figure 3.32b. Both isotropic and anisotropic models fail to predict the temperature fluctuations at $y/h = 0$, whereas in the other streamwise locations, the simulation results are in agreement with DNS data. The turbulent heat flux components along wall-normal and streamwise directions are reported respectively in Figure 3.33a and Figure 3.33b. The wall-normal turbulent heat flux is strongly underestimated near the heated wall for $y/h < 9$, for both anisotropic and isotropic simulations, while in the proximity of the outlet section $y/h > 12$ it is in good agreement with DNS data. The streamwise component is underestimated in the proximity of the heated wall for both models, but in the case of the isotropic model this field is almost null.

The Nusselt number profile along the heated wall is shown in Figure 3.34. If compared with the forced convection case, the Nusselt number presents larger values for all locations at the heated wall and a qualitatively similar shape as for the forced convection case. In the profile we can observe a

local minimum $Nu \approx 1.4$, corresponding to the vortex behind the step, and a local maximum $Nu \approx 2.2$, corresponding to the start of the wall jet. The heat transfer is strongly increased by the presence of buoyancy forces. The Nusselt prediction is in good agreement with DNS data, in particular the position of the minimum is accurately estimated with both isotropic and anisotropic models.

PART II

Optimal control

CHAPTER 4

Optimal control of Boussinesq equations

The optimization of complex systems in engineering is a crucial aspect that encourages and promotes research in the optimal control field. For flow control or optimization, we mean the attempt to control the mechanical and/or the thermodynamic state of a fluid to achieve desired purposes. Thus, optimization problems have three main ingredients. First, there is the objective, which is the reason why we want to control the flow. There are many objectives of interest in engineering applications, i.e. flow matching, drag minimization, enhancing or reducing turbulence. Mathematically, such an objective is expressed as a cost or objective functional. Next, there are controls or design parameters. We can have boundary controls, such as injection or suction of fluid [85] and heating or cooling temperature controls [86, 87, 88]; distributed control such as heat sources or magnetic fields [26]; lastly, shape controls such as geometric domains [89]. Finally, there exist constraints that determine what type of flow one is interested in, for example, viscous or inviscid flow, compressible or incompressible flow, stationary or time-dependent flow. Mathematically, the constraints are expressed in terms of a specific set of partial differential equations for the state variables. We can also have constraints motivated by practical necessities. The opti-

mization problem is then to find state and control variables that minimize the objective functional, subject to the requirement that the constraints are satisfied [25].

Liquid metals are widely studied as coolant fluids in Generation IV nuclear reactors or concentrating solar power plants. In the design of engineering devices such as heat exchangers, nuclear cores, and primary or secondary circuit pipes, optimization techniques can be used to find the optimal wall temperature or wall-normal heat flux to achieve specified objectives, as a target mean temperature, a velocity profile or a certain turbulence enhancement/reduction. In particular, we focus on applications in which buoyancy forces have a strong influence on the flow, such as in lead-cooled fast reactors (LFR). The thermodynamic properties of lead allow a high level of natural circulation cooling in the primary system of an LFR. For core cooling, LFR designs are generally characterized by the existence of strong natural circulation characteristics, during both operation and shutdown conditions [21]. In this framework, we focus on the optimal control of buoyant flows. Firstly, we study optimal control problems for thermally convected flows considering the Boussinesq system of equations, i.e. the coupled Navier-Stokes and temperature equations. This example is useful to introduce the adjoint method for optimal control. Then, to consider a more realistic model of the flow in a heat exchanger or nuclear core, we will consider the role of turbulence and the mathematical complexity that turbulence introduces in Chapter 5.

The structure of the Chapter is the following. First, we introduce some functional spaces, their norms, and some bilinear and trilinear forms that are used to express the weak formulation of the partial differential equations. Then, we formulate the optimization problem considering three different control mechanisms, which are Dirichlet boundary control, Neumann boundary control, and distributed control. For each case, we aim to study the optimal control problem from a mathematical point of view. To do so, we present the weak form of the boundary value problem and prove the existence of a solution. Then, we state the optimization problem and we claim the existence of an optimal solution. We use the method of Lagrange multipliers and we show that suitable Lagrange multipliers exist. Finally, we obtain the optimality system and we propose a numerical algorithm for the solution of such a system. After the mathematical analysis, we show some numerical results obtained considering the three different control

mechanisms and varying the objectives.

4.1. Notation

We introduce some functional spaces and their norms. We use standard notation $H^s(\mathcal{O})$ for Sobolev space of order s with respect to the set $\mathcal{O}$, which can be the flow domain $\Omega \subset \mathbb{R}^n$, with $n = 2, 3$, or its boundary Γ or a part of it. Of course, $H^0(\mathcal{O}) = L^2(\mathcal{O})$. Corresponding Sobolev spaces of vector-valued functions will be denoted by $\mathbf{H}^s(\mathcal{O})$. Of special interest is the space

$$\mathbf{H}^1(\Omega) = \left\{ v_i \in L^2(\Omega) \middle| \frac{\partial v_i}{\partial x_j} \in L^2(\Omega) \text{ for } i, j = 1, \ldots, n \right\}$$

and the subspace

$$\mathbf{H}^1_{\Gamma_j}(\Omega) = \left\{ \mathbf{v} \in \mathbf{H}^1(\Omega) | \mathbf{v} = \mathbf{0} \text{ on } \Gamma_j \right\},$$

where Γ_j is a subset of Γ. Also, we write $\mathbf{H}^1_0(\Omega) = \mathbf{H}^1_\Gamma(\Omega)$. Let $\mathbf{H}^{1*}_{\Gamma_s}(\Omega)$ denote the dual space of $\mathbf{H}^1_{\Gamma_s}(\Omega)$. Note that $\mathbf{H}^{1*}_{\Gamma_s}(\Omega)$ is a subspace of $\mathbf{H}^{-1}(\Omega)$, where the latter is the dual space of $\mathbf{H}^1_0(\Omega)$. We define the space of square integrable functions having zero mean over Ω as

$$L^2_0(\Omega) = \left\{ q \in L^2(\Omega) \middle| \int_\Omega q d\mathbf{x} = 0 \right\}.$$

We also define the solenoidal spaces

$$\mathbf{V} = \{ \mathbf{v} \in \mathbf{H}^1(\Omega) \,|\, \nabla \cdot \mathbf{v} = 0 \}, \quad \mathbf{V}_0 = \{ \mathbf{v} \in \mathbf{H}^1_0(\Omega) \,|\, \nabla \cdot \mathbf{v} = 0 \}.$$

It is well known that $\mathbf{V}$ and $\mathbf{V}_0$ are separable Hilbert spaces [90]. A Hilbert space is separable if and only if it admits a countable orthonormal basis. Norms of functions belonging to $H^m(\mathcal{O})$ are denoted by $\|\cdot\|_{m,\mathcal{O}}$. We define, for $(fg) \in L^1(\mathcal{O})$ and $(\mathbf{u} \cdot \mathbf{v}) \in L^1(\mathcal{O})$

$$(f, g)_\mathcal{O} = \int_\mathcal{O} fg d\mathbf{x}, \qquad (\mathbf{u}, \mathbf{v})_\mathcal{O} = \int_\mathcal{O} \mathbf{u} \cdot \mathbf{v} d\mathbf{x}.$$

Whenever possible, we will neglect the domain label. Thus, the inner product in $L^2(\Omega)$ and $\mathbf{L}^2(\Omega)$ are both denoted by $(\cdot, \cdot)$. This notation will also be employed to denote pairings between Sobolev spaces and their duals.

We will use the bilinear forms

$$a(\mathbf{u}, \mathbf{v}) = \int_\Omega \nabla \mathbf{u} : \nabla \mathbf{v} d\mathbf{x} \qquad \forall \mathbf{u}, \mathbf{v} \in \mathbf{H}^1(\Omega), \tag{4.1}$$

$$a(T,\theta) = \int_\Omega \nabla T \cdot \nabla \theta d\mathbf{x} \qquad \forall T, \theta \in H^1(\Omega)\,, \tag{4.2}$$

$$b(\mathbf{u}, q) = -\int_\Omega q \nabla \cdot \mathbf{u} d\mathbf{x} \qquad \forall q \in L^2_0(\Omega), \forall \mathbf{u} \in \mathbf{H}^1(\Omega)\,, \tag{4.3}$$

and the trilinear forms

$$c(\mathbf{w}, \mathbf{u}, \mathbf{v}) = \int_\Omega \mathbf{w} \cdot \nabla \mathbf{u} \cdot \mathbf{v} d\mathbf{x} \qquad \forall \mathbf{w}, \mathbf{u}, \mathbf{v} \in \mathbf{H}^1(\Omega)\,, \tag{4.4}$$

$$c(\mathbf{w}, T, \theta) = \int_\Omega \mathbf{w} \cdot \nabla T \theta d\mathbf{x} \qquad \forall \mathbf{w} \in \mathbf{H}^1(\Omega), \forall T, \theta \in H^1(\Omega)\,. \tag{4.5}$$

These forms are continuous in the sense that there exist constants c_a, c_b and c_c such that

$$|a(\mathbf{u}, \mathbf{v})| \leq c_a \|\mathbf{u}\|_1 \|\mathbf{v}\|_1 \qquad \forall \mathbf{u}, \mathbf{v} \in \mathbf{H}^1(\Omega)\,, \tag{4.6}$$

$$|a(T, \theta)| \leq c_a \|T\|_1 \|\theta\|_1 \qquad \forall T, \theta \in H^1(\Omega)\,, \tag{4.7}$$

$$|b(\mathbf{u}, q)| \leq c_b \|\mathbf{v}\|_1 \|q\|_0 \qquad \forall q \in L^2_0(\Omega), \forall \mathbf{v} \in \mathbf{H}^1(\Omega), \tag{4.8}$$

$$|c(\mathbf{w}, \mathbf{u}, \mathbf{v})| \leq c_c \|\mathbf{w}\|_1 \|\mathbf{u}\|_1 \|\mathbf{v}\|_1 \qquad \forall \mathbf{w}, \mathbf{u}, \mathbf{v} \in \mathbf{H}^1(\Omega)\,, \tag{4.9}$$

$$|c(\mathbf{w}, T, \theta)| \leq c_c \|\mathbf{w}\|_1 \|T\|_1 \|\theta\|_1 \qquad \forall \mathbf{w} \in \mathbf{H}^1(\Omega), \forall T, \theta \in H^1(\Omega)\,. \tag{4.10}$$

Moreover, we have

$$c(\mathbf{u}, \mathbf{v}, \mathbf{v}) = 0 \qquad \forall \mathbf{u} \in \mathbf{V}, \forall \mathbf{v} \in \mathbf{H}^1(\Omega)\,, \tag{4.11}$$

$$c(\mathbf{u}, T, T) = 0 \qquad \forall \mathbf{u} \in \mathbf{V}, \forall T \in H^1(\Omega)\,. \tag{4.12}$$

Furthermore, we have the coercivity properties

$$a(\mathbf{v}, \mathbf{v}) \geq C_a \|\mathbf{v}\|_1^2 \qquad \forall \mathbf{v} \in \mathbf{H}^1(\Omega)\,, \tag{4.13}$$

$$a(T, T) \geq C_a \|T\|_1^2 \qquad \forall T \in H^1(\Omega)\,, \tag{4.14}$$

and

$$\sup_{\mathbf{v} \neq \mathbf{0} \in \mathbf{H}^1_0(\Omega)} \frac{b(\mathbf{v}, q)}{\|\mathbf{v}\|_1} \geq C_b \|q\|_0 \qquad \forall q \in L^2_0(\Omega)\,, \tag{4.15}$$

for some constants C_a and $C_b > 0$.

4.2. Optimal control of Boussinesq equations

In this chapter, we aim to study optimal control problems for stationary incompressible flows in mixed or natural convection regime. In this application, the dependence on the temperature field cannot be neglected

in the Navier-Stokes equation. Thus, temperature and velocity fields are mutual dependent through buoyancy forces and advection. These flows are governed by the Boussinesq equations derived in Chapter 1

$$\nabla \cdot \mathbf{u} = 0 \qquad \text{in } \Omega\,, \tag{4.16}$$

$$\mathbf{u} \cdot \nabla \mathbf{u} + \nabla p - \nu \Delta \mathbf{u} = \mathbf{f} - \beta \mathbf{g} T \qquad \text{in } \Omega\,, \tag{4.17}$$

$$\mathbf{u} \cdot \nabla T - \alpha \Delta T = Q \qquad \text{in } \Omega\,. \tag{4.18}$$

where Ω is a regular bounded open set in $\mathbb{R}^d$, $d = 2$ or 3 with boundary Γ. We have dropped the Einstein notation and we have indicated with Δ the Laplace operator $\nabla \cdot \nabla = \nabla^2 = \Delta$. In (4.16)-(4.18), $\mathbf{u}$, p and T denote the velocity, pressure and temperature fields, while $\mathbf{f}$ is a body force, Q is a heat source and $\mathbf{g}$ is the gravitational acceleration. The coefficients α, ν and β are the fluid thermal diffusivity, kinematic viscosity and coefficient of expansion respectively. The system (4.16)-(4.18) is closed with appropriate boundary conditions on $\partial\Omega$. For the velocity field we set a Dirichlet boundary condition, while for the temperature we consider a mixed boundary condition

$$\begin{aligned} &\mathbf{u} = \mathbf{w} && \text{on } \partial\Omega\,, \\ &T = g_t && \text{on } \Gamma_d\,, \\ &\alpha \nabla T \cdot \mathbf{n} = g_{t,n} && \text{on } \Gamma_n\,, \end{aligned} \tag{4.19}$$

where Γ_d and Γ_n indicate boundaries where Dirichlet and Neumann boundary conditions are respectively applied, with $\Gamma_d \cup \Gamma_n = \Gamma = \partial\Omega$.

We formulate our control problem as a constrained minimization of the following objective functional

$$\mathcal{T}(\mathbf{u}, T) = \frac{\alpha_u}{2} \int_{\Omega_d} |\mathbf{u} - \mathbf{u}_d|^2 d\mathbf{x} + \frac{\alpha_T}{2} \int_{\Omega_d} |T - T_d|^2 d\mathbf{x}\,, \tag{4.20}$$

with the Boussinesq equations (4.16)-(4.18) as constraints. In (4.20) the functions $\mathbf{u}_d$ and T_d are given desired velocity and temperature distributions. The terms in the functional (4.20) measure the $L^2(\Omega)$ distance between the velocity $\mathbf{u}$ and the target field $\mathbf{u}_d$, and/or between the temperature T and the target field T_d. The non-negative penalty parameters α_u and α_T can be used to change the relative importance of the terms appearing in the definition of the functional. If $\alpha_u = 0$ we have as objective a temperature matching case, if $\alpha_T = 0$ we consider a velocity matching case. The control can be a volumetric heat source, a boundary temperature, or a heat flux. In

all these cases, the control has to be limited to avoid unbounded solutions. To do so, we can add a constraint limiting the value of the admissible control, or we can penalize the objective functional $\mathcal{T}$ adding a regularization term. With this second approach, we do not need to impose any a priori constraints on the size of the control. Let c be the control belonging to a Hilbert space $H^s(\mathcal{O})$, we can then define a cost functional

$$\mathcal{J}(\mathbf{u}, T, c) = \frac{\alpha_u}{2}\int_{\Omega_d} |\mathbf{u} - \mathbf{u}_d|^2 d\mathbf{x} + \frac{\alpha_T}{2}\int_{\Omega_d} |T - T_d|^2 d\mathbf{x} + \\ +\lambda ||c||_{H^s(\mathcal{O})}\,, \tag{4.21}$$

where the last term contains the $H^s(\mathcal{O})$-norm of the control c penalized with a parameter λ. The value of the parameter λ is used to change the relative importance of objective-terms and cost-terms. The real goal of the optimization is to minimize the first terms appearing in (4.21).

4.2.1. Dirichlet boundary control

In a Dirichlet boundary control problem, we aim to control the fluid state acting on the temperature on a portion of the boundary $\Gamma_c \subseteq \Gamma_d$. The boundary condition reported in (4.19) can be written in this case as

$$\begin{aligned} &\mathbf{u} = \mathbf{w} && \text{on } \partial\Omega\,, \\ &T = g_t && \text{on } \Gamma_i\,, \\ &T = g_t + T_c && \text{on } \Gamma_c\,, \\ &\alpha \nabla T \cdot \mathbf{n} = g_{t,n} && \text{on } \Gamma_n\,, \end{aligned} \tag{4.22}$$

where $\Gamma_i = \Gamma_d \setminus \Gamma_c$. In (4.22) g_t, $g_{t,n}$ and $\mathbf{w}$ are given functions, while T_c is the control. Thus Γ_i and Γ_c denote the portions of Γ_d where temperature control is and is not applied, respectively. The cost functional is given as follows

$$\mathcal{J}(\mathbf{u}, T, T_c) = \frac{\alpha_u}{2}\int_{\Omega_d} |\mathbf{u} - \mathbf{u}_d|^2 d\mathbf{x} + \frac{\alpha_T}{2}\int_{\Omega_d} |T - T_d|^2 d\mathbf{x} + \\ +\frac{\lambda}{2}\int_{\Gamma_c} (|T_c|^2 + |\nabla_s T_c|^2) d\mathbf{x}\,, \tag{4.23}$$

where ∇_s denotes the surface gradient operator, i.e. $\nabla_s f := \nabla f - \mathbf{n}(\mathbf{n}\cdot\nabla f)$. The cost contribution measures the $H^1(\Gamma_c)$-norm of the control T_c.

Weak formulation

The weak form of the boundary value problem (4.16)-(4.18) and (4.22) is given as follows: find $(\mathbf{u}, p, T) \in \mathbf{H}^1(\Omega) \times L^2_0(\Omega) \times H^1(\Omega)$ such that

$$\begin{aligned} & b(\mathbf{u}, q) = 0 && \forall q \in L^2_0(\Omega)\,, \\ & \nu a(\mathbf{u}, \mathbf{v}) + c(\mathbf{u}, \mathbf{u}, \mathbf{v}) + b(\mathbf{v}, p) = (\mathbf{f}, \mathbf{v}) + \\ & \qquad - \beta(\mathbf{g}T, \mathbf{v}) && \forall \mathbf{v} \in \mathbf{H}^1_0(\Omega)\,, \\ & \alpha a(T, \varphi) + c(\mathbf{u}, T, \varphi) = (Q, \varphi) + (g_{t,n}, \varphi)_{\Gamma_n} && \forall \varphi \in H^1_{\Gamma_d}(\Omega)\,, \\ & (T, s_T)_{\Gamma_d} = (g_t, s_T)_{\Gamma_d} + (T_c, s_T)_{\Gamma_c} && \forall s_T \in H^{-1/2}(\Gamma_d)\,. \end{aligned} \tag{4.24}$$

One may compute the normal heat flux on Γ_d as

$$q_n = -\alpha \nabla T \cdot \mathbf{n}|_{\Gamma_d}\,. \tag{4.25}$$

The existence of the solution of the system (4.24) has been proved in [87]. Here we report the cited theorem.

Theorem 4.1. *For every $g_t \in H^1(\Gamma_i)$, $T_c \in H^1(\Gamma_c)$, $g_{t,n} \in L^2(\Gamma_n)$, $Q \in L^2(\Omega)$, $\mathbf{f} \in \mathbf{L}^2(\Omega)$, $\mathbf{w} \in \mathbf{H}^1(\Gamma)$, the Boussinesq equations (4.24) have a solution $(\mathbf{u}, p, T) \in \mathbf{H}^1(\Omega) \times H^1(\Omega) \times L^2_0(\Omega)$. Moreover if $(\mathbf{u}, p, T)$ is a solution of (4.24), then $(\mathbf{u}, p, T) \in \mathbf{V} \cap \mathbf{H}^2(\Omega) \times L^2_0(\Omega) \cap H^1(\Omega) \times H^s(\Omega) (1 \leq s \leq \frac{3}{2})$ and there is a continuos function P_s for each s such that*

$$\begin{aligned} \|\mathbf{u}\|_2 + \|p\|_1 + \|T\|_s \leq P_s(\|\mathbf{f}\|_0 + \|Q\|_0 + \|g_{t,n}\|_{0,\Gamma_n} + \|g_t\|_{1,\Gamma_i} + \\ + \|T_c\|_{1,\Gamma_c} + \|\mathbf{w}\|_{1,\Gamma})\,. \end{aligned} \tag{4.26}$$

Proof. The proof of this result can be found in [87]. □

The optimization problem and existence of optimal solution

We state the optimal control problem. We look for a $(\mathbf{u}, p, T, T_c) \in \mathbf{H}^1(\Omega) \times L^2_0(\Omega) \times H^1(\Omega) \times H^1_0(\Gamma_c)$ such that the cost functional (4.23) is minimized subject to the constraints (4.24). The admissible set of states and controls is

$$\begin{aligned} \mathcal{U}_{ad} = \{(\mathbf{u}, p, T, T_c) \in \mathbf{H}^1(\Omega) \times L^2_0(\Omega) \times H^1(\Omega) \times H^1_0(\Gamma_c) : \\ \mathcal{J}(\mathbf{u}, T, T_c) < \infty \text{ and (4.24) is satified.}\} \end{aligned} \tag{4.27}$$

Then $(\hat{\mathbf{u}}, \hat{p}, \hat{T}, \hat{T}_c) \in \mathcal{U}_{ad}$ is called an optimal solution if there exists $\varepsilon > 0$ such that

$$\begin{aligned} \mathcal{J}(\hat{\mathbf{u}}, \hat{p}, \hat{T}, \hat{T}_c,) \leq \mathcal{J}(\mathbf{u}, p, T, T_c) \quad \forall (\mathbf{u}, p, T, T_c) \in \mathcal{U}_{ad} \text{ satisfying} \\ \|\mathbf{u} - \hat{\mathbf{u}}\|_1 + \|p - \hat{p}\|_0 + \|T - \hat{T}\|_1 + \|T_c - \hat{T}_c\|_{1,\Gamma_c} < \varepsilon \,. \end{aligned} \tag{4.28}$$

We now show that an optimal solution exists.

Theorem 4.2. *Let $\mathcal{U}_{ad}$ be not empty. There exists at least one optimal solution $(\hat{\mathbf{u}}, \hat{p}, \hat{T}, \hat{T}_c) \in \mathcal{U}_{ad}$.*

Proof. The existence of an optimal solution can be proved based on standard techniques. Let $\{\mathbf{u}^{(n)}, p^{(n)}, T^{(n)}, T_c^{(n)}\}$ be a sequence in $\mathcal{U}_{ad}$ such that

$$\lim_{n\to\infty} \mathcal{J}(\mathbf{u}^{(n)}, p^{(n)}, T^{(n)}, T_c^{(n)}) = \inf_{(\mathbf{v},q,S,z)\in\mathcal{U}_{ad}} \mathcal{J}(\mathbf{v}, q, S, z) \,. \tag{4.29}$$

By the definition of $\mathcal{U}_{ad}$ we have

$$\begin{aligned} & b(\mathbf{u}^{(n)}, q) = 0 && \forall q \in L_0^2(\Omega) \,, \\ & \nu a(\mathbf{u}^{(n)}, \mathbf{v}) + c(\mathbf{u}^{(n)}, \mathbf{u}^{(n)}, \mathbf{v}) + b(\mathbf{v}, p^{(n)}) = \\ & \qquad = (\mathbf{f}, \mathbf{v}) - \beta(\mathbf{g}T^{(n)}, \mathbf{v}) && \forall \mathbf{v} \in \mathbf{H}_0^1(\Omega) \,, \\ & \alpha a(T^{(n)}, \varphi) + c(\mathbf{u}^{(n)}, T^{(n)}, \varphi) = (Q, \varphi) + \\ & \qquad + (g_{t,n}, \varphi)_{\Gamma_n} && \forall \varphi \in H_{\Gamma_d}^1(\Omega) \,, \\ & (T^{(n)}, s_T)_{\Gamma_d} = (g_t, s_T)_{\Gamma_d} + (T_c^{(n)}, s_T)_{\Gamma_c} && \forall s_T \in H^{-1/2}(\Gamma_d) \,. \end{aligned} \tag{4.30}$$

By (4.23) and (4.27) we can see that $\{\|T_c^{(n)}\|_{1,\Gamma_c}\}$ is uniformly bounded. Also by (4.26) we have that $\{\|\mathbf{u}^{(n)}\|_1\}$, $\{\|p^{(n)}\|_0\}$ and $\{\|T^{(n)}\|_1\}$ are uniformly bounded. We may then extract subsequences $\{\mathbf{u}^{(n)}, p^{(n)}, T^{(n)}, T_c^{(n)}\}$ converging to $(\hat{\mathbf{u}}, \hat{p}, \hat{T}, \hat{T}_c)$

$$\begin{aligned} T_c^{(n)} &\rightharpoonup \hat{T}_c && \text{in } H_0^1(\Gamma_c) \,, \\ \mathbf{u}^{(n)} &\rightharpoonup \hat{\mathbf{u}} && \text{in } \mathbf{H}^1(\Omega) \,, && \text{and } \nabla\mathbf{u}^{(n)} \rightharpoonup \nabla\hat{\mathbf{u}} \text{ in } L^2(\Omega) \,, \\ T^{(n)} &\rightharpoonup \hat{T} && \text{in } H^1(\Omega) \,, && \text{and } \nabla T^{(n)} \rightharpoonup \nabla\hat{T} \text{ in } L^2(\Omega) \,, \\ p^{(n)} &\rightharpoonup \hat{p} && \text{in } L_0^2(\Omega) \,, \\ \mathbf{u}^{(n)} &\to \hat{\mathbf{u}} && \text{in } \mathbf{L}^2(\Omega) \,, \\ T^{(n)}|_\Gamma &\to \hat{T}|_\Gamma && \text{in } L^2(\Gamma) \,, \\ \mathbf{u}^{(n)}|_\Gamma &\to \hat{\mathbf{u}}|_\Gamma && \text{in } \mathbf{L}^2(\Gamma) \,. \end{aligned}$$

The symbols of full and half arrows denote strong and weak convergence [87]. The last two convergence results above follow from the compact embeddings $\mathbf{H}^1(\Omega) \subset \mathbf{L}^2(\Omega)$ and $H^{1/2}(\Gamma_c) \subset L^2(\Gamma_c)$. We may pass to the limit in (4.30) to determine that $(\hat{\mathbf{u}}, \hat{p}, \hat{T}, \hat{T}_c)$ satisfies (4.24). Indeed, the only troublesome term passing to the limit is the nonlinearity $c(\cdot,\cdot,\cdot)$. However, note that

$$c(\mathbf{u}^{(n)}, \mathbf{u}^{(n)}, \mathbf{v}) = \int_\Gamma (\mathbf{u}^{(n)} \cdot \mathbf{n})\mathbf{u}^{(n)} \cdot \mathbf{v} ds - \int_\Omega \mathbf{u}^{(n)} \cdot \nabla \mathbf{v} \cdot \mathbf{u}^{(n)} d\mathbf{x}\,, \quad (4.31)$$

$\forall \mathbf{v} \in C^\infty(\bar{\Omega})$, where $\bar{\Omega}$ indicates the closure of Ω. Since $\mathbf{u}^{(n)} \to \hat{\mathbf{u}}$ in $\mathbf{L}^2(\Omega)$ and $\mathbf{u}^{(n)}|_\Gamma \to \hat{\mathbf{u}}|_\Gamma$ in $\mathbf{L}^2(\Gamma)$, we have that

$$\lim_{n\to\infty} c(\mathbf{u}^{(n)}, \mathbf{u}^{(n)}, \mathbf{v}) = \int_\Gamma (\hat{\mathbf{u}}\cdot\mathbf{n})\hat{\mathbf{u}}\cdot\mathbf{v} ds - \int_\Omega \hat{\mathbf{u}}\cdot\nabla\mathbf{v}\cdot\hat{\mathbf{u}} d\mathbf{x} = c(\hat{\mathbf{u}}, \hat{\mathbf{u}}, \mathbf{v})\,, \quad (4.32)$$

$\forall \mathbf{v} \in C^\infty(\bar{\Omega})$. Since $C^\infty(\bar{\Omega})$ is dense in $H^1(\Omega)$ we also have that

$$\lim_{n\to\infty} c(\mathbf{u}^{(n)}, \mathbf{u}^{(n)}, \mathbf{v}) = c(\hat{\mathbf{u}}, \hat{\mathbf{u}}, \mathbf{v})\,, \qquad \forall \mathbf{v} \in H^1(\Omega)\,. \quad (4.33)$$

Thus, $(\hat{\mathbf{u}}, \hat{p}, \hat{T}, \hat{T}_c)$ satisfies (4.24). □

The existence of Lagrange multipliers

We wish to use the method of Lagrange multipliers to turn the constrained optimization problem (4.27) into an unconstrained one. We first show that the suitable Lagrange multipliers exist. Now we consider all the constraint equations and the functional in two mappings in order to study their differential properties. It is convenient to define the following functional spaces

$$\mathbf{B}_1 = \mathbf{H}^1(\Omega) \times L^2_0(\Omega) \times H^1(\Omega) \times H^1_0(\Gamma_c) \times H^{-\frac{1}{2}}(\Gamma_d)\,, \quad (4.34)$$

$$\mathbf{B}_2 = \mathbf{H}^{-1}(\Omega) \times L^2_0(\Omega) \times H^{1*}_{\Gamma_i}(\Omega) \times H^{\frac{1}{2}}(\Gamma_d)\,, \quad (4.35)$$

$$\mathbf{B}_3 = \mathbf{H}^1_0(\Omega) \times L^2_0(\Omega) \times H^1(\Omega) \times H^1_0(\Gamma_c) \times H^{-\frac{1}{2}}(\Gamma_d)\,. \quad (4.36)$$

Let $M : \mathbf{B}_1 \to \mathbf{B}_2$ denote the generalized constraint equations, i.e. $M(\mathbf{z}) = \mathbf{l}$ for $\mathbf{z} = (\mathbf{u}, p, T, T_c, q_n) \in \mathbf{B}_1$ and $(\mathbf{l}_1, l_2, l_3, l_4) \in \mathbf{B}_2$ if and only if

$$\begin{aligned}
&\nu a(\mathbf{u}, \mathbf{v}) + c(\mathbf{u}, \mathbf{u}, \mathbf{v}) + b(\mathbf{v}, p) - (\mathbf{f}, \mathbf{v}) + \\
&\qquad + \beta(\mathbf{g}T, \mathbf{v}) = (\mathbf{l}_1, \mathbf{v}) && \forall \mathbf{v} \in \mathbf{H}^1_0(\Omega)\,, \\
&b(\mathbf{u}, q) = (l_2, q) && \forall q \in L^2_0(\Omega)\,, \\
&\alpha a(T, \varphi) + c(\mathbf{u}, T, \varphi) - (Q, \varphi) - (g_{t,n}, \varphi)_{\Gamma_n} + && \quad (4.37) \\
&\qquad - (q_n, \varphi)_{\Gamma_c} = (l_3, \varphi) && \forall \varphi \in H^1_{\Gamma_i}(\Omega)\,, \\
&(T, s_T)_{\Gamma_d} - (g_t, s_T)_{\Gamma_d} - (T_c, s_T)_{\Gamma_c} = \\
&\qquad = (l_4, s_T)_{\Gamma_d} && \forall s_T \in H^{-1/2}(\Gamma_d)\,.
\end{aligned}$$

Thus, the constraint (4.24) can be expressed as $M(\mathbf{u}, p, T, T_c, q_n) = \mathbf{0}$. Let $(\hat{\mathbf{u}}, \hat{p}, \hat{T}, \hat{T}_c) \in \mathbf{H}^1(\Omega) \times L^2_0(\Omega) \times H^1(\Omega) \times H^1_0(\Gamma_c)$ denote an optimal solution in the sense of (4.28). Then, consider the nonlinear operator $N : \mathbf{B}_1 \to \mathbb{R} \times \mathbf{B}_2$ defined by

$$N(\mathbf{u}, p, T, T_c, q_n) = \begin{pmatrix} \mathcal{J}(\mathbf{u}, T, T_c) - \mathcal{J}(\hat{\mathbf{u}}, \hat{T}, \hat{T}_c) \\ M(\mathbf{u}, p, T, T_c, q_n) \end{pmatrix}. \tag{4.38}$$

Given $\mathbf{z} = (\mathbf{u}, p, T, T_c, q_n) \in \mathbf{B}_1$ the operator $M'(\mathbf{z}) : \mathbf{B}_3 \to \mathbf{B}_2$ may be defined as $M'(\mathbf{z}) \cdot \tilde{\mathbf{z}} = \tilde{\mathbf{l}}$ for $\tilde{\mathbf{z}} = (\tilde{\mathbf{u}}, \tilde{p}, \tilde{T}, \tilde{T}_c, \tilde{q}_n) \in \mathbf{B}_3$ and $\tilde{\mathbf{l}} = (\tilde{\mathbf{l}}_1, \tilde{l}_2, \tilde{l}_3, \tilde{l}_4) \in \mathbf{B}_2$ if and only if

$$\begin{aligned}
&\nu a(\tilde{\mathbf{u}}, \mathbf{v}) + c(\tilde{\mathbf{u}}, \mathbf{u}, \mathbf{v}) + c(\mathbf{u}, \tilde{\mathbf{u}}, \mathbf{v}) + b(\mathbf{v}, \tilde{p}) + \\
&\qquad + \beta(\mathbf{g}\tilde{T}, \mathbf{v}) = (\tilde{\mathbf{l}}_1, \mathbf{v}) && \forall \mathbf{v} \in \mathbf{H}^1_0(\Omega)\,, \\
&b(\tilde{\mathbf{u}}, q) = (\tilde{l}_2, q) && \forall q \in L^2_0(\Omega)\,, \\
&\alpha a(\tilde{T}, \varphi) + c(\tilde{\mathbf{u}}, T, \varphi) + c(\mathbf{u}, \tilde{T}, \varphi) + \\
&\qquad - (\tilde{q}_n, \varphi)_{\Gamma_c} = (\tilde{l}_3, \varphi) && \forall \varphi \in H^1_{\Gamma_i}(\Omega)\,, \\
&(\tilde{T}, s_T)_{\Gamma_d} - (\tilde{T}_c, s_T)_{\Gamma_c} = (\tilde{l}_4, s_T)_{\Gamma_d} && \forall s_T \in H^{-1/2}(\Gamma_d)\,.
\end{aligned} \tag{4.39}$$

The operator $N'(\mathbf{z}) : \mathbf{B}_3 \to \mathbb{R} \times \mathbf{B}_2$ may be defined as $N'(\mathbf{z}) \cdot \tilde{\mathbf{z}} = (\tilde{a}, \tilde{\mathbf{l}})$ for $\tilde{a} \in \mathbb{R}$ if and only if

$$\begin{aligned}
&\alpha_u(\mathbf{u} - \mathbf{u}_d, \tilde{\mathbf{u}})_{\Omega_d} + \alpha_T(T - T_d, \tilde{T})_{\Omega_d} + \\
&\qquad + \lambda(T_c, \tilde{T}_c)_{\Gamma_c} + \lambda(\nabla_s T_c, \nabla_s \tilde{T}_c)_{\Gamma_c} = \tilde{a} \\
&\nu a(\tilde{\mathbf{u}}, \mathbf{v}) + c(\tilde{\mathbf{u}}, \mathbf{u}, \mathbf{v}) + c(\mathbf{u}, \tilde{\mathbf{u}}, \mathbf{v}) + b(\mathbf{v}, \tilde{p}) + \\
&\qquad + \beta(\mathbf{g}\tilde{T}, \mathbf{v}) = (\tilde{\mathbf{l}}_1, \mathbf{v}) && \forall \mathbf{v} \in \mathbf{H}^1_0(\Omega)\,, \\
&b(\tilde{\mathbf{u}}, q) = (\tilde{l}_2, q) && \forall q \in L^2_0(\Omega)\,, \\
&\alpha a(\tilde{T}, \varphi) + c(\tilde{\mathbf{u}}, T, \varphi) + c(\mathbf{u}, \tilde{T}, \varphi) + \\
&\qquad - (\tilde{q}_n, \varphi)_{\Gamma_c} = (\tilde{l}_3, \varphi) && \forall \varphi \in H^1_{\Gamma_i}(\Omega)\,, \\
&(\tilde{T}, s_T)_{\Gamma_d} - (\tilde{T}_c, s_T)_{\Gamma_c} = (\tilde{l}_4, s_T)_{\Gamma_d} && \forall s_T \in H^{-1/2}(\Gamma_d)\,.
\end{aligned}$$

The differential operator M' is rather complex. Many equations in this operator are non-coercive elliptic equations with advection term driven by the velocity field $\mathbf{u} \in \mathbf{H}^1(\Omega)$. The existence result for this class of equations can be obtained not in the Lax-Milgram setting, but by using a Leray-Schauder Topological Degree argument. In order to deal with these equations, we introduce the following theorem.

Theorem 4.3. *Let $\Omega \subset \mathbb{R}^n$ be a bounded open subset with boundary Γ. Let $\Gamma_d \subset \Gamma$ be a set with positive measure and $\Gamma_n \subseteq \Gamma \setminus \Gamma_d$. Consider*

$$\begin{aligned} -\nabla \cdot (A^T \nabla y) + (\mathbf{u} \cdot \nabla) y + by &= f && \text{in } \Omega \\ y &= y_1 && \text{on } \Gamma_d \\ A^T \nabla y \cdot \mathbf{n} &= y_n && \text{on } \Gamma_n \,, \end{aligned} \tag{4.40}$$

with $b \in L^{n_*/2}(\Omega)$, $b \geq 0$ a.e. on Ω, $\mathbf{u} \in \mathbf{L}^{n_*}(\Omega)$, and $f \in H^{1*}_{\Gamma_D}(\Omega)$ where $n_* = n$ when $n \geq 3$, $n_* \in]2, \infty[$ when $n = 2$. If A is a function which satisfies these two properties:

1. *$\exists\, \alpha_A > 0$ such that $A(x)\xi \cdot \xi \geq \alpha_A |\xi|^2$ for a.e. $x \in \Omega$ and for all $\xi \in \mathbb{R}^n$;*
2. *$\exists\, \Lambda_A > 0$ such that $|A(x)| \leq \Lambda_A$ for a.e. $x \in \Omega$;*

then, there exists a unique solution $y \in H^1(\Omega)$ of (4.40).

Proof. The proof of this result is based on a Leray-Schauder Topological Degree argument and can be found in [91]. □

Lemma 4.1. *Let $\mathbf{z}_0 \in \mathbf{B_1}$. Then we have that*

1. *the operator $M'(\mathbf{z}_0)$ has closed range in $\mathbf{B_2}$,*
2. *the operator $N'(\mathbf{z}_0)$ has closed range but is not onto in $\mathbb{R} \times \mathbf{B_2}$,*

Proof. In order to proof *1.* we can split the range operator $M'(\mathbf{z}_0)$ in a product of range spaces for all its components and apply well known results. The range operator $M'(\mathbf{z}_0)$ can be split into the Navier Stokes and temperature equations. First, let us consider the Navier Stokes derivative operator

$$\begin{aligned} &\nu a(\widetilde{\mathbf{u}}, \mathbf{v}) + c(\widetilde{\mathbf{u}}, \mathbf{u}, \mathbf{v}) + c(\mathbf{u}, \widetilde{\mathbf{u}}, \mathbf{v}) + \\ &\qquad + b(\mathbf{v}, \widetilde{p}) = (\widetilde{\mathbf{l}}_1^*, \mathbf{v}) && \forall \mathbf{v} \in \mathbf{H}_0^1(\Omega)\,, \\ &(\widetilde{\mathbf{l}}_1^*, \mathbf{v}) = -\beta(\mathbf{g}\widetilde{T}, \mathbf{v}) + (\widetilde{\mathbf{l}}_1, \mathbf{v}) && \forall \mathbf{v} \in \mathbf{H}_0^1(\Omega)\,, \\ &b(\widetilde{\mathbf{u}}, q) = (\widetilde{l}_2, q) && \forall q \in L_0^2(\Omega)\,, \end{aligned} \tag{4.41}$$

The question of the closeness of the range $(\widetilde{\mathbf{l}}_1^*, \widetilde{l}_2)$ in $\mathbf{H}^{-1}(\Omega) \times L_0^2(\Omega)$ of (4.41) is discussed in many papers, see for examples [92]. Since $\mathbf{z}_0$ is an optimal solution, $\widetilde{T}$ and $\widetilde{q}_n$ solve the equations

$$\begin{aligned} &\alpha a(\widetilde{T}, \varphi) + c(\mathbf{u}, \widetilde{T}, \varphi) - (\widetilde{q}_n, \varphi)_{\Gamma_c} = (\widetilde{l}_3^*, \varphi) && \forall \varphi \in H^1_{\Gamma_i}(\Omega)\,, \\ &(\widetilde{T}, s_T)_{\Gamma_d} = (\widetilde{l}_4^*, s_T)_{\Gamma_d} && \forall s_T \in H^{-1/2}(\Gamma_d)\,, \end{aligned} \tag{4.42}$$

with

$$\begin{aligned}(\widetilde{l}_3^*, \varphi) &= (\widetilde{l}_3, \varphi) - c(\widetilde{\mathbf{u}}, T, \varphi) \qquad \forall \varphi \in H^1_{\Gamma_i}(\Omega)\,, \\ (\widetilde{l}_4^*, s_T)_{\Gamma_d} &= (\widetilde{T}_c, s_T)_{\Gamma_c} + (\widetilde{l}_4, s_T)_{\Gamma_d} \quad \forall s_T \in H^{-1/2}(\Gamma_d)\,.\end{aligned} \tag{4.43}$$

For $(\widetilde{l}_3, \widetilde{l}_4) \in H^{1*}_{\Gamma_i}(\Omega) \times H^{1/2}(\Gamma_d)$ we have $(\widetilde{l}_3^*, \widetilde{l}_4^*) \in H^{1*}_{\Gamma_i}(\Omega) \times H^{1/2}(\Gamma_d)$. By using the result in Theorem 4.3 for each $(\widetilde{l}_3^*, \widetilde{l}_4^*)$ we have a solution and therefore the range of the mapping $M'(\mathbf{z}_0)$ for the energy equation is onto. Starting from *1.*, the proof of *2.* can be found easily by using the standard techniques in [92, 93]. □

Theorem 4.4. *Let* $\hat{\mathbf{z}} = (\hat{\mathbf{u}}, \hat{p}, \hat{T}, \hat{T}_c, \hat{q}_n) \in \mathbf{H}^1(\Omega) \times L^2_0(\Omega) \times H^1(\Omega) \times H^1_0(\Gamma_c) \times H^{-1/2}(\Gamma_c)$ *denote an optimal solution in the sense of* (4.28)*. Then there exists a nonzero Lagrange multiplier* $(\Lambda, \hat{\mathbf{u}}_a, \hat{p}_a, \hat{T}_a, \hat{q}_a) \in \mathbb{R} \times \mathbf{B}_2^*$ *satisfying the Euler equations*

$$\Lambda \mathcal{J}'(\hat{\mathbf{u}}, \hat{T}, \hat{T}_c) \cdot \widetilde{\mathbf{z}} + \langle (\hat{\mathbf{u}}_a, \hat{p}_a, \hat{T}_a, \hat{q}_a), M'(\hat{\mathbf{z}}) \cdot \widetilde{\mathbf{z}} \rangle = 0\,, \quad \forall \widetilde{\mathbf{z}} \in \mathbf{B}_3 \tag{4.44}$$

where $\langle \cdot, \cdot \rangle$ *denotes the duality pairing between* $\mathbf{B}_2$ *and* $\mathbf{B}_2^*$*.*

Proof. From Lemma 4.1, we have that the range of $N'(\hat{\mathbf{z}})$ is a closed, proper subspace of $\mathbb{R} \times \mathbf{B}_2$. Then, from the Hahn-Banach theorem, there exists a nonzero element of $\mathbb{R} \times \mathbf{B}_2^*$ that nullifies the range of $N'(\hat{\mathbf{z}})$. Then, there exists $(\Lambda, \hat{\mathbf{u}}_a, \hat{p}_a, \hat{T}_a, \hat{q}_a) \in \mathbb{R} \times \mathbf{B}_2^*$ such that

$$\begin{aligned}&\langle (\widetilde{a}, \widetilde{\mathbf{l}}_1, \widetilde{l}_2, \widetilde{l}_3, \widetilde{l}_4), (\Lambda, \hat{\mathbf{u}}_a, \hat{p}_a, \hat{T}_a, \hat{q}_a) \rangle = 0 \\ &\qquad \forall (\widetilde{a}, \widetilde{\mathbf{l}}_1, \widetilde{l}_2, \widetilde{l}_3, \widetilde{l}_4) \text{ belonging to the range of } N'(\widehat{\mathbf{z}})\,.\end{aligned} \tag{4.45}$$

Note that $\Lambda \neq 0$ since otherwise we would have that $\langle (\widetilde{\mathbf{l}}_1, \widetilde{l}_2, \widetilde{l}_3, \widetilde{l}_4), (\hat{\mathbf{u}}_a, \hat{p}_a, \hat{T}_a, \hat{q}_a) \rangle = 0$ for all $\widetilde{\mathbf{l}} \in \mathbf{B}_2$. This would imply $(\hat{\mathbf{u}}_a, \hat{p}_a, \hat{T}_a, \hat{q}_a) = 0$ contradicting the fact that $(\Lambda, \hat{\mathbf{u}}_a, \hat{p}_a, \hat{T}_a, \hat{q}_a) \neq 0$. Clearly, using the definition of $N'(\widehat{\mathbf{z}})$, (4.44) and (4.45) are equivalent. □

The optimality system

Dropping the $\widehat{(\cdot)}$ notation for optimal solution, we derive now the optimality system using (4.44). The Euler equations (4.44) are equivalent to

$$\begin{aligned}\alpha_u \Lambda(\mathbf{u} - \mathbf{u}_d, \widetilde{\mathbf{u}})_{\Omega_d} &+ \alpha_T \Lambda(T - T_d, \widetilde{T})_{\Omega_d} + \Lambda\lambda(T_c, \widetilde{T}_c)_{\Gamma_c} + \\ &+ \Lambda\lambda(\nabla_s T_c, \nabla_s \widetilde{T}_c)_{\Gamma_c} + b(\widetilde{\mathbf{u}}, p_a) + \nu a(\widetilde{\mathbf{u}}, \mathbf{u}_a) + \\ &+ c(\widetilde{\mathbf{u}}, \mathbf{u}, \mathbf{u}_a) + b(\mathbf{u}_a, \widetilde{p}) + c(\mathbf{u}, \widetilde{\mathbf{u}}, \mathbf{u}_a) + \beta(\mathbf{g}\widetilde{T}, \mathbf{u}_a) + \\ &+ \alpha a(\widetilde{T}, T_a) + c(\widetilde{\mathbf{u}}, T, T_a) + c(\mathbf{u}, \widetilde{T}, T_a) - (\widetilde{q}_n, T_a)_{\Gamma_c} + \\ &+ (\widetilde{T}, q_a)_{\Gamma_d} - (\widetilde{T}_c, q_a)_{\Gamma_c} = 0\,.\end{aligned} \tag{4.46}$$

By extracting the terms involved in the same variation and setting $\Lambda = -1$ we obtain the following equations

$$\begin{aligned}
&b(\mathbf{u}_a, \widetilde{p}) = 0\,, && \forall \widetilde{p} \in L^2_0(\Omega)\\
&\nu a(\widetilde{\mathbf{u}}, \mathbf{u}_a) + c(\mathbf{u}, \widetilde{\mathbf{u}}, \mathbf{u}_a) + c(\widetilde{\mathbf{u}}, \mathbf{u}, \mathbf{u}_a) + \\
&\qquad + b(\widetilde{\mathbf{u}}, p_a) = \alpha_u(\mathbf{u} - \mathbf{u}_d, \widetilde{\mathbf{u}})_{\Omega_d} + \\
&\qquad - c(\widetilde{\mathbf{u}}; T, T_a)\,, && \forall \widetilde{\mathbf{u}} \in \mathbf{H}^1_0(\Omega)\\
&\alpha a(\widetilde{T}, T_a) + c(\mathbf{u}, \widetilde{T}, T_a) + (\widetilde{T}, q_a)_{\Gamma_c} = \\
&\qquad = -(\beta \mathbf{g}\widetilde{T}, \mathbf{u}_a) + \alpha_T(T - T_d, \widetilde{T})_{\Omega_d}\,, && \forall \widetilde{T} \in H^1_{\Gamma_i}(\Omega)\\
&(T_a, \widetilde{q}_n)_{\Gamma_c} = 0\,, && \forall \widetilde{q}_n \in H^{-1/2}(\Gamma_c)
\end{aligned} \tag{4.47}$$

and the control equation

$$\lambda_1(T_c, \widetilde{T}_c)_{\Gamma_c} + \lambda_1(\nabla_s T_c, \nabla_s \widetilde{T}_c)_{\Gamma_c} + (q_a, \widetilde{T}_c)_{\Gamma_c} = 0\,, \tag{4.48}$$

$\forall \widetilde{T}_c \in H^1_0(\Gamma_c)$ with $q_a = -\alpha \nabla T_a \cdot \mathbf{n}|_{\Gamma_c}$ on Γ_c. The necessary conditions for an optimum are that equations (4.24) and (4.47) are satisfied. This system of equations is called optimality system. Integrations by parts may be used to show that the system constitutes a weak formulation of the boundary value problem for state equations

$$\begin{aligned}
&\nabla \cdot \mathbf{u} = 0 && \text{in } \Omega\,,\\
&\mathbf{u} \cdot \nabla \mathbf{u} + \nabla p - \nu \Delta \mathbf{u} = \mathbf{f} - \beta \mathbf{g} T && \text{in } \Omega\,,\\
&\mathbf{u} \cdot \nabla T - \alpha \Delta T = Q && \text{in } \Omega\,,\\
&\mathbf{u} = \mathbf{w} && \text{on } \Gamma\,,\\
&\alpha \nabla T \cdot \mathbf{n}|_{\Gamma_n} = g_{t,n} && \text{on } \Gamma_n\,,\\
&T = g_t && \text{on } \Gamma_i\,,\\
&T = g_t + T_c && \text{on } \Gamma_c\,,
\end{aligned} \tag{4.49}$$

and adjoint equations

$$\begin{aligned}
&\nabla \cdot \mathbf{u}_a = 0 && \text{in } \Omega\,,\\
&\mathbf{u}_a \cdot (\nabla \mathbf{u})^T - \mathbf{u} \cdot \nabla \mathbf{u}_a + \nabla p_a - \nu \Delta \mathbf{u}_a = \\
&\qquad = -T \nabla T_a + \alpha_u(\mathbf{u} - \mathbf{u}_d) && \text{in } \Omega\,,\\
&-\alpha \Delta T_a - \mathbf{u} \cdot \nabla T_a = -\beta \mathbf{g} \cdot \mathbf{u}_a + \alpha_T(T - T_d) && \text{in } \Omega\,,\\
&\mathbf{u}_a = 0 && \text{on } \Gamma\,,\\
&\nabla T_a \cdot \mathbf{n}|_{\Gamma_n} = 0 && \text{on } \Gamma_n\,,\\
&T_a = 0 && \text{on } \Gamma_d\,,
\end{aligned} \tag{4.50}$$

and control equation

$$\begin{aligned} -\Delta_s T_c + T_c - \frac{\alpha \nabla T_a \cdot \mathbf{n}|_{\Gamma_c}}{\lambda} = 0 \quad & \text{on } \Gamma_c\,, \\ T_c = 0 \quad & \text{on } \partial\Gamma_c\,, \end{aligned} \tag{4.51}$$

where Δ_s denotes the surface Laplacian. The optimality system in the strong form consists of the Boussinesq system (4.49), the adjoint of Boussinesq equations (4.50) and the control equations (4.51).

Numerical algorithm

The optimality system consists of three groups of equations: the state equations (4.24), the adjoint state equations (4.47) and the optimality conditions for T_c (4.48). Due to the non-linearity and large dimension of this system, a one-shot solver cannot be implemented. We may construct an iterative method to iterate among the three groups of equations so that at each iteration we are dealing with a smaller size system of equations. We consider a gradient method for the solution of the optimality problem and the gradient of the functional is determined with the help of the solution of the adjoint system.

Let us consider the gradient method for the following minimization problem: find $T_c \in H_0^1(\Gamma_c)$ such that $\mathcal{F}(T_c) := \mathcal{J}(\mathbf{u}(T_c), T(T_c), T_c)$ is minimized. Given $T_c^{(0)}$, we can define the sequence

$$T_c^{(n+1)} = T_c^{(n)} - \rho^{(n)} \frac{d\mathcal{F}(T_c^{(n)})}{dT_c^{(n)}}\,, \tag{4.52}$$

recursively, where $\rho^{(n)}$ is a variable step size. Let $\hat{T}_c$ be a solution of the minimization problem, thus the following necessary condition holds

$$\frac{d\mathcal{F}(\hat{T}_c)}{d\hat{T}_c} = \frac{d\mathcal{J}(\mathbf{u}(\hat{T}_c), T(\hat{T}_c), \hat{T}_c)}{d\hat{T}_c} = 0\,, \tag{4.53}$$

then at the optimum state the equality $T_c^{(n+1)} = T_c^{(n)}$ holds. For each fixed T_c, the Gâteaux derivative $(d\mathcal{F}(T_c)/dT_c) \cdot \widetilde{T}_c$ for every direction $\widetilde{T}_c \in H^1(\Gamma_c)$ may be computed

$$\begin{aligned} \frac{d\mathcal{F}(T_c)}{dT_c} \cdot \widetilde{T}_c = {} & \lambda(\nabla_s T_c, \nabla_s \widetilde{T}_c)_{\Gamma_c} + \lambda(T_c, \widetilde{T}_c)_{\Gamma_c} + \alpha_u(\mathbf{u} - \mathbf{u}_d, \widetilde{\mathbf{u}})_{\Omega_d} \\ & + \alpha_T(T - T_d, \widetilde{T})_{\Omega_d}\,, \end{aligned} \tag{4.54}$$

where $\tilde{\mathbf{u}}$ and $\widetilde{T}$ are the solution of $M'(\mathbf{z}) \cdot \tilde{\mathbf{z}} = \mathbf{0}$, that is

$$\begin{aligned}
&b(\tilde{\mathbf{u}}, q) = 0 && \forall q \in L^2_0(\Omega)\,,\\
&\nu a(\tilde{\mathbf{u}}, \mathbf{v}) + c(\tilde{\mathbf{u}}, \mathbf{u}, \mathbf{v}) + c(\mathbf{u}, \tilde{\mathbf{u}}, \mathbf{v}) + b(\mathbf{v}, \widetilde{p}) = \\
&\qquad = -\beta(\mathbf{g}\widetilde{T}, \mathbf{v}) && \forall \mathbf{v} \in \mathbf{H}^1_0(\Omega)\,,\\
&\alpha a(\widetilde{T}, \varphi) + c(\tilde{\mathbf{u}}, T, \varphi) + c(\mathbf{u}, \widetilde{T}, \varphi) = (\widetilde{q}_n, \varphi)_{\Gamma_c} && \forall \varphi \in H^1_{\Gamma_i}(\Omega)\,,\\
&(\widetilde{T}, s_T)_{\Gamma_c} - (\widetilde{T}_c, s_T)_{\Gamma_c} = 0 && \forall s_T \in H^{-1/2}(\Gamma_c)\,.
\end{aligned} \tag{4.55}$$

Let $(\mathbf{u}, p, T, q_n) \in \mathbf{H}^1(\Omega) \times L^2_0(\Omega) \times H^1(\Omega) \times H^{-1/2}(\Gamma_c)$ be the solution of the state problem (4.24) and let $(\mathbf{u}_a, p_a, T_a, q_a) \in \mathbf{H}^1_0(\Omega) \times L^2_0(\Omega) \times H^1_{\Gamma_i}(\Omega) \times H^{-1/2}(\Gamma_c)$ be the solution of the adjoint problem (4.47). Setting $(\mathbf{v}, q, \varphi, s_T) \in \mathbf{H}^1_0(\Omega) \times L^2_0(\Omega) \times H^1_{\Gamma_i}(\Omega) \times H^{-1/2}(\Gamma_c)$ equal to ($\mathbf{u}_a$, p_a, T_a, q_a) $\in \mathbf{H}^1_0(\Omega) \times L^2_0(\Omega) \times H^1_{\Gamma_i}(\Omega) \times H^{-1/2}(\Gamma_c)$ in (4.55) we have that

$$\begin{aligned}
&b(\tilde{\mathbf{u}}, p_a) = 0 && \forall p_a \in L^2_0(\Omega)\,,\\
&\nu a(\tilde{\mathbf{u}}, \mathbf{u}_a) + c(\tilde{\mathbf{u}}, \mathbf{u}, \mathbf{u}_a) + c(\mathbf{u}, \tilde{\mathbf{u}}, \mathbf{u}_a) + \\
&\qquad + b(\mathbf{u}_a, \widetilde{p}) = -\beta(\mathbf{g}\widetilde{T}, \mathbf{u}_a) && \forall \mathbf{u}_a \in \mathbf{H}^1_0(\Omega)\,,\\
&\alpha a(\widetilde{T}, T_a) + c(\tilde{\mathbf{u}}, T, T_a) + c(\mathbf{u}, \widetilde{T}, T_a) + \\
&\qquad - (\widetilde{q}_n, T_a)_{\Gamma_c} = 0 && \forall T_a \in H^1_{\Gamma_i}(\Omega)\,,\\
&(\widetilde{T}, q_a)_{\Gamma_c} - (\widetilde{T}_c, q_a)_{\Gamma_c} = 0 && \forall q_a \in H^{-1/2}(\Gamma_c)\,.
\end{aligned} \tag{4.56}$$

Comparing (4.56) and (4.47), we find that

$$\alpha_u(\mathbf{u} - \mathbf{u}_d, \tilde{\mathbf{u}})_{\Omega_d} + \alpha_T(T - T_d, \widetilde{T})_{\Omega_d} = (\widetilde{T}_c, q_a)_{\Gamma_c}\,. \tag{4.57}$$

Thus, the Gâteaux derivative may be computed as

$$\frac{d\mathcal{F}(T_c)}{dT_c} \cdot \widetilde{T}_c = \lambda(\nabla_s T_c, \nabla_s \widetilde{T}_c)_{\Gamma_c} + \lambda(T_c, \widetilde{T}_c)_{\Gamma_c} + (\widetilde{T}_c, q_a)_{\Gamma_c}\,, \tag{4.58}$$

or

$$\frac{d\mathcal{F}(T_c)}{dT_c} = -\lambda \Delta_s T_c + \lambda T_c + q_a\,. \tag{4.59}$$

The optimization algorithm is reported in the following.

a) Initialization:

   1. choose tolerance τ and $T_c^{(0)}$; set $n = 0$ and $\rho^{(0)} = 1$;
   2. solve for $(\mathbf{u}^{(0)}, p^{(0)}, T^{(0)})$ from (4.24) with $T_c = T_c^{(0)}$;

3. evaluate $\mathcal{J}^{(0)} = \mathcal{J}(\mathbf{u}^{(0)}, T^{(0)}, T_c^{(0)})$ using (4.23);

b) main loop:

1. set $n = n + 1$;
2. solve for $(\mathbf{u}_a^{(n)}, p_a^{(n)}, T_a^{(n)})$ from (4.47);
3. solve for $T_c^{(n)}$ from

$$T_c^{(n)} = T_c^{(n-1)} - \rho^{(n)}\Big(- \Delta_s T_c^{(n-1)} + T_c^{(n-1)} + \\ + \frac{\alpha}{\lambda}\nabla T_a^{(n)} \cdot \mathbf{n}|_{\Gamma_c}\Big), \tag{4.60}$$

or

$$-\Delta_s T_c^{(n)} + T_c^{(n)} = -\Delta_s T_c^{(n-1)} + T_c^{(n-1)} + \\ -\rho^{(n)}\Big(- \Delta_s T_c^{(n-1)} + T_c^{(n-1)} + \\ + \frac{\alpha}{\lambda}\nabla T_a^{(n)} \cdot \mathbf{n}|_{\Gamma_c}\Big). \tag{4.61}$$

4. solve for $(\mathbf{u}^{(n)}, p^{(n)}, T^{(n)})$ from (4.24) with $T_c = T_c^{(n)}$;
5. evaluate $\mathcal{J}^{(n)} = \mathcal{J}(\mathbf{u}^{(n)}, T^{(n)}, T_c^{(n)})$ using (4.23);
   i) if $\mathcal{J}^{(n)} > \mathcal{J}^{(n-1)}$, set $\rho^{(n)} = 0.5\rho^{(n)}$ and go to step b) 3.;
   ii) if $\mathcal{J}^{(n)} < \mathcal{J}^{(n-1)}$, set $\rho^{(n+1)} = 1$ and go to step b) 1.;
   iii) if $|\mathcal{J}^{(n)} - \mathcal{J}^{(n-1)}|/|\mathcal{J}^{(n)}| < \tau$ stop.

In the algorithm we propose two forms, (4.60) and (4.61), for the control update. With (4.61), we enforce the belonging of T_c to $H_0^1(\Gamma_c)$ and we give more regularity to the control.

4.2.2. Neumann boundary control

In a Neumann boundary control problem, we aim to control the state by acting on the heat flux on a portion of the boundary $\Gamma_c \subseteq \Gamma_n$. The general boundary conditions reported in (4.19), can be written in this case as

$$\begin{aligned} &\mathbf{u} = \mathbf{w} && \text{on } \partial\Omega\,, \\ &T = g_t && \text{on } \Gamma_d\,, \\ &\alpha\nabla T \cdot \mathbf{n} = g_{t,n} && \text{on } \Gamma_i\,, \\ &\alpha\nabla T \cdot \mathbf{n} = h && \text{on } \Gamma_c\,, \end{aligned} \tag{4.62}$$

where $\Gamma_i = \Gamma_n \setminus \Gamma_c$. In (4.22) g_t, $g_{t,n}$ and $\mathbf{w}$ are given functions, while h is the control. Thus Γ_i and Γ_c denote the portions of Γ_n where the control is applied or not, respectively.

The cost functional is given as follows

$$\mathcal{J}(\mathbf{u}, T, h) = \frac{\alpha_u}{2} \int_{\Omega_d} |\mathbf{u} - \mathbf{u}_d|^2 d\mathbf{x} + \frac{\alpha_T}{2} \int_{\Omega_d} |T - T_d|^2 d\mathbf{x} + \\ + \frac{\lambda}{2} \int_{\Gamma_c} |h|^2 d\mathbf{x}\,. \tag{4.63}$$

The cost contribution measures the $L^2(\Gamma_c)$-norm of the control h.

Weak formulation

The weak form of the boundary value problem (4.16)-(4.18) and (4.62) is given as follows: find $(\mathbf{u}, p, T) \in \mathbf{H}^1(\Omega) \times L^2_0(\Omega) \times H^1(\Omega)$ such that

$$\begin{aligned} & b(\mathbf{u}, q) = 0 && \forall q \in L^2_0(\Omega)\,, \\ & \nu a(\mathbf{u}, \mathbf{v}) + c(\mathbf{u}, \mathbf{u}, \mathbf{v}) + b(\mathbf{v}, p) = (\mathbf{f}, \mathbf{v}) + \\ & \qquad - \beta(\mathbf{g}T, \mathbf{v}) && \forall \mathbf{v} \in \mathbf{H}^1_0(\Omega)\,, \\ & \alpha a(T, \varphi) + c(\mathbf{u}, T, \varphi) = (Q, \varphi) + (g_{t,n}, \varphi)_{\Gamma_i} + \\ & \qquad + (h, \varphi)_{\Gamma_c} && \forall \varphi \in H^1_{\Gamma_d}(\Omega)\,. \end{aligned} \tag{4.64}$$

The existence of the solution of the system (4.64) can be easily derived from Theorem 4.1 and has been proved in [23].

The optimization problem and existence of optimal solution

We state the optimal control problem. We look for a $(\mathbf{u}, p, T, h) \in \mathbf{H}^1(\Omega) \times L^2_0(\Omega) \times H^1(\Omega) \times L^2(\Gamma_c)$ such that the cost functional (4.63) is minimized subject to the constraints (4.64). The admissible set of states and controls is

$$\begin{aligned} \mathcal{U}_{ad} = \{ & (\mathbf{u}, p, T, h) \in \mathbf{H}^1(\Omega) \times L^2_0(\Omega) \times H^1(\Omega) \times L^2(\Gamma_c) : \\ & \mathcal{J}(\mathbf{u}, T, h) < \infty \text{ and (4.64) is satified.}\} \end{aligned} \tag{4.65}$$

Then $(\hat{\mathbf{u}}, \hat{p}, \hat{T}, \hat{h}) \in \mathcal{U}_{ad}$ is called an optimal solution if there exists $\varepsilon > 0$ such that

$$\begin{aligned} & \mathcal{J}(\hat{\mathbf{u}}, \hat{p}, \hat{T}, \hat{h}) \leq \mathcal{J}(\mathbf{u}, p, T, h) \quad \forall (\mathbf{u}, p, T, h) \in \mathcal{U}_{ad} \text{ satisfying} \\ & \qquad \|\mathbf{u} - \hat{\mathbf{u}}\|_1 + \|p - \hat{p}\|_0 + \|T - \hat{T}\|_1 + \|h - \hat{h}\|_{0,\Gamma_c} < \varepsilon\,. \end{aligned} \tag{4.66}$$

We now show that an optimal solution exists.

Theorem 4.5. *Let $\mathcal{U}_{ad}$ be not empty. There exists at least one optimal solution $(\hat{\mathbf{u}}, \hat{p}, \hat{T}, \hat{h}) \in \mathcal{U}_{ad}$.*

Proof. Let $\{\mathbf{u}^{(n)}, p^{(n)}, T^{(n)}, h^{(n)}\}$ be a sequence in $\mathcal{U}_{ad}$ such that

$$\lim_{n\to\infty} \mathcal{J}(\mathbf{u}^{(n)}, p^{(n)}, T^{(n)}, h^{(n)}) = \inf_{(\mathbf{v},q,S,z)\in\mathcal{U}_{ad}} \mathcal{J}(\mathbf{v}, q, S, z)\,. \tag{4.67}$$

By the definition of $\mathcal{U}_{ad}$ we have

$$\begin{aligned} &b(\mathbf{u}^{(n)}, q) = 0 && \forall q \in L^2_0(\Omega)\,,\\ &\nu a(\mathbf{u}^{(n)}, \mathbf{v}) + c(\mathbf{u}^{(n)}, \mathbf{u}^{(n)}, \mathbf{v}) + b(\mathbf{v}, p^{(n)}) = \\ &\qquad = (\mathbf{f}, \mathbf{v}) - \beta(\mathbf{g}T^{(n)}, \mathbf{v}) && \forall \mathbf{v} \in \mathbf{H}^1_0(\Omega)\,,\\ &\alpha a(T^{(n)}, \varphi) + c(\mathbf{u}^{(n)}, T^{(n)}, \varphi) = (Q, \varphi) + \\ &\qquad + (g_{t,n}, \varphi)_{\Gamma_i} + (h^{(n)}, \varphi)_{\Gamma_c} && \forall \varphi \in H^1_{\Gamma_d}(\Omega)\,, \end{aligned} \tag{4.68}$$

By (4.63) and (4.65) we easily see that $\{\|h^{(n)}\|_{0,\Gamma_c}\}$ is uniformly bounded. Also, by (4.26) we have that $\{\|\mathbf{u}^{(n)}\|_1\}$, $\{\|p^{(n)}\|_0\}$ and $\{\|T^{(n)}\|_1\}$ are uniformly bounded. We may then extract subsequences $\{\mathbf{u}^{(n)}, p^{(n)}, T^{(n)}, h^{(n)}\}$ converging to $(\hat{\mathbf{u}}, \hat{p}, \hat{T}, \hat{h})$

$$\begin{aligned} h^{(n)} &\rightharpoonup \hat{h} && \text{in } L^2(\Gamma_c)\,, && \\ \mathbf{u}^{(n)} &\rightharpoonup \hat{\mathbf{u}} && \text{in } \mathbf{H}^1(\Omega)\,, && \text{and } \nabla\mathbf{u}^{(n)} \rightharpoonup \nabla\hat{\mathbf{u}} \text{ in } L^2(\Omega)\,,\\ T^{(n)} &\rightharpoonup \hat{T} && \text{in } H^1(\Omega)\,, && \text{and } \nabla T^{(n)} \rightharpoonup \nabla\hat{T} \text{ in } L^2(\Omega)\,,\\ p^{(n)} &\rightharpoonup \hat{p} && \text{in } L^2_0(\Omega)\,, && \\ \mathbf{u}^{(n)} &\to \hat{\mathbf{u}} && \text{in } \mathbf{L}^2(\Omega)\,, && \\ T^{(n)}|_\Gamma &\to \hat{T}|_\Gamma && \text{in } L^2(\Gamma)\,, && \\ \mathbf{u}^{(n)}|_\Gamma &\to \hat{\mathbf{u}}|_\Gamma && \text{in } \mathbf{L}^2(\Gamma)\,. && \end{aligned}$$

We may pass to the limit in (4.68) to determine that $(\hat{\mathbf{u}}, \hat{p}, \hat{T}, \hat{h})$ satisfies (4.64). □

The existence of Lagrange multipliers

Also for the Neumann control, we consider all the constraint equations and the functional in two mappings in order to study their differential properties. The following functional spaces are now defined

$$\mathbf{B}_1 = \mathbf{H}^1(\Omega) \times L^2_0(\Omega) \times H^1(\Omega) \times L^2(\Gamma_c)\,, \tag{4.69}$$

$$\mathbf{B}_2 = \mathbf{H}^{-1}(\Omega) \times L^2_0(\Omega) \times H^{1*}_{\Gamma_d}(\Omega)\,, \tag{4.70}$$

$$\mathbf{B}_3 = \mathbf{H}^1_0(\Omega) \times L^2_0(\Omega) \times H^1_{\Gamma_d}(\Omega) \times L^2(\Gamma_c)\,. \tag{4.71}$$

Let $M : \mathbf{B}_1 \to \mathbf{B}_2$ denote the generalized constraint equations, i.e. $M(\mathbf{z}) = \mathbf{l}$ for $\mathbf{z} = (\mathbf{u}, p, T, h) \in \mathbf{B}_1$ and $\mathbf{l} = (\mathbf{l}_1, l_2, l_3) \in \mathbf{B}_2$ if and only if

$$\begin{aligned}
&\nu a(\mathbf{u}, \mathbf{v}) + c(\mathbf{u}, \mathbf{u}, \mathbf{v}) + b(\mathbf{v}, p) - (\mathbf{f}, \mathbf{v}) + \\
&\qquad + \beta(\mathbf{g}T, \mathbf{v}) = (\mathbf{l}_1, \mathbf{v}) && \forall \mathbf{v} \in \mathbf{H}^1_0(\Omega)\,, \\
&b(\mathbf{u}, q) = (l_2, q) && \forall q \in L^2_0(\Omega)\,, \\
&\alpha a(T, \varphi) + c(\mathbf{u}, T, \varphi) - (Q, \varphi) - (g_{t,n}, \varphi)_{\Gamma_i} + \\
&\qquad - (h, \varphi)_{\Gamma_c} = (l_3, \varphi) && \forall \varphi \in H^1_{\Gamma_d}(\Omega)\,.
\end{aligned} \tag{4.72}$$

Thus, the constraints (4.64) can be expressed as $M(\mathbf{u}, p, T, h) = \mathbf{0}$. Let $(\hat{\mathbf{u}}, \hat{p}, \hat{T}, \hat{h}) \in \mathbf{H}^1(\Omega) \times L^2_0(\Omega) \times H^1(\Omega) \times L^2(\Gamma_c)$ denote an optimal solution in the sense of (4.66). Then, consider the nonlinear operator $N : \mathbf{B}_1 \to \mathbb{R} \times \mathbf{B}_2$ defined by

$$N(\mathbf{u}, p, T, h) = \begin{pmatrix} \mathcal{J}(\mathbf{u}, T, h) - \mathcal{J}(\hat{\mathbf{u}}, \hat{T}, \hat{h}) \\ M(\mathbf{u}, p, T, h) \end{pmatrix}. \tag{4.73}$$

Given $\mathbf{z} = (\mathbf{u}, p, T, h) \in \mathbf{B}_1$ the operator $M'(\mathbf{z}) : \mathbf{B}_3 \to \mathbf{B}_2$ may be defined as $M'(\mathbf{z}) \cdot \widetilde{\mathbf{z}} = \widetilde{\mathbf{l}}$ for $\widetilde{\mathbf{z}} = (\widetilde{\mathbf{u}}, \widetilde{p}, \widetilde{T}, \widetilde{h}) \in \mathbf{B}_3$ and $\widetilde{\mathbf{l}} = (\widetilde{\mathbf{l}}_1, \widetilde{l}_2, \widetilde{l}_3) \in \mathbf{B}_2$ if and only if

$$\begin{aligned}
&\nu a(\widetilde{\mathbf{u}}, \mathbf{v}) + c(\widetilde{\mathbf{u}}, \mathbf{u}, \mathbf{v}) + c(\mathbf{u}, \widetilde{\mathbf{u}}, \mathbf{v}) + b(\mathbf{v}, \widetilde{p}) + \\
&\qquad + \beta(\mathbf{g}\widetilde{T}, \mathbf{v}) = (\widetilde{\mathbf{l}}_1, \mathbf{v}) && \forall \mathbf{v} \in \mathbf{H}^1_0(\Omega)\,, \\
&b(\widetilde{\mathbf{u}}, q) = (\widetilde{l}_2, q) && \forall q \in L^2_0(\Omega)\,, \\
&\alpha a(\widetilde{T}, \varphi) + c(\widetilde{\mathbf{u}}, T, \varphi) + c(\mathbf{u}, \widetilde{T}, \varphi) - (\widetilde{h}, \varphi)_{\Gamma_c} = \\
&\qquad = (\widetilde{l}_3, \varphi) && \forall \varphi \in H^1_{\Gamma_d}(\Omega)\,.
\end{aligned} \tag{4.74}$$

The operator $N'(\mathbf{z}) : \mathbf{B}_3 \to \mathbb{R} \times \mathbf{B}_2$ may be defined as $N'(\mathbf{z}) \cdot \widetilde{\mathbf{z}} = (\widetilde{a}, \widetilde{\mathbf{l}})$ for $\widetilde{a} \in \mathbb{R}$ if and only if

$$\begin{aligned}
&\alpha_u(\mathbf{u} - \mathbf{u}_d, \widetilde{\mathbf{u}})_{\Omega_d} + \alpha_T(T - T_d, \widetilde{T})_{\Omega_d} + \\
&\qquad + \lambda_1(h, \widetilde{h})_{\Gamma_c} = \widetilde{a} \\
&\nu a(\widetilde{\mathbf{u}}, \mathbf{v}) + c(\widetilde{\mathbf{u}}, \mathbf{u}, \mathbf{v}) + c(\mathbf{u}, \widetilde{\mathbf{u}}, \mathbf{v}) + b(\mathbf{v}, \widetilde{p}) + \\
&\qquad + \beta(\mathbf{g}\widetilde{T}, \mathbf{v}) = (\widetilde{\mathbf{l}}_1, \mathbf{v}) && \forall \mathbf{v} \in \mathbf{H}^1_0(\Omega)\,, \\
&b(\widetilde{\mathbf{u}}, q) = (\widetilde{l}_2, q) && \forall q \in L^2_0(\Omega)\,, \\
&\alpha a(\widetilde{T}, \varphi) + c(\widetilde{\mathbf{u}}, T, \varphi) + c(\mathbf{u}, \widetilde{T}, \varphi) - (\widetilde{h}, \varphi)_{\Gamma_c} = \\
&\qquad = (\widetilde{l}_3, \varphi) && \forall \varphi \in H^1_{\Gamma_d}(\Omega)\,.
\end{aligned} \tag{4.75}$$

Lemma 4.2. *Let* $\mathbf{z}_0 \in \mathbf{B_1}$. *Then we have that*

1. *the operator* $M'(\mathbf{z}_0)$ *has closed range in* $\mathbf{B_2}$,
2. *the operator* $N'(\mathbf{z}_0)$ *has closed range but is not onto in* $\mathbb{R} \times \mathbf{B_2}$,

Proof. The proof follows standard techniques, see the Proof of Lemma 4.1. □

Theorem 4.6. *Let* $\hat{\mathbf{z}} = (\hat{\mathbf{u}}, \hat{p}, \hat{T}, \hat{h}) \in \mathbf{H}^1(\Omega) \times L_0^2(\Omega) \times H^1(\Omega) \times L^2(\Gamma_c)$ *denote an optimal solution in the sense of* (4.66). *Then there exists a nonzero Lagrange multiplier* $(\Lambda, \hat{\mathbf{u}}_a, \hat{p}_a, \hat{T}_a) \in \mathbb{R} \times \mathbf{B}_2^*$ *satisfying the Euler equations*

$$\Lambda \mathcal{J}'(\hat{\mathbf{u}}, \hat{T}, \hat{h}) \cdot \widetilde{\mathbf{z}} + \langle (\hat{\mathbf{u}}_a, \hat{p}_a, \hat{T}_a), M'(\hat{\mathbf{z}}) \cdot \widetilde{\mathbf{z}} \rangle = 0\,, \quad \forall \widetilde{\mathbf{z}} \in \mathbf{B}_3 \tag{4.76}$$

where $\langle \cdot, \cdot \rangle$ *denotes the duality pairing between* $\mathbf{B}_2$ *and* $\mathbf{B}_2^*$.

Proof. From Lemma 4.2, we have that the range of $N'(\hat{\mathbf{z}})$ is a closed, proper subspace of $\mathbb{R} \times \mathbf{B}_2$. Then, from the Hahn-Banach theorem, there exists a nonzero element of $\mathbb{R} \times \mathbf{B}_2^*$ that nullifies the range of $N'(\hat{\mathbf{z}})$. Then, there exists $(\Lambda, \hat{\mathbf{u}}_a, \hat{p}_a, \hat{T}_a) \in \mathbb{R} \times \mathbf{B}_2^*$ such that

$$\begin{aligned} &\langle (\widetilde{a}, \widetilde{\mathbf{l}}_1, \widetilde{l}_2, \widetilde{l}_3), (\Lambda, \hat{\mathbf{u}}_a, \hat{p}_a, \hat{T}_a) \rangle = 0 \\ &\qquad \forall (\widetilde{a}, \widetilde{\mathbf{l}}_1, \widetilde{l}_2, \widetilde{l}_3) \text{ belonging to the range of } N'(\hat{\mathbf{z}})\,. \end{aligned} \tag{4.77}$$

Note that $\Lambda \neq 0$ since otherwise we would have that $\langle (\widetilde{\mathbf{l}}_1, \widetilde{l}_2, \widetilde{l}_3), (\hat{\mathbf{u}}_a, \hat{p}_a, \hat{T}_a) \rangle = 0$ for all $\widetilde{\mathbf{l}} \in \mathbf{B}_2$. This would imply $(\hat{\mathbf{u}}_a, \hat{p}_a, \hat{T}_a) = 0$ contradicting the fact that $(\Lambda, \hat{\mathbf{u}}_a, \hat{p}_a, \hat{T}_a) \neq 0$. Clearly, using the definition of $N'(\hat{\mathbf{z}})$, (4.76) and (4.77) are equivalent. □

The optimality system

Dropping the $\hat{(\cdot)}$ notation for optimal solution, we derive now the optimality system using (4.76). The Euler equations (4.76) are equivalent to

$$\begin{aligned} \alpha_u \Lambda (\mathbf{u} - \mathbf{u}_d, \widetilde{\mathbf{u}})_{\Omega_d} + \alpha_T \Lambda (T - T_d, \widetilde{T})_{\Omega_d} + \Lambda \lambda_1 (h, \widetilde{h})_{\Gamma_c} + \\ + b(\widetilde{\mathbf{u}}, p_a) + \nu a(\widetilde{\mathbf{u}}, \mathbf{u}_a) + c(\widetilde{\mathbf{u}}, \mathbf{u}, \mathbf{u}_a) + b(\mathbf{u}_a, \widetilde{p}) + \\ + c(\mathbf{u}, \widetilde{\mathbf{u}}, \mathbf{u}_a) + \beta(\mathbf{g}\widetilde{T}, \mathbf{u}_a) + \alpha a(\widetilde{T}, T_a) + c(\widetilde{\mathbf{u}}, T, T_a) + \\ + c(\mathbf{u}, \widetilde{T}, T_a) - (\widetilde{h}, T_a)_{\Gamma_c} = 0\,. \end{aligned} \tag{4.78}$$

By extracting the terms involved in the same variation and setting $\Lambda = -1$ we obtain the following equations

$$\begin{aligned}
&b(\mathbf{u}_a, \widetilde{p}) = 0\,, && \forall \widetilde{p} \in L^2_0(\Omega)\\
&\nu a(\widetilde{\mathbf{u}}, \mathbf{u}_a) + c(\mathbf{u}, \widetilde{\mathbf{u}}, \mathbf{u}_a) + c(\widetilde{\mathbf{u}}, \mathbf{u}, \mathbf{u}_a) + b(\widetilde{\mathbf{u}}, p_a) = \\
&\qquad = \alpha_u(\mathbf{u} - \mathbf{u}_d, \widetilde{\mathbf{u}})_{\Omega_d} - c(\widetilde{\mathbf{u}}; T, T_a)\,, && \forall \widetilde{\mathbf{u}} \in \mathbf{H}^1_0(\Omega) \quad (4.79)\\
&\alpha a(\widetilde{T}, T_a) + c(\mathbf{u}, \widetilde{T}, T_a) = -(\beta \mathbf{g}\widetilde{T}, \mathbf{u}_a) + \\
&\qquad + \alpha_T(T - T_d, \widetilde{T})_{\Omega_d}\,, && \forall \widetilde{T} \in H^1_{\Gamma_d}(\Omega)
\end{aligned}$$

and the control equation

$$\lambda(h, \widetilde{h})_{\Gamma_c} + (\widetilde{h}, T_a)_{\Gamma_c} = 0\,, \tag{4.80}$$

for all $\widetilde{h} \in L^2(\Gamma_c)$. The necessary conditions for an optimum are that equations (4.64) and (4.79) are satisfied. This system of equations is called optimality system. Integrations by parts may be used to show that the system constitutes a weak formulation of the boundary value problem

$$\begin{aligned}
&\nabla \cdot \mathbf{u} = 0 && \text{in } \Omega\,,\\
&\mathbf{u} \cdot \nabla \mathbf{u} + \nabla p - \nu \Delta \mathbf{u} = \mathbf{f} - \beta \mathbf{g} T && \text{in } \Omega\,,\\
&\mathbf{u} \cdot \nabla T - \alpha \Delta T = Q && \text{in } \Omega\,,\\
&\mathbf{u} = \mathbf{w} && \text{on } \Gamma\,, \qquad (4.81)\\
&\alpha \nabla T \cdot \mathbf{n}|_{\Gamma_i} = g_{t,n} && \text{on } \Gamma_i\,,\\
&\alpha \nabla T \cdot \mathbf{n}|_{\Gamma_c} = h && \text{on } \Gamma_c\,,\\
&T = g_t && \text{on } \Gamma_d\,,
\end{aligned}$$

and adjoint equations

$$\begin{aligned}
&\nabla \cdot \mathbf{u}_a = 0 && \text{in } \Omega\,,\\
&\mathbf{u}_a \cdot (\nabla \mathbf{u})^T - \mathbf{u} \cdot \nabla \mathbf{u}_a + \nabla p_a - \nu \Delta \mathbf{u}_a = \\
&\qquad = -T \nabla T_a + \alpha_u(\mathbf{u} - \mathbf{u}_d) && \text{in } \Omega\,,\\
&-\alpha \Delta T_a - \mathbf{u} \cdot \nabla T_a = -\beta \mathbf{g} \cdot \mathbf{u}_a + \alpha_T(T - T_d) && \text{in } \Omega\,, \qquad (4.82)\\
&\mathbf{u}_a = 0 && \text{on } \Gamma\,,\\
&\nabla T_a \cdot \mathbf{n}|_{\Gamma_n} = 0 && \text{on } \Gamma_n\,,\\
&T_a = 0 && \text{on } \Gamma_d\,,
\end{aligned}$$

and control equation

$$h = -\frac{T_a}{\lambda} \quad \text{on } \Gamma_c\,. \tag{4.83}$$

The optimality system in the strong form consists of the Boussinesq system (4.81), the adjoint of Boussinesq equations (4.82) and the control equations (4.83).

Numerical algorithm

Let us consider the gradient method for the following minimization problem: find $h \in L^2(\Gamma_c)$ such that $\mathcal{F}(h) := \mathcal{J}(\mathbf{u}(h), T(h), h)$ is minimized. Given $h^{(0)}$, we can define the sequence

$$h^{(n+1)} = h^{(n)} - \rho^{(n)} \frac{d\mathcal{F}(h^{(n)})}{dh^{(n)}}\,, \tag{4.84}$$

recursively, where $\rho^{(n)}$ is a variable step size. For each fixed T_c, the Gâteaux derivative $(d\mathcal{F}(h)/dh) \cdot \widetilde{h}$ for every direction $\widetilde{h} \in L^2(\Gamma_c)$ may be computed

$$\frac{d\mathcal{F}(h)}{dh} \cdot \widetilde{h} = \lambda(h, \widetilde{h})_{\Gamma_c} + \alpha_u(\mathbf{u} - \mathbf{u}_d, \widetilde{\mathbf{u}})_{\Omega_d} + \alpha_T(T - T_d, \widetilde{T})_{\Omega_d}\,, \tag{4.85}$$

where $\widetilde{\mathbf{u}}$ and $\widetilde{T}$ are the solution of $M'(\mathbf{z}) \cdot \widetilde{\mathbf{z}} = \mathbf{0}$, that is

$$\begin{aligned}
&b(\widetilde{\mathbf{u}}, q) = 0 && \forall q \in L^2_0(\Omega)\,,\\
&\nu a(\widetilde{\mathbf{u}}, \mathbf{v}) + c(\widetilde{\mathbf{u}}, \mathbf{u}, \mathbf{v}) + c(\mathbf{u}, \widetilde{\mathbf{u}}, \mathbf{v}) + b(\mathbf{v}, \widetilde{p}) = \\
&\qquad = -\beta(\mathbf{g}\widetilde{T}, \mathbf{v}) && \forall \mathbf{v} \in \mathbf{H}^1_0(\Omega)\,,\\
&\alpha a(\widetilde{T}, \varphi) + c(\widetilde{\mathbf{u}}, T, \varphi) + c(\mathbf{u}, \widetilde{T}, \varphi) = (\widetilde{h}, \varphi)_{\Gamma_c} && \forall \varphi \in H^1_{\Gamma_d}(\Omega)\,.
\end{aligned} \tag{4.86}$$

Let $(\mathbf{u}, p, T) \in \mathbf{H}^1(\Omega) \times L^2_0(\Omega) \times H^1(\Omega)$ be the solution of the state problem (4.64) and let $(\mathbf{u}_a, p_a, T_a) \in \mathbf{H}^1_0(\Omega) \times L^2_0(\Omega) \times H^1_{\Gamma_d}(\Omega)$ be the solution of the adjoint problem (4.79). Setting $(\mathbf{v}, q, \varphi) \in \mathbf{H}^1_0(\Omega) \times L^2_0(\Omega) \times H^1_{\Gamma_d}(\Omega)$ equal to $(\mathbf{u}_a, p_a, T_a) \in \mathbf{H}^1_0(\Omega) \times L^2_0(\Omega) \times H^1_{\Gamma_d}(\Omega)$ in (4.55) and comparing the resulting equation with (4.79), we find that

$$\alpha_u(\mathbf{u} - \mathbf{u}_d, \widetilde{\mathbf{u}})_{\Omega_d} + \alpha_T(T - T_d, \widetilde{T})_{\Omega_d} = (\widetilde{h}, T_a)_{\Gamma_c}\,. \tag{4.87}$$

Thus, the Gâteaux derivative may be computed as

$$\frac{d\mathcal{F}(h)}{dh} = h + \frac{T_a}{\lambda}\,. \tag{4.88}$$

The optimization algorithm is then given as follows

a) Initialization:

1. choose tolerance τ and $h^{(0)}$; set $n = 0$ and $\rho^{(0)} = 1$;
2. solve for $(\mathbf{u}^{(0)}, p^{(0)}, T^{(0)})$ from (4.64) with $h = h^{(0)}$;
3. evaluate $\mathcal{J}^{(0)} = \mathcal{J}(\mathbf{u}^{(0)}, T^{(0)}, h^{(0)})$ using (4.63);

b) main loop:

1. set $n = n + 1$;
2. solve for $(\mathbf{u}_a^{(n)}, p_a^{(n)}, T_a^{(n)})$ from (4.79);
3. solve for $h^{(n)}$ from
$$h^{(n)} = h^{(n-1)} - \rho^{(n)}\Big(h^{(n-1)} + \frac{T_a^{(n)}}{\lambda}\Big); \tag{4.89}$$
4. solve for $(\mathbf{u}^{(n)}, p^{(n)}, T^{(n)})$ from (4.64) with $h = h^{(n)}$;
5. evaluate $\mathcal{J}^{(n)} = \mathcal{J}(\mathbf{u}^{(n)}, T^{(n)}, h^{(n)})$ using (4.63);
   i) if $\mathcal{J}^{(n)} > \mathcal{J}^{(n-1)}$, set $\rho^{(n)} = 0.5\rho^{(n)}$ and go to step b) 3.;
   ii) if $\mathcal{J}^{(n)} < \mathcal{J}^{(n-1)}$, set $\rho^{(n+1)} = 1$ and go to step b) 1.;
   iii) if $|\mathcal{J}^{(n)} - \mathcal{J}^{(n-1)}|/|\mathcal{J}^{(n)}| < \tau$ stop.

4.2.3. Distributed control

The aim of a distributed control problem is to control the flow state using a heat source acting on the domain Ω as control mechanism. In (4.18) the heat source Q is the control of the optimal control problem. The boundary conditions are the ones reported in (4.19) where $\mathbf{w}$, g_t and $g_{t,n}$ are given functions. The cost functional is formulated as follows

$$\mathcal{J}(\mathbf{u}, T, Q) = \frac{\alpha_u}{2}\int_{\Omega_d} |\mathbf{u} - \mathbf{u}_d|^2 d\mathbf{x} + \frac{\alpha_T}{2}\int_{\Omega_d} |T - T_d|^2 d\mathbf{x} + \\ + \frac{\lambda}{2}\int_{\Omega} |Q|^2 d\mathbf{x}\,, \tag{4.90}$$

where the cost contribution measures the $L^2(\Omega)$-norm of the control Q.

Weak formulation

The weak form of the boundary value problem (4.16)-(4.19) is given as follows: find $(\mathbf{u}, p, T) \in \mathbf{H}^1(\Omega) \times L_0^2(\Omega) \times H^1(\Omega)$ such that

$$\begin{aligned} &b(\mathbf{u}, q) = 0 && \forall q \in L_0^2(\Omega)\,, \\ &\nu a(\mathbf{u}, \mathbf{v}) + c(\mathbf{u}, \mathbf{u}, \mathbf{v}) + b(\mathbf{v}, p) = (\mathbf{f}, \mathbf{v}) - \beta(\mathbf{g}T, \mathbf{v}) && \forall \mathbf{v} \in \mathbf{H}_0^1(\Omega)\,, \\ &\alpha a(T, \varphi) + c(\mathbf{u}, T, \varphi) = (Q, \varphi) + (g_{t,n}, \varphi)_{\Gamma_n} && \forall \varphi \in H_{\Gamma_d}^1(\Omega)\,, \end{aligned} \tag{4.91}$$

The existence of the solution of the system (4.91) has been proved in [23].

The optimization problem and existence of optimal solution

We enunciate the optimal control problem. We look for a $(\mathbf{u},\ p,\ T,\ Q) \in \mathbf{H}^1(\Omega) \times L^2_0(\Omega) \times H^1(\Omega) \times L^2(\Omega)$ such that the cost functional (4.90) is minimized subject to the constraints (4.91). The admissible set of states and controls is

$$\begin{aligned} \mathcal{U}_{ad} = \{(\mathbf{u}, p, T, Q) \in \mathbf{H}^1(\Omega) \times L^2_0(\Omega) \times H^1(\Omega) \times L^2(\Omega) : \\ \mathcal{J}(\mathbf{u}, T, Q) < \infty \text{ and (4.91) is satified.}\} \end{aligned} \tag{4.92}$$

Then $(\hat{\mathbf{u}}, \hat{p}, \hat{T}, \hat{Q}) \in \mathcal{U}_{ad}$ is called an optimal solution if there exists $\varepsilon > 0$ such that

$$\begin{aligned} \mathcal{J}(\hat{\mathbf{u}}, \hat{p}, \hat{T}, \hat{Q}) \leq \mathcal{J}(\mathbf{u}, p, T, Q) \quad \forall (\mathbf{u}, p, T, Q) \in \mathcal{U}_{ad} \text{ satisfying} \\ \|\mathbf{u} - \hat{\mathbf{u}}\|_1 + \|p - \hat{p}\|_0 + \|T - \hat{T}\|_1 + \|Q - \hat{Q}\|_0 < \varepsilon\,. \end{aligned} \tag{4.93}$$

Theorem 4.7. *Let $\mathcal{U}_{ad}$ be not empty. There exists at least one optimal solution $(\hat{\mathbf{u}}, \hat{p}, \hat{T}, \hat{Q}) \in \mathcal{U}_{ad}$.*

Proof. Let $\{\mathbf{u}^{(n)}, p^{(n)}, T^{(n)}, Q^{(n)}\}$ be a sequence in $\mathcal{U}_{ad}$ such that

$$\lim_{n\to\infty} \mathcal{J}(\mathbf{u}^{(n)}, p^{(n)}, T^{(n)}, Q^{(n)}) = \inf_{(\mathbf{v},q,S,z)\in\mathcal{U}_{ad}} \mathcal{J}(\mathbf{v}, q, S, z)\,. \tag{4.94}$$

By the definition of $\mathcal{U}_{ad}$ in (4.92) we have

$$\begin{aligned} & b(\mathbf{u}^{(n)}, q) = 0 && \forall q \in L^2_0(\Omega)\,, \\ & \nu a(\mathbf{u}^{(n)}, \mathbf{v}) + c(\mathbf{u}^{(n)}, \mathbf{u}^{(n)}, \mathbf{v}) + b(\mathbf{v}, p^{(n)}) = \\ & \qquad = (\mathbf{f}, \mathbf{v}) - \beta(\mathbf{g}T^{(n)}, \mathbf{v}) && \forall \mathbf{v} \in \mathbf{H}^1_0(\Omega)\,, \\ & \alpha a(T^{(n)}, \varphi) + c(\mathbf{u}^{(n)}, T^{(n)}, \varphi) = (Q^{(n)}, \varphi) + \\ & \qquad + (g_{t,n}, \varphi)_{\Gamma_n} && \forall \varphi \in H^1_{\Gamma_d}(\Omega)\,. \end{aligned} \tag{4.95}$$

By (4.90) and (4.92) we easily see that $\{\|Q^{(n)}\|_0\}$ is uniformly bounded. Also by (4.26) we have that $\{\|\mathbf{u}^{(n)}\|_1\}$, $\{\|p^{(n)}\|_0\}$ and $\{\|T^{(n)}\|_1\}$ are uniformly bounded. We may then extract subsequences $\{\mathbf{u}^{(n)},\ p^{(n)},\ T^{(n)},\ Q^{(n)}\}$ converging to $(\hat{\mathbf{u}}, \hat{p}, \hat{T}, \hat{Q})$

$$\begin{aligned} & Q^{(n)} \rightharpoonup \hat{Q} && \text{in } L^2(\Omega)\,, && \\ & \mathbf{u}^{(n)} \rightharpoonup \hat{\mathbf{u}} && \text{in } \mathbf{H}^1(\Omega)\,, && \text{and } \nabla\mathbf{u}^{(n)} \rightharpoonup \nabla\hat{\mathbf{u}} \text{ in } L^2(\Omega)\,, \\ & T^{(n)} \rightharpoonup \hat{T} && \text{in } H^1(\Omega)\,, && \text{and } \nabla T^{(n)} \rightharpoonup \nabla\hat{T} \text{ in } L^2(\Omega)\,, \\ & p^{(n)} \rightharpoonup \hat{p} && \text{in } L^2_0(\Omega)\,, && \end{aligned}$$

$$\begin{aligned}
\mathbf{u}^{(n)} &\to \hat{\mathbf{u}} && \text{in } \mathbf{L}^2(\Omega)\,,\\
T^{(n)}|_\Gamma &\to \hat{T}|_\Gamma && \text{in } L^2(\Gamma)\,,\\
\mathbf{u}^{(n)}|_\Gamma &\to \hat{\mathbf{u}}|_\Gamma && \text{in } \mathbf{L}^2(\Gamma)\,.
\end{aligned}$$

We may pass to the limit in (4.95) to determine that $(\hat{\mathbf{u}}, \hat{p}, \hat{T}, \hat{Q})$ satisfies (4.91). □

The existence of Lagrange multipliers

We define the following functional spaces

$$\mathbf{B}_1 = \mathbf{H}^1(\Omega) \times L^2_0(\Omega) \times H^1(\Omega) \times L^2(\Omega)\,, \tag{4.96}$$

$$\mathbf{B}_2 = \mathbf{H}^{-1}(\Omega) \times L^2_0(\Omega) \times H^{1*}_{\Gamma_d}(\Omega)\,, \tag{4.97}$$

$$\mathbf{B}_3 = \mathbf{H}^1_0(\Omega) \times L^2_0(\Omega) \times H^1_{\Gamma_d}(\Omega) \times L^2(\Omega)\,. \tag{4.98}$$

Let $M : \mathbf{B}_1 \to \mathbf{B}_2$ denote the generalized constraint equations, i.e. $M(\mathbf{z}) = \mathbf{l}$ for $\mathbf{z} = (\mathbf{u}, p, T, Q) \in \mathbf{B}_1$ and $\mathbf{l} = (\mathbf{l}_1, l_2, l_3) \in \mathbf{B}_2$ if and only if

$$\begin{aligned}
&\nu a(\mathbf{u}, \mathbf{v}) + c(\mathbf{u}, \mathbf{u}, \mathbf{v}) + b(\mathbf{v}, p) - (\mathbf{f}, \mathbf{v}) + \\
&\qquad + \beta(\mathbf{g}T, \mathbf{v}) = (\mathbf{l}_1, \mathbf{v}) && \forall \mathbf{v} \in \mathbf{H}^1_0(\Omega)\,,\\
&b(\mathbf{u}, q) = (l_2, q) && \forall q \in L^2_0(\Omega)\,,\\
&\alpha a(T, \varphi) + c(\mathbf{u}, T, \varphi) - (Q, \varphi) - (g_{t,n}, \varphi)_{\Gamma_n} = \\
&\qquad = (l_3, \varphi) && \forall \varphi \in H^1_{\Gamma_d}(\Omega)\,,
\end{aligned} \tag{4.99}$$

Thus, the constraints (4.91) can be expressed as $M(\mathbf{u}, p, T, Q) = \mathbf{0}$. Let $(\hat{\mathbf{u}}, \hat{p}, \hat{T}, \hat{Q}) \in \mathbf{H}^1(\Omega) \times L^2_0(\Omega) \times H^1(\Omega) \times L^2(\Omega)$ denote an optimal solution in the sense of (4.93). Then, consider the nonlinear operator $N : \mathbf{B}_1 \to \mathbb{R} \times \mathbf{B}_2$ defined by

$$N(\mathbf{u}, p, T, Q) = \begin{pmatrix} \mathcal{J}(\mathbf{u}, T, Q) - \mathcal{J}(\hat{\mathbf{u}}, \hat{T}, \hat{Q}) \\ M(\mathbf{u}, p, T, Q) \end{pmatrix}. \tag{4.100}$$

Given $\mathbf{z} = (\mathbf{u}, p, T, Q) \in \mathbf{B}_1$ the operator $M'(\mathbf{z}) : \mathbf{B}_3 \to \mathbf{B}_2$ may be defined as $M'(\mathbf{z}) \cdot \widetilde{\mathbf{z}} = \widetilde{\mathbf{l}}$ for $\widetilde{\mathbf{z}} = (\widetilde{\mathbf{u}}, \widetilde{p}, \widetilde{T}, \widetilde{Q}) \in \mathbf{B}_3$ and $\widetilde{\mathbf{l}} = (\widetilde{\mathbf{l}}_1, \widetilde{l}_2, \widetilde{l}_3) \in \mathbf{B}_2$ if and only if

$$\begin{aligned}
&\nu a(\widetilde{\mathbf{u}}, \mathbf{v}) + c(\widetilde{\mathbf{u}}, \mathbf{u}, \mathbf{v}) + c(\mathbf{u}, \widetilde{\mathbf{u}}, \mathbf{v}) + b(\mathbf{v}, \widetilde{p}) + \\
&\qquad + \beta(\mathbf{g}\widetilde{T}, \mathbf{v}) = (\widetilde{\mathbf{l}}_1, \mathbf{v}) && \forall \mathbf{v} \in \mathbf{H}^1_0(\Omega)\,,\\
&b(\widetilde{\mathbf{u}}, q) = (\widetilde{l}_2, q) && \forall q \in L^2_0(\Omega)\,,\\
&\alpha a(\widetilde{T}, \varphi) + c(\widetilde{\mathbf{u}}, T, \varphi) + c(\mathbf{u}, \widetilde{T}, \varphi) - (\widetilde{Q}, \varphi) = \\
&\qquad = (\widetilde{l}_3, \varphi) && \forall \varphi \in H^1_{\Gamma_d}(\Omega)\,,
\end{aligned} \tag{4.101}$$

The operator $N'(\mathbf{z}) : \mathbf{B}_3 \to \mathbb{R} \times \mathbf{B}_2$ may be defined as $N'(\mathbf{z}) \cdot \widetilde{\mathbf{z}} = (\widetilde{a}, \widetilde{\mathbf{l}})$ for $\widetilde{a} \in \mathbb{R}$ if and only if

$$\begin{aligned}
&\alpha_u(\mathbf{u} - \mathbf{u}_d, \widetilde{\mathbf{u}})_{\Omega_d} + \alpha_T(T - T_d, \widetilde{T})_{\Omega_d} + \\
&\qquad + \lambda(Q, \widetilde{Q}) = \widetilde{a} \\
&\nu a(\widetilde{\mathbf{u}}, \mathbf{v}) + c(\widetilde{\mathbf{u}}, \mathbf{u}, \mathbf{v}) + c(\mathbf{u}, \widetilde{\mathbf{u}}, \mathbf{v}) + b(\mathbf{v}, \widetilde{p}) + \\
&\qquad + \beta(\mathbf{g}\widetilde{T}, \mathbf{v}) = (\widetilde{\mathbf{l}}_1, \mathbf{v}) \qquad \forall \mathbf{v} \in \mathbf{H}_0^1(\Omega)\,, \\
&b(\widetilde{\mathbf{u}}, q) = (\widetilde{l}_2, q) \qquad \forall q \in L_0^2(\Omega)\,, \\
&\alpha a(\widetilde{T}, \varphi) + c(\widetilde{\mathbf{u}}, T, \varphi) + c(\mathbf{u}, \widetilde{T}, \varphi) - (\widetilde{Q}, \varphi) = \\
&\qquad = (\widetilde{l}_3, \varphi) \qquad \forall \varphi \in H_{\Gamma_d}^1(\Omega)\,,
\end{aligned} \tag{4.102}$$

Lemma 4.3. *Let $\mathbf{z}_0 \in \mathbf{B_1}$. Then we have that*

1. *the operator $M'(\mathbf{z}_0)$ has closed range in $\mathbf{B_2}$,*
2. *the operator $N'(\mathbf{z}_0)$ has closed range but is not onto in $\mathbb{R} \times \mathbf{B_2}$,*

Proof. The proof follows standard techniques, see the Proof of Lemma 4.1. □

Theorem 4.8. *Let $\hat{\mathbf{z}} = (\hat{\mathbf{u}}, \hat{p}, \hat{T}, \hat{Q}) \in \mathbf{H}^1(\Omega) \times L_0^2(\Omega) \times H^1(\Omega) \times L^2(\Omega)$ denote an optimal solution in the sense of (4.93). Then there exists a nonzero Lagrange multiplier $(\Lambda, \hat{\mathbf{u}}_a, \hat{p}_a, \hat{T}_a) \in \mathbb{R} \times \mathbf{B}_2^*$ satisfying the Euler equations*

$$\Lambda \mathcal{J}'(\hat{\mathbf{u}}, \hat{T}, \hat{Q}) \cdot \widetilde{\mathbf{z}} + \langle (\hat{\mathbf{u}}_a, \hat{p}_a, \hat{T}_a), M'(\hat{\mathbf{z}}) \cdot \widetilde{\mathbf{z}} \rangle = 0\,, \quad \forall \widetilde{\mathbf{z}} \in \mathbf{B}_3 \tag{4.103}$$

where $\langle \cdot, \cdot \rangle$ denotes the duality pairing between $\mathbf{B}_2$ and $\mathbf{B}_2^*$.

Proof. From Lemma 4.3, we have that the range of $N'(\hat{\mathbf{z}})$ is a closed, proper subspace of $\mathbb{R} \times \mathbf{B}_2$. Then, from the Hahn-Banach theorem, there exists a nonzero element of $\mathbb{R} \times \mathbf{B}_2^*$ that nullifies the range of $N'(\hat{\mathbf{z}})$. Then, there exists $(\Lambda, \hat{\mathbf{u}}_a, \hat{p}_a, \hat{T}_a) \in \mathbb{R} \times \mathbf{B}_2^*$ such that

$$\begin{aligned}
&\langle (\widetilde{a}, \widetilde{\mathbf{l}}_1, \widetilde{l}_2, \widetilde{l}_3), (\Lambda, \hat{\mathbf{u}}_a, \hat{p}_a, \hat{T}_a) \rangle = 0 \\
&\qquad \forall (\widetilde{a}, \widetilde{\mathbf{l}}_1, \widetilde{l}_2, \widetilde{l}_3) \text{ belonging to the range of } N'(\hat{\mathbf{z}})\,.
\end{aligned} \tag{4.104}$$

Note that $\Lambda \neq 0$ since otherwise we would have that $\langle (\widetilde{\mathbf{l}}_1, \widetilde{l}_2, \widetilde{l}_3), (\hat{\mathbf{u}}_a, \hat{p}_a, \hat{T}_a) \rangle = 0$ for all $\widetilde{\mathbf{l}} \in \mathbf{B}_2$. This would imply $(\hat{\mathbf{u}}_a, \hat{p}_a, \hat{T}_a) = 0$ contradicting the fact that $(\Lambda, \hat{\mathbf{u}}_a, \hat{p}_a, \hat{T}_a) \neq 0$. Clearly, using the definition of $N'(\hat{\mathbf{z}})$, (4.103) and (4.104) are equivalent. □

The optimality system

Dropping the $\widehat{(\cdot)}$ notation for optimal solution, we derive now the optimality system using the Euler equation (4.103)

$$\begin{aligned}\alpha_u\Lambda(\mathbf{u}-\mathbf{u}_d,\tilde{\mathbf{u}})_{\Omega_d}+\alpha_T\Lambda(T-T_d,\widetilde{T})_{\Omega_d}+\Lambda\lambda(Q,\widetilde{Q})+\\ +b(\tilde{\mathbf{u}},p_a)+\nu a(\tilde{\mathbf{u}},\mathbf{u}_a)+c(\tilde{\mathbf{u}},\mathbf{u},\mathbf{u}_a)+b(\mathbf{u}_a,\widetilde{p})+\\ +c(\mathbf{u},\tilde{\mathbf{u}},\mathbf{u}_a)+\beta(\mathbf{g}\widetilde{T},\mathbf{u}_a)+\alpha a(\widetilde{T},T_a)+c(\tilde{\mathbf{u}},T,T_a)+\\ +c(\mathbf{u},\widetilde{T},T_a)-(\widetilde{Q},T_a)=0\,.\end{aligned} \tag{4.105}$$

By extracting the terms involved in the same variation and setting $\Lambda=-1$ we obtain the following equations

$$\begin{aligned}&b(\mathbf{u}_a,\widetilde{p})=0\,, && \forall\widetilde{p}\in L^2_0(\Omega)\\ &\nu a(\tilde{\mathbf{u}},\mathbf{u}_a)+c(\mathbf{u},\tilde{\mathbf{u}},\mathbf{u}_a)+c(\tilde{\mathbf{u}},\mathbf{u},\mathbf{u}_a)+b(\tilde{\mathbf{u}},p_a)=\\ &\qquad=\alpha_u(\mathbf{u}-\mathbf{u}_d,\tilde{\mathbf{u}})_{\Omega_d}-c(\tilde{\mathbf{u}};T,T_a)\,, && \forall\tilde{\mathbf{u}}\in\mathbf{H}^1_0(\Omega)\\ &\alpha a(\widetilde{T},T_a)+c(\mathbf{u},\widetilde{T},T_a)=-(\beta\mathbf{g}\widetilde{T},\mathbf{u}_a)+\\ &\qquad+\alpha_T(T-T_d,\widetilde{T})_{\Omega_d}\,, && \forall\widetilde{T}\in H^1_{\Gamma_d}(\Omega)\end{aligned} \tag{4.106}$$

and the control equation

$$\lambda(Q,\widetilde{Q})+(\widetilde{Q},T_a)=0\,,\quad\forall\widetilde{Q}\in L^2(\Omega)\,. \tag{4.107}$$

The necessary conditions for an optimum are that equations (4.91) and (4.106) are satisfied. This system of equations is the optimality system and we can use integrations to show that the system constitutes a weak formulation of the boundary value problem for state equations

$$\begin{aligned}&\nabla\cdot\mathbf{u}=0 && \text{in }\Omega\,,\\ &\mathbf{u}\cdot\nabla\mathbf{u}+\nabla p-\nu\Delta\mathbf{u}=\mathbf{f}-\beta\mathbf{g}T && \text{in }\Omega\,,\\ &\mathbf{u}\cdot\nabla T-\alpha\Delta T=Q && \text{in }\Omega\,,\\ &\mathbf{u}=\mathbf{w} && \text{on }\Gamma\,,\\ &\alpha\nabla T\cdot\mathbf{n}|_{\Gamma_n}=g_{t,n} && \text{on }\Gamma_n\,,\\ &T=g_t && \text{on }\Gamma_d\,,\end{aligned} \tag{4.108}$$

and adjoint equations

$$\begin{aligned}
&\nabla \cdot \mathbf{u}_a = 0 && \text{in } \Omega\,,\\
&\mathbf{u}_a \cdot (\nabla \mathbf{u})^T - \mathbf{u} \cdot \nabla \mathbf{u}_a + \nabla p_a - \nu \Delta \mathbf{u}_a = \\
&\qquad = -T \nabla T_a + \alpha_u (\mathbf{u} - \mathbf{u}_d) && \text{in } \Omega\,,\\
&-\alpha \Delta T_a - \mathbf{u} \cdot \nabla T_a = -\beta \mathbf{g} \cdot \mathbf{u}_a + \alpha_T (T - T_d) && \text{in } \Omega\,,\\
&\mathbf{u}_a = 0 && \text{on } \Gamma\,,\\
&\nabla T_a \cdot \mathbf{n}|_{\Gamma_n} = 0 && \text{on } \Gamma_n\,,\\
&T_a = 0 && \text{on } \Gamma_d\,,
\end{aligned} \tag{4.109}$$

and control equation

$$Q = -\frac{T_a}{\lambda} \quad \text{in } \Omega\,. \tag{4.110}$$

The optimality system in the strong form consists of the Boussinesq system (4.108), the adjoint of Boussinesq equations (4.109) and the control equation (4.110).

Numerical algorithm

Let us consider the gradient method for the following minimization problem: find $Q \in L^2(\Omega)$ such that $\mathcal{F}(Q) := \mathcal{J}(\mathbf{u}(Q), T(Q), Q)$ is minimized. Given $Q^{(0)}$, we can define the sequence

$$Q^{(n+1)} = Q^{(n)} - \rho^{(n)} \frac{d\mathcal{F}(Q^{(n)})}{dQ^{(n)}}\,, \tag{4.111}$$

recursively, where $\rho^{(n)}$ is a variable step size. Let $\hat{Q}_c$ be a solution of the minimization problem, thus at the optimum $d\mathcal{F}(\hat{Q})/d\hat{Q} = 0$ and $Q^{(n+1)} = Q^{(n)}$. The Gâteaux derivative $(d\mathcal{F}(Q)/dQ) \cdot \widetilde{Q}$ for every direction $\widetilde{Q} \in L^2(\Omega)$ may be computed

$$\frac{d\mathcal{F}(Q)}{dQ} \cdot \widetilde{Q} = \lambda(Q, \widetilde{Q}) + \alpha_u (\mathbf{u} - \mathbf{u}_d, \widetilde{\mathbf{u}})_{\Omega_d} + \alpha_T (T - T_d, \widetilde{T})_{\Omega_d}\,, \tag{4.112}$$

where $\widetilde{\mathbf{u}}$ and $\widetilde{T}$ are the solution of $M'(\mathbf{z}) \cdot \widetilde{\mathbf{z}} = \mathbf{0}$. Using similar techniques presented in the previous sections, it is possible to find that

$$\alpha_u (\mathbf{u} - \mathbf{u}_d, \widetilde{\mathbf{u}})_{\Omega_d} + \alpha_T (T - T_d, \widetilde{T})_{\Omega_d} = (\widetilde{Q}, T_a)\,. \tag{4.113}$$

Thus, the Gâteaux derivative may be computed as

$$\frac{d\mathcal{F}(Q)}{dQ} = Q + \frac{T_a}{\lambda}\,. \tag{4.114}$$

The optimization algorithm is then given as follows

a) Initialization:
   1. choose tolerance τ and $Q^{(0)}$; set $n = 0$ and $\rho^{(0)} = 1$;
   2. solve for $(\mathbf{u}^{(0)}, p^{(0)}, T^{(0)})$ from (4.91) with $Q = Q^{(0)}$;
   3. evaluate $\mathcal{J}^{(0)} = \mathcal{J}(\mathbf{u}^{(0)}, T^{(0)}, Q^{(0)})$ using (4.90);

b) main loop:
   1. set $n = n + 1$;
   2. solve for $(\mathbf{u}_a^{(n)}, p_a^{(n)}, T_a^{(n)})$ from (4.106);
   3. solve for $Q^{(n)}$ from

$$Q^{(n)} = Q^{(n-1)} - \rho^{(n)}\Big(Q^{(n-1)} + \frac{T_a^{(n)}}{\lambda}\Big)\,; \tag{4.115}$$

   4. solve for $(\mathbf{u}^{(n)}, p^{(n)}, T^{(n)})$ from (4.64) with $Q = Q^{(n)}$;
   5. evaluate $\mathcal{J}^{(n)} = \mathcal{J}(\mathbf{u}^{(n)}, T^{(n)}, Q^{(n)})$ using (4.63);
      i) if $\mathcal{J}^{(n)} > \mathcal{J}^{(n-1)}$, set $\rho^{(n)} = 0.5\rho^{(n)}$ and go to step b) 3.;
      ii) if $\mathcal{J}^{(n)} < \mathcal{J}^{(n-1)}$, set $\rho^{(n+1)} = 1$ and go to step b) 1.;
      iii) if $|\mathcal{J}^{(n)} - \mathcal{J}^{(n-1)}|/|\mathcal{J}^{(n)}| < \tau$ stop.

4.3. Numerical results

In this section, we report some numerical results obtained by using the mathematical models shown in the previous sections. We have derived the optimality systems for Dirichlet, Neumann, and distributed optimal control problems. The main difference between the three control problems is in the nature of the control equations. For Neumann and distributed control, the control equation is an algebraic equation that states that the control is proportional to the adjoint temperature, see Equation (4.83) and (4.110). In contrast, when we have a Dirichlet boundary control, the control equation is a partial differential equation with the normal adjoint temperature gradient as source term, as reported in (4.51). Thus, the adjoint temperature T_a

Table 4.1: Boussinesq control: physical properties employed for the numerical simulations.

Property	Symbol	Value	Units
Viscosity	μ	0.00181	$Pa\,s$
Density	ρ	10340	kg/m^3
Thermal conductivity	λ	10.72	$W/(mK)$
Specific heat	c	145.75	$J/(kgK)$
Coefficient of expansion	β	2.5684×10^{-4}	K^{-1}

plays a key role in all three control mechanisms, as well as the regularization parameter λ which appears in the denominator of the source terms. The adjoint temperature T_a is dependent on the objectives of velocity and temperature fields. If the objective is on the temperature field, the dependence is direct through the term $\alpha_T(T - T_d)$ appearing in the right-hand side of the adjoint temperature equation (4.47), (4.79) and (4.106). If the objective is on the velocity field, the control mechanism is indirect, since the term $\alpha_u(\mathbf{u} - \mathbf{u}_d)$ acts as a source in the adjoint velocity equation. In its turn, the adjoint velocity appears in the source term of the adjoint temperature $\beta\mathbf{g} \cdot \mathbf{u}_a$.

The solvers for the adjoint variables have been implemented in the finite element code FEMuS. Also, the algorithms presented in the previous sections have been included into the finite element library. Several numerical simulations have been performed varying the control mechanism (wall temperature, wall-normal heat flux, volumetric heat source), the objectives and the weight of the regularization coefficients.

4.3.1. Dirichlet boundary control

We show numerical results for the Dirichlet boundary control. The geometry considered is a square cavity with $L = 0.01m$. The domain $\Omega = [0, L] \times [0, L] \in \mathbb{R}^2$ is reported in Figure 4.1. The boundary conditions are reported in (4.22), where $\Gamma_d = \Gamma_1 \cup \Gamma_3$, $\Gamma_i = \Gamma_3$, $\Gamma_c = \Gamma_1$ and $\Gamma_n = \Gamma_2 \cup \Gamma_4$. We set $\mathbf{f} = \mathbf{0}$ and $Q = 0$ in (4.24), and $\mathbf{g}_u = \mathbf{0}$, $g_{t,n} = 0$, $g_t = 493K$ on Γ_3 and $g_t = 503K$ on Γ_1 in (4.22). For the reference case, we set $T_c^{(0)} = 0$ then on $\Gamma_c = \Gamma_1$ we have $T^{(0)} = g_t$. We have considered liquid lead with the properties reported in Table 4.1. We discretize the numerical problem in a finite element framework, and we consider a 20×20 uniform

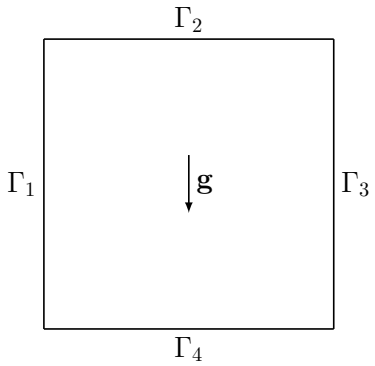

Figure 4.1: Computational domain for the optimal control of Boussinesq equations.

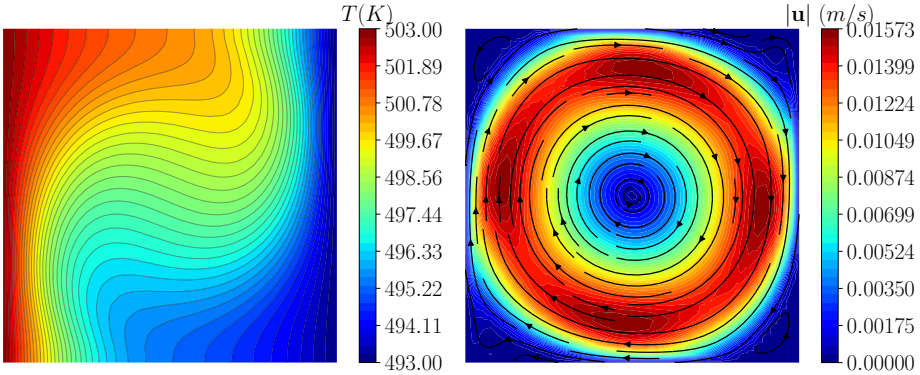

Figure 4.2: Uncontrolled solution: contours of temperature field $T^{(0)}$ (a); contours and streamlines of velocity field $\mathbf{u}^{(0)}$ (b).

quadrangular mesh formed by biquadratic elements. The temperature and velocity contours on the computational domain are reported in Figure 4.2a and b respectively. Lead flows in the cavity and forms a clockwise vortex due to buoyancy forces caused by the heated cavity wall. The bulk velocity is $U_b = 0.008765m/s$. The corresponding Reynolds number is 500. The Richardson number, which represents the importance of natural convection relative to forced convection, is computed as $Ri = gL\Delta T\beta/U_b^2$ and is equal to 3.28. The Grashof number, which measures the ratio of the buoyancy to the viscous force acting on a fluid, is given by $Gr = RiRe^2 = 8.2 \times 10^5$. Lastly, the Rayleigh number $Ra = GrPr$ is equal to 2×10^4. In Figure 4.2 we can observe the typical features of temperature and velocity profiles for $Ra \approx 10^4$. The shape of the isotherms shows which is the dominant

heat transfer mechanism between conduction and convection. For low Ra values, almost vertical isotherms appear, because heat is transferred by conduction between the hot wall and cold one. As the isotherms depart from the vertical position, the heat transfer mechanism changes from conduction to convection. Concerning the velocity field, for low values of Ra a central vortex appears as the dominant characteristic of the flow. As Ra increases, the vortex tends to become elliptic at $Ra \approx 10^4$, while it breaks up into two vortices only at $Ra = 10^5$ [94].

Temperature matching case. Firstly, we aim to test the optimization algorithm with a temperature matching case. Let (4.23) be the objective functional with $\alpha_u = 0$, $\alpha_T = 1$ and $\Omega_d = [0.45L; 0.55L] \times [0.75L; 0.85L]$. The region Ω_d is indicated in Figure 4.3a. We set $T_d = 450K$ then in Ω_d we aim obtaining cooler fluid than in the uncontrolled case. We consider four different values of the regularization parameter λ, i.e. $10^{-5}, 10^{-6}, 10^{-7}$ and 10^{-8}. The reference objective functional is $\mathcal{J}^{(0)} = 0.001250$. For the numerical simulations, we use the algorithm for Dirichlet boundary problems presented in the previous sections, and we choose for the update of the control the Equation (4.61).

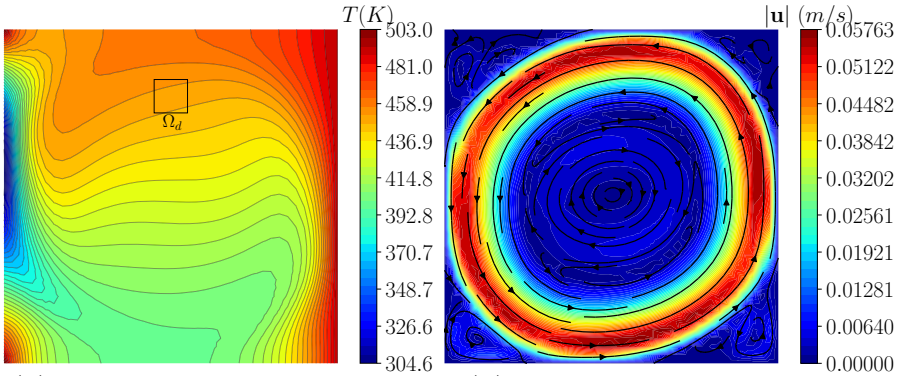

Figure 4.3: Temperature matching case with Dirichlet boundary control: optimal solution for $\lambda = 10^{-7}$. Contours of the temperature (a) and velocity magnitude with velocity streamlines (b).

The contours of the optimal solution in terms of temperature and velocity fields are reported respectively in Figure 4.3a and b for $\lambda = 10^{-7}$. The region Ω_d where the objective is set is highlighted with a black square in Figure 4.3a. From the contours, we can see that the optimal temperature

field assumes values close to the target temperature $T_d = 450K$. To achieve the objective, the temperature on the left wall decreases with respect to the reference case. For this reason, the motion changes, and we obtain a counterclockwise vortex, as depicted by the streamlines in Figure 4.3b.

Table 4.2: Temperature matching case with Dirichlet boundary control: objective functional, percentage reduction and number of iterations of the optimization algorithm for different λ values.

λ	10^{-5}	10^{-6}	10^{-7}	10^{-8}	Reference
$\mathcal{J}^{(n)} \times 10^6$	3.110	2.179	2.091	1.979	1250
% Reduction	-99.75	-99.82	-99.83	-99.84	0
Iterations n	6	5	6	10	0

In Table 4.2 we report the objective functional values $\mathcal{J}^{(n)}$ corresponding to the optimal state for each numerical simulations. We also report the value of the reference objective functional $\mathcal{J}^{(0)}$ and the percentage reduction for each case evaluated as $(\mathcal{J}^{(n)} - \mathcal{J}^{(0)})/\mathcal{J}^{(0)}$. In addition, the number of iterations n of the optimization algorithm is included in Table 4.2. With the lowest value of λ, we have the lowest functional value, $\mathcal{J}^{(10)} = 1.979 \times 10^{-6}$, and the greatest percentage reduction.

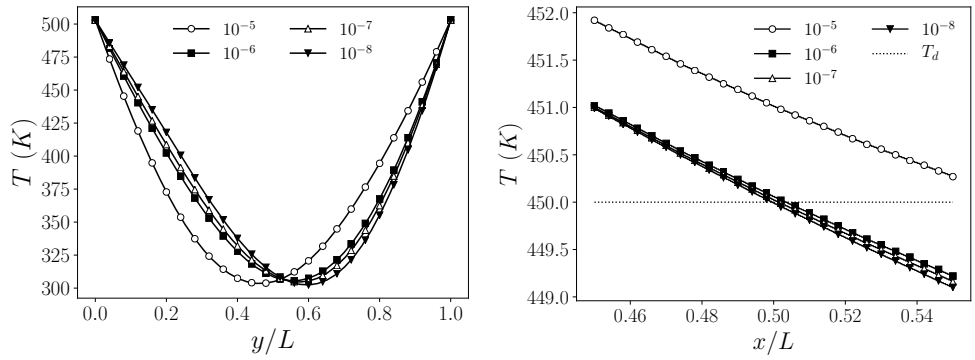

(a) (b)

Figure 4.4: Temperature matching case with Dirichlet boundary control: temperature profiles on the controlled boundary Γ_c (a) and on the region Ω_d along the line $y/L = 0.8$ (b). Numerical results for $\lambda = 10^{-5}, 10^{-6}, 10^{-7}$ and 10^{-8}.

Temperature profiles along the boundary Γ_c are reported in Figure 4.4a for the different values of the regularization parameter λ. As λ decreases,

the minimum of the profiles moves towards $y/L = 1$. In Figure 4.4b the temperature is plotted along a line at $y/L = 0.8$ for $0.45 < y/L < 0.55$ in the region Ω_d. We can see that for the lowest values of λ, the optimal solutions tend to the target profile T_d. The case $\lambda = 10^{-5}$ is the farthest from the objective, as we can also deduce from the functional values reported in Table 4.2.

Velocity matching case. The second test for the Dirichlet optimal control is a velocity matching case. The objective functional is the one reported in Equation (4.23) setting $\alpha_u = 1$, $\alpha_T = 0$ and $\Omega_d = [0.15L; 0.25L] \times [0.45L; 0.55L]$. The region Ω_d is represented in Figure 4.5c. We aim to control the y-component of the velocity then we set $v_d = 0.05m/s$. In the reference case, the mean value of v on Ω_d is equal to $0.0159m/s$ then we aim to accelerate the fluid near the controlled boundary Γ_c. We consider different values of the regularization parameter λ, i.e. $10^{-10}, 10^{-11}, 10^{-12}$, 10^{-13}, and 10^{-14}. The considered values are lower than those used for the temperature matching test. We also tested higher values of the regularization parameter, but the control was ineffective in those cases. Indeed, it is easier to achieve an objective on the temperature field than on the velocity field, since the control parameter T_c (or h, or Q) depends directly on the adjoint temperature but indirectly on the adjoint velocity. The reference objective functional is $\mathcal{J}^{(0)} = 7.011 \times 10^{-10}$.

In Figure 4.5 the optimal solution obtained with $\lambda = 10^{-13}$ is reported. In Figure 4.5a the contours of the optimal temperature field are shown. On Γ_c, the left wall of the domain, the temperature shows a sharp variation. In the lower part of Γ_c we have a maximum for the temperature, while in the higher part of Γ_c there is the minimum value of T. The hot portion of the wall causes the fluid to be accelerated to the desired velocity at the region Ω_d. The resulting velocity field is shown in 4.5b, where contours of the velocity magnitude and streamlines are reported. The contours of the y-component of the velocity are represented in Figure 4.5c, where the region Ω_d is highlighted. At the hot wall, the fluid is accelerated and reaches the desired velocity values in Ω_d.

In Table 4.3 we report the objective functional values $\mathcal{J}^{(n)}$, the number of iterations n of the optimization algorithm and the percentage reduction with respect to the reference $\mathcal{J}^{(0)}$. For the highest values of λ, the control is poor and the functional is quite similar to the reference value. However,

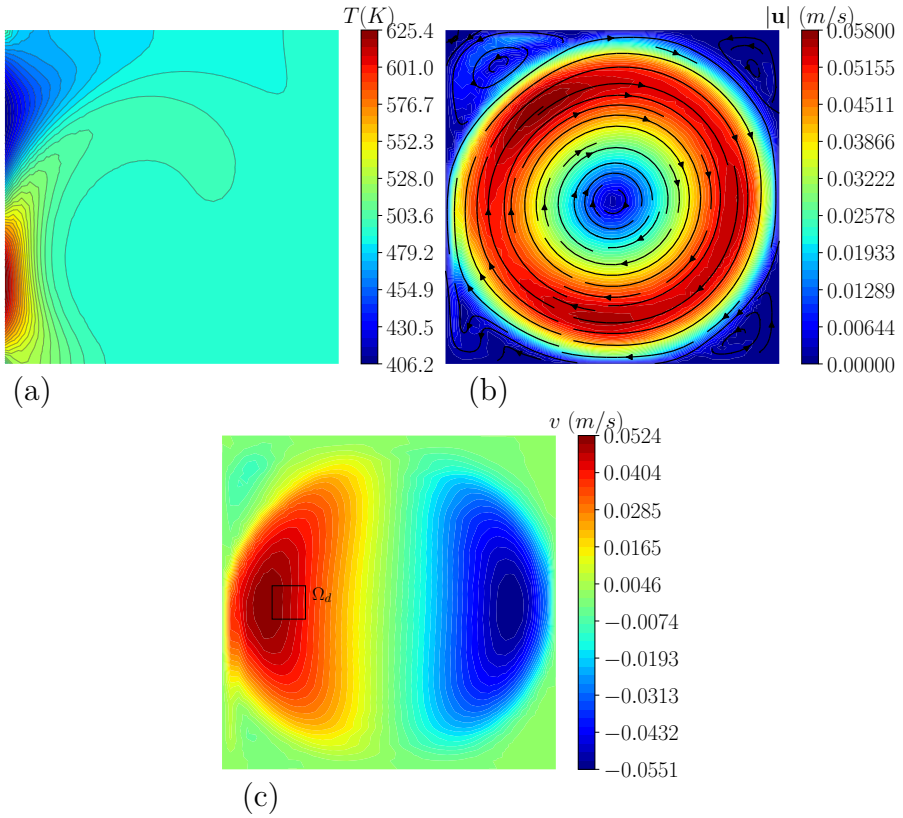

Figure 4.5: Velocity matching case with Dirichlet boundary control: optimal solution for $\lambda = 10^{-13}$. Contours of the temperature field (a), contours and streamlines of the velocity field (b), contours of the y-component of velocity field (c).

Table 4.3: Velocity matching case with Dirichlet boundary control: objective functional, percentage reduction and number of iterations of the optimization algorithm for different λ values.

λ	10^{-10}	10^{-11}	10^{-12}	10^{-13}	10^{-14}	Reference
$\mathcal{J}^{(n)} \times 10^{12}$	586.3	413.6	137.4	9.767	8.796	701.1
% Reduction	−16.4	−41.01	−80.40	−98.61	−98.74	0
Iterations n	5	5	4	6	5	0

we can observe a strong functional reduction for the cases with $\lambda \leq 10^{-13}$. The optimal solution shown in Figure 4.5 corresponds to a case with a strong functional reduction, but it is characterized by strong temperature

variations on Γ_c.

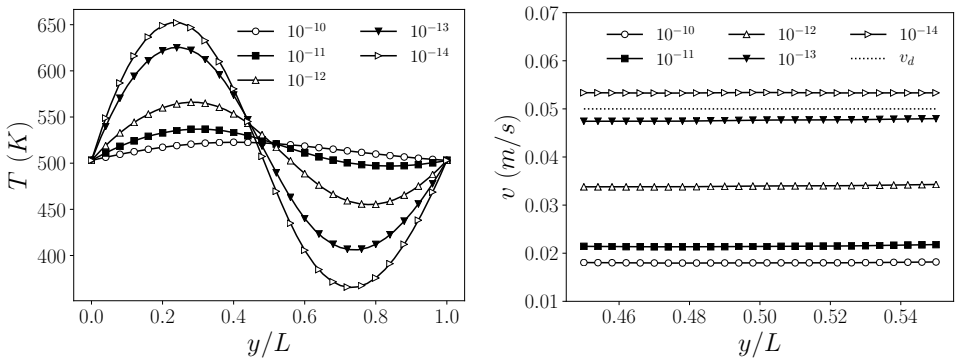

(a) (b)

Figure 4.6: Velocity matching case with Dirichlet boundary control: temperature profiles on the controlled boundary Γ_c (a) and velocity v on the region Ω_d along the line $x/L = 0.2$ (b). Numerical results for $\lambda = 10^{-10}, 10^{-11}, 10^{-12}, 10^{-13}$ and 10^{-14}.

Temperature profiles along the boundary Γ_c are reported in Figure 4.6a for the different values of regularization parameter λ. For $\lambda = 10^{-10}$, the profile has only a stationary point at $y/L \approx 0.5$. For lower values of λ, there is a change of concavity in the temperature profiles and an inflection point at $y/L \approx 0.5$. As λ decreases, the maximum is located at $0.2 < y/L < 0.4$ and its value increases, while the minimum is located at $0.6 < y/L < 0.8$ and its value decreases. As expected, with low values of regularization parameters, the $H^{-1}(\Gamma_c)$-norm of the control weighs less in the objective functional and more irregular functions are accepted as optimal solution. In Figure 4.6b, the y-component of the velocity is plotted along a line at $x/L = 0.2$ for $0.45 < y/L < 0.55$ in the region Ω_d. The profile of velocity is reported for all values of λ and also the target velocity profile v_d is shown. For the lowest values of λ (10^{-13}, 10^{-14}), the optimal solutions tend to the target profile v_d, while the highest values of λ ($10^{-10}, 10^{-11}$, 10^{-12}) brings to the farthest solutions from the objective, as we have deduced from the functional values in Table 4.3. However, when λ is small (10^{-13}, 10^{-14}), the maximum values of temperature increase (from $503K$ up to 650) and the minimum values decrease (from $503K$ down to $400K$). This deep variation is due to the fact that the target v_d is quite far from the reference case and the temperature on Γ_c has to change considerably to reach the objective. However, in the context of nuclear reactor design, the temperature is limited

from below to avoid solidification and from above to avoid material failure. Thus, in order to include these limits, it would be possible to consider as additional constraints the maximum and minimum acceptable temperature values. These kinds of constraints are called inequality constraints. For each additional constraint, we would obtain ad additional adjoint equation. In Chapter 5 the treatment of inequality constraints is described and may be applied to reduce the variation range of temperature.

A second case for the velocity matching test is now considered. The objective is set on the x-component of velocity field and we aim to achieve a counterclockwise flow. Let us consider $\Omega_d = [0.45L; 0.55L] \times [0.75L; 0.85L]$. This region is highlighted in Figure 4.7c. In the reference case, the mean value of u on Ω_d is $0.0129m/s$, then we set as target profile a uniform value $u_d = -0.02m/s$. The simulations have been performed considering different values of λ, namely $10^{-10}, 10^{-11}$ and 10^{-12}. The reference objective functional is $\mathcal{J}^{(0)} = 5.425 \times 10^{-10}$.

In Figure 4.7 the optimal temperature and velocity fields obtained with $\lambda = 10^{-11}$ are reported. In Figure 4.7a the contours of the optimal temperature field are shown. The resulting velocity field is shown in 4.7b, where contours of the velocity magnitude and streamlines are reported. We can easily observe that a counterclockwise flow is driven by the buoyancy forces. The contours of the x-component of the velocity are represented in Figure 4.7c, where the region Ω_d is highlighted. We also report the optimal solution obtained with $\lambda = 10^{-12}$ in Figure 4.8. In this case, the solution is quite unexpected. Figure 4.8a shows contours of the optimal temperature field. At the bottom of the left wall ($\Gamma_c = \Gamma_1$), the temperature is higher than the temperature on the right wall ($\Gamma_i = \Gamma_3$), while at the top of Γ_c the temperature is lower than the temperature on Γ_3. This profile induces buoyancy forces which cause two vortexes, a smaller clockwise vortex behind the bottom-left corner and a bigger counterclockwise vortex in the center of the cavity, as shown in Figure 4.8b. The contours of the x-component of velocity are reported in Figure 4.8c, where the region Ω_d is put in evidence. There, the x-component of velocity is quite uniform and close to the target value u_d.

In Table 4.4 we report the objective functional values $\mathcal{J}^{(n)}$, the percentage reduction and the number of iterations n of the optimization algorithm. For the highest value of λ (10^{-10}), the control is poor and the functional value is quite similar to the reference value. For the other values of λ,

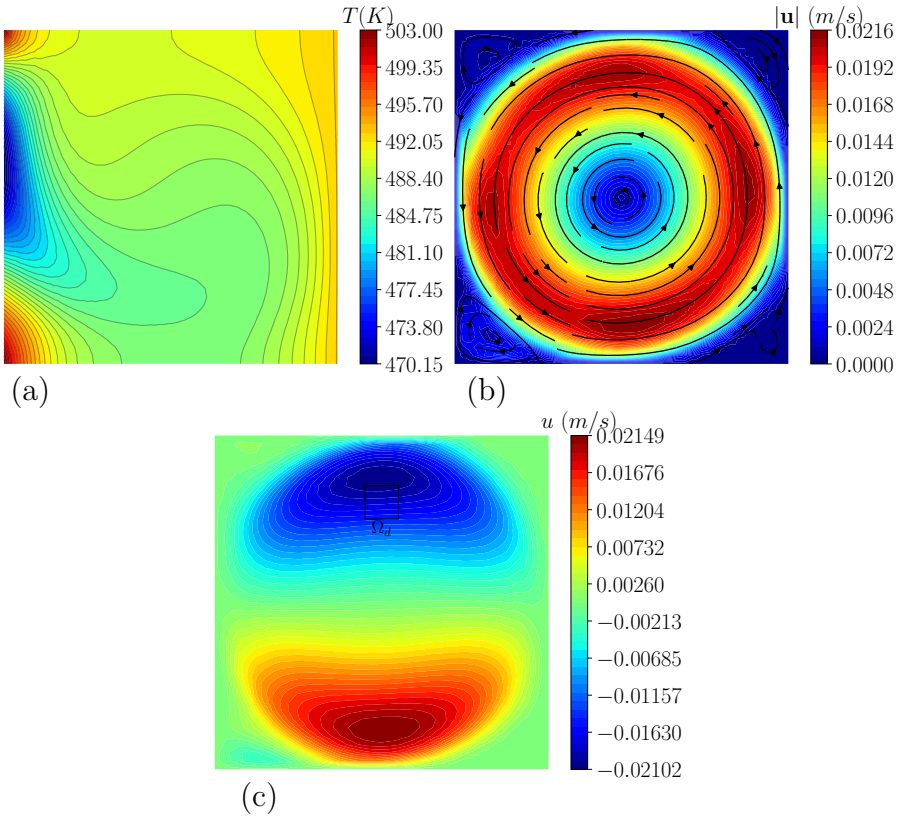

Figure 4.7: Velocity matching case with Dirichlet boundary control: optimal solution for $\lambda = 10^{-11}$. Contours of the temperature field (a), contours and streamlines of the velocity field (b), contours of the x-component of the velocity field.

Table 4.4: Velocity matching case with Dirichlet boundary control: objective functional, percentage reduction and number of iterations of the optimization algorithm for different λ values.

λ	10^{-10}	10^{-11}	10^{-12}	Reference
$\mathcal{J}^{(n)} \times 10^{13}$	246.6	36.04	1.677	5423
% Reduction	−54.53	−93.35	−99.69	0
Iterations n	4	10	9	0

the control is more effective. As observed in the previous test cases, with the lowest value of λ, we have the lowest functional value and the greatest percentage reduction.

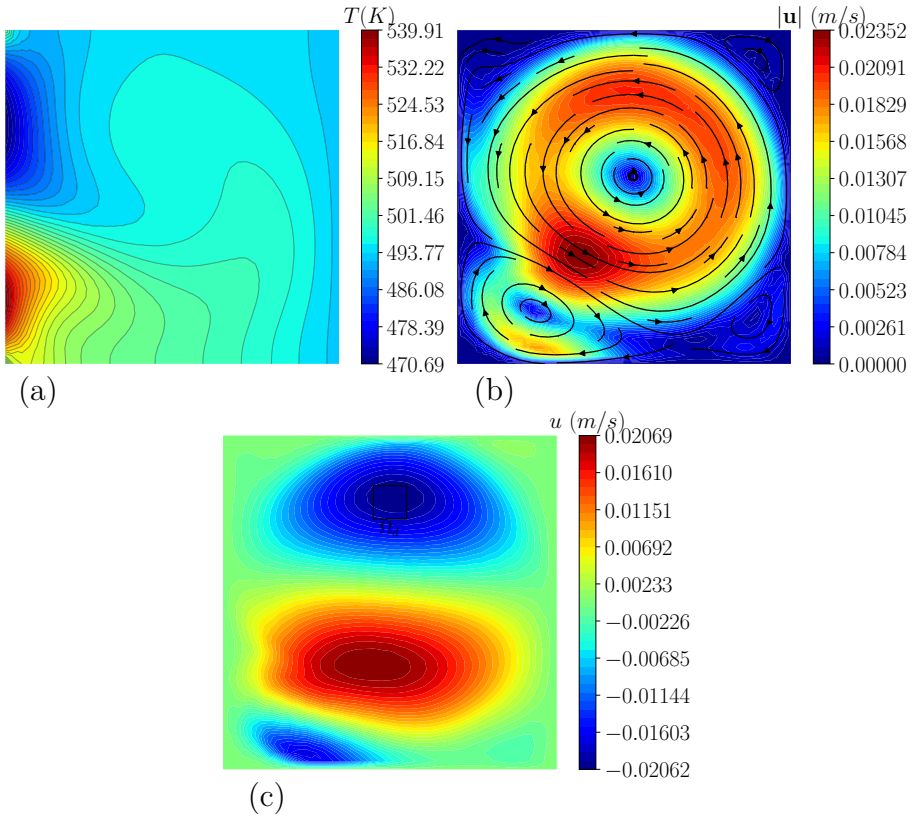

Figure 4.8: Velocity matching case with Dirichlet boundary control: optimal solution for $\lambda = 10^{-12}$. Contours of the temperature field (a), contours and streamlines of the velocity field (b), contours of the x-component of the velocity field.

In Figure 4.9a, the temperature profiles along the boundary Γ_c are shown for the different values of the regularization parameter λ (10^{-10}, 10^{-11}, 10^{-12}). For $\lambda = 10^{-10}$ and $\lambda = 10^{-11}$, the profiles present a minimum point at $0.4 < y/L < 0.7$. The temperature on Γ_c is lower than the temperature on the opposite wall Γ_i, namely $T = 493K$, to get a counterclockwise flow. For $\lambda = 10^{-12}$, the optimal solution is unexpected, as previously noted. There is a variation of concavity in the profile and an inflection point at $y/L \approx 0.5$. For $y/L < 0.5$, the temperature on Γ_c is higher than the temperature on Γ_3, while at the top of the controlled wall, for $y/L > 0.5$, the temperature on Γ_c is lower than the temperature on Γ_3. In Figure 4.9b, the x-component of the velocity is plotted along a line at $y/L = 0.8$ for $0.45 < x/L < 0.55$ in the region Ω_d. The profiles of velocity are reported for all values of λ and also the target velocity profile u_d is shown. We can observe that in all

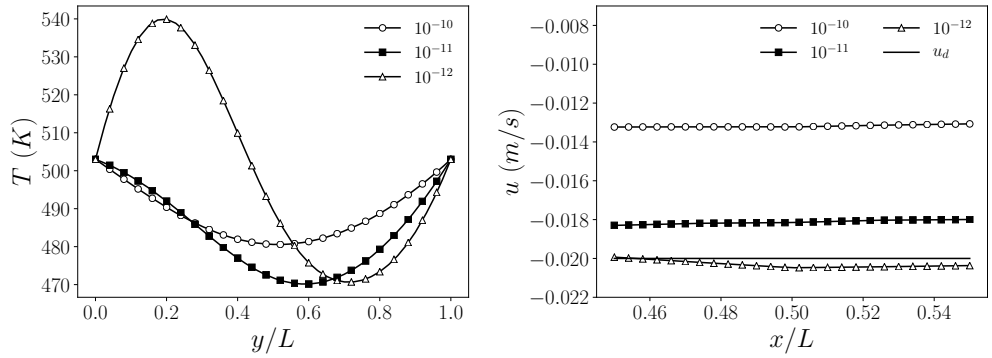

Figure 4.9: Velocity matching case with Dirichlet boundary control: temperature profile on the controlled boundary Γ_c (a) and velocity u on the region Ω_d along the line $y/L = 0.8$ (b). Numerical results for $\lambda = 10^{-10}, 10^{-11}$ and 10^{-12}.

cases the flow changes from clockwise to counterclockwise with a negative x-component of velocity in the top of the cavity. Also in this test, the lowest value of λ brings to the velocity profile nearest to the target profile.

4.3.2. Neumann boundary control

For the Neumann control problem, we consider the geometry reported in Figure 4.1. The boundary conditions are reported in (4.62), where $\Gamma_d = \Gamma_3$, $\Gamma_n = \Gamma_1 \cup \Gamma_2 \cup \Gamma_4$, $\Gamma_i = \Gamma_2 \cup \Gamma_4$, $\Gamma_c = \Gamma_1$. We set $g_{t,n} = 0$, $g_t = 493K$ and $\mathbf{g}_u = \mathbf{0}$ in (4.62) and $\mathbf{f} = \mathbf{0}$, $Q = 0$ in (4.64). The wall-normal heat flux h acting on Γ_c is the control of the problem. To compute the reference case, we set $h^{(0)} = 0$. Thus, the uncontrolled problem consists of three thermally-insulated walls, i.e., the left (Γ_1), bottom (Γ_2), and top (Γ_4) walls, and a wall with a fixed temperature, which is the right wall (Γ_3). The reference case is a trivial problem, characterized by a uniform and constant temperature, no buoyancy forces, and still fluid.

We have performed several tests varying the objective. We report the numerical results obtained considering the same objective on the x-component of velocity studied also with the Dirichlet control. We recall the main simulation parameters. Let $\Omega_d = [0.45L; 0.55L] \times [0.75L; 0.85L]$ be the region where we aim to achieve the objective, and let $u_d = -0.02m/s$ be the target velocity profile. In the reference case, the fluid is still, then $u = 0$ in Ω_d. The simulations have been performed considering different values of λ, namely 10^{-4}, $10^{-5}, 10^{-6}$ and 10^{-7}. The reference objective functional is

$\mathcal{J}^{(0)} = 2.061 \times 10^{-10}$.

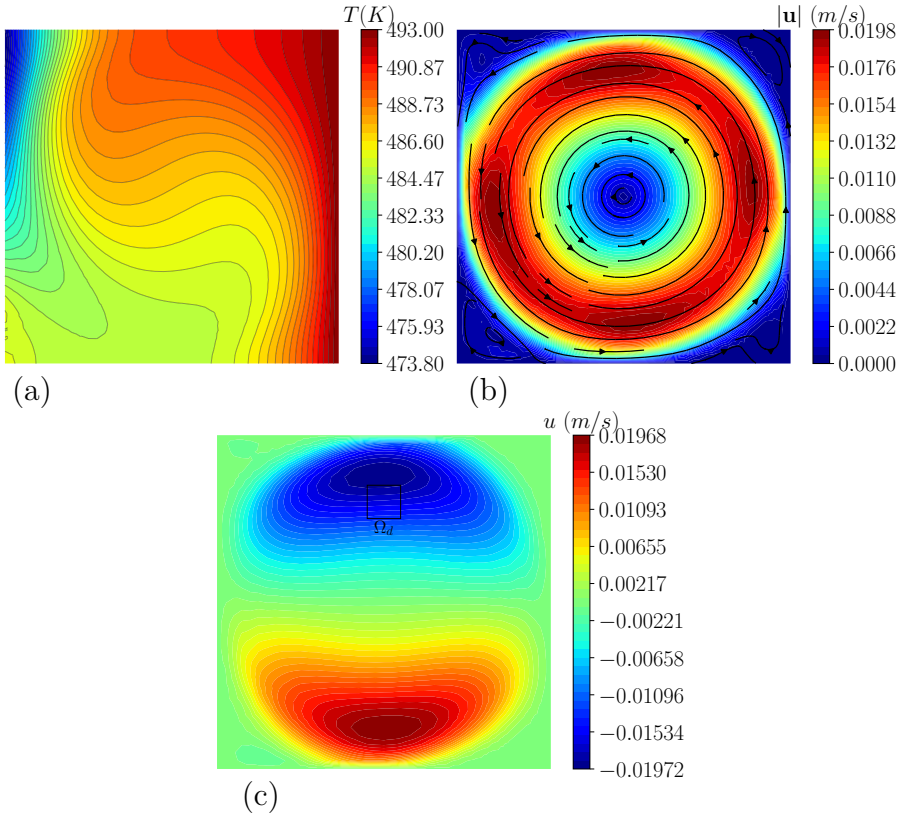

Figure 4.10: Velocity matching case with Neumann boundary control: optimal solution for $\lambda = 10^{-6}$. Contours of the temperature field (a), streamlines and contours of the velocity field (b) and contours of x-component of velocity (c).

λ	10^{-4}	10^{-5}	10^{-6}	10^{-7}	Reference
$\mathcal{J}^{(n)} \times 10^{12}$	30.58	30.14	8.454	1.536	206.1
% Reduction	−85.16	−85.8	−95.90	−99.25	0
Iterations n	4	14	9	7	0

Table 4.5: Velocity matching case with Neumann boundary control: objective functional, percentage of reduction and number of iterations of the optimization algorithm for the reference case and different λ values.

In Table 4.5 the objective functional values $\mathcal{J}^{(n)}$ and the number of iterations n of the optimization algorithm are reported for all the values of

λ. The percentage reductions are also reported. In all tests we have large functional reductions. However, for the lowest values of λ the control is more effective.

The optimal solution obtained with $\lambda = 10^{-6}$ is reported in Figure 4.10. The contours of the temperature field T over the domain can be observed in Figure 4.10a. The heat flux imposed on the left wall is outgoing and the wall is cooler than in the reference case, with a minimum value around 473 K. In Figure 4.10b, the streamlines of the velocity field and the contours of the velocity magnitude are reported. The formation of a counterclockwise vortex is shown in this picture. The contours of the x-component of the velocity field, indicated with u, are reported in Figure 4.10 and the region Ω_d is highlighted.

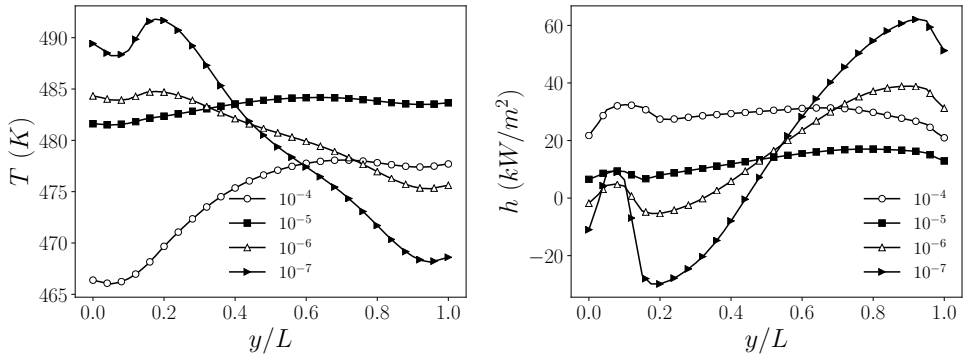

Figure 4.11: Velocity matching case with Neumann boundary control: temperature profile $T^{(n)}$ (a) and wall-normal heat flux $h^{(n)}$ (b) on the controlled boundary Γ_c. Numerical results for $\lambda = 10^{-4}, 10^{-5}, 10^{-6}$ and 10^{-7}.

In Figure 4.11a, the temperature profiles along the boundary Γ_c are shown for the different values of the regularization parameter λ (10^{-4}, 10^{-5}, 10^{-6}, 10^{-7}). Comparing these profiles with the temperature profiles of Figure 4.9a obtained for a Dirichlet control, we observe very different trends. With a Dirichlet control, the temperature on Γ_c belongs to the Hilbert space $H^1(\Gamma_c)$ and the control T_c nullifies at the extremities of the boundary, i.e., $T_c = 0K$ on $\partial\Gamma_c$. For this reason, with a Dirichlet control, $T = g_t = 503K$ at $y/L = 0$ and $y/L = 1$. With Neumann controls, we do not have constraints on the temperature value on $\partial\Gamma_c$ and we obtain different shapes of the profiles. In Figure 4.11b, the control parameter h expressed in kW/m^2 is reported along Γ_c. With the highest values of λ (10^{-4}, 10^{-5}), the control is

quite uniform and regular, but it is less effective on the functional reduction. With the lowest values of λ (10^{-6}, 10^{-7}), the profiles of the control h are sharp and present changes of sign.

4.3.3. Distributed control

For the distributed control problem, we consider the geometry reported in Figure 4.1. The boundary conditions are reported in (4.19), where $\Gamma_d = \Gamma_1 \cup \Gamma_3$, $\Gamma_n = \Gamma_2 \cup \Gamma_4$. We set $\mathbf{f} = \mathbf{0}$, $\mathbf{g}_u = \mathbf{0}$ in (4.91), while in (4.19) we have $g_{t,n} = 0$, $g_t = 493K$ on Γ_3, $g_t = 503K$ on Γ_1. The volumetric heat source Q is the control acting on the domain Ω. For the reference case, we consider $Q^{(0)} = 0$. Thus, the reference case is the one considered for the Dirichlet boundary control. The buoyancy forces put in motion the liquid lead and a clockwise vortex is formed. The contours and streamlines of temperature and velocity are reported in Figure 4.2.

We have performed several tests, varying objectives and values of the regularization parameter λ. We show the results for a velocity matching case. Let us consider $\Omega_d = [0.15L; 0.25L] \times [0.45L; 0.55L]$. We aim to control the y-component of the velocity then we set $v_d = 0.05m/s$, as in the first velocity matching case presented for the Dirichlet boundary control. In the reference case, the mean value of v on Ω_d is equal to $0.0159m/s$ then we aim to accelerate the fluid near the controlled boundary Γ_c. We consider several values of the regularization coefficient, namely 10^{-10}, 10^{-11} and 10^{-12}.

Table 4.6: Velocity matching case with distributed control: objective functional $\mathcal{J}^{(n)}$, percentage reduction and number of iterations n of the optimization algorithm for different values of λ.

λ	10^{-10}	10^{-11}	10^{-12}	Reference
$\mathcal{J}^{(n)} \times 10^{13}$	2.792	2.229	2.159	2061
% Reduction	-99.96	-99.97	-99.97	0
Iterations n	3	13	35	0

In Table 4.6 the objective functional values $\mathcal{J}^{(n)}$, the percentage reductions and the number of iterations n of the optimization algorithm are reported for all values of λ. Thus, in all the tests, the functional is strongly reduced by a factor of 10^3. This is an expected result since the optimal control Q can act on the whole domain and its influence is strong on the

distribution of the temperature field and buoyancy forces. In contrast, with boundary control problems, the control can act only on a portion of the boundary and its impact is less effective on the solution.

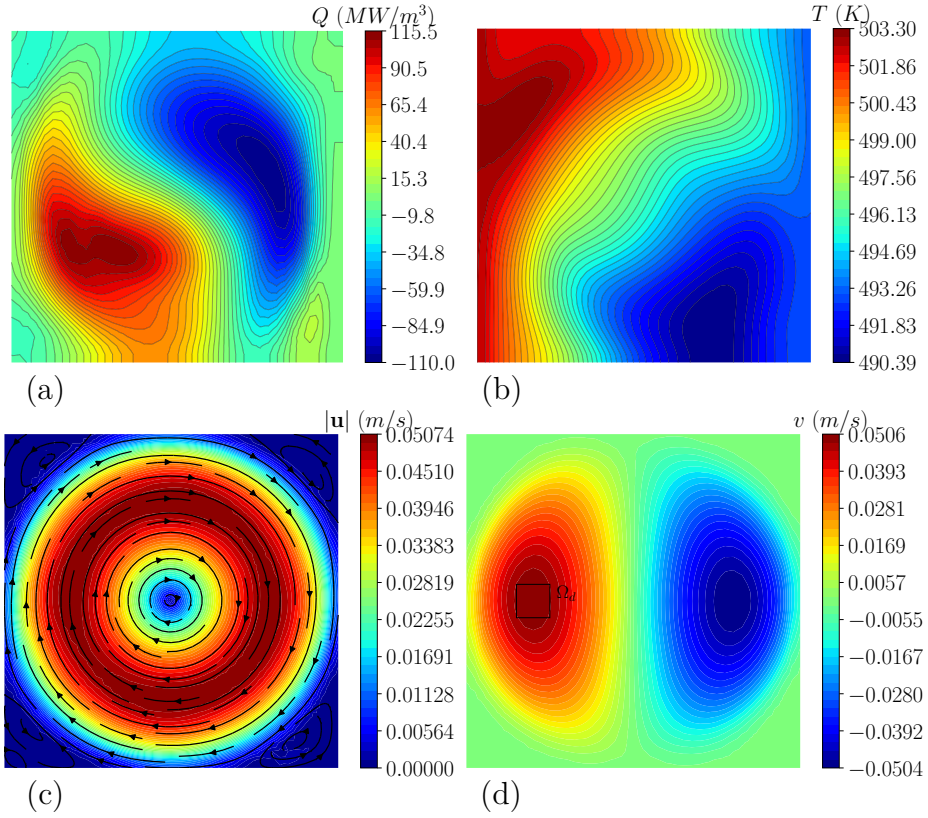

Figure 4.12: Velocity matching case with distributed control: contours of the control $Q^{(n)}$ (a), temperature field $T^{(n)}$ (b), streamlines and contours of velocity field (c), contours of the y-component of velocity (d) for $\lambda = 10^{-11}$.

In Figure 4.12 the contours of the optimal solution for $\lambda = 10^{-11}$ are shown. The optimal control $Q^{(n)}$ expressed in MW/m^3 is reported in Figure 4.12a. The heat source is not uniform over the domain, being positive in the proximity of the hottest wall ($T = 503K$ on Γ_1) and negative near the coolest wall ($T = 493K$ on Γ_3). This heat source distribution influences the temperature solution reported in Figure 4.12b. The isotherms are more stretched than in the reference case, and the fluid is locally hotter than $503K$ and cooler than $493K$ due to the volumetric heat source. The streamlines and contours of the velocity field are reported in Figure 4.12c. Figure 4.12d shows the region Ω_d and the contours of the y-component of velocity. The

solution is almost uniform of Ω_d and close to the target value $v_d = 0.02m/s$. Comparing 4.12d and 4.5c, we can observe that the distributed control is the most effective in achieving the objective. The greater effectiveness of distributed control can be also seen by comparing Table 4.6 and the first three columns of Table 4.3. With the same coefficient λ (10^{-10}, 10^{-11} and 10^{-12}), the distributed control involves much greater reductions in the functional $\mathcal{J}^{(n)}$ than the Dirichlet control. Moreover, by observing Figure 4.12b and Figure 4.5a, with a distributed control the optimal temperature solution is more uniform and regular than with a Dirichlet optimal control, which can lead to temperature variations that may not be acceptable in a practical context, as a nuclear reactor.

CHAPTER 5

Optimal control of turbulent buoyant flows

In Chapter 4 optimal control problems for incompressible Newtonian buoyant flows have been presented and discussed. Dirichlet, Neumann, and distributed optimal control problems have been analyzed, and the optimality system has been derived for each case. However, in most engineering applications flows and heat transfer phenomena are in turbulent conditions, thus we need to include the turbulence in the set of constraint equations. In particular, we consider a RANS approach. For simplicity, we adopt a linear eddy viscosity model for the closure of Reynolds stresses. For the eddy viscosity, we choose the Wilcox k-ω model reported in (2.14) and (2.15). For the closure of the turbulent heat flux, we consider the SGDH model with the Reynolds analogy of (2.33).

Even though the adopted turbulence model presents some deficiencies, see Chapter 2, the aim of formulating and analyzing an optimal control problem for turbulent flows including buoyancy effects in a RANS framework poses significant challenges and, to the best of our knowledge, has not yet been published in the literature. Several works in literature are focused on the optimal control of the heat transfer in forced convection flows, where the coupling between the Navier-Stokes and energy equations is only a one-

way coupling and the turbulence is not considered [86, 88]. In the case of natural or mixed convection flows in laminar conditions, the mathematical analysis of the optimal control for the Oberbeck-Boussinesq system has been considered in several works focusing on stationary distributed and boundary controls [23, 95, 22, 96]. The mathematical analysis and numerical simulations of the optimal control for turbulent flows have been investigated in past works [97, 98, 85], but the temperature dependence has not been included.

Thus, this Ph.D. thesis aims to provide a mathematical analysis of the optimal control for Reynolds-Averaged Navier-Stokes and energy equations closed with the Wilcox k-ω model and the Reynolds analogy. We consider the Dirichlet boundary control problem, but the discussion can be easily extended to Neumann and distributed controls, referring to theorems and results reported in Chapter 4.

We consider the Reynolds-Averaged Navier-Stokes and energy system. The state is defined by the mean velocity $\mathbf{u}$, pressure p and temperature field T, closed with the k-ω turbulence model introduced in Equations (2.14) and (2.15) [99]. The eddy viscosity ν_t is given by k over ω. To close the energy equation, we consider the Reynolds analogy with Pr_t assumed to be constant. We drop the notation $\langle\cdot\rangle$ for mean variables. We consider an open bounded domain Ω with boundary $\Gamma = \partial\Omega$ and the following governing state equations

$$\nabla \cdot \mathbf{u} = 0\,, \tag{5.1}$$

$$(\mathbf{u}\cdot\nabla)\mathbf{u} + \nabla p - \nabla\cdot[(\nu+\nu_t)\mathbf{S}(\mathbf{u})] = \mathbf{f} - b\mathbf{g}(T-T_0)\,, \tag{5.2}$$

$$(\mathbf{u}\cdot\nabla)T = \nabla\cdot\left[\left(\alpha + \frac{\nu_t}{Pr_t}\right)\nabla T\right] + Q\,, \tag{5.3}$$

$$(\mathbf{u}\cdot\nabla)k - \nabla\left[(\nu+\sigma_k\nu_t)\cdot\nabla k\right] = S_k + S_{k,b} - \beta^*\,k\,\omega\,, \tag{5.4}$$

$$(\mathbf{u}\cdot\nabla)\omega - \nabla\left[(\nu+\sigma_\omega\nu_t)\cdot\nabla\omega\right] = S_\omega + S_{k,b} - \beta\omega^2\,. \tag{5.5}$$

In (5.2), we have introduced the symmetric tensor $\mathbf{S}(\mathbf{u}) = \nabla\mathbf{u} + \nabla\mathbf{u}^T$. With b we indicate the coefficient of thermal expansion. The k-ω dynamical production terms S_k and S_ω for turbulence equations are defined by

$$S_k = \nu_t\mathbf{S}(\mathbf{u}) : \nabla\mathbf{u} = \frac{1}{2}\nu_t\mathbf{S}^2(\mathbf{u})\,, \tag{5.6}$$

$$S_\omega = \gamma\frac{\omega}{k}\nu_t\mathbf{S}(\mathbf{u}) : \nabla\mathbf{u} = \frac{1}{2}\gamma\mathbf{S}^2(\mathbf{u})\,, \tag{5.7}$$

where $\mathbf{S}^2(\mathbf{u}) = \mathbf{S}(\mathbf{u}) : \mathbf{S}(\mathbf{u})$ is the squared norm of the strain rate tensor. The production terms due to buoyancy in k-ω equations are modeled according to [100, 101]. The source terms depending on the interaction between gravity and the turbulent heat flux components are modeled as

$$S_{k,b} = b\frac{\nu_t}{Pr_t}\mathbf{g} \cdot \nabla T\,, \tag{5.8}$$

$$S_{\omega,b} = b\frac{\gamma}{Pr_t}\mathbf{g} \cdot \nabla T\,. \tag{5.9}$$

The coefficients σ_k, σ_ω, γ, β and β^* are model constants reported in Equation (2.16) [99].

We use a near wall approach for the solution of the turbulence problem, so the RANS equations are integrated through the viscous layer where near-wall boundary conditions are imposed. By using Taylor expansion of for turbulent variables, with respect to the distance from the wall δ, we obtain

$$u_t = \frac{\tau_w}{\nu}\delta\,, \quad k = a_1\delta^2\,, \quad \omega = \frac{2\nu}{\beta^*\delta^2}\,, \tag{5.10}$$

where with u_t we indicate the tangential component of the velocity, τ_w represents the wall shear stress and a_1 is a constant. The boundary conditions of the problem can be then formulated as

$$\begin{aligned}
&\mathbf{u} = \mathbf{g}_u && \text{on } \Gamma\,,\\
&k = g_k && \text{on } \Gamma\,,\\
&\omega = g_\omega && \text{on } \Gamma\,,\\
&T = g_t && \text{on } \Gamma_i\,,\\
&T = g_t + T_c && \text{on } \Gamma_c\,,\\
&\alpha\nabla T \cdot \mathbf{n} = g_{t,n} && \text{on } \Gamma_n\,,
\end{aligned} \tag{5.11}$$

where $\Gamma \setminus \Gamma_n = \Gamma_d$ and $\Gamma_d \setminus \Gamma_c = \Gamma_i$. In (5.11) we have considered for all dynamic variables Dirichlet boundary conditions, while for the temperature a mixed boundary condition where g_t and $g_{t,n}$ are given functions and T_c is the control. The functions $\mathbf{g}_u$, g_k and g_ω are given. Their expressions for wall boundaries are reported in (5.10).

The system of equations (5.2)-(5.5) defines the state variable ($\mathbf{u}$, p, T, k, ω) when this is completed with suitable boundary conditions (5.11). However, the above system may not have a solution in many physical situations

when k and ω become too large or too small. The k and ω equations have the typical pattern of the diffusion-reaction equations and therefore, introducing some assumptions, their solutions can be constrained inside a precise interval limited by the roots of the equation defined only by the right-hand side nonlinear terms. In an infinite medium or when advection and diffusion terms are negligible the equations (5.4)-(5.5) reduce to the nonlinear right-hand side terms

$$S_k + S_{k,b} - \beta^* k\omega = 0\,, \tag{5.12}$$
$$S_\omega + S_{\omega,b} - \beta\omega^2 = 0\,, \tag{5.13}$$

that imply

$$k = \sqrt{\nu_t \frac{S_k + S_{k,b}}{\beta^*}}\,, \qquad \omega = \sqrt{\frac{S_\omega + S_{\omega,b}}{\beta}}\,. \tag{5.14}$$

While $S_k \geq 0$ and $S_\omega \geq 0$, the sign of $S_{k,b}$ and $S_{\omega,b}$ is not defined *a priori*, so we must impose $S_k + S_{k,b} \geq 0$ and $S_\omega + S_{\omega,b} \geq 0$. To consider these lower bounds, we can define

$$S'_k = \max\left[S_k + S_{k,b}, 0\right]\,, \tag{5.15}$$
$$S'_\omega = \max\left[S_\omega + S_\omega, 0\right]\,. \tag{5.16}$$

Moreover, to keep the Navier-Stokes solutions in standard functional classes and have turbulent fields bounded in well-defined intervals, we must regularize the modeling of the turbulence sources. This is achieved by limiting the total turbulence production terms $P_k = S'_k$ and $P_\omega = S'_\omega$ under the maximum value of the respective dissipation terms. Therefore, given arbitrary limiting values k_1 and ω_1 we define

$$P_k = \min\left[S'_k,\, \beta^* k_1 \omega\right]\,, \tag{5.17}$$
$$P_\omega = \min\left[S'_\omega, \beta\omega_1^2\right]\,. \tag{5.18}$$

In the rest of the chapter, we label k_1 and ω_1 with k_{max} and ω_{max} since they will be proved to be the limits for k and ω fields. The two relations (5.17) and (5.18) assure that, in the case of unbounded gradient velocity, the dissipation term can cope with the turbulence sources and keep k and ω limited. Thus, the state equations for k and ω that we will consider in the next sections are the following

$$(\mathbf{u}\cdot\nabla)k - \nabla\left[(\nu + \sigma_k\nu_t)\cdot\nabla k\right] = P_k - \beta^*\, k\,\omega\,, \tag{5.19}$$

$$(\mathbf{u}\cdot\nabla)\omega - \nabla\left[(\nu+\sigma_\omega\nu_t)\cdot\nabla\omega\right] = P_\omega - \beta\omega^2\,. \tag{5.20}$$

The definition of ν_t can lead to singularities when $\omega \approx 0$. For this reason we bound the value of ν_t as

$$\nu_t = \min\left[\frac{k}{\omega}, \nu_{max}\right]. \tag{5.21}$$

Note that the introduced constants k_{max}, ω_{max} and ν_{max} can be chosen as large as needed in order to assure the regularity of the problem together with the accuracy of the physical solution. By doing so, the solution of Navier-Stokes equations remains unchanged while only the turbulence source terms are modeled to avoid singularities.

We aim to minimize the cost functional

$$\begin{aligned}\mathcal{J}(\mathbf{u},k,T_c) = \frac{\alpha_u}{2}\int_{\Omega_d}|\mathbf{u}-\mathbf{u}_d|^2 d\mathbf{x} + \frac{\alpha_k}{2}\int_{\Omega_d}|k-k_d|^2 d\mathbf{x} + \\ + \frac{\lambda_1}{2}\int_{\Gamma_c}|T_c|^2 d\mathbf{x} + \frac{\lambda_2}{2}\int_{\Gamma_c}|\nabla_s T_c|^2 d\mathbf{x}\,,\end{aligned} \tag{5.22}$$

under the constraints (5.2)-(5.3), (5.11) and (5.19)-(5.20) in order to have a desired velocity $\mathbf{u}_d$ or a desired turbulent kinetic energy k_d located over a certain domain $\Omega_d \subseteq \Omega$. A more general expression for the cost contribution has been considered in (5.22) where two regularization parameters λ_1 and λ_2 have been introduced. The parameter λ_2 is non-negative while λ_1 is positive. The cost contribution measures the $H^1(\Gamma_c)$-norm of the control T_c. When $\lambda_2 = 0$, the cost contribution reduces to the measure of $L^2(\Gamma_c)$-norm, while if $\lambda_1 = \lambda_2$ we obtain the same cost term considered in functional (4.23). The choice of them is a key point for the numerical solution of the problem because high values of λ_1 and λ_2 can result in a poor control, while low values can lead to convergence issues due to the enlargement of the functional space of the control variable T_c. The constants α_u, α_k are non-negative. In particular, when $\alpha_u = 0$ or $\alpha_k = 0$ the objective functional can be used to control only the turbulent kinetic energy or the velocity field, respectively.

5.1. Variational formulation of the state problem

For spaces, norms and scalar products we use the same notations introduced in Chapter 4. We introduce the following continuous bilinear and trilinear forms useful to derive the weak form of the introduced system

$$a(\nu;\mathbf{u},\mathbf{v}) = \frac{1}{2}\int_\Omega \nu\mathbf{S}(\mathbf{u}):\mathbf{S}(\mathbf{v})d\mathbf{x}\,, \tag{5.23}$$

$$b(\mathbf{u},\psi) = -\int_\Omega \psi \nabla\cdot\mathbf{u}\, d\mathbf{x}\,, \tag{5.24}$$

$$a(k;T,\varphi) = k\int_\Omega \nabla T\cdot\nabla\varphi\, d\mathbf{x}\,. \tag{5.25}$$

for all $\mathbf{u}\in\mathbf{H}^1(\Omega)\,,\mathbf{v}\in\mathbf{H}^1(\Omega)\,,\psi\in L^2_0(\Omega)\,,T\in H^1(\Omega)$ and $\varphi\in H^1(\Omega)$. Also we introduce the following continuous trilinear forms

$$c(\mathbf{w};\mathbf{u},\mathbf{v}) = \frac{1}{2}\left[\int_\Omega(\mathbf{w}\cdot\nabla)\mathbf{u}\cdot\mathbf{v}\, d\mathbf{x} - \int_\Omega(\mathbf{w}\cdot\nabla)\mathbf{v}\cdot\mathbf{u}\, d\mathbf{x}\right], \tag{5.26}$$

$$c(\mathbf{u},T,\varphi) = \int_\Omega(\mathbf{u}\cdot\nabla T)\varphi\, d\mathbf{x}\,, \tag{5.27}$$

for all $\mathbf{w}\in\mathbf{V}(\Omega)$, $\mathbf{u}\in\mathbf{H}^1(\Omega)\,,\mathbf{v}\in\mathbf{H}^1(\Omega)\,,T\in H^1(\Omega)$ and $\varphi\in H^1(\Omega)$. It is clear that $c(\mathbf{w};\mathbf{v},\mathbf{v})=0$ for all $\mathbf{w}\in\mathbf{V}(\Omega)$ and $c(\mathbf{u},\phi,\phi)=0$ for all $\varphi\in H^1(\Omega)$. A detailed discussion on these trilinear forms can be found in [102].

We consider the following formulation of the direct problem for the Navier Stokes and energy system (5.2)-(5.3).

$$\begin{aligned}
&a(\nu+\nu_t;\mathbf{u},\mathbf{v}) + c(\mathbf{u};\mathbf{u},\mathbf{v}) + b(\mathbf{v},p) = \\
&\qquad = (\mathbf{f},\mathbf{v}) - (b(T-T_0)\mathbf{g},\mathbf{v}) \qquad \forall\mathbf{v}\in\mathbf{H}^1_0(\Omega)\\
&b(\mathbf{u},q) = 0 \qquad \forall q\in L^2_0(\Omega)\\
&a\Big(\alpha+\frac{\nu_t}{Pr_t};T,\varphi\Big) + c(\mathbf{u};T,\varphi) = \\
&\qquad = (Q,\varphi) + (\varphi,g_{t,n})_{\Gamma_n} \qquad \forall\varphi\in H^1_{\Gamma_d}(\Omega)\\
&(T,s_T)_{\Gamma_d} = (g_t,s_T)_{\Gamma_d} + (T_c,s_T)_{\Gamma_c} \qquad \forall s_T\in H^{-1/2}(\Gamma_d)\,.
\end{aligned} \tag{5.28}$$

We also consider the following formulation of the direct problem for turbulence equations (5.19)-(5.20).

$$\begin{aligned}
&c(\mathbf{u};k,\psi) + a(\nu+\nu_t\sigma_k;k,\psi) = (P_k,\psi) + \\
&\qquad - (\beta^*\, k\omega,\psi) \qquad \forall\psi\in H^1_0(\Omega)\\
&c(\mathbf{u};\omega,\phi) + a(\nu+\nu_t\sigma_\omega;\omega,\phi) = (P_\omega,\phi) + \\
&\qquad - (\beta\,\omega^2,\phi) \qquad \forall\phi\in H^1_0(\Omega)
\end{aligned} \tag{5.29}$$

Note that Γ_d and Γ_n are the portion of the boundary where Dirichlet and Neumann boundary conditions on the temperature field are imposed, respectively. Moreover, one may compute the normal heat flux on Γ_d as

$$q_n = -\Big(\alpha+\frac{\nu_t}{Pr_t}\Big)\nabla T\cdot\mathbf{n}|_{\Gamma_d}\in H^{-1/2}(\Gamma_d)\,.$$

The existence of the solution of system (5.28) can be reduced to Theorem 4.1 since system (5.28) and (4.24) are the same except for the diffusion coefficients. Thus, it is sufficient to add as hypothesis the non-negativity of the eddy viscosity ν_t. Here we report the theorem.

Theorem 5.1. *For every $\nu_t \geq 0 \in L^\infty(\Omega)$, $g_t \in H^1(\Gamma_d)$, $T_c \in H^1(\Gamma_c)$, $g_{t,n} \in L^2(\Gamma_n)$, $Q \in L^2(\Omega)$, $\mathbf{f} \in \mathbf{L}^2(\Omega)$, $\mathbf{g}_u \in \mathbf{H}^1(\Gamma)$, the Boussinesq equations (4.24) have a solution $(\mathbf{u}, p, T) \in \mathbf{H}^1(\Omega) \times H^1(\Omega) \times L^2_0(\Omega)$. Moreover if $(\mathbf{u}, p, T)$ is a solution of (4.24), then $(\mathbf{u}, p, T) \in \mathbf{V} \cap \mathbf{H}^2(\Omega) \times L^2_0(\Omega) \cap H^1(\Omega) \times H^s(\Omega) (1 \leq s \leq \frac{3}{2})$ and there is a continuos function P_s for each s such that*

$$\begin{aligned} \|\mathbf{u}\|_2 + \|p\|_1 + \|T\|_s \leq P_s(\|\mathbf{f}\|_0 + \|Q\|_0 + \|g_{t,n}\|_{0,\Gamma_n} + \|g_t\|_{1,\Gamma_d} + \\ + \|T_c\|_{1,\Gamma_c} + \|\mathbf{g}_u\|_{1,\Gamma}) \,. \end{aligned} \tag{5.30}$$

Proof. The proof of this result can be found in [87]. □

We now introduce the existence of the solution for the k-ω turbulence system.

Theorem 5.2. *Let Ω be an open, bounded set with Lipschitz-continuous boundary Γ. Let $\mathbf{u} \in \mathbf{V}(\Omega)$, g_k and g_ω in $H^1(\Omega) \cup L^\infty(\Omega)$ and ν_t, P_k, P_ω as defined in (5.21), (5.17) and (5.18), respectively. Then*

1. *there exists at least one solution $(k, \omega) \in H^1(\Omega) \times H^1(\Omega)$ of (5.29);*
2. *let ω_{max} and k_{max} be positive real constants and*

$$k_{sup} = \sup\{\sup_\Gamma\{g_k\}, k_{max}\} \,, \tag{5.31}$$

$$\omega_{inf} = \inf\{\inf_\Gamma\{g_\omega\}, \inf_\Omega\{\sqrt{P_\omega/\beta}\}\} \,, \tag{5.32}$$

$$\omega_{sup} = \sup\{\sup_\Gamma\{g_\omega\}, \omega_{max}\} \,, \tag{5.33}$$

then

$$0 \leq k \leq k_{sup} \,, \tag{5.34}$$

$$0 \leq \omega_{inf} \leq \omega \leq \omega_{sup} \,. \tag{5.35}$$

Proof. The proof of this Theorem can be found in [97, 103]. □

By using previous theorems we can prove the existence of the solution of the associated boundary value problem.

Theorem 5.3. *There exists a solution* $(\mathbf{u}, p, T, k, \omega)$ *of the associated boundary value problem in* (5.28)-(5.29).

Proof. To prove the existence of the solution, we rely on the Schauder's fixed point theorem and we follow standard techniques (e.g. see [104]). To simplify the notation, we consider now the presented physical system with $\mathbf{g}_u = \mathbf{0}$ and $g_t = g_{t,n} = g_k = g_\omega = T_c = 0$. For a given set $(\mathbf{u}_1,\ p_1,\ T_1,\ k_1,\ \omega_1) \in \mathbf{H}^1_0(\Omega) \times H^1_{\Gamma_d}(\Omega) \times L^2_0(\Omega) \times H^1_0(\Omega) \times H^1_0(\Omega)$, $(\mathbf{u}, p, T)$ and (k, ω) are the state of the following system

$$
\begin{aligned}
& b(\mathbf{u}, q) = 0 && \forall\, q \in L^2_0(\Omega) \\
& a(\nu + \nu_{t1}; \mathbf{u}, \mathbf{v}) + c(\mathbf{u}_1; \mathbf{u}, \mathbf{v}) + b(\mathbf{v}, p_1) = (\mathbf{f}, \mathbf{v}) + \\
& \qquad - (b(T_1 - T_0)\mathbf{g}, \mathbf{v}) && \forall \mathbf{v} \in \mathbf{H}^1_0(\Omega) \\
& a\Big(\alpha + \frac{\nu_{t1}}{Pr_t}; T, \varphi\Big) + c(\mathbf{u}_1; T, \varphi) = (Q, \varphi) && \forall \varphi \in H^1_{\Gamma_d}(\Omega) \\
& c(\mathbf{u}_1; k, \psi) + a(\nu + \nu_{t1}\sigma_k; k, \psi) = (P_{k1}, \psi) + \\
& \qquad - (\beta^*\, k\omega_1, \psi) && \forall \psi \in H^1_0(\Omega) \\
& c(\mathbf{u}_1; \omega, \phi) + a(\nu + \nu_{t1}\sigma_\omega; \omega, \phi) = (P_{\omega 1}, \phi) + \\
& \qquad - (\beta\, \omega\omega_1, \phi) && \forall \phi \in H^1_0(\Omega)
\end{aligned}
\tag{5.36}
$$

where $\nu_{t1} = \nu_t(k_1, \omega_1)$, $P_{k1} = P_k(\mathbf{u}_1, T_1, k_1, \omega_1)$, $P_{\omega 1} = P_\omega(\mathbf{u}_1, T_1)$. Under the imposed hypotheses, we can now prove the existence of the solution of the split system (5.36). In fact, from Theorem 5.1 we have that $\|\mathbf{u}\|_2 + \|p\|_1 + \|T\|_s$ is uniformly bounded, with $1 \le s \le 3/2$. Moreover, from Theorem 5.2 we have that $\|k\|_1$ and $\|\omega\|_1$ are uniformly bounded by the constants C_k and C_ω as a function of the given values k_{max} and ω_{max}.

Let $D = \mathbf{H}^1_0(\Omega) \times L^2_0(\Omega) \times H^1_{\Gamma_d}(\Omega) \times H^1_0(\Omega) \times H^1_0(\Omega)$ and $A = \mathbf{H}^1_0(\Omega)$ $\times L^2_0(\Omega)\ \times H^1_{\Gamma_d}(\Omega)\ \times H^1_0(\Omega)\ \times H^1_0(\Omega)$. We consider now the mapping $\mathcal{T}$: $D \to A$ such that

$$
\begin{aligned}
& \mathbf{u} = \mathbf{u}(\mathbf{u}_1, p_1, T_1, k_1, \omega_1)\,, \\
& p = p((\mathbf{u}_1, p_1, T_1, k_1, \omega_1)\,, \\
& T = T(\mathbf{u}_1, p_1, T_1, k_1, \omega_1)\,, \\
& k = k(\mathbf{u}_1, p_1, T_1, k_1, \omega_1)\,, \\
& \omega = \omega(\mathbf{u}_1, p_1, T_1, k_1, \omega_1)\,.
\end{aligned}
\tag{5.37}
$$

We endow the product space $\mathbf{H}^1_0(\Omega) \times L^2_0(\Omega) \times H^1_{\Gamma_d}(\Omega) \times H^1_0(\Omega) \times H^1_0(\Omega)$ with the norm $\|(\mathbf{u}_1, p_1, T_1, k_1, \omega_1)\| = \|\mathbf{u}_1\|_2 + \|p_1\|_1 + \|T_1\|_s + \|k_1\|_1 + \|\omega_1\|_1$. It can

be proved that $\mathcal{T}$ is a continuous mapping with respect to the introduced norm. Let R denote the constant $R = C_{u,p,T} + C_k + C_\omega$, where $C_{u,T} = P_s(\|\mathbf{f}\|_0 + \|Q\|_0 + \|g_{t,n}\|_{0,\Gamma_n} + \|g_t\|_{1,\Gamma_d} + \|T_c\|_{1,\Gamma_c} + \|\mathbf{g}_u\|_{1,\Gamma})$ for each s. For all $(\mathbf{u}_1, p_1, T_1, k_1, \omega_1) \in D$ we have $\|(\mathbf{u}, p, T, k, \omega)\| = \|\mathbf{u}\|_2 + \|p\|_1 + \|T\|_s + \|k\|_1 + \|\omega\|_1 < C_{u,T} + C_k + C_\omega = R$. Therefore

$$\mathcal{T}(B_R) \subset B_R\,, \tag{5.38}$$

where B_R is the ball of radius R. The condition (5.38) derives from Theorem 5.1 and 5.2, and represents a mandatory hypothesis for the Schauder's fixed point theorem. In fact, the theorem states that for a separated topological vector space D, a convex subset $B_R \subset D$, a continuous mapping of B_R into itself $\mathcal{T}$, such that $\mathcal{T}(B_R)$ is contained in a compact subset of B_R, equipped with the topology inherited from D, then $\mathcal{T}$ has a fixed point, namely, there exists $x \in B_R$ such that $\mathcal{T}(x) = x$. In conclusion, we can now apply the fixed point theorem to the system (5.36), and therefore there exists a solution of the system. □

5.2. The optimal control problem

In this section, we present the model for the optimal control of the presented state system, and prove the existence of an optimal solution. We first recall that, according to the Theorem 5.2, the set of all admissible functions k and ω is determined by

$$\begin{aligned}\mathcal{T}_{ad} = \Big\{ &(k,\omega) \in H^1(\Omega) \times H^1(\Omega) \,|\, 0 \le \omega_{inf} \le \omega \le \omega_{sup} \\ &\text{and } 0 \le k \le k_{sup} \Big\}\,,\end{aligned} \tag{5.39}$$

where ω_{inf}, ω_{sup} and k_{sup} have been introduced above.

In this work, we aim to control the temperature $T = g_t + T_c$ on a portion of the boundary $\Gamma_c \subseteq \Gamma_d \subset \Gamma$ to have a desired velocity $\mathbf{u}_d$ or a desired turbulence kinetic energy k_d on a certain domain $\Omega_d \subseteq \Omega$. The optimal control problem can be summarized as follows

> Given g_k, $g_\omega \in H^{\frac{1}{2}}(\Gamma)$, $g_t \in H^{\frac{1}{2}}(\Gamma_d)$ and $\mathbf{g}_u \in \mathbf{H}^{\frac{1}{2}}(\Gamma)$, find a state-control set $(\mathbf{u}, p, T, T_c, k, \omega, P_k, P_\omega, \nu_t) \in \mathbf{H}^1(\Omega) \times L^2_0(\Omega) \times H^1(\Omega) \times H^1_0(\Gamma_c) \times \mathcal{T}_{ad} \times L^2(\Omega) \times L^2(\Omega) \times L^2(\Omega)$ which minimizes the cost functional (5.22) under the constraints (5.28)-(5.29).

We also recall that P_k, P_ω and ν_t are defined in (5.17), (5.18) and (5.21), respectively. We can now define the admissible set of states and controls as

$$\begin{aligned}\mathcal{S}_{ad} = \Big\{ & (\mathbf{u}, p, T, T_c, k, \omega, P_k, P_\omega, \nu_t) \in \mathbf{H}^1(\Omega) \times L^2_0(\Omega) \times H^1(\Omega) \times \\ & \times H^1_0(\Gamma_c) \times \mathcal{T}_{ad} \times L^2(\Omega) \times L^2(\Omega) \times L^2(\Omega) \\ & \text{such that } \mathcal{J}(\mathbf{u}, T, T_c, k) < \infty \Big\}.\end{aligned} \tag{5.40}$$

Since the main statement of the optimal control problem is the minimization of the functional (5.22), the problem can be reformulated as follows. We say that $(\widehat{\mathbf{u}}, \widehat{p}, \widehat{T}, \widehat{T_c}, \widehat{k}, \widehat{\omega}, \widehat{P}_k, \widehat{P}_\omega, \widehat{\nu_t}) \in \mathcal{S}_{ad}$ is an *optimal solution* if there exists $M > 0$ such that

$$\begin{aligned}&\mathcal{J}(\widehat{\mathbf{u}}, \widehat{T}, \widehat{T_c}, \widehat{k}) < \mathcal{J}(\mathbf{u}, T, T_c, k),\ \forall\, (\mathbf{u}, p, T, T_c, k, \omega, P_k, P_\omega, \nu_t) \in \mathcal{S}_{ad} \\ &\text{satisfying} \quad \|\mathbf{u} - \widehat{\mathbf{u}}\|_1 + \|p - \widehat{p}\|_0 + \|T - \widehat{T}\|_1 + \|k - \widehat{k}\|_1 + \\ &\qquad + \|\omega - \widehat{\omega}\|_1 + \|P_k - \widehat{P}_k\|_0 + \|P_\omega - \widehat{P}_\omega\|_0 + \\ &\qquad + \|T_c - \widehat{T}_c\|_{1,\Gamma_c} < M\,.\end{aligned} \tag{5.41}$$

We now turn to the question of the existence of optimal solutions for the problem (5.41).

Theorem 5.4. *Let $\mathcal{S}_{ad}$ be not empty. There exists at least one optimal solution $(\widehat{\mathbf{u}}, \widehat{p}, \widehat{T}, \widehat{T}_c, \widehat{k}, \widehat{\omega}, \widehat{P}_k, \widehat{P}_\omega, \widehat{\nu}_t) \in \mathcal{S}_{ad}$.*

Proof. The proof of the existence of an optimal solution is obtained with standard techniques, and the interested reader can consult [93, 105]. Since the set of the values of $\mathcal{J}$ is bounded from below, there exists a minimizing sequence $(\mathbf{u}_m,\ p_m,\ T_m,\ T_{cm},\ k_m,\ \omega_m,\ P_{km},\ P_{\omega m},\ \nu_{tm}) \in \mathbf{H}^1(\Omega) \times L^2_0(\Omega) \times H^1(\Omega) \times H^1_0(\Gamma_c) \times \mathcal{T}_{ad} \times L^2(\Omega) \times L^2(\Omega) \times L^2(\Omega)$. As defined in (5.17), (5.18) and (5.21), the sequences P_{km}, $P_{\omega m}$ and ν_{tm} are uniformly bounded. Since P_{km} and $P_{\omega m}$ are bounded, then also k_m and ω_m are uniformly bounded in $\mathcal{T}_{ad}$. From Theorem 5.1, we can also state that $\mathbf{u}_m$ and T_m are uniformly bounded in $\mathbf{H}^1(\Omega)$ and $H^1(\Omega)$, respectively. Following standard techniques, we can now extract subsequences $(\mathbf{u}_n,\ p_n,\ T_n,\ T_{cn},\ k_n,\ \omega_n,\ P_{kn},\ P_{\omega n},\ \nu_{tn})$ converging to $(\widehat{\mathbf{u}},\ \widehat{p},\ \widehat{T},\ \widehat{T}_c,\ \widehat{k},\ \widehat{\omega},\ \widehat{P}_k,\ \widehat{P}_\omega,\ \widehat{\nu}_t)$. To prove that the limit of the sub-sequence satisfies the problem we pass to the limit the equation problem. Following [104, 93], we can state that the solution of all the linear and the nonlinear operators converges to the solution of the equation problem. □

5.3. The Lagrange multiplier method

5.3.1. Preliminaries

In this section, we show that the Lagrange multiplier technique is well-posed and can be used to obtain the first-order necessary condition. In particular, we introduce the Lagrangian map and we show that it is strictly differentiable.

We recall the inequality constraints introduced in (5.15)-(5.21) and define auxiliary variables which allows us to transform them into equality constraints [106]. Let us consider the source $S'_k = \max[S_k + S_{k,b}, 0]$ defined by (5.15). It is easy to show that finding S'_k from (5.15) is equivalent to solve the following system of equation

$$S'_k(S'_k - (S_k + S_{k,b})) = 0\,, \tag{5.42}$$
$$r_{k1}^2 - S'_k - (S'_k - (S_k + S_{k,b})) = 0\,. \tag{5.43}$$

From (5.15) we have $S'_k = S_k + S_{kb}$ or $S'_k = 0$ that satisfies (5.42). When $S_k + S_{kb} \geq 0$ we have $S'_k = S_k + S_{kb} = r_{k1}^2 \geq 0$ for some real number r_{k1}^2. Otherwise, when $S_k + S_{kb} \leq 0$ we have $S'_k = 0$ and $(S_k + S_{kb}) = -r_{k1}^2 \leq 0$ for some real number r_{k1}^2 that satisfies (5.43). The value $r_{k1}^2 = 0$ is attained when $S'_k = (S_k + S_{k,b}) = 0$. Vice-versa from (5.42) we have $S'_k = 0$ and/or $S'_k = S_k + S_{k,b}$. From (5.43), S'_k is zero when $S_k + S_{k,b} \leq 0$ and $S'_k = S_k + S_{k,b}$ when $S'_k \geq 0$. With the same arguments the source P_k, defined in (5.17), satisfies

$$(S'_k - P_k)(\beta^* k_{max}\omega - P_k) = 0\,, \tag{5.44}$$
$$r_{k2}^2 - (S'_k - P_k) - (\beta^* k_{max}\omega - P_k) = 0\,, \tag{5.45}$$

for some $r_{k2} \in L^2(\Omega)$. By using similar arguments, finding P_k in (5.17) it is equivalent to solve (5.44) and find a real r_{k2}^2 in (5.45).

Similarly, let us consider the definition of $S'_\omega = \max[S_\omega + S_{\omega,b}, 0]$ in (5.18). When $S_\omega + S_{\omega b} \geq 0$ we have $S'_\omega = S_\omega + S_{\omega b}$ and $S'_\omega - (S_\omega + S_{\omega b}) = r_{\omega 1}^2 \geq 0$ for some real number $r_{\omega 1}^2$. Otherwise, when $S_\omega + S_{\omega b} \leq 0$ we have $S'_\omega = 0$ and $-(S_\omega + S_{\omega b}) = r_{\omega 1}^2 \geq 0$ for some real number $r_{\omega 1}^2$. In this case, we have that S'_ω satisfies

$$S'_\omega(S'_\omega - (S_\omega + S_{\omega,b})) = 0\,, \tag{5.46}$$
$$r_{\omega 1}^2 - S'_\omega - (S'_\omega - (S_\omega + S_{\omega,b})) = 0\,, \tag{5.47}$$

for some $r_{\omega 1} \in L^2(\Omega)$. Vice-versa, when (5.46) is satisfied and there exists a $r^2_{\omega 1}$ we have $S'_\omega = S_\omega + S_{\omega b}$ with $S'_\omega \geq 0$ or $S'_\omega = 0$ with $S_\omega + S_{\omega,b} \leq 0$ which implies (5.18). With the same arguments the source P_ω, defined in (5.18), satisfies

$$(S'_\omega - P_\omega)(\beta\omega^2_{max} - P_\omega) = 0\,, \tag{5.48}$$
$$r^2_{\omega 2} - (S'_\omega - P_\omega) - (\beta\omega^2_{max} - P_\omega) = 0\,, \tag{5.49}$$

for some $r_{\omega 2} \in L^2(\Omega)$. Finding P_ω from (5.15) is equivalent to solve (5.48)-(5.49).

Finally, the inequality (5.21) can be replaced by

$$(k - \nu_t\omega)(\nu_{max} - \nu_t) = 0\,, \tag{5.50}$$
$$r^2_\nu - (k - \nu_t\omega) - \omega(\nu_{max} - \nu_t) = 0\,, \tag{5.51}$$

for some $r_\nu \in L^2(\Omega)$.

Now we consider all the constraint equations and the functional in two mappings in order to study their differential properties. It is convenient to define the functional spaces $\mathbf{B_1}$, $\mathbf{B_2}$ and $\mathbf{B_3}$. Let Γ_i be the portion of boundary Γ_d where there is no control, $\Gamma_i = \Gamma_d \setminus \Gamma_c$, then we introduce the following functional spaces

$$\mathbf{B_1} = \mathbf{B_{1e}} \times \mathbf{B_c}\,, \mathbf{B_2} = \mathbf{B_{2e}} \times \mathbf{B_c}\,, \mathbf{B_3} = \mathbf{B_{3e}} \times \mathbf{B_c}\,, \tag{5.52}$$

where

$$\begin{aligned}
\mathbf{B_{1e}} &= \mathbf{H}^1(\Omega) \times L^2_0(\Omega) \times H^1(\Omega) \times H^1_0(\Gamma_c) \times H^{-\frac{1}{2}}(\Gamma_d) \times \mathcal{T}_{ad}\,,\\
\mathbf{B_{2e}} &= \mathbf{H}^{-1}(\Omega) \times L^2_0(\Omega) \times H^{1*}(\Omega) \times H^{\frac{1}{2}}(\Gamma_d) \times (H^{-1}(\Omega))^2\,,\\
\mathbf{B_{3e}} &= \mathbf{H}^1_0(\Omega) \times L^2_0(\Omega) \times H^1_{\Gamma_i}(\Omega) \times \times H^1_0(\Gamma_c) \times H^{-\frac{1}{2}}(\Gamma_d) \times\\
&\quad \times (H^1_0(\Omega))^2\,,\\
\mathbf{B_c} &= (L^2(\Omega))^4 \times (L^2(\Omega))^4 \times (L^2(\Omega))^2\,.
\end{aligned} \tag{5.53}$$

We equip $\mathbf{B_1}, \mathbf{B_2}, \mathbf{B_3}$ with the usual graph norms for the product spaces involved.

Given $\mathbf{z}_0 = (\mathbf{u}, p, T, T_c, q_n, k, \omega, S'_k, r_{k1}, P_k, r_{k2}, S'_\omega, r_{\omega 1}, P_\omega, r_{\omega 2}, \nu_t, r_\nu) \in \mathbf{B_1}$, we can now define the nonlinear mapping $M : \mathbf{B_1} \to \mathbf{B_2}$ at $\mathbf{z}_0$ by $M(\mathbf{z}_0) \cdot \mathbf{z}_0 = \mathbf{b}$ with $\mathbf{b} = (\mathbf{l}_1, l_2, l_3, l_4, l_5, l_6, \mathbf{l}_k, \mathbf{l}_\omega, \mathbf{l}_\nu)$ if and only if the follow-

ing equations hold

$$\begin{aligned}
&a(\nu+\nu_t;\mathbf{u},\mathbf{v})+c(\mathbf{u};\mathbf{u},\mathbf{v})+b(\mathbf{v},p)-(\mathbf{f},\mathbf{v})\\
&\qquad+(b(T-T_0)\mathbf{g},\mathbf{v})=(\mathbf{l}_1,\mathbf{v}) && \forall\mathbf{v}\in\mathbf{H}_0^1(\Omega)\,,\\
&b(\mathbf{u},q)=(l_2,q) && \forall\, q\in L_0^2(\Omega)\,,\\
&a\Big(\alpha+\frac{\nu_t}{Pr_t};T,\varphi\Big)+c(\mathbf{u};T,\varphi)-(q_n,\varphi)_{\Gamma_d}\\
&\qquad-(g_{t,n},\varphi)_{\Gamma_n}=(l_3,\varphi) && \forall\varphi\in H^1(\Omega)\,,\\
&(T,s_T)_{\Gamma_d}-(T_c,s_T)_{\Gamma_c}-(g_t,s_T)_{\Gamma_d}=\\
&\qquad=(l_4,s_T)_{\Gamma_d} && \forall s_T\in H^{-1/2}(\Gamma_d)\,,\\
&c(\mathbf{u};k,\psi)+a(\nu+\nu_t\sigma_k;k,\psi)-(P_k,\psi)+\\
&\qquad+(\beta^*k\omega,\psi)=(l_5,\psi) && \forall\psi\in H_0^1(\Omega)\,,\\
&c(\mathbf{u};\omega,\phi)+a(\nu+\nu_t\sigma_\omega;\omega,\phi)-(P_\omega,\phi)+\\
&\qquad+(\beta\omega^2,\phi)=(l_6,\phi) && \forall\phi\in H_0^1(\Omega)\,,
\end{aligned}\tag{5.54}$$

and

$$\begin{aligned}
&S_k'\Big(S_k'-\frac{1}{2}\nu_t\mathbf{S}^2(\mathbf{u})-\frac{b\nu_t}{Pr_t}\mathbf{g}\cdot\nabla T\Big)=l_{k0}\,,\\
&r_{k1}^2-S_k'-\Big(S_k'-\frac{1}{2}\nu_t\mathbf{S}^2(\mathbf{u})-\frac{b\nu_t}{Pr_t}\mathbf{g}\cdot\nabla T\Big)=l_{k1}\,,\\
&(S_k'-P_k)(\beta^*k_{max}\omega-P_k)=l_{k2}\,,\\
&r_{k2}^2-(S_k'-P_k)-(\beta^*k_{max}\omega-P_k)=l_{k3}\,,\\
&S_\omega'\Big(S_\omega'-\frac{1}{2}\gamma\mathbf{S}^2(\mathbf{u})-\frac{\gamma b}{Pr_t}\mathbf{g}\cdot\nabla T\Big)=l_{\omega0}\,,\\
&r_{\omega1}^2-S_\omega'-\Big(S_\omega'-\frac{1}{2}\gamma\mathbf{S}^2(\mathbf{u})-\frac{\gamma b}{Pr_t}\mathbf{g}\cdot\nabla T\Big)=l_{\omega1}\,,\\
&(S_\omega'-P_\omega)(\beta\omega_{max}^2-P_\omega)=l_{\omega2}\,,\\
&r_{\omega2}^2-(S_\omega'-P_\omega)-(\beta\omega_{max}^2-P_\omega)=l_{\omega3}\\
&(k-\nu_t\omega)(\nu_{max}-\nu_t)=l_{\nu0}\,,\\
&r_\nu^2-(k-\nu_t\omega)-\omega(\nu_{max}-\nu_t)=l_{\nu1}\,,
\end{aligned}\tag{5.55}$$

where all the equations of (5.55) hold in Ω. From the definition of $\mathbf{b}$, we can state that the set of constraint equations in our optimal control problem can be expressed as $M(\mathbf{z}_0)\cdot\mathbf{z}_0=\mathbf{0}$.

Let $\widehat{\mathbf{z}}=(\widehat{\mathbf{u}},\widehat{p},\widehat{T},\widehat{T}_c,\widehat{q}_n,\widehat{k},\widehat{\omega},\widehat{S}_k',\widehat{r}_{k1},\widehat{P}_k,\widehat{r}_{k2},\widehat{S}_\omega',\widehat{r}_{\omega1},\widehat{P}_\omega,\widehat{r}_{\omega2},\widehat{\nu}_t,\widehat{r}_\nu)\in\mathbf{B}_1$, we define the nonlinear mapping $Q:\mathbf{B}_1\to\mathbb{R}\times\mathbf{B}_2$. For $a\in\mathbb{R}$ we set

$Q(\mathbf{z}_0)\cdot\widehat{\mathbf{z}} = (a,\mathbf{b})$ if and only if

$$Q(\mathbf{z}_0)\cdot\widehat{\mathbf{z}} = \begin{pmatrix} \mathcal{J}(\mathbf{u},T,k,T_c) - \mathcal{J}(\widehat{\mathbf{u}},\widehat{T},\widehat{k},\widehat{T}_c) \\ M(\mathbf{z}_0)\cdot\widehat{\mathbf{z}} \end{pmatrix} = \begin{pmatrix} a \\ \mathbf{b} \end{pmatrix}. \tag{5.56}$$

5.3.2. Mapping differentiability

We now introduce the notion of map differentiability, and we show that the mappings M and Q introduced above are strictly differentiable. For the definition of the differentiability, see [107].

Lemma 5.1. *Let* $\mathbf{z}_0 \in \mathbf{B}_1$, $\widetilde{\mathbf{z}}_0 = (\widetilde{\mathbf{u}},\widetilde{p},\widetilde{T},\widetilde{T}_c,\widetilde{q}_n,\widetilde{k},\widetilde{\omega},\widetilde{S}'_k,\widetilde{r}_{k1},\widetilde{P}_k,\widetilde{r}_{k2},\widetilde{S}'_\omega,\widetilde{r}_{\omega 1},\widetilde{P}_\omega,\ \widetilde{r}_{\omega 2},\widetilde{\nu}_t,\widetilde{r}_\nu) \in \mathbf{B}_3$ *and* $\overline{\mathbf{b}} = (\overline{\mathbf{l}}_1,\overline{l}_2,\overline{l}_3,\overline{l}_4,\overline{l}_5,\overline{l}_6,\overline{\mathbf{l}}_k,\overline{\mathbf{l}}_\omega,\overline{\mathbf{l}}_\nu) \in \mathbf{B}_2$. *Let consider, as derivative map, the bounded linear operator* $M' : \mathbf{B_3} \to \mathbf{B_2}$, *where* $M'(\mathbf{z}_0)\cdot\widetilde{\mathbf{z}}_0 = \overline{\mathbf{b}}$, *defined as*

$$\begin{aligned}
&a(\widetilde{\nu}_t;\mathbf{u},\mathbf{v}) + a(\nu+\nu_t;\widetilde{\mathbf{u}},\mathbf{v}) + c(\widetilde{\mathbf{u}};\mathbf{u},\mathbf{v}) + c(\mathbf{u};\widetilde{\mathbf{u}},\mathbf{v}) + \\
&\qquad + b(\mathbf{v},\widetilde{p}) + (b\mathbf{g}\widetilde{T},\mathbf{v}) = (\overline{\mathbf{l}}_1,\mathbf{v}),\\
&b(\widetilde{\mathbf{u}},q) = (\overline{l}_2,q),\\
&a\Big(\frac{\widetilde{\nu}_t}{Pr_t};T,\varphi\Big) + a\Big(\alpha+\frac{\nu_t}{Pr_t};\widetilde{T},\varphi\Big) + c(\widetilde{\mathbf{u}};T,\varphi) + \\
&\qquad + c(\mathbf{u};\widetilde{T},\varphi) - (\widetilde{q}_n,\varphi)_{\Gamma_d} = (\overline{l}_3,\varphi),\\
&(\widetilde{T},s_T)_{\Gamma_d} - (\widetilde{T}_c,s_T)_{\Gamma_c} = (\overline{l}_4,s_T)_{\Gamma_d},\\
&c(\widetilde{\mathbf{u}};k,\psi) + c(\mathbf{u};\widetilde{k},\psi) + a(\widetilde{\nu}_t\sigma_k;k,\psi) + a(\nu+\nu_t\sigma_k;\widetilde{k},\psi) + \\
&\qquad - (\widetilde{P}_k,\psi) + (\beta^*\widetilde{k}\omega,\psi) + (\beta^* k\widetilde{\omega},\psi) = (\overline{l}_5,\psi),\\
&c(\widetilde{\mathbf{u}};\omega,\phi) + c(\mathbf{u};\widetilde{\omega},\phi) + a(\widetilde{\nu}_t\sigma_\omega;\omega,\phi) + a(\nu+\nu_t\sigma_\omega;\widetilde{\omega},\phi) + \\
&\qquad - (\widetilde{P}_\omega,\phi) + 2(\beta\omega\widetilde{\omega},\phi) = (\overline{l}_6,\phi),
\end{aligned} \tag{5.57}$$

for all $\mathbf{v}\in\mathbf{H}^1_0(\Omega)$, $q\in L^2_0(\Omega)$, $\varphi\in H^1(\Omega)$, $s_T\in H^{-1/2}(\Gamma_d)$, $\forall\psi\in H^1_0(\Omega)$, $\phi\in H^1_0(\Omega)$ *and*

$$\begin{aligned}
&\widetilde{S}'_k\Big(S'_k - (S_k+S_{k,b})\Big) + S'_k\Big(\widetilde{S}'_k - \frac{1}{2}\widetilde{\nu}_t\mathbf{S}^2(\mathbf{u}) - \nu_t\mathbf{S}(\mathbf{u}):\mathbf{S}(\widetilde{\mathbf{u}}) + \\
&\qquad - \frac{b\widetilde{\nu}_t}{Pr_t}\mathbf{g}\cdot\nabla T - \frac{b\nu_t}{Pr_t}\mathbf{g}\cdot\nabla\widetilde{T}\Big) = \overline{l}_{k0},\\
&2r_{k1}\widetilde{r}_{k1} - 2\widetilde{S}'_k - \frac{1}{2}\widetilde{\nu}_t\mathbf{S}^2(\mathbf{u}) - \nu_t\mathbf{S}(\mathbf{u}):\mathbf{S}(\widetilde{\mathbf{u}}) + \frac{b\widetilde{\nu}_t}{Pr_t}\mathbf{g}\cdot\nabla T + \\
&\qquad + \frac{b\nu_t}{Pr_t}\mathbf{g}\cdot\nabla\widetilde{T} = \overline{l}_{k1},
\end{aligned}$$

$$
\begin{aligned}
&(\widetilde{S}'_k - \widetilde{P}_k)(\beta^* k_{max}\omega - P_k) + (S'_k - P_k)(\beta^* k_{max}\widetilde{\omega} - \widetilde{P}_k) = \bar{l}_{k2}\,,\\
&2r_{k2}\,\widetilde{r}_{k2} - \widetilde{S}'_k - \beta^* k_{max}\widetilde{\omega} + 2\widetilde{P}_k = \bar{l}_{k3}\,,\\
&\widetilde{S}'_\omega\Big(S'_\omega - (S_\omega + S_{\omega,b})\Big) + S'_\omega\Big(\widetilde{S}'_\omega - \gamma\mathbf{S}(\mathbf{u}) : \mathbf{S}(\widetilde{\mathbf{u}}) + \\
&\qquad - \frac{\gamma b}{Pr_t}\mathbf{g}\cdot\nabla\widetilde{T}\Big) = \bar{l}_{\omega 0}\,,\\
&2r_{\omega 1}\,\widetilde{r}_{\omega 1} - 2\widetilde{S}'_\omega + \gamma\mathbf{S}(\mathbf{u}) : \mathbf{S}(\widetilde{\mathbf{u}}) + \frac{\gamma b}{Pr_t}\mathbf{g}\cdot\nabla\widetilde{T} = \bar{l}_{\omega 1}\,,\\
&(\widetilde{S}'_\omega - \widetilde{P}_\omega)(\beta\omega_{max}^2 - P_\omega) - \widetilde{P}_\omega(S'_\omega - P_\omega) = \bar{l}_{\omega 2}\,,\\
&2r_{\omega 2}\,\widetilde{r}_{\omega 2} - \widetilde{S}'_\omega + 2\widetilde{P}_\omega = \bar{l}_{\omega 3}\,,\\
&(\widetilde{k} - \widetilde{\nu}_t\omega - \nu_t\widetilde{\omega})(\nu_{max} - \nu_t) - (k - \nu_t\omega)\widetilde{\nu}_t = \bar{l}_{\nu 0}\,,\\
&2r_\nu\widetilde{r}_\nu - \widetilde{k} + 2\widetilde{\nu}_t\omega + 2\nu_t\widetilde{\omega} - \widetilde{\omega}\nu_{max} = \bar{l}_{\nu 1}\,.
\end{aligned}
\tag{5.58}
$$

Consider the nonlinear operator $Q' : \mathbf{B_3} \to \mathbb{R}\times\mathbf{B_2}$, *where* $Q'(\mathbf{z}_0)\cdot\widetilde{\mathbf{z}}_0 = (\bar{a},\bar{\mathbf{b}})$ *for* $\bar{a}\in\mathbb{R}$. *If we set*

$$
\begin{aligned}
\mathcal{J}'(\mathbf{u},T,k,T_c)\cdot\widetilde{\mathbf{z}}_0 = \alpha_u\int_{\Omega_d}(\mathbf{u}-\mathbf{u}_d)\cdot\widetilde{\mathbf{u}}d\mathbf{x} + \alpha_k\int_{\Omega_d}(k-k_d)\widetilde{k}d\mathbf{x} + \\
+ \lambda_1\int_{\Gamma_c}T_c\widetilde{T}_c d\mathbf{x} + \lambda_2\int_{\Gamma_c}\nabla_s T_c\cdot\nabla_s\widetilde{T}_c d\mathbf{x}\,,
\end{aligned}
\tag{5.59}
$$

then the strict derivative of Q *at a point* $\mathbf{z}_0$ *is given by* Q' *if and only if*

$$
\begin{pmatrix} \mathcal{J}'(\mathbf{u},T,k,T_c)\cdot\widetilde{\mathbf{z}}_0 \\ M'(\mathbf{z}_0)\cdot\widetilde{\mathbf{z}}_0 \end{pmatrix} = \begin{pmatrix} \bar{a} \\ \bar{\mathbf{b}} \end{pmatrix}. \tag{5.60}
$$

Proof. The linearity and the boundedness of the operators M' and Q' follows from the continuity of the forms $a(\cdot;\cdot,\cdot)$, $b(\cdot,\cdot)$ and $c(\cdot;\cdot,\cdot)$ for both scalar and vector functions. The proof that M' is the strict derivative of the mapping M also follows from the continuity of the trilinear form $c(\cdot;\cdot,\cdot)$ and bilinear form $a(\cdot;\cdot,\cdot)$. The procedure is standard, and similar proofs have been reported in [93, 89]. Indeed, it can be proved that for a given $\mathbf{z}_0 = (\mathbf{u},p,T,T_c,q_n,k,\omega,S'_k,r_{k1},P_k,r_{k2},S'_\omega,r_{\omega 1},P_\omega,r_{\omega 2},\ \nu_t,r_t)\in\mathbf{B}_1$, then for any $\varepsilon>0$, and considering $\mathbf{z}_1,\mathbf{z}_2\in\mathbf{B}_1$ such that, for an appropriate $\delta=\delta(\varepsilon)$, we have $\|\mathbf{z}_0-\mathbf{z}_1\|_{\mathbf{B}_1}<\delta$ and $\|\mathbf{z}_0-\mathbf{z}_2\|_{\mathbf{B}_1}<\delta$, we obtain

$$
\|M(\mathbf{z}_1) - M(\mathbf{z}_2) - M'(\mathbf{z}_0)\cdot(\mathbf{z}_1-\mathbf{z}_2)\|_{\mathbf{B}_2} \le \varepsilon\|\mathbf{z}_1-\mathbf{z}_2\|_{\mathbf{B}_1}\,.
$$

This proves that the mapping M is strictly differentiable on all $\mathbf{B}_1$ and its strict derivative is given by M'. Using again standard techniques, it is

easy to show that the mapping Q is strictly differentiable and that its strict derivative is given by Q' [93, 89]. □

We now recall the fact that the introduced variables r_{k1}, $r_{\omega 1}, r_{k2}$, $r_{\omega 2}$, and r_ν are equal to zero when the turbulence sources in k and ω satisfy both limits at the same time in all the relations (5.15)-(5.21). This may be a problem for the optimization if this is verified over domain with positive measure. However, this is not a problem if this happens over points or boundary regions with zero measure. For this reason we introduce the following subsets

$$\Omega_{P_k} = \left\{ \mathbf{x} \in \Omega : S'_k = S_k + S_{k,b} = 0 \text{ or } P_k = \beta^* k_{max}\, \omega = S'_k \right\},$$
$$\Omega_{P_\omega} = \left\{ \mathbf{x} \in \Omega : S'_\omega = S_\omega + S_{\omega,b} = 0 \text{ or } P_\omega = \beta \omega^2_{max} = S'_\omega \right\},$$
$$\Omega_\nu = \left\{ \mathbf{x} \in \Omega : \nu_t = \nu_{max} = k/\omega \right\}.$$

These sets are used to assure the validity of the Lagrange multiplier technique around the region where the minimum point should be searched.

The differential operator M' is rather complex. Many equations in this operator are non-coercive elliptic equations with advection term driven by the velocity field $\mathbf{u} \in \mathbf{H}^1(\Omega)$. The existence result for this class of equations can be obtained not in the Lax-Milgram setting, but by using a Leray-Schauder Topological Degree argument. In order to deal with these equations, we use Theorem 4.3 introduced in the Chapter 4.

Lemma 5.2. *Let $\mathbf{z}_0 \in \mathbf{B_1}$. Then, if the region $\Omega_{P_k} \cup \Omega_{P_\omega} \cup \Omega_{S_\nu}$ has zero measure, we have that*

1. *the operator $M'(\mathbf{z}_0)$ has closed range in $\mathbf{B_2}$,*

2. *the operator $Q'(\mathbf{z}_0)$ has closed range in $\mathbb{R} \times \mathbf{B_2}$,*

3. *the operator $Q'(\mathbf{z}_0)$ is not onto in $\mathbb{R} \times \mathbf{B_2}$.*

Proof. In order to prove 1. we can split the range operator $M'(\mathbf{z}_0)$ in a product of range spaces for all its components and apply well known results. The operator range of M' can be split into four parts: the Navier-Stokes, the temperature, the k-ω model and the turbulence source constraint derivative

equations. First, let us consider the Navier-Stokes derivative operator

$$\begin{aligned}
&a(\nu+\nu_t;\tilde{\mathbf{u}},\mathbf{v})+c(\tilde{\mathbf{u}};\mathbf{u},\mathbf{v})+c(\mathbf{u};\tilde{\mathbf{u}},\mathbf{v})+\\
&\qquad+b(\mathbf{v},\widetilde{p})=(\bar{\mathbf{l}}_1^*,\mathbf{v}) && \forall\mathbf{v}\in\mathbf{H}_0^1(\Omega)\,,\\
&(\bar{\mathbf{l}}_1^*,\mathbf{w})=(\bar{\mathbf{l}}_1,\mathbf{w})-(b\mathbf{g}\widetilde{T},\mathbf{w})-a(\widetilde{\nu}_t;\mathbf{u},\mathbf{w}) && \forall\mathbf{w}\in\mathbf{H}_0^1(\Omega)\,,\\
&b(\tilde{\mathbf{u}},q)=(\bar{l}_2,q) && \forall\, q\in L_0^2(\Omega)\,,
\end{aligned}\tag{5.61}$$

with $\nu_t\in L^\infty(\Omega)$ and $\nu+\nu_t>0$. The question of the closeness of the range $(\bar{\mathbf{l}}_1^*,\bar{l}_2)$ in $H^{-1}(\Omega)\times L_0^2(\Omega)$ of (5.61) is discussed in many papers, see for examples [92, 97, 86].

Since $\mathbf{z}_0$ is an optimal solution, $\widetilde{T}$ and $\widetilde{q}_n$ solve the equations

$$\begin{aligned}
&a\Big(\alpha+\frac{\nu_t}{Pr_t};\widetilde{T},\varphi\Big)+c(\mathbf{u};\widetilde{T},\varphi)-(\widetilde{q}_n,\varphi)_{\Gamma_d}=\\
&\qquad=(\bar{l}_3^*,\varphi) && \forall\varphi\in H^1(\Omega)\,,\\
&(\widetilde{T},s_T)_{\Gamma_d}=(\bar{l}_4^*,s_T)_{\Gamma_d} && \forall s_T\in H^{-1/2}(\Gamma_d)\,,
\end{aligned}\tag{5.62}$$

with

$$\begin{aligned}
&(\bar{l}_3^*,\varphi)=(\bar{l}_3,\varphi)-a\Big(\frac{\widetilde{\nu}_t}{Pr_t};T,\varphi\Big)-c(\tilde{\mathbf{u}};T,\varphi) && \forall\varphi\in H^1(\Omega)\,,\\
&(\bar{l}_4^*,s_T)_{\Gamma_d}=(\widetilde{T}_c,s_T)_{\Gamma_c}+(\bar{l}_4,s_T)_{\Gamma_d} && \forall s_T\in H^{-1/2}(\Gamma_d)\,,
\end{aligned}\tag{5.63}$$

For $(\bar{l}_3,\bar{l}_4)\in H^{1*}(\Omega)\times H^{1/2}(\Gamma)$ we have $(\bar{l}_3^*,\bar{l}_4^*)\in H^{1*}(\Omega)\times H^{1/2}(\Gamma)$. By using the result in Theorem 4.3 for each $(\bar{l}_3^*,\bar{l}_4^*)\in H^{1*}(\Omega)\times H^{1/2}(\Gamma)$ we have a solution and therefore the range of the mapping $M'(\mathbf{z}_0)$ for the energy equation is onto.

Now we consider the k-ω system in M'. Since $\mathbf{z}_0$ is an optimal solution, the system reduces to

$$\begin{aligned}
&a(\nu+\nu_t\sigma_k;\tilde{k},\phi)+c(\mathbf{u};\tilde{k},\phi)+(\beta^*\omega\tilde{k},\phi)=\\
&\qquad=(\bar{l}_5^*,\phi) && \forall\phi\in H_0^1(\Omega)\,,\\
&(\bar{l}_5^*,\phi)=(\bar{l}_5,\phi)-a(\tilde{\nu}_t\sigma_k;k,\phi)-c(\tilde{\mathbf{u}};k,\phi)+\\
&\qquad-(\beta^*\tilde{\omega}k,\phi)+(\tilde{P}_k,\phi) && \forall\phi\in H_0^1(\Omega)\,,\\
&a(\nu+\nu_t\sigma_\omega;\tilde{\omega},\psi)+c(\mathbf{u};\tilde{\omega},\psi)+(2\beta\omega\tilde{\omega},\psi)=\\
&\qquad=(\bar{l}_6^*,\psi) && \forall\psi\in H_0^1(\Omega)\,,\\
&(\bar{l}_6^*,\psi)=(\bar{l}_6,\psi)-a(\tilde{\nu}_t\sigma_\omega;\omega,\psi)-c(\tilde{\mathbf{u}};\omega,\psi)+\\
&\qquad+(\tilde{P}_\omega,\psi) && \forall\psi\in H_0^1(\Omega)\,,
\end{aligned}\tag{5.64}$$

with homogeneous Dirichlet boundary conditions. It is possible to show that the equation for $\tilde{\omega}$ in (5.64) has a solution for all $\bar{l}_6^*$ and also that the equation for $\tilde{k}$ can be solved for all $\bar{l}_4^*$. In fact, since $\nu + \nu_t$ is a positive function in $L^\infty(\Omega)$ and thanks to the Sobolev compact embeddings $\mathbf{H}^1(\Omega) \hookrightarrow \mathbf{L}^q(\Omega)$ which holds for $1 \leq q < \infty$ when $n = 2$ and for $1 \leq q \leq 6$ when $n = 3$, we have that $\mathbf{u} \in \mathbf{H}^1(\Omega)$ verifies the hypothesis in Theorem 4.3 both with $n = 2$ and with $n = 3$.

Finally, we focus on the system (5.58) under the assumption that $\mathbf{z}_0$ is an optimal solution. From this we have that $\mathbf{S}^2(\mathbf{u})$ is bounded and $\nu_t \in L^\infty(\Omega)$. If we assume that the region $\Omega_\nu \cup \Omega_{P_k} \cup \Omega_{P_\omega}$ has a measure zero then $r_\nu, r_{k1}, r_{k2}, r_{\omega 1}, r_{\omega 2}$ cannot be zero a.e. on the domain Ω. Therefore the equations can be solved a.e. in Ω for all $\mathbf{l}_\nu = (l_{\nu 0}, l_{\nu 1}) \in L^2(\Omega) \times L^2(\Omega)$, $\mathbf{l}_k = (l_{k0}, l_{k1}, l_{k2}) \in L^2(\Omega) \times L^2(\Omega) \times L^2(\Omega)$ and $\mathbf{l}_\omega = (l_{\omega 0}, l_{\omega 1}, l_{\omega 2}) \in L^2(\Omega) \times L^2(\Omega) \times L^2(\Omega)$ as a function of $\tilde{\nu}_t$, $\tilde{r}_{\nu 1}$, $\tilde{k}$, $\tilde{r}_{k1}$, $\tilde{r}_{k2}$ and $\tilde{\omega}$, $\tilde{r}_{\omega 1}$ and $\tilde{r}_{\omega 2}$, respectively.

Starting from 1., the proof of 2. and 3. can be found easily by using the standard techniques in [92, 93, 97]. □

Theorem 5.5. *Let $\hat{\mathbf{z}} \in \mathbf{B}_1$ denote an optimal solution. Then there exists a nonzero Lagrange multiplier $(\Lambda, \hat{\mathbf{z}}_a) = (\Lambda, \hat{\mathbf{u}}_a, \hat{p}_a, \widehat{T}_a, \hat{q}_a, \hat{k}_a, \hat{\omega}_a, \widehat{S'}_{ka}, \hat{r}_{k1a}, \widehat{P}_{ka}, \hat{r}_{k2a}, \widehat{S'}_{\omega a}, \widehat{P}_{\omega a}, \hat{r}_{\omega 1a}, \hat{r}_{\omega 2a}, \hat{\nu}_a, \hat{r}_{\nu a}) \in \mathbb{R} \times \mathbf{B}_2^*$ satisfying the Euler equations*

$$\Lambda \mathcal{J}'(\hat{\mathbf{u}}, \hat{k}, \widehat{T}, \widehat{T}_c) \cdot \tilde{\mathbf{z}}_0 + \langle \hat{\mathbf{z}}_a, M'(\hat{\mathbf{z}}) \cdot \tilde{\mathbf{z}}_0 \rangle = 0 \qquad \forall \tilde{\mathbf{z}}_0 \in \mathbf{B}_3 \tag{5.65}$$

where $\langle \cdot, \cdot \rangle$ denotes the duality pairing between $\mathbf{B}_2$ and $\mathbf{B}_2^*$.

Proof. From Lemma 5.2, we have that the range of $Q'(\hat{\mathbf{z}})$ is a closed, proper subspace of $\mathbb{R} \times \mathbf{B}_2$. Then, from the Hahn-Banach theorem, there exists a nonzero element of $\mathbb{R} \times \mathbf{B}_2^*$ that nullifies the range of $Q'(\hat{\mathbf{z}})$. Therefore, there exists $(\Lambda, \hat{\mathbf{u}}_a, \hat{p}_a, \widehat{T}_a, \hat{q}_a, \hat{k}_a, \hat{\omega}_a, \widehat{S'}_{ka}, \hat{r}_{k1a}, \widehat{P}_{ka}, \hat{r}_{k2a}, \widehat{S'}_{\omega a}, \hat{r}_{\omega 1a}, \widehat{P}_{\omega a}, \hat{r}_{\omega 2a}, \hat{\nu}_a, \hat{r}_{\nu a}) \in \mathbb{R} \times \mathbf{B}_2^*$ such that

$$\langle (\bar{a}, \bar{\mathbf{b}}), (\Lambda, \hat{\mathbf{z}}_a) \rangle = 0\,, \tag{5.66}$$

for all $(\bar{a}, \bar{\mathbf{b}}) = (\bar{a}, \bar{\mathbf{l}}_1, \bar{l}_2, \bar{l}_3, \bar{l}_4, \bar{l}_5, \bar{l}_6, \bar{\mathbf{l}}_\nu, \bar{\mathbf{l}}_k, \bar{\mathbf{l}}_\omega)$ belonging to the range of $Q'(\hat{\mathbf{z}})$, where $\langle \cdot, \cdot \rangle$ denotes the duality pairing between $\mathbb{R} \times \mathbf{B}_2$ and $\mathbb{R} \times \mathbf{B}_2^*$. Note that $\Lambda \neq 0$ since otherwise we would have that $\langle \bar{\mathbf{b}}, \hat{\mathbf{z}}_a \rangle = 0$ for all $\bar{\mathbf{b}} \in \mathbf{B}_2$. This would imply $\hat{\mathbf{z}}_a = 0$ contradicting the fact that $(\Lambda, \hat{\mathbf{z}}_a) \neq 0$. Clearly, using the definition of $Q'(\hat{\mathbf{z}})$, (5.65) and (5.66) are equivalent. □

5.3.3. The optimality system

Dropping the $\widehat{(\cdot)}$ notation for optimal solution, we derive now the optimality system using (5.65). We introduce the following equations

$$\Lambda\lambda_1(T_c,\widetilde{T}_c)_{\Gamma_c}+\Lambda\lambda_2(\nabla_s T_c,\nabla_s\widetilde{T}_c)_{\Gamma_c}=(q_a,\widetilde{T}_c)_{\Gamma_c}\,, \tag{5.67}$$

for all $\widetilde{T}_c\in H_0^1(\Gamma_c)$

$$\begin{aligned}
&b(\mathbf{u}_a,\widetilde{p})=0\,,\\
&a(\nu+\nu_t;\widetilde{\mathbf{u}},\mathbf{u}_a)+c(\mathbf{u};\widetilde{\mathbf{u}},\mathbf{u}_a)+c(\widetilde{\mathbf{u}};\mathbf{u},\mathbf{u}_a)+b(\widetilde{\mathbf{u}},p_a)=\\
&\qquad=-\alpha_u\Lambda((\mathbf{u}-\mathbf{u}_d),\widetilde{\mathbf{u}})_{\Omega_d}-c(\widetilde{\mathbf{u}};T,T_a)-c(\widetilde{\mathbf{u}};k,k_a)+\\
&\qquad-c(\widetilde{\mathbf{u}};\omega,\omega_a)+a(\nu_t(r_{k1a}-S'_{ka}S'_k)+\\
&\qquad+\gamma(r_{\omega 1a}-S'_{\omega a}S'_\omega);\mathbf{u},\widetilde{\mathbf{u}})\,,
\end{aligned} \tag{5.68}$$

for all $(\widetilde{\mathbf{u}},\widetilde{p})\in\mathbf{H}_0^1(\Omega)\times L_0^2(\Omega)$

$$\begin{aligned}
&a(\alpha+\frac{\nu_t}{Pr_t};\widetilde{T},T_a)+c(\mathbf{u};\widetilde{T},T_a)+(\widetilde{T},q_a)_{\Gamma_d}=-(b\mathbf{g}\widetilde{T},\mathbf{u}_a)+\\
&\qquad+\Big(\frac{b}{Pr_t}\mathbf{g}\cdot\nabla\widetilde{T},\nu_t(r_{k1a}-S'_{ka}S'_k)+\gamma(r_{\omega 1a}-S'_{\omega a}S'_\omega)\Big)\\
&(T_a,\widetilde{q}_n)_{\Gamma_d}=0\,,
\end{aligned} \tag{5.69}$$

for all $(\widetilde{T},\widetilde{q}_n)\in H^1_{\Gamma_i}(\Omega)\times H^{-\frac{1}{2}}(\Gamma_d)$

$$\begin{aligned}
&a(\nu+\nu_t\sigma_k;\widetilde{k},k_a)+c(\mathbf{u};\widetilde{k},k_a)+(\beta^*\widetilde{k}\omega,k_a)=\\
&\qquad=-\alpha_k\Lambda((k-k_d),\widetilde{k})_{\Omega_d}-(\widetilde{k},\nu_a(\nu_{max}-\nu_t)-r_{\nu a})\,,\\
&a(\nu+\nu_t\sigma_\omega;\widetilde{\omega},\omega_a)+c(\mathbf{u};\widetilde{\omega},\omega_a)+(2\beta\omega\widetilde{\omega},\omega_a)=\\
&\qquad=-(\beta^*k\widetilde{\omega},k_a)-(P_{ka}(S'_k-P_k)-r_{k2a},\beta^*k_{max}\widetilde{\omega})+\\
&\qquad+(\nu_t\nu_a(\nu_{max}-\nu_t)-r_{\nu a}(2\nu_t-\nu_{max}),\widetilde{\omega})\,,
\end{aligned} \tag{5.70}$$

for all $(\widetilde{k},\widetilde{\omega})\in H_0^1(\Omega)\times H_0^1(\Omega)$. We also introduce the algebraic system

$$\begin{aligned}
&\nu_a\omega\Big(\nu_{max}+\frac{k}{\omega}-2\nu_t\Big)=\frac{\mathbf{S}(\mathbf{u}):\mathbf{S}(\mathbf{u}_a)}{2}+\frac{\nabla T\cdot\nabla T_a}{Pr_t}+\\
&\qquad+\sigma_k\nabla k\cdot\nabla k_a+\sigma_\omega\nabla\omega\cdot\nabla\omega_a+2r_{\nu a}\omega+\\
&\qquad-(S'_{ka}S'_k-r_{k1a})\Big(\frac{1}{2}\mathbf{S}^2(\mathbf{u})+\frac{b}{Pr_t}\mathbf{g}\cdot\nabla T\Big)\,,\\
&S'_{ka}\Big(2S'_k-\frac{1}{2}\nu_t\mathbf{S}^2(\mathbf{u})-\frac{b\nu_t}{Pr_t}\mathbf{g}\cdot\nabla T\Big)=2r_{k1a}+r_{k2a}+
\end{aligned}$$

$$
\begin{aligned}
&\quad - P_{ka}(\beta^* k_{max}\omega - P_k)\,, \qquad (5.71)\\
&S'_{\omega a}\Big(2S'_\omega - \frac{1}{2}\gamma \mathbf{S}^2(\mathbf{u}) - \frac{\gamma b}{Pr_t}\mathbf{g}\cdot\nabla T\Big) = 2r_{\omega 1a} + r_{\omega 2a} +\\
&\quad - P_{\omega a}(\beta\omega_{max}^2 - P_\omega)\,,\\
&P_{ka}(\beta^* k_{max}\omega + S'_k - 2P_k) = 2r_{k2a} - k_a\,,\\
&P_{\omega a}(\beta\omega_{max}^2 + S'_\omega - 2P_\omega) = 2r_{\omega 2a} - \omega_a\,.
\end{aligned}
$$

Lastly, we have

$$
r_{k1a}r_{k1} = r_{k2a}r_{k2} = r_{\omega 1a}r_{\omega 1} = r_{\omega 2a}r_{\omega 2} = r_{\nu a}r_\nu = 0\,. \qquad (5.72)
$$

In (5.67) q_a is given by the normal adjoint temperature gradient as follows

$$
q_a = -\Big(\alpha + \frac{\nu_t}{Pr_t}\Big)\nabla T_a\cdot\mathbf{n} \quad \text{on } \Gamma_d\,. \qquad (5.73)
$$

Theorem 5.6. *Let $\mathbf{z}\in\mathbf{B}_1$ denote a solution of the optimal control problem. Then, if the region $\Omega_{P_k}\cup\Omega_{P_\omega}\cup\Omega_\nu$ has zero measure, the control variable $T_c\in H_0^1(\Gamma_c)$ is the solution of (5.67).*

Also, $(\mathbf{u}_a, p_a)\in\mathbf{H}_0^1(\Omega)\times L_0^2(\Omega)$ is solution of (5.68). In addition, $(T_a, q_a)\in H^1(\Omega)\times H^{-\frac{1}{2}}(\Gamma_d)$ is the solution of (5.69) under the condition (5.73). Also, $(k_a,\omega_a)\in H_0^1(\Omega)\times H_0^1(\Omega)$ is solution of (5.70).

Moreover, $(\nu_a, S'_{ka}, S'_{\omega a}, P_{ka}, P_{\omega a})\in (L^2(\Omega))^5$ are solutions of the algebraic equations (5.71), and $(r_{k1a}, r_{k2a}, r_{\omega 1a}, r_{\omega 2a}, r_{\nu a})\in (L^2(\Omega))^5$ satisfy (5.72).

Proof. The Euler equations (5.65) are equivalent to

$$
\begin{aligned}
\Lambda(&\alpha_u((\mathbf{u}-\mathbf{u}_d),\widetilde{\mathbf{u}})_{\Omega_d} + \alpha_k((k-k_d),\widetilde{k})_{\Omega_d} + \lambda_1(T_c,\widetilde{T}_c)_{\Gamma_c} +\\
&+\lambda_2(\nabla_s T_c, \nabla_s\widetilde{T}_c)_{\Gamma_c}) + a(\widetilde{\nu}_t;\mathbf{u},\mathbf{u}_a) + a(\nu+\nu_t;\widetilde{\mathbf{u}},\mathbf{u}_a) +\\
&+c(\widetilde{\mathbf{u}};\mathbf{u},\mathbf{u}_a) + c(\mathbf{u};\widetilde{\mathbf{u}},\mathbf{u}_a) + b(\mathbf{u}_a,\widetilde{p}) + (b\mathbf{g}\widetilde{T},\mathbf{u}_a) +\\
&+b(\widetilde{\mathbf{u}},p_a) + c(\widetilde{\mathbf{u}};T,T_a) + c(\mathbf{u};\widetilde{T},T_a) + a\Big(\frac{\widetilde{\nu}_t}{Pr_t};T,T_a\Big) +\\
&+a\Big(\alpha+\frac{\nu_t}{Pr_t};\widetilde{T},T_a\Big) - (\widetilde{q}_n,T_a)_{\Gamma_d} + (\widetilde{T},q_a)_{\Gamma_d} - (\widetilde{T}_c,q_a)_{\Gamma_c}\\
&+c(\widetilde{\mathbf{u}};k,k_a) + c(\mathbf{u};\widetilde{k},k_a) + a(\widetilde{\nu}_t\sigma_k;k,k_a) - (\widetilde{P}_k,k_a) +\\
&+a(\nu+\nu_t\sigma_k;\widetilde{k},k_a) + (\beta^*\widetilde{k}\omega,k_a) + (\beta^* k\widetilde{\omega},k_a) +\\
&+c(\widetilde{\mathbf{u}};\omega,\omega_a) + c(\mathbf{u};\widetilde{\omega},\omega_a) + a(\widetilde{\nu}_t\sigma_\omega;\omega,\omega_a) - (\widetilde{P}_\omega,\omega_a) +\\
&+a(\nu+\nu_t\sigma_\omega;\widetilde{\omega},\omega_a) + 2(\beta\omega\widetilde{\omega},\omega_a) +
\end{aligned}
$$

$$
\begin{aligned}
&+\Big(S'_{ka},\widetilde{S}'_k\Big(S'_k-\frac{1}{2}\nu_t\mathbf{S}^2(\mathbf{u})-\frac{b\nu_t}{Pr_t}\mathbf{g}\cdot\nabla T\Big)+\\
&+S'_k\Big(\widetilde{S}'_k-\frac{1}{2}\widetilde{\nu}_t\mathbf{S}^2(\mathbf{u})-\nu_t\mathbf{S}(\mathbf{u}):\mathbf{S}(\widetilde{\mathbf{u}})-\frac{b\widetilde{\nu}_t}{Pr_t}\mathbf{g}\cdot\nabla T+\\
&-\frac{b\nu_t}{Pr_t}\mathbf{g}\cdot\nabla\widetilde{T}\Big)\Big)+\Big(r_{k1a},2r_{k1}\widetilde{r}_{k1}-2\widetilde{S}'_k+\frac{1}{2}\widetilde{\nu}_t\mathbf{S}^2(\mathbf{u})+\\
&+\nu_t\mathbf{S}(\mathbf{u}):\mathbf{S}(\widetilde{\mathbf{u}})+\frac{b\widetilde{\nu}_t}{Pr_t}\mathbf{g}\cdot\nabla T+\frac{b\nu_t}{Pr_t}\mathbf{g}\cdot\nabla\widetilde{T}\Big)+\\
&+(P_{ka},(\widetilde{S}'_k-\widetilde{P}_k)(\beta^*k_{max}\omega-P_k)+(S'_k-P_k)(\beta^*k_{max}\widetilde{\omega}+\\
&-\widetilde{P}_k))+(r_{k2a},2r_{k2}\widetilde{r}_{k2}-\widetilde{S}'_k-\beta^*k_{max}\widetilde{\omega}+2\widetilde{P}_k)+\\
&+\Big(S'_{\omega a},\widetilde{S}'_\omega\Big(S'_\omega-\frac{1}{2}\gamma\mathbf{S}^2(\mathbf{u})-\frac{\gamma b}{Pr_t}\mathbf{g}\cdot\nabla T\Big)+\\
&+S'_\omega\Big(\widetilde{S}'_\omega-\gamma\mathbf{S}(\mathbf{u}):\mathbf{S}(\widetilde{\mathbf{u}})-\frac{\gamma b}{Pr_t}\mathbf{g}\cdot\nabla\widetilde{T}\Big)\Big)+\\
&+\Big(r_{\omega 1a},2r_{\omega 1}\widetilde{r}_{\omega 1}-2\widetilde{S}'_\omega+\gamma\mathbf{S}(\mathbf{u}):\mathbf{S}(\widetilde{\mathbf{u}})+\frac{\gamma b}{Pr_t}\mathbf{g}\cdot\nabla\widetilde{T}\Big)+\\
&+(P_{\omega a},(\widetilde{S}'_\omega-\widetilde{P}_\omega)(\beta\omega^2_{max}-P_\omega)-\widetilde{P}_\omega(S'_\omega-P_\omega))+\\
&+(r_{\omega 2a},2r_{\omega 2}\widetilde{r}_{\omega 2}-\widetilde{S}'_\omega+2\widetilde{P}_\omega)+\\
&+(\nu_a,(\widetilde{k}-\widetilde{\nu}_t\omega-\nu_t\widetilde{\omega})(\nu_{max}-\nu_t)-(k-\nu_t\omega)\widetilde{\nu}_t)+\\
&+(r_{\nu a},2r_\nu\widetilde{r}_\nu-\widetilde{k}+2\widetilde{\nu}_t\omega+2\nu_t\widetilde{\omega}-\widetilde{\omega}\nu_{max})=0\,,
\end{aligned}
$$

for all $\mathbf{z}\in\mathbf{B}_1$. In order to satisfy the integral on the boundary, we set homogeneous Dirichlet boundary conditions for the adjoint variables $(\mathbf{u}_a,k_a,\omega_a)$. By extracting the terms involved in the same variation, we obtain (5.67)-(5.72). □

If the region $\Omega_{P_k}\cup\Omega_{P_\omega}\cup\Omega_{S_\nu}$ has zero measure, then $r_{k1},r_{k2},r_{\omega 1},r_{\omega 2}$ and r_ν are almost everywhere different from zero. From (5.72) we note that if $r_{k1}\neq 0$, then $r_{k1a}=0$. This is true also for $r_{k2a},r_{\omega 1a},r_{\omega 2a}$ and $r_{\nu a}$. By setting $\Lambda=-1$, the final adjoint system reduces to

$$
\lambda_1(T_c,\widetilde{T}_c)_{\Gamma_c}+\lambda_2(\nabla_s T_c,\nabla_s\widetilde{T}_c)_{\Gamma_c}+(q_a,\widetilde{T}_c)_{\Gamma_c}=0\,,
\tag{5.74}
$$

for all $\widetilde{T}_c\in H^1_0(\Gamma_c)$,

$$
\begin{aligned}
&b(\mathbf{u}_a,\widetilde{p})=0\,,\\
&a(\nu+\nu_t;\widetilde{\mathbf{u}},\mathbf{u}_a)+c(\mathbf{u};\widetilde{\mathbf{u}},\mathbf{u}_a)+c(\widetilde{\mathbf{u}};\mathbf{u},\mathbf{u}_a)+b(\widetilde{\mathbf{u}},p_a)=\\
&\qquad=\alpha_u((\mathbf{u}-\mathbf{u}_d),\widetilde{\mathbf{u}})_{\Omega_d}-c(\widetilde{\mathbf{u}};T,T_a)-c(\widetilde{\mathbf{u}};k,k_a)+\\
&\qquad-c(\widetilde{\mathbf{u}};\omega,\omega_a)-a(\nu_t S'_{ka}S'_k+\gamma S'_{\omega a}S'_\omega;\mathbf{u},\widetilde{\mathbf{u}})\,,
\end{aligned}
\tag{5.75}
$$

for all $(\widetilde{\mathbf{u}}, \widetilde{p}) \in \mathbf{H}^1_0(\Omega) \times L^2_0(\Omega)$,

$$\begin{aligned} a\Big(\alpha + \frac{\nu_t}{Pr_t}; \widetilde{T}, T_a\Big) + c(\mathbf{u}; \widetilde{T}, T_a) + (\widetilde{T}, q_a)_{\Gamma_c} = -(b\mathbf{g}\widetilde{T}, \mathbf{u}_a) + \\ - \Big(\frac{b}{Pr_t}\mathbf{g} \cdot \nabla\widetilde{T}, \nu_t S'_{ka} S'_k + \gamma S'_{\omega a} S'_\omega\Big)\,, \end{aligned} \tag{5.76}$$

for all $\widetilde{T} \in H^1_{\Gamma_i}(\Omega)$,

$$\begin{aligned} &a(\nu + \nu_t\sigma_k; \widetilde{k}, k_a) + c(\mathbf{u}; \widetilde{k}, k_a) + (\beta^*\widetilde{k}\omega, k_a) = \\ &\qquad = \alpha_k((k - k_d), \widetilde{k})_{\Omega_d} - (\widetilde{k}, \nu_a(\nu_{max} - \nu_t))\,, \\ &a(\nu + \nu_t\sigma_\omega; \widetilde{\omega}, \omega_a) + c(\mathbf{u}; \widetilde{\omega}, \omega_a) + (2\beta\omega\widetilde{\omega}, \omega_a) = -(\beta^* k\widetilde{\omega}, k_a) + \\ &\qquad - (P_{ka}(S'_k - P_k), \beta^* k_{max}\widetilde{\omega}) + (\nu_t\nu_a(\nu_{max} - \nu_t), \widetilde{\omega})\,, \end{aligned} \tag{5.77}$$

for all $(\widetilde{k}, \widetilde{\omega}) \in H^1_0(\Omega) \times H^1_0(\Omega)$. Lastly, in the case in which $\Omega_{P_k} \cup \Omega_{P_\omega} \cup \Omega_{S_\nu}$ has zero measure, we have the following algebraic equations

$$\begin{aligned} &\nu_a r^2_\nu = \frac{\mathbf{S}(\mathbf{u}) : \mathbf{S}(\mathbf{u}_a)}{2} + \frac{\nabla T \cdot \nabla T_a}{Pr_t} + \sigma_k \nabla k \cdot \nabla k_a + \\ &\qquad + \sigma_\omega \nabla\omega \cdot \nabla\omega_a - S'_{ka} S'_k \Big(\frac{1}{2}\mathbf{S}^2(\mathbf{u}) + \frac{b}{Pr_t}\mathbf{g} \cdot \nabla T\Big)\,, \\ &S'_{ka} r^2_{k1} = -P_{ka}(\beta^* k_{max}\omega - P_k)\,, \\ &S'_{\omega a} r^2_{\omega 1} = -P_{\omega a}(\beta\omega^2_{max} - P_\omega)\,, \\ &P_{ka} r^2_{k2} = -k_a\,, \\ &P_{\omega a} r^2_{\omega 2} = -\omega_a\,. \end{aligned} \tag{5.78}$$

Furthermore, in the case in which no bounds are reached, we have

$$\nu_t = \frac{k}{\omega}\,, \quad P_k = S'_k = S_k + S_{kb}\,, \quad P_\omega = S'_\omega + S_{\omega b}\,, \tag{5.79}$$

then the adjoint system (5.75)-(5.78) simplifies and in particular

$$S'_{ka} S'_k = k_a\,, \quad S'_{\omega a} S'_\omega = \omega_a\,. \tag{5.80}$$

Thus, the equations for adjoint velocity and pressure reduce to

$$\begin{aligned} &b(\mathbf{u}_a, \widetilde{p}) = 0\,, \\ &a(\nu + \nu_t; \widetilde{\mathbf{u}}, \mathbf{u}_a) + c(\mathbf{u}; \widetilde{\mathbf{u}}, \mathbf{u}_a) + c(\widetilde{\mathbf{u}}; \mathbf{u}, \mathbf{u}_a) + b(\widetilde{\mathbf{u}}, p_a) = \\ &\qquad = \alpha_u((\mathbf{u} - \mathbf{u}_d), \widetilde{\mathbf{u}})_{\Omega_d} - c(\widetilde{\mathbf{u}}; T, T_a) - c(\widetilde{\mathbf{u}}; k, k_a) + \\ &\qquad - c(\widetilde{\mathbf{u}}; \omega, \omega_a) - a(\nu_t k_a + \gamma\omega_a; \mathbf{u}, \widetilde{\mathbf{u}})\,, \end{aligned} \tag{5.81}$$

for all $(\widetilde{\mathbf{u}}, \widetilde{p}) \in \mathbf{H}_0^1(\Omega) \times L_0^2(\Omega)$, while the adjoint temperature equation is the following

$$\begin{aligned} a\Big(\alpha + \frac{\nu_t}{Pr_t}; \widetilde{T}, T_a\Big) + c(\mathbf{u}; \widetilde{T}, T_a) + (\widetilde{T}, q_a)_{\Gamma_c} = -(b\mathbf{g}\widetilde{T}, \mathbf{u}_a) + \\ - \Big(\frac{b}{Pr_t}\mathbf{g} \cdot \nabla \widetilde{T}, \nu_t k_a + \gamma \omega_a\Big), \end{aligned} \tag{5.82}$$

for all $\widetilde{T} \in H^1_{\Gamma_i}(\Omega)$. The adjoint equations for k_a and ω_a simplify

$$\begin{aligned} &a(\nu + \nu_t\sigma_k; \widetilde{k}, k_a) + c(\mathbf{u}; \widetilde{k}, k_a) + (\beta^* \widetilde{k}\omega, k_a) = \\ &\qquad = \alpha_k((k - k_d), \widetilde{k})_{\Omega_d} - (\widetilde{k}, \nu_a(\nu_{max} - \nu_t)), \\ &a(\nu + \nu_t\sigma_\omega; \widetilde{\omega}, \omega_a) + c(\mathbf{u}; \widetilde{\omega}, \omega_a) + (2\beta\omega\widetilde{\omega}, \omega_a) = -(\beta^* k\widetilde{\omega}, k_a) + \\ &\qquad + (\nu_t\nu_a(\nu_{max} - \nu_t), \widetilde{\omega}), \end{aligned} \tag{5.83}$$

for all $(\widetilde{k}, \widetilde{\omega}) \in H_0^1(\Omega) \times H_0^1(\Omega)$. Furthermore, if no bounds are reached, we have $r_\nu^2 = \omega(\nu_t - \nu_{max})$, thus the adjoint viscosity equation reduces to

$$\begin{aligned} \nu_a\omega(\nu_{max} - \nu_t) = -\frac{\mathbf{S}(\mathbf{u}) : \mathbf{S}(\mathbf{u}_a)}{2} - \frac{\nabla T \cdot \nabla T_a}{Pr_t} - \sigma_k \nabla k \cdot \nabla k_a + \\ - \sigma_\omega \nabla\omega \cdot \nabla\omega_a + k_a\Big(\frac{1}{2}\mathbf{S}^2(\mathbf{u}) + \frac{b}{Pr_t}\mathbf{g} \cdot \nabla T\Big). \end{aligned} \tag{5.84}$$

Integrations by parts may be used to show that the system (5.75)-(5.76) constitutes a weak formulation of the boundary value problem for adjoint equations

$$\begin{aligned} &\nabla \cdot \mathbf{u}_a = 0 && \text{in } \Omega, \\ &\mathbf{u}_a \cdot (\nabla\mathbf{u})^T - \mathbf{u} \cdot \nabla\mathbf{u}_a + \nabla p_a - \nabla \cdot [(\nu + \nu_t)\mathbf{S}(\mathbf{u}_a)] = \\ &\qquad = \alpha_u(\mathbf{u} - \mathbf{u}_d) - T\nabla T_a - k\nabla k_a - \omega\nabla\omega_a + \\ &\qquad + \frac{1}{2}\nabla \cdot [(\nu_t k_a + \gamma\omega_a)\mathbf{S}(\mathbf{u})] && \text{in } \Omega, \\ &\nabla \cdot \Big[\Big(\alpha + \frac{\nu_t}{Pr_t}\Big)\nabla T_a\Big] - \mathbf{u} \cdot \nabla T_a = -b\mathbf{g} \cdot \mathbf{u}_a + \\ &\qquad + \frac{b}{Pr_t}\mathbf{g} \cdot \nabla(\nu_t k_a + \gamma\omega_a) && \text{in } \Omega, \\ &\nabla \cdot [(\nu + \sigma_k\nu_t)\nabla k_a] - \mathbf{u} \cdot \nabla k_a + \beta^*\omega k_a = && \text{in } \Omega, \\ &\qquad = \alpha_k(k - k_d) - \nu_a(\nu_{max} - \nu_t) && \\ &\nabla \cdot [(\nu + \sigma_\omega\nu_t)\nabla\omega_a] - \mathbf{u} \cdot \nabla\omega_a + 2\beta\omega\omega_a = \end{aligned} \tag{5.85}$$

$$
\begin{aligned}
&= -\beta^* k k_a + \nu_t \nu_a (\nu_{max} - \nu_t) && \text{in } \Omega\,,\\
&\mathbf{u}_a = 0 && \text{on } \Gamma\\
&\nabla T_a \cdot \mathbf{n}|_{\Gamma_n} = 0 && \text{on } \Gamma_n\,,\\
&T_a = 0 && \text{on } \Gamma_d\,,\\
&k_a = 0 && \text{on } \Gamma\,,\\
&\omega_a = 0 && \text{on } \Gamma\,,
\end{aligned}
$$

and control equation

$$
\begin{aligned}
&-\Delta_s T_c + T_c - \frac{\alpha \nabla T_a \cdot \mathbf{n}|_{\Gamma_c}}{\lambda} = 0 \quad && \text{on } \Gamma_c\,,\\
&T_c = 0 && \text{on } \partial\Gamma_c\,,
\end{aligned}
\tag{5.86}
$$

5.3.4. Numerical algorithm

The optimality system consists of three groups of equations: the state equations (5.28)-(5.29), the adjoint state equations (5.81)-(5.84) and the optimality conditions for T_c (5.74). Since the coupled solution of the system is extremely expensive, we uncouple the state, adjoint, and control equations. We may construct an iterative method to iterate among the three groups of equations so that at each iteration we are dealing with a smaller size system of equations. We consider a gradient method for the solution of the optimality problem and the gradient of the functional is determined with the help of the solution of the adjoint system. Let us consider the gradient method for the following minimization problem: find $T_c \in H_0^1(\Gamma_c)$ such that $\mathcal{F}(T_c) := \mathcal{J}(\mathbf{u}(T_c), k(T_c), T_c)$ is minimized, with $\mathcal{J}$ reported in Equation (5.22). Given $T_c^{(0)}$, we can define the sequence

$$
T_c^{(n+1)} = T_c^{(n)} - \rho^{(n)} \frac{d\mathcal{F}(T_c^{(n)})}{dT_c^{(n)}}\,,
\tag{5.87}
$$

recursively, where $\rho^{(n)}$ is a variable step size. Let $\hat{T}_c$ be a solution of the minimization problem, thus the following necessary condition holds

$$
\frac{d\mathcal{F}(\hat{T}_c)}{d\hat{T}_c} = \frac{d\mathcal{J}(\mathbf{u}(\hat{T}_c), k(\hat{T}_c), \hat{T}_c)}{d\hat{T}_c} = 0\,,
\tag{5.88}
$$

then at the optimum state the equality $T_c^{(n+1)} = T_c^{(n)}$ holds. For each fixed T_c, the Gâteaux derivative $(d\mathcal{F}(T_c)/dT_c) \cdot \widetilde{T}_c$ for every direction $\widetilde{T}_c \in H^1(\Gamma_c)$

may be computed

$$\frac{d\mathcal{F}(T_c)}{dT_c}\cdot\widetilde{T}_c = \lambda_1(T_c,\widetilde{T}_c)_{\Gamma_c} + \lambda_2(\nabla_s T_c,\nabla_s\widetilde{T}_c)_{\Gamma_c} + \alpha_u(\mathbf{u}-\mathbf{u}_d,\widetilde{\mathbf{u}})_{\Omega_d} + \\ + \alpha_k(k-k_d,\widetilde{k})_{\Omega_d}\,, \tag{5.89}$$

where $\widetilde{\mathbf{u}}$ and $\widetilde{k}$ are the solution of $M'(\mathbf{z})\cdot\widetilde{\mathbf{z}}=\mathbf{0}$, obtained by setting $\bar{\mathbf{b}}=\mathbf{0}$ in Equations (5.57) and (5.58). Following the procedure described in Chapter 4 for the Dirichlet optimal control, we find that

$$\alpha_u(\mathbf{u}-\mathbf{u}_d,\widetilde{\mathbf{u}})_{\Omega_d} + \alpha_k(k-k_d,\widetilde{k})_{\Omega_d} = (\widetilde{T}_c,q_a)_{\Gamma_c}\,. \tag{5.90}$$

Thus, the Gâteaux derivative may be computed as

$$\frac{d\mathcal{F}(T_c)}{dT_c}\cdot\widetilde{T}_c = \lambda_2(\nabla_s T_c,\nabla_s\widetilde{T}_c)_{\Gamma_c} + \lambda_1(T_c,\widetilde{T}_c)_{\Gamma_c} + (\widetilde{T}_c,q_a)_{\Gamma_c}\,, \tag{5.91}$$

or

$$\frac{d\mathcal{F}(T_c)}{dT_c} = -\lambda_2\Delta_s T_c + \lambda_1 T_c + q_a\,. \tag{5.92}$$

The optimization algorithm is reported in the following.

a) Initialization:
   1. choose tolerance τ and $T_c^{(0)}$; set $n=0$ and $\rho=1$;
   2. solve for $(\mathbf{u}^{(0)},p^{(0)},T^{(0)},k^{(0)},\omega^{(0)})$ from equations (5.28)-(5.29) with $T_c=T_c^{(0)}$;
   3. evaluate $\mathcal{J}^{(0)}=\mathcal{J}(\mathbf{u}^{(0)},k^{(0)},T_c^{(0)})$ using (5.22);

b) main loop:
   1. set $n=n+1$;
   2. solve for $(\mathbf{u}_a^{(n)},p_a^{(n)},T_a^{(n)},k_a^{(n)},\omega_a^{(n)})$ from (5.81)-(5.83);
   3. solve for $T_c^{(n)}$ from

$$-\Delta_s T_c^{(n)} + T_c^{(n)} = -\Delta_s T_c^{(n-1)} + T_c^{(n-1)} + \\ -\rho^{(n)}\Big(-\frac{\lambda_2}{\lambda_1}\Delta_s T_c^{(n-1)} + T_c^{(n-1)} + \\ +\frac{\alpha}{\lambda_1}\nabla T_a^{(n)}\cdot\mathbf{n}|_{\Gamma_c}\Big)\,. \tag{5.93}$$

   4. solve for $(\mathbf{u}^{(n)},p^{(n)},T^{(n)},k^{(n)},\omega^{(n)})$ with $T_c=T_c^{(n)}$;

5. evaluate $\mathcal{J}^{(n)} = \mathcal{J}(\mathbf{u}^{(n)}, k^{(n)}, T_c^{(n)})$ using (4.23);
   i) if $\mathcal{J}^{(n)} > \mathcal{J}^{(n-1)}$, set $\rho^{(n)} = 0.5\rho^{(n)}$ and go to step b) 3.;
   ii) if $\mathcal{J}^{(n)} < \mathcal{J}^{(n-1)}$, set $\rho^{(n+1)} = 1$ and go to step b) 1.;
   iii) if $|\mathcal{J}^{(n)} - \mathcal{J}^{(n-1)}|/|\mathcal{J}^{(n)}| < \tau$ stop.

The chosen form for the update of the control (5.93) allows enforcing the belonging of T_c to $H_0^1(\Gamma_c)$ and giving more regularity to the control.

5.4. Numerical results

In this section, we report the results obtained by solving the optimality system (5.28)-(5.29), (5.74) and (5.81)-(5.84). Finite element solvers for the adjoint temperature T_a, adjoint turbulent kinetic energy k_a, adjoint specific dissipation rate ω_a, and adjoint viscosity ν_a have been implemented and integrated into the finite element code FEMuS. The constraints on the eddy viscosity (5.21) and on the source terms for turbulent kinetic energy and its specific dissipation rate (5.15)-(5.18) have been included. Also, the gradient algorithm has been implemented in the finite element code.

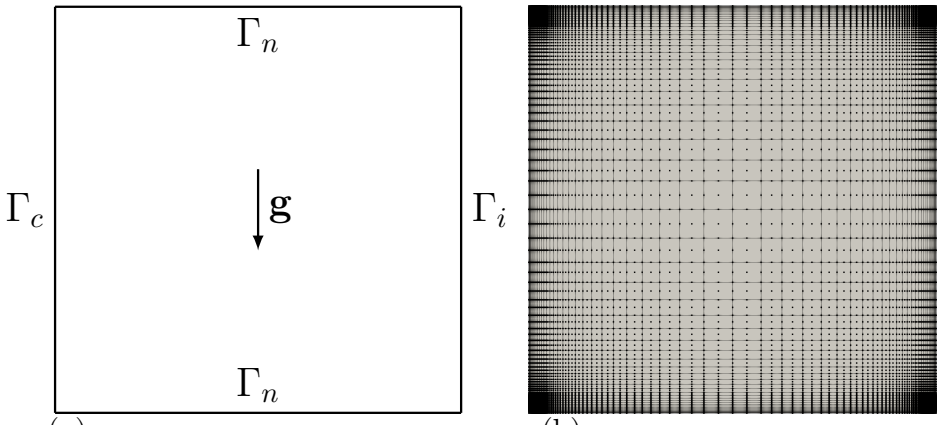

Figure 5.1: Computational domain (a) and computational grid with biquadratic elements (b) for the optimal control of turbulent buoyant flows.

We study a two-dimensional cavity where the flow is driven by buoyancy forces. Let us consider the domain $\Omega = [0, L] \times [0, L] \in \mathbb{R}^2$ reported in Figure 5.1. In our computations, we consider $L = 0.1m$. We set in (5.28)-(5.29) $\mathbf{f} = \mathbf{0}$, $Q = 0$, $\mathbf{g}_u = \mathbf{0}$ and $g_{t,n} = 0$, while $g_k = a_1\delta^2$ and $g_\omega = 2\nu/\beta^*\delta^2$ where

δ is the distance from the wall. Moreover, the function g_t on Γ_d is given as

$$g_t = \begin{cases} 493\ K \text{ on } \Gamma_i\,, \\ 503\ K \text{ on } \Gamma_c\,. \end{cases} \tag{5.94}$$

For the reference case, we set $T_c^{(0)} = 0$. Thus, the horizontal walls of the cavity Γ_n are assumed to be perfectly adiabatic, while the vertical walls are kept isothermal, with the left wall Γ_c at high temperature ($503K$) and the right wall Γ_i at low temperature ($493K$). The interior of the cavity is filled with liquid lead and all properties are calculated at a reference temperature $493K$ and are reported in Table 4.1.

We discretize the numerical problem in a finite element framework, and we consider the computational grid reported in Figure 5.1b consisting of 3960 biquadratic elements where the cells are clustered near the walls to have the first mesh point in the viscous layer and $y^+ < 1$. The computational grid is reported in Figure 5.1b. It is possible to compute the friction velocity u_τ and the corresponding friction Reynolds number. The values of the friction quantities change along the walls, but the maximum values are $u_\tau = 0.00338m/s$ and $Re_\tau = 1895$.

In Figure 5.2 we report the contours of the temperature and velocity fields for the reference case. Due to the heat transfer through the vertical walls, density changes result in a recirculating flow. From the evaluation of the bulk velocity ($U_b = 0.00414m/s$), we can evaluate the Reynolds and Rayleigh numbers, $Re = 2321$ and $Ra = 1.9 \times 10^7$. Since the flow becomes turbulent at $Ra > 10^6$ [94, 108], the considered reference case is in turbulent conditions. We can observe the typical feature of velocity and temperature profiles for $10^6 < Ra < 10^8$ in Figure 5.2. The isotherms at the center of the cavity are horizontal and become vertical only at the boundary layers. The velocity magnitude at the center of the cavity is very small compared with those at the boundaries where the fluid is moving fast, forming narrow vortices and improving the stratification of the flow at the central part of the cavity.

Since the presented optimal control problem allows controlling the velocity $\mathbf{u}_d$ and the turbulence kinetic energy k_d on Ω_d, we consider two different control cases. In particular, we report a velocity matching case, and a turbulent kinetic energy enhancement case.

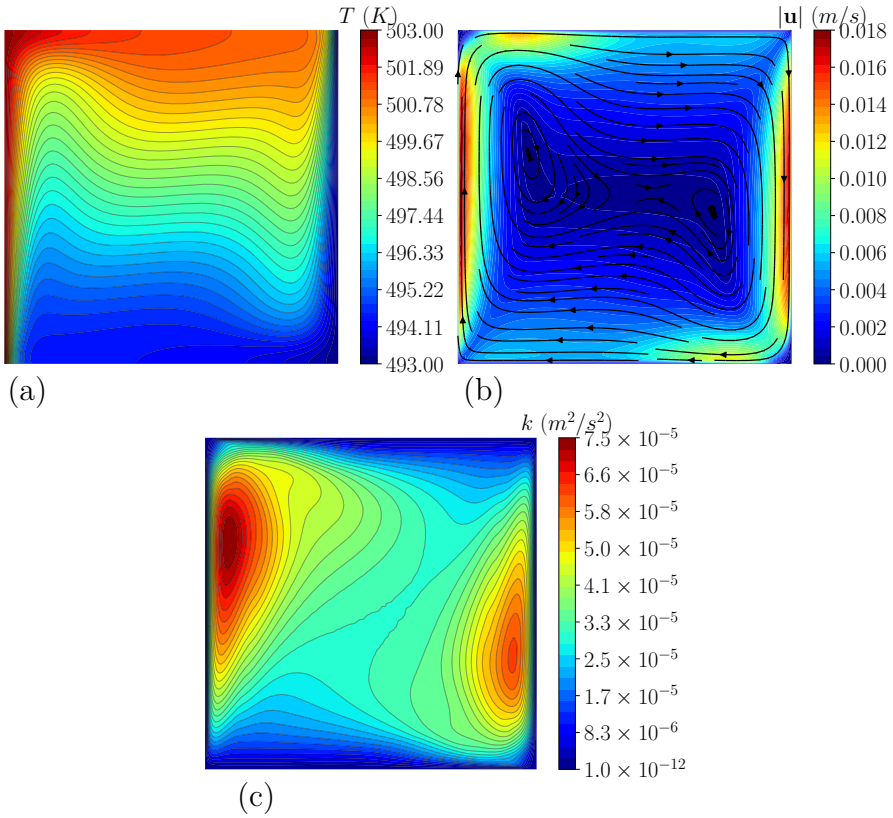

Figure 5.2: Uncontrolled solution: contours of temperature field (a); contours and streamlines of velocity field (b); contours of turbulent kinetic energy field.

Velocity matching case. We first consider a velocity matching case, imposing $\alpha_u = 1$ and $\alpha_k = 0$ in the objective functional reported in Equation (5.22). We set $\Omega_d = [0.45L; 0.55L] \times [0.85L; 0.95L]$. We aim to control the x-component of the velocity $\mathbf{u} = (u, v)$ by setting $u_d = -0.01m/s$. In the reference case, the average x-component of the velocity on Ω_d is $u_b = 0.0047m/s$. Thus, our goal is transforming the clockwise vortex into a counterclockwise flow. The reference functional $\mathcal{J}^{(0)}$ measures 1.562×10^{-8}. We consider different values of regularization coefficients. Firstly, we set $\lambda_1 = \lambda_2 = \lambda$ to have the exact $H^1(\Gamma_c)$-norm as cost contribution in (5.22). Then, we consider different values for the two regularization parameters to show the influence of λ_2 on the control.

Let us consider $\lambda_1 = \lambda_2 = \lambda$. Numerical simulations are performed for different values of λ, namely 10^{-6}, 10^{-7} and 10^{-8}. In Table 5.1 we report the objective functional values $\mathcal{J}^{(n)}$ and the number of iterations n of the

Table 5.1: Velocity matching case: objective functional, percentage reduction and number of iterations of the optimization algorithm for different $\lambda = \lambda_1 = \lambda_2$ values.

λ	10^{-6}	10^{-7}	10^{-8}	Reference
$\mathcal{J}^{(n)} \times 10^9$	14.15	3.128	1.882	15.62
% Reduction	−9.41	−80.0	−87.9	0
Iterations n	9	4	2	0

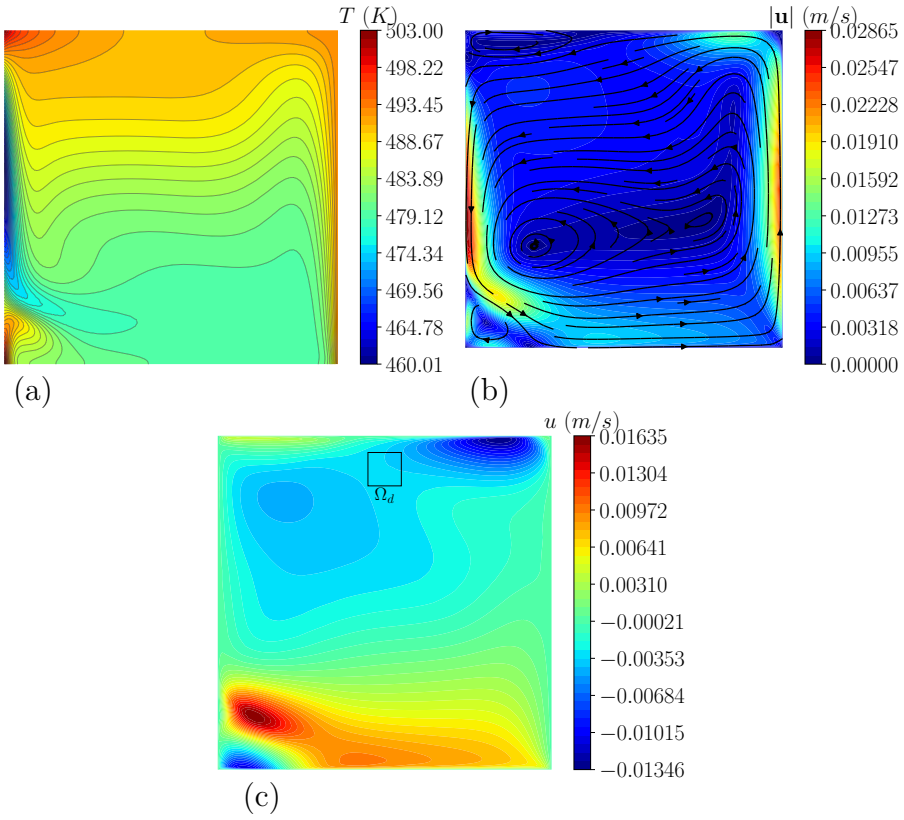

Figure 5.3: Velocity matching case: optimal solution for $\lambda = 10^{-7}$. Contours of the temperature field (a), streamlines and contours of the velocity field (b) and contours of x-component of velocity (c).

optimization algorithm. Also, the percentage reduction of the functional $\mathcal{J}^{(n)}$ with respect to the reference value is reported. For the highest value of λ (10^{-6}), the control is poor and the functional is quite similar to the reference value. With the lowest value of λ, we have the lowest functional

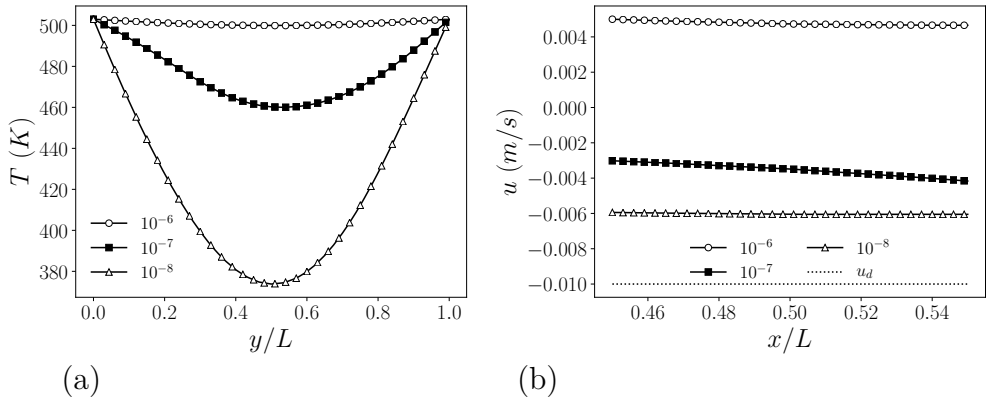

Figure 5.4: Velocity matching case: temperature profiles on the controlled boundary Γ_c (a) and x-component of velocity profiles on the region Ω_d along the line $y/L = 0.9$ (b). Numerical results for $\lambda = 10^{-6}, 10^{-7}$ and 10^{-8}.

value and the greatest percentage reduction.

In Figure 5.3a contours of the controlled temperature field are shown for $\lambda = 10^{-7}$. To obtain a reverse flow, the average temperature along Γ_c must be lower than the temperature along the opposite wall, Γ_d. At the boundaries of the wall, we have $T_c = 0$ on $\partial\Gamma_c$ and $T = g_t$, as stated by Equation (5.86). Contours and streamlines of velocity field are shown in Figure 5.3b. We can observe the formation of a counterclockwise vortex and the increase of the velocity magnitude, as asked with the objective. In Figure 5.3c, contours of the x-component of the velocity are reported and the region Ω_d is highlighted.

The temperature profiles along the controlled boundary Γ_c are reported for the different values of $\lambda = \lambda_1 = \lambda_2$ in Figure 5.4a. As observed from the functional values in Table 5.1, the control in the case $\lambda = 10^{-6}$ has no effect and we obtain a temperature profile almost uniform and equal to the reference. As λ decreases, the temperature profile presents a stationary point for $0.4 < y/L < 0.6$. The minimum value decreases as λ decreases. In Figure 5.4b, the x-component of the velocity is plotted along a line at $y/L = 0.9$ for $0.45 < x/L < 0.55$ in the region Ω_d. The profiles of velocity are reported for all values of λ and also the target velocity profile u_d is shown. We can observe that in cases with $\lambda \leq 10^{-7}$ the flow changes from clockwise to counterclockwise with a negative x-component of velocity in the top of the cavity. With $\lambda = 10^{-6}$, the control is too poor and ineffective since we still have a clockwise vortex.

During the control process, depending on the values of λ, the optimal temperature fields show considerable changes with respect to the reference case. In Table 5.2 we report the bulk velocity U_b and the average temperature differences between the left and right wall boundaries ΔT_{avg}. Rayleigh and Reynolds numbers are also reported for the considered values of λ. As λ decreases, Re and Ra increase and the flow becomes more turbulent. The condition $y^+ < 1$ is still observed for all the simulations.

Table 5.2: Velocity matching case: comparison of bulk velocity, average temperature difference, bulk Reynolds number and Rayleigh number for different values of λ.

λ	$U_b(mm/s)$	ΔT_{avg} (K)	Re_b	Ra
Reference	4.14	10	2321	1.9×10^7
10^{-6}	3.87	2	2170	3.9×10^6
10^{-7}	5.40	22	3028	4.3×10^7
10^{-8}	7.25	77	4065	1.5×10^8

Table 5.3: Velocity matching case: objective functional, percentage reduction and number of iterations of the optimization algorithm for different λ_2 values and $\lambda_1 = 10^{-7}$.

λ_2	10^{-6}	10^{-7}	10^{-8}	10^{-9}	Reference
$\mathcal{J}^{(n)} \times 10^9$	8.491	3.128	0.9115	0.1765	15.62
% Reduction	-45.6	-80.0	-94.2	-98.9	0
Iterations n	4	4	21	36	0

We consider now separate choices for λ_1 and λ_2. Let λ_1 be equal to 10^{-7}, for λ_2 we consider different values, namely 10^{-6}, $10^{-7}, 10^{-8}$ and 10^{-9}. The case with $\lambda_2 = 10^{-7}$ is a standard case with $\lambda_1 = \lambda_2 = \lambda$ previously described with optimal solution reported in Figure 5.3.

In Table 5.3 the values of objective functional and the percentage reductions are reported for the different choices of λ_2. Also, the number of iterations of the numerical algorithm is included. Holding constant λ_1, we can analyze the impact of the coefficient λ_2 which penalizes the norm of the surface gradient of the control T_c in the cost contribution. If $\lambda_2 \to 0$, the control belongs to $L^2(\Gamma_c)$ instead of $H^1(\Gamma_c)$. We can observe that for

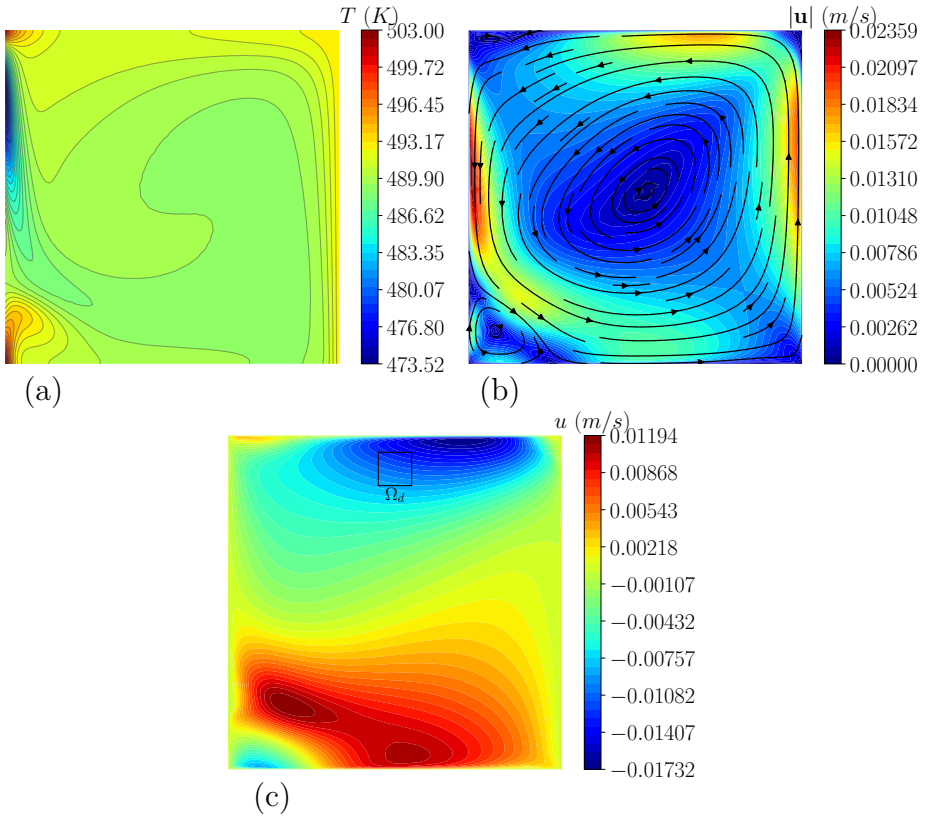

Figure 5.5: Velocity matching case: optimal solution for $\lambda_1 = 10^{-7}$ and $\lambda_2 = 10^{-9}$. Contours of the temperature field (a), streamlines and contours of the velocity field (b) and contours of x-component of velocity (c).

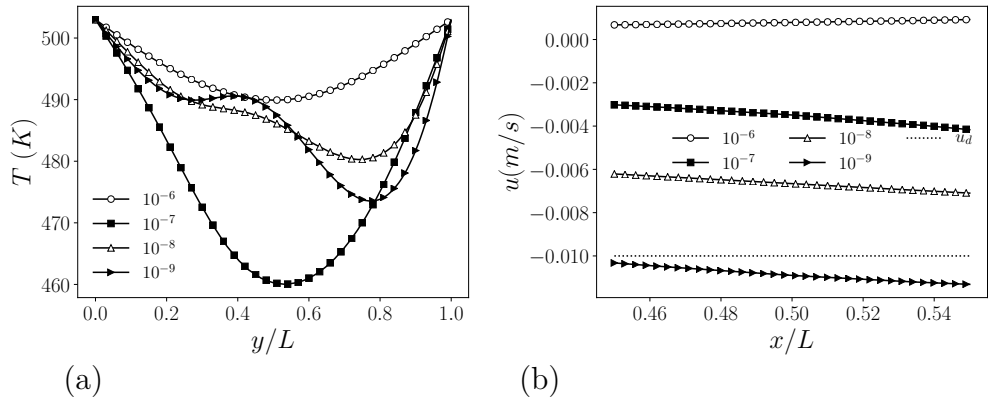

Figure 5.6: Velocity matching case: temperature profiles on the controlled boundary Γ_c (a) and x-component of velocity profiles on the region Ω_d along the line $y/L = 0.9$ (b). Numerical results for $\lambda_2 = 10^{-6}, 10^{-7}, 10^{-8}, 10^{-9}$ and $\lambda_1 = 10^{-7}$.

$\lambda_2 > \lambda_1$ the control is less effective and the functional reduction is poor. For $\lambda_2 < \lambda_1$ we observe large functional decreases.

Contours of the optimal temperature field are shown in Figure 5.5a for $\lambda_1 = 10^{-7}$ and $\lambda_2 = 10^{-9}$. Streamlines and contours of the optimal velocity field are reported in Figure 5.5b. Comparing Figure 5.5 and 5.3, we can observe that with a lower regularization parameter λ_2, the solution is sharper and more irregular. The velocity field on Ω_d is nearer to the target profile u_d. This aspect can be observed also by Figure 5.6b where the velocity u is plotted on Ω_d at $y/L = 0.9$ and $0.45 < x/L < 0.55$ for different values of λ_2. The lowest value of λ_2 (10^{-9}) brings the optimal solution with the largest functional reduction. With the highest value of λ_2 (10^{-6}), in contrast, we have poor control and a counterclockwise flow with low velocity magnitude. Lastly, in Figure 5.6a the temperature profiles on Γ_d are reported for all values of λ_2. As noticed by the previous comparisons, with low values of λ_2 the control is more effective and the temperature on the boundary presents stationary and inflection points.

Turbulence kinetic energy enhancement case. In the second test we aim to enhance the turbulence inside the cavity. This goal can be achieved considering in the objective functional (5.22) $\alpha_u = 0$ and $\alpha_k = 1$. The turbulent kinetic energy contours for the reference case are reported in Figure 5.2c. As target profile of turbulent kinetic energy we may set $k_d = 0.0001 m^2/s^2$ since in the reference case the turbulent kinetic energy is everywhere smaller than this value, in particular $k^{(0)}_{max} \approx 7.5 \times 10^{-5}\ m^2/s^2$. Let $\Omega_d = [0.10L; 0.20L] \times [0.45L, 0.55L]$ be the region where we aim to minimize the functional (5.22). In the reference case, the functional value is $\mathcal{J}^{(0)} = 1.818 \times 10^{-13}$.

The choice of values for the regularization parameters is crucial. A turbulence enhancement problem is more complex than a velocity or temperature matching problem. As we have observed in Chapter 4, a control problem with an objective on the temperature field is the easiest to solve, since the distance from the objective T_d appears as a source term in the adjoint temperature equation and the control depends on the normal gradient of T_a. Thus, the link between objective and control is almost direct. With a velocity control problem, this link is indirect. Indeed, the distance from the objective $\mathbf{u}_d$ appears as a source term in the adjoint Navier-Stokes equation. The adjoint velocity $\mathbf{u}_a$, in its turn, appears as a source term in

the adjoint temperature equation. Thus, the objective acts on $\mathbf{u}_a$, which influences T_a, which gives the control T_c. With a turbulence optimization problem, the link is even more indirect. Analyzing the optimality system in strong form (5.85), the distance from the objective k_d appears in the equation for the adjoint turbulent kinetic energy k_a. The gradient of this adjoint variable appears as a source term in the adjoint temperature equation, but this contribution is negligible. Thus, k_a influences only the adjoint velocity $\mathbf{u}_a$, which affects the adjoint temperature T_a. For this reason, we need very low regularization parameters to make the control effective.

Table 5.4: Turbulence enhancement case: objective functional, percentage reduction and number of iterations of the optimization algorithm for different $\lambda = \lambda_1 = \lambda_2$ values.

λ	10^{-11}	10^{-12}	10^{-13}	Reference
$\mathcal{J}^{(n)} \times 10^{14}$	16.35	4.079	2.561	18.18
% Reduction	-10.1	-77.6	-85.9	0
Iterations n	6	3	2	0

Table 5.5: Turbulence enhancement case: comparison of bulk velocity, average temperature difference, bulk Reynolds number and Rayleigh number for different values of λ.

λ	$U_b(mm/s)$	ΔT_{avg} (K)	Re_b	Ra
Reference	4.14	10	2321	1.9×10^7
10^{-11}	4.36	11	2445	2.1×10^7
10^{-12}	5.24	19	2938	3.7×10^7
10^{-13}	6.19	33	3471	6.5×10^7

We report the numerical results for $\lambda = \lambda_1 = \lambda_2$ with regularization parameter values equal to 10^{-11}, 10^{-12} and 10^{-13}. In Table 5.4 the functional values at the end of the optimization process $\mathcal{J}^{(n)}$ are reported for each regularization parameter. Also, the number of iterations of the optimization algorithm is included. We can observe that the case with $\lambda = 10^{-11}$ is ineffective since $\mathcal{J}^{(n)} \approx \mathcal{J}^{(0)}$. For lower values of λ, we have satisfactory functional reductions. The case with the lowest value of λ is the one with the strongest functional reduction.

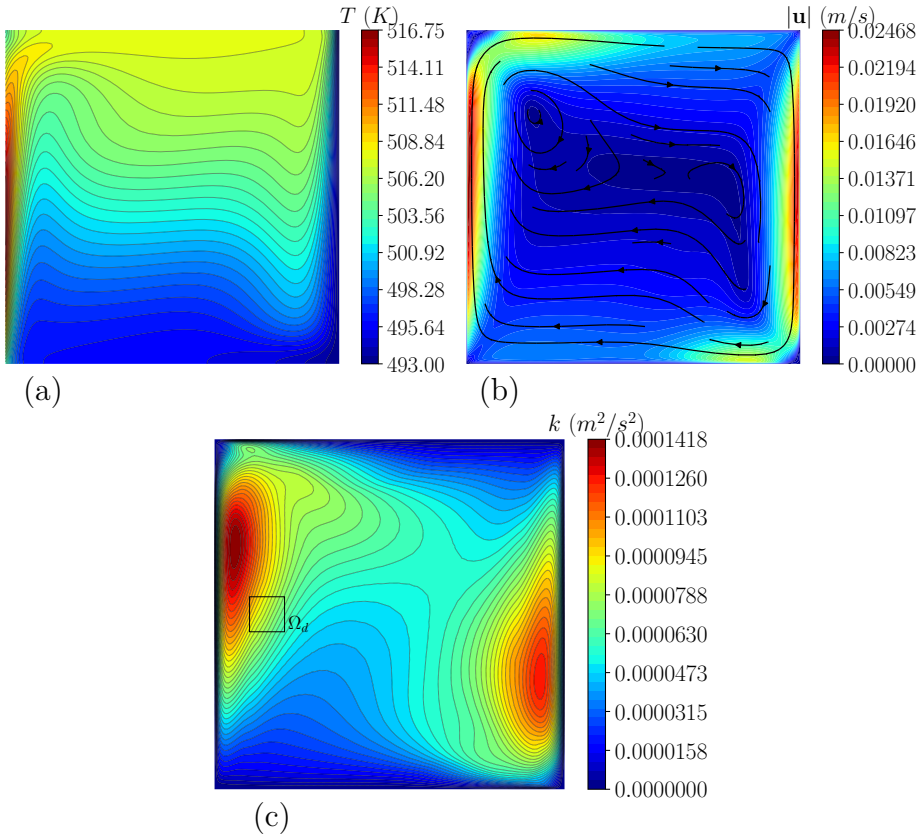

Figure 5.7: Turbulence enhancement case: optimal solution for $\lambda_1 = \lambda_2 = \lambda = 10^{-12}$. Contours of optimal temperature field $T^{(n)}$ (a), contours and streamlines of optimal velocity field $\mathbf{u}^{(n)}$ (b), contours of turbulent kinetic energy $k^{(n)}$.

In Figure 5.7c the optimal distribution of turbulent kinetic energy is reported for $\lambda = \lambda_1 = \lambda_2 = 10^{-12}$. The maximum values of turbulent kinetic energy are located in the proximity of Ω_d and in the left top corner near the controlled boundary. This peak is due to the strong temperature gradients in that region that can be observed in Figure 5.7c. Here, the temperature profile on the domain is reported. The temperature on Γ_c has increased and the buoyancy forces are more effective than in the uncontrolled case. The fluid accelerates and the turbulence increases. However, on Ω_d the turbulent kinetic energy mean value is higher than the target k_d.

The temperature profiles on Γ_d are reported in Figure 5.8a for each value of λ. When $\lambda = 10^{-11}$, the control is very poor and the temperature profile is approximately the same as the reference case. With $\lambda = 10^{-12}$ and 10^{-13}, the temperature on Γ_c is higher than in the reference case. The

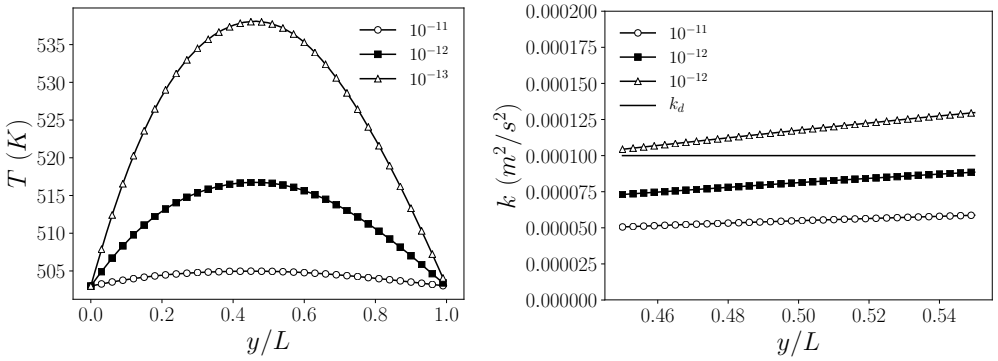

(a) (b)

Figure 5.8: Turbulence enhancement case: temperature profiles on the controlled boundary Γ_c (a) and turbulent kinetic energy profiles on the region Ω_d along the line $x/L = 0.155$ (b). Numerical results for $\lambda = 10^{-11}, 10^{-12}$ and 10^{-13}.

temperature difference between the two vertical walls increases, buoyancy effects are strong and the turbulence in the cavity is enhanced. In Figure 5.8b the turbulent kinetic energy profile on Ω_d is plotted at $x/L = 0.15$ for $0.45 < y/L < 0.55$. With the lowest values of λ, we obtain a good match of the optimal solution with the target profile k_d reported with a solid line in the graph.

In Table 5.5 we report the bulk velocity U_b and the average temperature differences between the left and right wall boundaries ΔT_{avg}. Rayleigh and Reynolds numbers are also reported. For all the considered values of λ, the flow becomes more turbulent. The condition $y^+ < 1$ on first mesh points is still observed for all the simulations.

Conclusion

This Ph.D. thesis deals with the development of a numerical platform for the modeling and the optimal control of liquid metal flows. Liquid metals with their interesting thermal properties are widely studied for heat transfer applications. In the nuclear context, they are investigated for liquid metals-cooled reactors. Due to the low Prandtl number, however, the standard turbulence models employed for common coolants, like water or air, are not appropriate, and more sophisticated models able to capture the flow and heat transfer anisotropy are necessary.

In this framework, one of the aims of this work was to present and validate a new anisotropic four-parameter turbulence model that derives from the isotropic four-parameter turbulence model widely studied and already implemented in the multigrid finite element code FEMuS. An Explicit Algebraic Stress Model (EASM) and an Explicit Algebraic Heat Flux Model (EAHMF) were proposed for the closure of the Reynolds stresses and turbulent heat flux instead of the first-order closure relations used in the isotropic version of the model. Special attention was given to the modeling of the dynamical and thermal time scales to overcome the local equilibrium hypothesis typical of algebraic models and to predict the near-wall and bulk behavior of turbulent quantities. The closure of the model and estimation of the time scales were performed with four transport equations for the logarithmic variables K-Ω-K_θ-Ω_θ and suitable near-wall boundary conditions were presented. For the validation of the new anisotropic four-parameter turbulence model, three different geometrical configurations were consid-

ered, i.e., plane channel, cylindrical pipe, and backward-facing step. For the first two geometries, the condition of fully developed flows was simulated in forced convection considering different Re and low Pr numbers. For the backward-facing step, both forced and mixed convection regimes with $Ri = 0.338$ were considered to include the effects of buoyancy forces in the validation study. The simulation results were compared with the available DNS data whenever possible and with the numerical results obtained by using the isotropic version of the model. For the cylindrical pipe, few DNS data are present in the literature for low Prandtl number fluids, then a validation based on integral quantities and empirical correlations was proposed. For all configurations, the prediction of the velocity and temperature fields is in good agreement with DNS reference data. For the forced convection over the backward-facing step configuration, we could observe a general improvement in the prediction of dynamical and thermal fields, above all in the estimation of the turbulent heat flux components. It can be concluded that the anisotropic four-parameter turbulence model represents a promising approach toward the accurate prediction of both turbulent momentum and heat flux for low Prandtl number fluids. Further simulations, including complex geometries, different Ri numbers, and natural convection cases, are necessary to extend the validation of the presented model.

Since buoyancy effects cannot be neglected in liquid metals-cooled reactors, in the design and study of these devices we need tools to simulate and optimize liquid metal flows and heat transfer in mixed and natural convection. Thus, the second aim of this work was to provide tools for the optimal control of turbulent buoyant flows. Firstly, a mathematical analysis for Dirichlet, Neumann, and distributed optimal control problems was proposed for the Boussinesq equations. Then, in the governing equations describing the state of the fluid we included the turbulence within a RANS framework. We proposed the mathematical analysis of a Dirichlet boundary optimal control problem for the Reynolds Averaged Navier-Stokes and energy system closed with a k-ω model and Reynolds analogy. In particular, by starting from the existence of the solution of the Navier-Stokes system coupled with the energy equation, and the existence of the solution of the k-ω turbulence model, the existence of the coupled associated boundary value problem was proved. We then introduced a boundary optimal control problem to obtain the desired velocity and/or desired turbulence kinetic energy on a domain, by controlling the temperature on a boundary. The

optimality system was obtained through the Lagrange multiplier method. In particular, we proved that the Lagrange multiplier technique is well-posed and can be used to obtain the first-order necessary condition. Lastly, a numerical algorithm based on the gradient method was introduced for the numerical implementation of the proposed optimality system in a finite element framework. Then, some numerical results were shown, considering both velocity matching and turbulent kinetic energy enhancement cases. In particular, the dependence on the regularization parameters was analyzed to show consistency with the expectations, the robustness of the algorithm, and the feasibility of the method.

List of figures

List of tables

Bibliography

[1] A. Heinzel, W. Hering, J. Konys, L. Marocco, K. Litfin, G. Müller, J. Pacio, C. Schroer, R. Stieglitz, L. Stoppel, *et al.*, "Liquid metals as efficient high-temperature heat-transport fluids," *Energy Technology*, vol. 5, no. 7, pp. 1026–1036, 2017. 3

[2] L. Marocco, G. Cammi, J. Flesch, and T. Wetzel, "Numerical analysis of a solar tower receiver tube operated with liquid metals," *International Journal of Thermal Sciences*, vol. 105, pp. 22–35, 2016. 3

[3] D. Frazer, E. Stergar, C. Cionea, and P. Hosemann, "Liquid metal as a heat transport fluid for thermal solar power applications," *Energy Procedia*, vol. 49, pp. 627–636, 2014. 3

[4] S. Manservisi and F. Menghini, "Triangular rod bundle simulations of a CFD κ-ε-κ_θ-ε_θ heat transfer turbulence model for heavy liquid metals," *Nuclear Engineering and Design*, vol. 273, pp. 251–270, 2014. 3, 61, 62, 63, 65

[5] X. Cheng and N. Tak, "Investigation on turbulent heat transfer to lead–bismuth eutectic flows in circular tubes for nuclear applications," *Nuclear Engineering and Design*, vol. 236, no. 4, pp. 385–393, 2006. 3

[6] J. Pacio, K. Litfin, A. Batta, M. Viellieber, A. Class, H. Doolaard, F. Roelofs, S. Manservisi, F. Menghini, and M. Böttcher, "Heat transfer to liquid metals in a hexagonal rod bundle with grid spacers: Ex-

perimental and simulation results," *Nuclear Engineering and Design*, vol. 290, pp. 27–39, 2015. 3

[7] F. Roelofs, A. Shams, I. Otic, M. Böttcher, M. Duponcheel, Y. Bartosiewicz, D. Lakehal, E. Baglietto, S. Lardeau, and X. Cheng, "Status and perspective of turbulence heat transfer modelling for the industrial application of liquid metal flows," *Nuclear Engineering and Design*, vol. 290, pp. 99–106, 2015. 3

[8] T. Schulenberg and R. Stieglitz, "Flow measurement techniques in heavy liquid metals," *Nuclear Engineering and Design*, vol. 240, no. 9, pp. 2077–2087, 2010. 3

[9] G. Grötzbach, *Anisotropy and Buoyancy in Nuclear Turbulent Heat Transfer: Critical Assessment and Needs for Modelling.* Citeseer, 2007. 4, 49, 61, 76, 77

[10] A. Shams, A. De Santis, L. Koloszar, A. V. Ortiz, and C. Narayanan, "Status and perspectives of turbulent heat transfer modelling in low-Prandtl number fluids," *Nuclear Engineering and Design*, vol. 353, p. 110220, 2019. 5, 50

[11] S. Manservisi and F. Menghini, "A CFD four parameter heat transfer turbulence model for engineering applications in heavy liquid metals," *International Journal of Heat and Mass Transfer*, vol. 69, pp. 312–326, 2014. 5, 50, 61, 62, 63, 65, 82

[12] R. Da Via, S. Manservisi, and F. Menghini, "A k-ω-k_θ-ω_θ four parameter logarithmic turbulence model for liquid metals," *International Journal of Heat and Mass Transfer*, vol. 101, pp. 1030–1041, 2016. 5, 50, 59, 61, 62, 63, 65, 76, 79, 81, 82, 88, 93

[13] R. Da Và, V. Giovacchini, and S. Manservisi, "A Logarithmic Turbulent Heat Transfer Model in Applications with Liquid Metals for $Pr = 0.01$–0.025," *Applied Sciences*, vol. 10, no. 12, p. 4337, 2020. 5, 50, 63, 65, 76, 79, 80, 81, 88, 93

[14] R. Da Và and S. Manservisi, "Numerical simulation of forced and mixed convection turbulent liquid sodium flow over a vertical backward facing step with a four parameter turbulence model," *Interna-*

tional Journal of Heat and Mass Transfer, vol. 135, pp. 591–603, 2019. 5, 50, 63, 79, 81, 102, 107

[15] A. Chierici, G. Barbi, G. Bornia, D. Cerroni, L. Chirco, R. Da Vià, V. Giovacchini, S. Manservisi, R. Scardovelli, and A. Cervone, "FEMuS-Platform: a numerical platform for multiscale and multiphysics code coupling," in *9th edition of the International Conference on Computational Methods for Coupled Problems in Science and Engineering (COUPLED PROBLEMS 2021)*, 2021. 5, 76, 84

[16] R. Da Vià, "Development of a computational platform for the simulation of low Prandtl number turbulent flows," 2019. 5, 79, 80, 81

[17] D. Cerroni, "Multiscale multiphysics coupling on a finite element platform," 2016. 5

[18] G. Barbi, V. Giovacchini, and S. Manservisi, "A New Anisotropic Four-Parameter Turbulence Model for Low Prandtl Number Fluids," *Fluids*, vol. 7, no. 1, p. 6, 2022. 5, 83

[19] G. Barbi, A. Chierici, L. Chirco, V. Giovacchini, S. Manservisi, and L. Sirotti, "Numerical simulation of a low Prandtl number flow with a four-parameters turbulence model through an explicit algebraic definition of Reynolds stress and turbulent heat flux," in *Journal of Physics: Conference Series*, vol. 2177, p. 012005, IOP Publishing, 2022. 5, 83

[20] G. Barbi, A. Chierici, V. Giovacchini, F. Quarta, and S. Manservisi, "Numerical simulation of a low Prandtl number flow over a backward facing step with an anisotropic four-equation turbulence model," in *Journal of Physics: Conference Series*, vol. 2177, p. 012006, IOP Publishing, 2022. 5, 83

[21] C. F. Smith and L. Cinotti, "Lead-cooled fast reactor," in *Handbook of Generation IV Nuclear Reactors*, pp. 119–155, Elsevier, 2016. 6, 122

[22] H.-C. Lee and S.-H. Kim, "Finite element approximation and computations of optimal Dirichlet boundary control problems for the Boussinesq equations," *Journal of the Korean Mathematical Society*, vol. 41, no. 4, pp. 681–715, 2004. 6, 168

[23] H.-C. Lee and O. Y. Imanuvilov, "Analysis of optimal control problems for the 2-D stationary Boussinesq equations," *Journal of mathematical analysis and applications*, vol. 242, no. 2, pp. 191–211, 2000. 6, 137, 143, 168

[24] E. Aulisa, G. Bornia, and S. Manservisi, "Boundary Control Problems in Convective Heat Transfer with Lifting Function Approach and Multigrid Vanka-Type Solvers," *Commun. Comput. Phys.*, vol. 189, pp. 621–649, 2015. 6

[25] M. D. Gunzburger, *Perspectives in flow control and optimization*, vol. 5. Siam, 2003. 6, 122

[26] H.-C. Lee and B. C. Shin, "Piecewise optimal distributed controls for 2D Boussinesq equations," *Mathematical methods in the applied sciences*, vol. 23, no. 3, pp. 227–254, 2000. 6, 121

[27] L. Chirco, V. Giovacchini, and S. Manservisi, "An adjoint-based temperature boundary optimal control approach for turbulent buoyancy-driven flows," in *Journal of Physics: Conference Series*, vol. 1599, p. 012041, IOP Publishing, 2020. 6

[28] A. Chierici, V. Giovacchini, and S. Manservisi, "Analysis and numerical results for boundary optimal control problems applied to turbulent buoyant flows," *International Journal of Numerical Analysis & Modeling*, vol. 19, no. 2-3, pp. 347–368, 2022. 6

[29] S. B. Pope, *Turbulent flows*. Cambridge university press, 2000. 17, 33, 42, 53, 55, 56, 66

[30] P. Bradshaw, T. Cebeci, and J. H. Whitelaw, "Engineering calculation methods for turbulent flow," *NASA STI/Recon Technical Report A*, vol. 82, p. 20300, 1981. 25, 51, 54

[31] T. Cebeci, *Analysis of turbulent flows with computer programs*. Butterworth-Heinemann, 2013. 25, 27, 36

[32] F. H. Harlow and P. I. Nakayama, "Turbulence transport equations," *The Physics of Fluids*, vol. 10, no. 11, pp. 2323–2332, 1967. 29, 54

[33] B. A. Younis, C. G. Speziale, and T. T. Clark, "A rational model for the turbulent scalar fluxes," *Proceedings of the Royal Society A: Mathematical, Physical and Engineering Sciences*, vol. 461, no. 2054, pp. 575–594, 2005. 30

[34] B. E. Launder, *Heat and Mass Transport*, p. 231–287. Berlin, Heidelberg: Springer Berlin Heidelberg, 1976. 31, 32, 74, 75

[35] R. D. Moser, J. Kim, and N. N. Mansour, "Direct numerical simulation of turbulent channel flow up to Re_τ= 590," *Physics of fluids*, vol. 11, no. 4, pp. 943–945, 1999. 36, 52, 55, 64, 207, 208

[36] B. Weigand, *Analytical methods for heat transfer and fluid flow problems*, vol. 263. Springer, 2004. 37

[37] F. Alcántara-Ávila, S. Hoyas, and M. J. Pérez-Quiles, "DNS of thermal channel flow up to Re_τ= 2000 for medium to low Prandtl numbers," *International Journal of Heat and Mass Transfer*, vol. 127, pp. 349–361, 2018. 38, 45, 46, 47, 83, 84, 207

[38] P. Bradshaw and G. P. Huang, "The law of the wall in turbulent flow," *Proceedings of the Royal Society of London. Series A: Mathematical and Physical Sciences*, vol. 451, no. 1941, pp. 165–188, 1995. 42, 44, 46

[39] J. Kim, P. Moin, and R. Moser, "Turbulence statistics in fully developed channel flow at low Reynolds number," *Journal of Fluid Mechanics*, vol. 177, pp. 133–166, 1987. 43, 207

[40] B. Kader, "Temperature and concentration profiles in fully turbulent boundary layers," *International Journal of Heat and Mass Transfer*, vol. 24, no. 9, pp. 1541–1544, 1981. 45, 46

[41] B. Kader and A. Yaglom, "Heat and mass transfer laws for fully turbulent wall flows," *International Journal of Heat and Mass Transfer*, vol. 15, no. 12, pp. 2329–2351, 1972. 45

[42] H. Kawamura, H. Abe, and Y. Matsuo, "DNS of turbulent heat transfer in channel flow with respect to Reynolds and Prandtl number effects," *International Journal of Heat and Fluid Flow*, vol. 20, no. 3, pp. 196–207, 1999. 47, 82, 83, 84

[43] A. De Santis and A. Shams, "Application of an algebraic turbulent heat flux model to a backward facing step flow at low Prandtl number," *Annals of Nuclear Energy*, vol. 117, pp. 32–44, 2018. 50, 102, 104

[44] A. Shams and A. De Santis, "Towards the accurate prediction of the turbulent flow and heat transfer in low-Prandtl fluids," *International Journal of Heat and Mass Transfer*, vol. 130, pp. 290–303, 2019. 50, 61, 65

[45] T. Gatski and C. Rumsey, "Linear and nonlinear eddy viscosity," *Closure strategies for turbulent and transitional flows*, p. 9, 2002. 51

[46] W. P. Jones and B. E. Launder, "The prediction of laminarization with a two-equation model of turbulence," *International journal of heat and mass transfer*, vol. 15, no. 2, pp. 301–314, 1972. 54

[47] K. Hanjalić and B. E. Launder, "A Reynolds stress model of turbulence and its application to thin shear flows," *Journal of Fluid Mechanics*, vol. 52, no. 4, pp. 609–638, 1972. 54

[48] T. Cebeci, *Turbulence models and their application: efficient numerical methods with computer programs*. Springer, 2004. 55, 56

[49] D. C. Wilcox, "Reassessment of the scale-determining equation for advanced turbulence models," *AIAA journal*, vol. 26, no. 11, pp. 1299–1310, 1988. 55, 56

[50] W. P. Jones and B. Launder, "The calculation of low-Reynolds-number phenomena with a two-equation model of turbulence," *International Journal of Heat and Mass Transfer*, vol. 16, no. 6, pp. 1119–1130, 1973. 57

[51] K. Abe, T. Kondoh, and Y. Nagano, "A new turbulence model for predicting fluid flow and heat transfer in separating and reattaching flows—I. Flow field calculations," *International Journal of Heat and Mass Transfer*, vol. 37, no. 1, pp. 139–151, 1994. 58

[52] K. Abe, T. Kondoh, and Y. Nagano, "On Reynolds-stress expressions and near-wall scaling parameters for predicting wall and homogeneous turbulent shear flows," *International Journal of Heat and Fluid Flow*, vol. 18, no. 3, pp. 266–282, 1997. 58, 66, 73, 74, 78

[53] G. Grötzbach, "Challenges in low-Prandtl number heat transfer simulation and modelling," *Nuclear Engineering and Design*, vol. 264, pp. 41–55, 2013. 60, 61, 77

[54] S. Manservisi and F. Menghini, "CFD simulations in heavy liquid metal flows for square lattice bare rod bundle geometries with a four parameter heat transfer turbulence model," *Nuclear Engineering and Design*, vol. 295, pp. 251–260, 2015. 63

[55] K. Abe, T. Kondoh, and Y. Nagano, "A new turbulence model for predicting fluid flow and heat transfer in separating and reattaching flows—II. Thermal field calculations," *International Journal of Heat and Mass Transfer*, vol. 38, no. 8, pp. 1467–1481, 1995. 65, 82

[56] W. M. Kays, "Turbulent Prandtl number. Where are we?," *ASME Transactions Journal of Heat Transfer*, vol. 116, no. 2, pp. 284–295, 1994. 65

[57] S. Pope, "A more general effective-viscosity hypothesis," *Journal of Fluid Mechanics*, vol. 72, no. 2, pp. 331–340, 1975. 66, 68, 70, 72

[58] T. B. Gatski and C. G. Speziale, "On explicit algebraic stress models for complex turbulent flows," *Journal of Fluid Mechanics*, vol. 254, pp. 59–78, 1993. 66, 67, 68, 69, 70, 71

[59] W. Rodi, "The prediction of free turbulent boundary layers by use of a two equation model of turbulence," 1972. 66, 67

[60] C. G. Speziale, S. Sarkar, and T. B. Gatski, "Modelling the pressure–strain correlation of turbulence: an invariant dynamical systems approach," *Journal of Fluid Mechanics*, vol. 227, pp. 245–272, 1991. 68

[61] A. Spencer, "Part III. Theory of invariants," *Continuum physics*, vol. 1, pp. 239–353, 1971. 70

[62] K.-i. Abe, T. Kondoh, and Y. Nagano, "A two-equation heat transfer model reflecting second-moment closures for wall and free turbulent flows," *International Journal of Heat and Fluid Flow*, vol. 17, no. 3, pp. 228–237, 1996. 74, 75, 76, 80

[63] H. Hattori, A. Morita, and Y. Nagano, "Nonlinear eddy diffusivity models reflecting buoyancy effect for wall-shear flows and heat transfer," *International Journal of Heat and Fluid Flow*, vol. 27, no. 4, pp. 671–683, 2006. 74, 77, 78

[64] H. Hattori and Y. Nagano, "Nonlinear two-equation model taking into account the wall-limiting behavior and redistribution of stress components," *Theoretical and Computational Fluid Dynamics*, vol. 17, no. 5, pp. 313–330, 2004. 78

[65] H. Hattori, N. Ohiwa, M. Kozuka, and Y. Nagano, "Improvement of the nonlinear eddy diffusivity model for rotational turbulent heat transfer at various rotating axes," *Fluid dynamics research*, vol. 41, no. 1, p. 012402, 2009. 78

[66] F. Ilinca, D. Pelletier, *et al.*, "A unified finite element algorithm for two-equation models of turbulence," *Computers & fluids*, vol. 27, no. 3, pp. 291–310, 1998. 79

[67] Y. Nagano and M. Shimada, "Development of a two-equation heat transfer model based on direct simulations of turbulent flows with different Prandtl numbers," *Physics of Fluids*, vol. 8, no. 12, pp. 3379–3402, 1996. 82

[68] I. Tiselj and L. Cizelj, "DNS of turbulent channel flow with conjugate heat transfer at Prandtl number 0.01," *Nuclear Engineering and Design*, vol. 253, pp. 153–160, 2012. 83, 84

[69] M. Niemann and J. Fröhlich, "Buoyancy-affected backward-facing step flow with heat transfer at low Prandtl number," *International Journal of Heat and Mass Transfer*, vol. 101, pp. 1237–1250, 2016. 83, 102, 107

[70] P. Moin and J. Kim, "Numerical investigation of turbulent channel flow," *Journal of Fluid Mechanics*, vol. 118, pp. 341–377, 1982. 84

[71] A. Vreman and J. G. Kuerten, "Comparison of direct numerical simulation databases of turbulent channel flow at Re_τ= 180," *Physics of Fluids*, vol. 26, no. 1, p. 015102, 2014. 84

[72] L. Redjem-Saad, M. Ould-Rouiss, and G. Lauriat, "Direct numerical simulation of turbulent heat transfer in pipe flows: Effect of Prandtl number," *International Journal of Heat and Fluid Flow*, vol. 28, no. 5, pp. 847–861, 2007. 98

[73] R. N. Lyon, *Forced convection heat transfer theory and experiments with liquid metals*, vol. 419. United States Atomic Energy Commission, Technical Information Service, 1949. 101

[74] P. Kirillov and P. Ushakov, "Heat transfer to liquid metals : Specific features, methods of investigation, and main relationships," *Thermal Engineering*, vol. 48, pp. 50–59, 2001. 101

[75] E. Skupinski, J. Tortel, and L. Vautrey, "Determination des coefficients de convection d'un alliage sodium-potassium dans un tube circulaire," *International Journal of Heat and Mass Transfer*, vol. 8, no. 6, pp. 937–951, 1965. 101

[76] C. A. Sleicher Jr, "Heat transfer in a pipe with turbulent flow and arbitrary wall-temperature distribution," tech. rep., 1955. 101

[77] W. Stromquist and U. A. E. Commission, *Effect of Wetting on Heat Transfer Characteristics of Liquid Metals: (thesis)*. ORO (Series) (Oak Ridge, Tennessee), United States Atomic Energy Commission, Technical Information Service, 1953. 101

[78] M. K. Ibragimov, V. Subbotin, and P. Ushakov, "Investigation of heat transfer in the turbulent flow of liquid metals in tubes," *The Soviet Journal of Atomic Energy*, vol. 8, no. 1, pp. 48–50, 1961. 101

[79] M. Niemann and J. Fröhlich, "Direct Numerical Simulation of turbulent heat transfer behind a backward-facing step at low Prandtl number," *PAMM*, vol. 14, no. 1, pp. 659–660, 2014. 102

[80] M. Niemann and J. Fröhlich, "Buoyancy Effects on Turbulent Heat Transfer Behind a Backward-Facing Step in Liquid Metal Flow," in *Direct and Large-Eddy Simulation X*, pp. 513–519, Springer, 2018. 102

[81] M. Niemann and J. Fröhlich, "Turbulence budgets in buoyancy-affected vertical backward-facing step flow at low Prandtl number," *Flow, Turbulence and Combustion*, vol. 99, no. 3, pp. 705–728, 2017. 102

[82] T. Schumm, M. Niemann, F. Magagnato, L. Marocco, B. Frohnapfel, and J. Fröhlich, "Numerical prediction of heat transfer in liquid metal applications," in *THMT-15. Proceedings of the Eighth International Symposium On Turbulence Heat and Mass Transfer*, Begel House Inc., 2015. 102

[83] V. Sobolev, "Database of thermophysical properties of liquid metal coolants for GEN-IV," 2011. 103

[84] N. Kasagi and A. Matsunaga, "Three-dimensional particle-tracking velocimetry measurement of turbulence statistics and energy budget in a backward-facing step flow," *International Journal of Heat and Fluid Flow*, vol. 16, no. 6, pp. 477–485, 1995. 108

[85] L. Chirco, A. Chierici, R. Da Vià, V. Giovacchini, and S. Manservisi, "Optimal Control of the Wilcox turbulence model with lifting functions for flow injection and boundary control," in *Journal of Physics: Conference Series*, vol. 1224, p. 012006, IOP Publishing, 2019. 121, 168

[86] M. D. Gunzburger, L. S. Hou, and T. P. Svobodny, "The approximation of boundary control problems for fluid flows with an application to control by heating and cooling," *Computers & fluids*, vol. 22, no. 2-3, pp. 239–251, 1993. 121, 168, 183

[87] H.-C. Lee, "Analysis and computational methods of Dirichlet boundary optimal control problems for 2D Boussinesq equations," *Advances in Computational Mathematics*, vol. 19, no. 1, pp. 255–275, 2003. 121, 127, 129, 173

[88] E. Aulisa, G. Bornia, and S. Manservisi, "Boundary control problems in convective heat transfer with lifting function approach and multigrid Vanka-type solvers," *Communications in Computational Physics*, vol. 18, no. 3, pp. 621–649, 2015. 121, 168

[89] M. D. Gunzburger, H. Kim, and S. Manservisi, "On a shape control problem for the stationary Navier-Stokes equations," *ESAIM: Mathematical Modelling and Numerical Analysis*, vol. 34, no. 6, pp. 1233–1258, 2000. 121, 181, 182

[90] F. Abergel and R. Temam, "On some control problems in fluid mechanics," *Theoretical and Computational Fluid Dynamics*, vol. 1, no. 6, pp. 303–325, 1990. 123

[91] J. Droniou, "Non-coercive linear elliptic problems," *Potential Analysis*, vol. 17, no. 2, pp. 181–203, 2002. 131

[92] M. Gunzburger, L. Hou, and T. P. Svobodny, "Analysis and finite element approximation of optimal control problems for the stationary navier-stokes equations with dirichlet controls," *ESAIM: Mathematical Modelling and Numerical Analysis*, vol. 25, no. 6, pp. 711–748, 1991. 131, 132, 183, 184

[93] M. D. Gunzburger and S. Manservisi, "Analysis and approximation of the velocity tracking problem for Navier–Stokes flows with distributed control," *SIAM Journal on Numerical Analysis*, vol. 37, no. 5, pp. 1481–1512, 2000. 132, 176, 181, 182, 184

[94] G. Barakos, E. Mitsoulis, and D. Assimacopoulos, "Natural convection flow in a square cavity revisited: laminar and turbulent models with wall functions," *International journal for numerical methods in fluids*, vol. 18, no. 7, pp. 695–719, 1994. 152, 193

[95] H.-C. Lee, "Optimal control problems for the two dimensional Rayleigh—Bénard type convection by a gradient method," *Japan journal of industrial and applied mathematics*, vol. 26, no. 1, pp. 93–121, 2009. 168

[96] H.-C. Lee, "Analysis and computations of Neumann boundary optimal control problems for the stationary Boussinesq equations," in *Proceedings of the 40th IEEE Conference on Decision and Control (Cat. No. 01CH37228)*, vol. 5, pp. 4503–4508, IEEE, 2001. 168

[97] S. Manservisi and F. Menghini, "Optimal control problems for the Navier–Stokes system coupled with the k-ω turbulence model," *Computers & Mathematics with Applications*, vol. 71, no. 11, pp. 2389–2406, 2016. 168, 173, 183, 184

[98] S. Manservisi and F. Menghini, "Numerical simulations of optimal control problems for the Reynolds averaged Navier–Stokes system

closed with a two-equation turbulence model," *Computers & Fluids*, vol. 125, pp. 130–143, 2016. 168

[99] D. C. Wilcox *et al.*, *Turbulence modeling for CFD*, vol. 2. DCW industries La Canada, CA, 1998. 168, 169

[100] S.-H. Peng and L. Davidson, "Computation of turbulent buoyant flows in enclosures with low-Reynolds-number k-ω models," *International Journal of heat and fluid flow*, vol. 20, no. 2, pp. 172–184, 1999. 169

[101] B. Devolder, P. Rauwoens, and P. Troch, "Application of a buoyancy-modified k-ω SST turbulence model to simulate wave run-up around a monopile subjected to regular waves using OpenFOAM®," *Coastal Engineering*, vol. 125, pp. 81–94, 2017. 169

[102] R. Temam, *Navier-Stokes equations: theory and numerical analysis*, vol. 343. American Mathematical Soc., 2001. 172

[103] F. Menghini, "Advanced computational fluid dynamics models for liquid metal flows," 2016. 173

[104] T. C. Rebollo and R. Lewandowski, *Mathematical and numerical foundations of turbulence models and applications*. Springer, 2014. 174, 176

[105] D. M. Bedivan, "Existence of a solution for complete least squares optimal shape problems," *Numerical Functional Analysis and Optimization*, vol. 18, no. 5-6, pp. 495–505, 1997. 176

[106] S. Manservisi and M. Gunzburger, "A variational inequality formulation of an inverse elasticity problem," *Applied numerical mathematics*, vol. 34, no. 1, pp. 99–126, 2000. 177

[107] V. M. Tikhomirov, "Fundamental principles of the theory of extremal problems," *New York*, 1986. 180

[108] J. Elder, "Turbulent free convection in a vertical slot," *Journal of Fluid Mechanics*, vol. 23, no. 1, pp. 99–111, 1965. 193